USING IR THERMOGRAPHY TO DETERMINE THE HEAT FLUX REMOVED BY SPRAY COOLING A HIGH-TEMPERATURE METALLIC SURFACE

by

CRISTINA PEDOTTO

B.S., Kansas State University, 2006

A THESIS

submitted in partial fulfillment of the requirements for the degree

MASTER OF SCIENCE

Department of Mechanical Engineering
College of Engineering

KANSAS STATE UNIVERSITY
Manhattan, Kansas

2008

Approved by:

Major Professor
Dr. Bruce Babin

Abstract

A significant body of literature exists for experiments in spray cooling applications that utilize one-dimensional heat transfer through a metal ingot to determine the average surface heat flux. Due to inherent non-uniformities in spray distributions, measurements that account for the two-dimensional effects are required. In this study, an infrared (IR) camera was used to capture the two-dimensional temperature distribution formed when spraying an electrically heated NiChrome surface with three different fluids. IR thermography captured the thermal response of the un-sprayed side of a 0.005-inch (0.125mm) think strip of NiChrome exposed to spray from a 90° full-cone nozzle at low mass fluxes (0.025 – 0.045 lb/ft^2-s / 0.122 – 0.220 kg/m^2-s) from a distance of approximately 5 to 11 inches (13 to 28cm). Results were measured for surface average temperatures ranging from 150 to 600°F (65 – 315°C).

Table of Contents

List of Figures

List of Tables

Acknowledgements

I would like to take this opportunity to thank all of the individuals that have helped me complete this study:

First I'd like to express my gratitude to Dr. Bruce Babin, my Major Advisor, for all his efforts in coordinating this entire research effort, mentoring the experimental design process, and assisting in the collection and processing of data. I really feel as though I have learned a lot from him during this entire experience. And most of all, I want to thank him for his patience. It's no secret I can be stubborn with some of my ideas and I really appreciate all of his patience and time he spent working with me until I felt as though I understood.

I would also like to thank Dr. Gregg Geiger and Michael Christiansen, my Industry Mentors for all their help with this project. They really helped me stay focused on completing project goals and not getting too worked up in some of the non-essential details. I will take so very much from them about project management and project focus that I know will be a valuable asset for me in the future.

I would also like to thank my Committee Members, Dr. B. Terry Beck and Dr. Steve Eckels, for their time and assistance in completing this project and my degree.

I would like to acknowledge Jason Selland, MNE Shop Manager, for all his help in designing the experimental apparatus, locating materials, and manufacturing custom pieces for the experiments.

Additionally, I would like to thank Josh VanMeter, a great editor and friend, for being my sounding board for ideas and helping me edit my writing from hundreds of miles away.

Thank you to all of the students who have helped with various stages of this process: Brandon Svitak, Jeff Smith, Alex Fox, Will Cromer, Zach Thomas, and Amy Howell. I would especially like to thank, Jared Goodnight, for his on-going assistance throughout the entire project. He was always willing to go above and beyond to help me and I am very grateful.

And, lastly, I'd like to thank my family: Dominic for being a person with whom I could discuss theoretical ideas; Kelly for assisting me in proofreading; Jamison for giving me the computer that served as a huge asset to my completion of this project; And, lastly, Mom & Dad for listening to me ramble about technical concepts they didn't quite understand, but nodded in agreement anyway and for always believing in me.

CHAPTER 1 - Introduction

Spray cooling can be described as the processes of removing heat from a hot surface by exposing the surface to fluid flow from a nozzle. The high heat flux removed by spray cooling makes it optimal for use in different facets of industry. When quenching of forged metals, industries may employ a spray cooling technique in an effort to control the cooling process so that parts do not experience unintentional thermal stresses during cooling that may cause the warping or fracture. Electronic equipment, especially those that use high-powered chips that perform millions of processes at ever increasing speeds, may also use a spray cooling technique in order to quickly remove large quantities of heat from their small surfaces. Laser diodes may also be cooled by spray cooling for the same reason. During quenching, the exposed surface is very hot, so it will take full advantage of the spray's cooling capacity initially to quickly cool the metal. While in electronic and laser diode applications, the spray is used to keep the equipment temperature within an operating range. This generally requires heat removal significantly below the fluid's cooling capacity so that there is a low risk of equipment failure due to thermal exposure.

This report will detail an experimental investigation of the effects of varied low mass flux, spray fluid, and spray angle on the amount of heat flux removed by spray cooling a smooth metallic surface. The mass flux at the sprayed surface is defined as the amount of fluid impacting the surface area over time. The experiment assumes that the mass flux at the surface is essentially constant, which is reasonable for the small test surface. The mass flux applied to the spray surface is relatively low, ranging from 0.025lb/ft^2-s to 0.045lb/ft^2-s.

A heated surface was sprayed with three different fluids – water, and two alternate fluids that will be referred to as Fluid 1 and Fluid 2 for this report.

The spray angle is defined for these experiments as the angle formed between the sprayed surface and the center axis of the spray nozzle so that spray normal to the surface is at a 90° spray angle as shown in Figure 1.1.

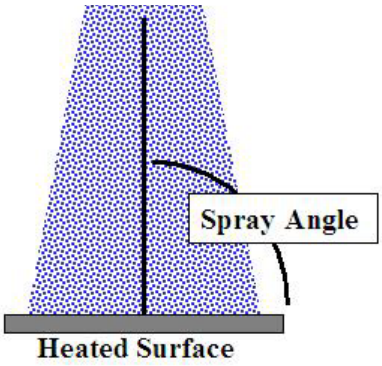

Figure 1.1 Spray angle defined as the angle between the spray surface and spray nozzle axis

The collected data will be used to determine associated trends that may be useful in optimizing spray cooling processes. Additionally, data will be used to predict the critical heat flux (CHF) for each spray scenario so that the cooling potential can be compared.

Spray cooling is often associated with boiling, where a volume of fluid is exposed to a hot surface and high quantities of heat are removed by changing the phase of the fluid from liquid to vapor. The main difference between the two processes it that in boiling, the surface is continually exposed to a liquid volume, and in spray cooling, the surface is exposed to liquid droplets that may not cover the surface completely at one point in time.

CHAPTER 2 - Literature Review

2.1 Dropwise Evaporation

Pool boiling, a type of boiling where the liquid is relatively stagnant during the phase change process, has been studied extensively by researchers. The associated heat flux in pool boiling is generally represented by a characteristic curve of the surface heat flux as it relates to a temperature difference for the process. If the initial fluid temperature is assumed to be close to saturation temperature, the x-axis is defined as the wall temperature minus the fluid's saturation temperature. If the initial fluid is sub-cooled, the x-axis is plotted as the wall temperature minus the fluid temperature. The y-axis is generally plotted as heat flux at the surface on a logarithmic scale. An example can be seen in Figure 2.1(A). In general, researchers describe the curve by defining four regions of heat transfer: convective heat transfer, nucleate boiling, transition boiling, and film boiling. Convective heat transfer occurs when the temperature of the boiling surface is above the liquid's saturation temperature. A transition to nucleate boiling is defined physically by the formation of vapor bubbles at the boiling surface and graphically by a change in the slope of the curve. At higher surface temperatures, the formation and detachment of vapor bubbles at the surface continues and increases in frequency. A peak in the heat flux at the surface graphically defines the shift from nucleate boiling to transition boiling. This local maximum is called the critical heat flux (CHF). Film boiling is defined physically when an insulating vapor layer is formed above the surface and graphically by significant increase in temperature with only small increases in applied heat flux. Transition boiling is the quasi-steady state heat transfer regime between nucleate boiling and film boiling. During transition boiling, large vapor pockets form vapor layers at the surface that cannot be maintained and detach from the surface as large, non-spherical bubbles. The non-uniform surface conditions, where some of the surface area is insulated by vapor pockets and the rest is covered with the liquid pool, causes the average surface heat flux to be between that of nucleate boiling and film boiling (Faghri &

Zhang, 2006). Surface history may affect the ratio of film boiling and nucleate boiling effects at the surface during the transition boiling regime.

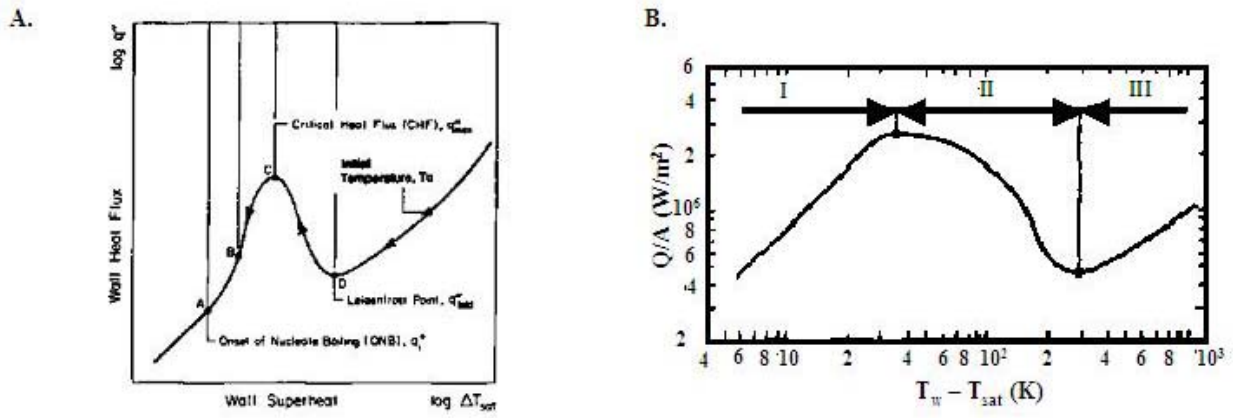

Figure 2.1 (A.) Pool boiling curve for water extracted from Mudawar & Valentine (1989). (B.) Boiling curve for liquid water impinging a hot surface extracted from Del Giudice & Comini (1979).

The phase change of a liquid drop on a surface is similar to pool boiling. The characteristic curve for phase change of an individual liquid drop impacting a hot surface is plotted in Figure 2.1(B). The heat transfer for a liquid drop, described by Del Giudice & Comini (1979), can be divided into three regimes: surface evaporation (I), film boiling (III), and transitional evaporation (II). When the hot surface is at a temperature only slightly above the fluid saturation temperature, the droplet impacts the surface and forms a disc-like thin film. Heat is conducted through the liquid film and evaporation occurs at the upper liquid-vapor interface reducing the diameter of the film not the overall thickness.

When the surface is at a temperature significantly above the saturation temperature, the droplet does not impact the surface. Rather, a thin layer of vapor is formed between the hot surface and the droplet. Heat is transferred by conduction through the vapor layer and by radiation from the surface. Phase change occurs at the vapor layer-liquid droplet interface. This mode of heat transfer is also referred to as film boiling, as it relates to the pool boiling phenomena of film boiling, or as the Leidenfrost effect (Del Giudice & Comini, 1979).

Transition evaporation occurs at surface temperatures between those of surface evaporation and film boiling. During this heat transfer regime, small vapor layers are formed within the impacted droplet reducing the overall heat transfer. It should be noted that there is no defined nucleate boiling regime where vapor bubbles form and detach from the surface in the phase change of a single droplet. It is speculated that this is because there may be no appreciable difference between nucleate boiling and transitional boiling in a thin film (Del Giudice & Comini, 1979).

Analytical models to predict heat transfer by phase change of a single drop based on liquid properties and impacted droplet diameter are presented by Del Guidice & Comini (1979) and Faghri & Zhang (2006) for surface temperatures slightly above saturation conditions. Analytical predictions were observed to agree with experimental findings (Del Guidice & Comini, 1979).

2.2 Experimental Methodology

The phase change of a single liquid droplet does not necessarily describe the heat transfer that will result from a field of impacting droplets. In order to broaden the understanding of spray cooling, experimental studies were necessary. A majority of spray cooling experiments - for example Lin & Ponnappan (2004) & (2002), Mudawar & Valentine (1989), Jai & Qui (2003), Grissom & Wierum (1980), Choi & Yao (1987), and Webb et al (1992) - used metal ingots heated by internal heaters surrounded by insulation to create a one-dimensional conduction heat transfer temperature profile between the sprayed surface and the central heaters. In general, thermocouple temperature measurements were recorded along a cylindrical ingot's axis and used to extrapolate a surface temperature assuming one dimensional conduction heat transfer through the ingot. A schematic of one of these experimental configurations is shown in Figure 2.1. Experiments that follow this basic style benefit from the innate stability and relatively slow response of the system due to the large thermal mass, but must assume uniform surface conditions, which may not be an accurate assumption. This experimental practice assumes a uniform temperature at the surface. However, this assumption is not strictly valid since phase change of individual fluid droplets is assumed to be the primary mode of heat transfer and the

entire surface does not experience contact with the sprayed fluid at a single point in time. Thus, it follows that the surface temperature will vary where and when the droplets strike.

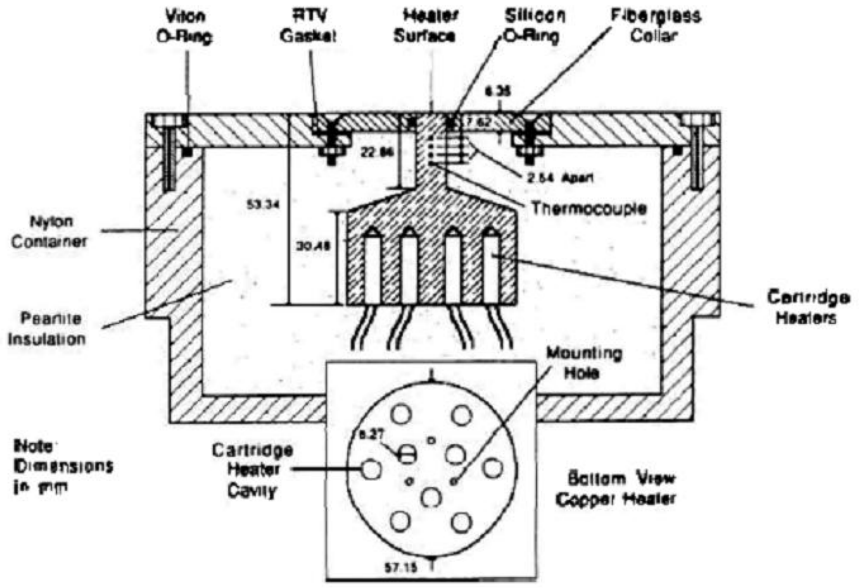

Figure 2.2 Ingot design used for experimental spray cooling studies extracted from Mudawar & Valentine (1989).

Other experiments (Ghodbane & Holman – 1991 and Lui & Wang – 2000) used a thin metal plate with thermocouples welded to the unsprayed side. For these experiments, current is run through the foil to heat the surface. Even with the use of thermocouples in these experiments, the reported average surface temperature maintains previous assumptions of uniform surface conditions. These experiments may have benefited from the quick thermal response of the metal plate. However, the welding of thermocouple wires may be detrimental: generating issues related to fin effects from the applied wire or electrical noise due to the positioning of the thermocouple on an electrically charged plate.

More unique experimental approaches were implemented by Horacek et al (2005) and Freund et al (2007). Horacek et al (2005) used an array of micro heaters set individually to a prescribed temperature via a digital potentiometer as a part of a Wheatstone bridge. Freund et al (2007) used Temperature Oscillation IR Thermography (TOIRT) to produce a two dimensional map of the heat transfer coefficient at the surface heated by radiation from a laser. Though this method

is able to measure two-dimensional surface temperatures and has a high experimental accuracy, it is not necessarily cost effective and has not been used in experiments with surface temperatures near CHF of water.

The non-uniform surface characteristics generated by impinging droplets on the sprayed surface suggest the assumption of a uniform surface temperature is invalid. Therefore, in the following experiment, a thin metal foil will be used as the spray surface instead of a metal ingot. In addition, to obtain a large number of temperature measurements without disrupting the uniform resistive heating of the foil, IR thermography will be employed instead of welded thermocouples to determine surface temperatures from the unsprayed side of the foil. A similar method was used by Schmidt & Boye (2001) in their investigation of the effects of droplet size and velocity on the spray cooling heat transfer.

2.3 IR Thermography

Infrared thermography is a non-contact, non-destructive temperature measurement method that uses a sensor to measure energy associated with infrared waves emitted by all objects within the focal view. Infrared devices have been used in research of convectively cooled surfaces (Sargent et al. (1998)) to measure two dimensional temperature profiles. These devices are also used regularly to observe the integrity of constructed insulation and in the prediction failure for mechanical devices (www.flirthermography.com).

All objects at temperatures above absolute zero emit infrared waves; this process is called thermal radiation. No medium is required to transfer heat through thermal radiation. A theoretical black body will absorb all impinging energy of all wavelengths from surrounding objects at higher temperatures. A black body will also emit energy uniformly in all wavelengths to surrounding objects at lower temperatures. The foundation of radiation heat transfer is based primarily upon the transfer of energy between black bodies with adjustments for gray bodies. Gray bodies are real objects that are assumed to absorb a constant portion of the impinging energy independent of wavelength. The ratio of the emittance of an object and the emittance of a black body is defined as the object's emissivity. A polished mirror surface will have an

emissivity around 0.1 while a surface painted with flat black paint will have an emissivity around 0.95. An object's emissivity has a significant impact on the rate of radiation heat transfer. (Incropera & DeWitt, 2002)

Infrared waves, generated as the mode of heat transfer in radiation heat transfer, are part of the electromagnetic spectrum not usually visible to the human eye slightly overlapping and extending to wavelengths just beyond the color red in the visible spectrum. The infrared range is composed of wavelengths between 0.75μm and 100μm (Incropera & DeWitt, 2002). An infrared camera is used to convert energy emittance from an object to a temperature reading given the object's emissivity, the distance between the camera and the object, the reflected temperature of surrounding objects, the ambient air temperature, and the relative humidity. The Flir ThermaCAM S65 used in testing uses a 320 by 240 pixel focal plane array (FPA) of uncooled microbolometers to capture the infrared image over a spectral range from 7.5μm to 13μm (Flir Systems, 2004). The camera works by taking advantage of the change in resistance of each microbolometer detector as it is exposed to infrared waves (Schaff, 2000). Each pixel in the array is used to describe the overall infrared image in the focal view of the camera's lens. Uncooled microbolometer detectors are considered less accurate than other cryogenically cooled detectors, but are more cost efficient and simpler to operate (Schaff, 2000).

2.4 Spray Cooling Parameters

Surface temperatures and the corresponding boiling regimes are not the only parameters that affect the amount heat transferred from the surface. Surface parameters, droplet dynamics, and spray characteristics can also affect the heat transfer from the surface.

Surface parameters such as roughness and fin geometry have been shown to affect the surface heat transfer. Pais et al (1992) concluded through an experimental study that as roughness increases the maximum heat transfer decreases. Surface fin geometry, studied by Silk et al (2006), also has a significant affect on heat transfer attributed mainly to more efficient drainage created by the fin pattern. To negate possible affects from changing surface parameters, the following study uses a smooth, non-finned filament for all tests.

The effects of droplet dynamics – droplet mean diameter, droplet mean velocity, and volumetric spray flux – were studied by Mudawar and Valentine (1989). The authors concluded that volumetric spray flux highly influenced all modes of heat transfer at the surface. While droplet mean diameter primarily affected the single-phase cooling and the determination of CHF, droplet mean velocity was also found to be influential during transitional cooling. The following experimental study uses a single spray nozzle, approximately constant nozzle inlet pressure, and minimal spray distance changes for all tests in order to assume a consistent droplet mean diameter and droplet mean velocity. Changes in heat flux associated with volumetric spray flux are investigated in the variation of mass flux at the heated surface.

Spray characteristics can be associated with varying spray liquid properties and spray geometry. The addition of sodium dodecyl sulphate (SDS), a surfactant that reduces the liquid's surface tension, to the liquid water spray was studied. Adding SDS was determined to be advantageous by Qiao & Chandra (1997) by increasing heat transfer during nucleate boiling and increasing CHF and Jia & Qiu (2003) by reducing superheat and generating larger, more stable CHF ranges. The following experiments will implement three different spray fluids to investigate the affects of spray fluid properties on heat transfer from the surface.

The following investigation will also address effects of spray geometry on the surface heat transfer by changing the impinging spray angle. A study by Silk, et al (2006) exposed surfaces to multiple spray angles and conclude a maximum heat transfer of 98 W/cm^2 for PF-5060 sprayed on a flat, horizontal surface at 15° from vertical. The effect of surface orientation was explored by Isachenko et al (1979), Ghodbane & Holman (1991), and Choi & Yao (1986) in spraying horizontally onto a vertically oriented surface forming a thin liquid film at the surface. The film flow along the vertical surface was found to be highly dependent on the Weber number by Ghodbane & Holman (1991) and Choi & Yao (1987) and is described as unstable due to the continual impact of droplets by Isachenko et al (1979). For all of the following tests, the surface is oriented horizontally and sprayed on from above to negate any affects attributed to surface orientation.

2.5 Summary of Spray Cooling Studies

The effects of various spray cooling parameters were considered for several analytical models developed to describe spray cooling. Many analytical models and experimental correlations take into consideration several relevant spray parameters such as spray mass flux at the surface, droplet velocity, droplet characteristic diameter, liquid surface tension, liquid and vapor density, liquid viscosity, and liquid to vapor latent heat removal in addition to spray and surface temperatures. A summary of some of the equations derived analytically or through experimental investigation in order to better predict spray cooling heat transfer is shown below in Table 2.1.

Table 2.1 Summary of Analytical and Experimental Correlations for Spray Cooling

Author	Eqn.	Correlations	Derivation Method	Parameters
Surface Evaporation Conditions				
Ghodbane & Holman (1991)	1	$\frac{qx}{\mu_f h_{fg}} = 10.55We^{0.6}\left(\frac{c_{pl}\Delta T}{h_{fg}}\right)$ q – heat flux x – distance from nozzle to heat source *We* based on droplet diameter and droplet velocity	Experimental Correlation	Freon 113 2200 < We < 13750 210 < D < 980μm 20°C < $T_{surface}$ < 90°C
Grissom & Wierum (1981)	2	$h^* = \frac{\pi k \lambda^*}{2b_o \lambda}\left[\frac{p+1}{2p+1}\right]$ h^* - flooding heat transfer coefficient q* - surface heat flux required to vaporize all impinging spray λ – latent heat of vaporization λ^* - [$\lambda + c_p(T_s - T_0)$] b_o – initial average droplet thickness p – coefficient relating droplet thickness to 'spread diameter' τ_t – total droplet evaporation time A_x – area reduction factor	Analytical	(T_w-T_{sat}< 20°C)
	3	$q^* = \frac{\pi \rho \lambda^* b_o}{4\tau_t A_x}$		
Lei & Lu (2005)	4	$h_{r(k)} = 9500\left(m_d NU\right)_{(k)}^{0.4}$ $h_{r(k)}$ – real heat transfer coefficient m_d – droplet mass N – droplet number flux U – mean droplet velocity	Experimental Correlation	Non-boiling Spray 50°C < T_w<10°C
Liu et al (1999)	5	$q = \dot{m}_L c_p\left(T_{sat} - T_L\right) + \dot{m}_L r_e h_{fg}$ ** Surface & Transitional Evaporation r_e – m_{vapor}/m_{liquid} (experimentally determined)	Analytical & Experimental	50°C<T_s<350°C
Jia & Qui (2003)	6	$q'' = \frac{\dot{M}_i\left(1-\varepsilon\right)\left(h_{fg} + C_{p,l}\left(T_{sat} - T_f\right)\right)}{A}$ ** Surface & Transitional Evaporation $\varepsilon = M_e/M_i$ - mass flux expelled over impacting mass flux (experimentally determined)	Analytical	50°C<T_s<160°C 22.7μm < D < 30.1μm
Mudawar & Valentine (1989)	7	Flooded Surface Condition $Nu_{32} = 2.512\,\mathrm{Re}_{32}^{0.76}\,\mathrm{Pr}_f^{0.56}$ $Re = Q''d/\nu_f$ – volumetric spray flux*droplet diameter / kinematic viscosity	Experimental Correlation	405μm < D_{32} < 1351μm 53 < ΔT_{max} < 125°C 10.9 < $v_{droplet}$ < 25.2m/s
	8	Nucleate Boiling $q'' = 1.87x10^{-5}\left(T_{sat} - T_f\right)^{5.55}$		

Author	Eqn.	Correlations	Derivation Method	Parameters
Transitional Evaporation Conditions				
Mudawar & Valentine (1989)	9	$\frac{q''_{CHF}}{\rho_g h_{fg} Q''} = 122.4\left[1+0.0118\left(\frac{\rho_g}{\rho_f}\right)^{1/4}\left(\frac{\rho_f c_{p,f}\Delta T_{sub}}{\rho_g h_{fg}}\right)\right]\left(\frac{\sigma}{\rho_f Q''^2 d_{32}}\right)^{0.198}$	Experimental Correlation	$405\mu m < D_{32} < 1351\mu m$ $53 < \Delta T_{max} < 125°C$ $10.9 < v_{droplet} < 25.2 m/s$
	10	$T_{\max} = 18\left[\left(\rho_g h_{fg} Q''\right)\left(\frac{\sigma}{\rho_f Q''^2 d_{32}}\right)^{0.198}\right]^{1/5.55} + T_f$ Q'' – volumetric spray flux d_{32} – Sauter mean diameter		
	11	Transition Boiling $\log\left(\frac{q''}{q''_{\max}}\right) = 4.78x10^5\left(\frac{u_m}{Q''}\right)^{-1.255}\left[\log\left(\frac{T_{sat}-T_f}{T_{\max}-T_f}\right)\right]^3 - 1.90x10^4\left(\frac{u_m}{Q''}\right)^{-.903}\left[\log\left(\frac{T_{sat}-T_f}{T_{\max}-T_f}\right)\right]^2$		
Film Boiling Conditions				
Mudawar & Valentine (1989)	12	$\frac{q''_{Leid}}{\rho_g h_{fg} Q''} = 0.145\left(\frac{u_m}{Q''}\right)^{0.834}$ u_m – droplet mean velocity Q'' – volumetric spray flux	Experimental Correlation	$405\mu m < D_{32} < 1351\mu m$ $53 < \Delta T_{max} < 125°C$ $10.9 < v_{droplet} < 25.2m$
Moriyama et al (1987)	13	$h_s = \frac{1.584\rho h_o q_W \overline{D}^4 \overline{v}}{\pi\sigma(d_{30})^3}$ h_o – heat transfer coefficient for a single drop (values obtained from published experimental data) d_{30} – volume-averaged diameter $\overline{D}$ - mean drop size at a given sampling location $\overline{v}$ - mean speed of droplets at a given sampling location	Experimental Correlation	$400 < T_W < 800°C$ $9.29 < d_{30} < 15.2\mu m$
Yao & Cox (2002)	14	$\varepsilon = \frac{q''}{G\left(h_{fg} + C_{p,l}(T_{sat}-T_l) + C_{p,v}(T_W - T_{sat})\right)}$	Experimental Correlation	$300 < \Delta T_{sat} < 800°C$ $2x10^{-3} < Re_s < 5$ (Accuracy ±33%) $6x10^{-10} < We_s < 3x10^{-2}$ (Accuracy ±17%)
	15	$\varepsilon = 2.5x10^{-4}\left[\mathrm{Re}_s\frac{T_{sat}}{\Delta T_{sub}+\Delta T_{sat}}\right]^{-1.05} + 2.5x10^{-2}\left[\mathrm{Re}_s\frac{T_{sat}}{\Delta T_{sub}+\Delta T_{sat}}\right]^{-0.4}$ G – liquid mass flux d – droplet diameter $Re_s = Gd/\mu$ $We_s = G^2 d/\rho\sigma$		
	16	$\varepsilon = 8x10^{-7}\left[We_s\frac{T_{sat}}{\Delta T_{sub}+\Delta T_{sat}}\right]^{-0.62} + 3.5x10^{-3}\left[We_s\frac{T_{sat}}{\Delta T_{sub}+\Delta T_{sat}}\right]^{-0.2}$		
	17	$T_{Leidenfrost} = 1400 We_s^{0.13}$		

Although attempts have been made to develop stand alone analytical models to accurately predict spray cooling heat transfer, many models are still partially empirical and rely on experimentally determined spray parameters. An example is the evaporation ratio, r_e, implemented in Eqn. 5 in Table 2.1 as the experimentally determined ratio between evaporating liquid and impinging liquid on the surface. Moriyama et al (1987) used an average heat transfer coefficient from a single drop, determined from previous experimental results (h_o in Eqn. 12), to correlate an overall spray heat transfer coefficient. Other examples of parameters not analytically defined are the droplet film thickness, b_o, in Eqn. 2 and Eqn. 3 and the mass ratio of impacting droplets compared to expelled droplets, ε, in Eqn. 6.

Frequently, in both analytical models and empirical correlations, non-dimensional Reynolds (Re) and Weber (We) numbers are used to describe the spray or droplet characteristics. In order to determine either of these parameters, a characteristic velocity and characteristic length must be used. Throughout the published literature, the characteristic length used is a form of the droplet mean diameter, with varying methods of determining an average, which is true for all correlations listed in Table 2.1. Similarly, the characteristic velocity is defined as the droplet mean velocity for most correlations, with the exception of Eqns. 15 through 17 where the overall spray velocity defined as the mass flux divided by the liquid density. Yao & Cox (2002) compare the use of droplet velocity to spray velocity in defining We and Re numbers. Their analytical model predicts spray cooling heat transfer at surface temperatures above 400°C by means of a spray heat transfer effectiveness. Comparing their results with experimental data for water spray, the authors conclude that the use of spray mass velocity greatly improves the overall correlation of effectiveness and more accurately reflects the behavior of real sprays.

Based upon these conclusions and because a mean droplet velocity is not established in this study, the characteristic spray velocity for this study for all phases of heat transfer will be based upon an overall spray velocity defined as the mass flux divided by the liquid density.

2.6 Experimental Predictions

A general prediction of spray cooling heat flux using a sample of the analytical equations listed in Table 2.1 can be seen below in Figure 2.3. It should be noted that because a mean droplet velocity is not measured during these tests the mean droplet velocity used in the development of correlation equations 7, 11, and 12 has been substituted with the spray velocity (mass flux divided by liquid density). This substitution may affect the validity of the predictions. In order to achieve a more accurate prediction, equations were chosen based on how well the correlation criteria listed in the last column of Table 2.1 fit the intended experimental parameters for this work and if all listed variables could be estimated without experimentation. Therefore, the general predictions shown in Figure 2.3 below are based upon Eqns. 5 through 12 and Eqns. 14 through 16 listed in Table 2.1.

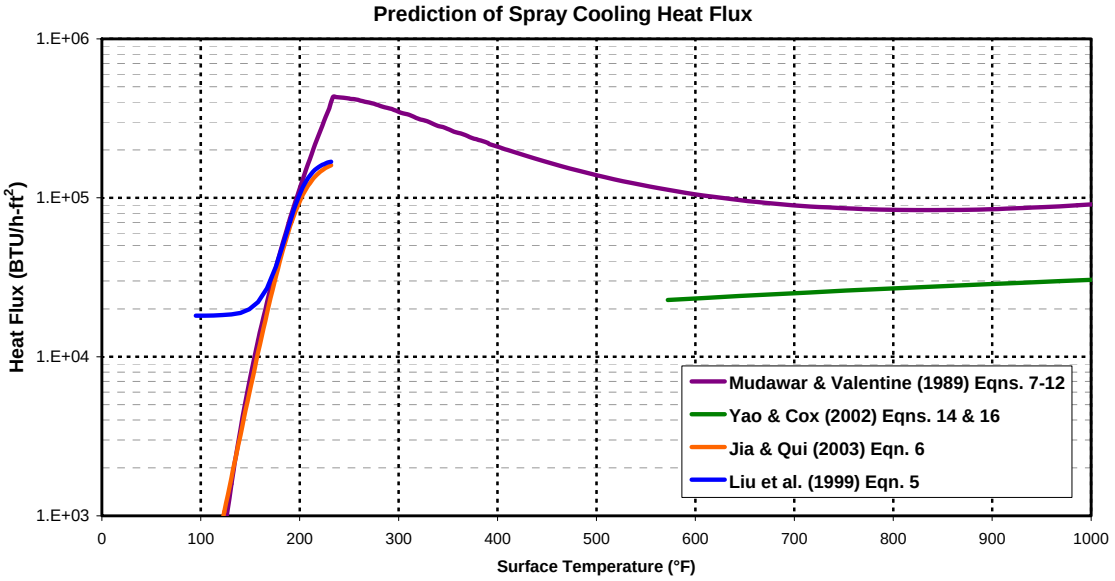

Figure 2.3 General Prediction of Spray Cooling Heat Flux for water sprayed at 0.035lb.ft^3-s.

The CHF values for water sprayed at 0.035lb/ft^3-s calculated using Eqns. 5, 6, and 9 are listed in Table 2.2. Eqn. 9 from Table 2.1 predicts a CHF value more than twice that predicted by both Eqns. 5 and 6. Because the correlation was developed based on an experimental mass flux that is higher and an experimental droplet size that is larger than those used in the prediction, it is reasonable to conclude that the Mudawar (1989) correlation may over-predict CHF. Eqns. 5 and 6 are based upon basic heat transfer principles of available energy during phase change, so the

predicted CHF values are considered more reasonable for this analysis. In this analysis, the Mudawar correlation (Eqns. 7 through 12) is assumed to be more accurate in the prediction of the general curve shape and in the prediction of surface temperatures that correspond to changing heat transfer regimes. This assumption is based on the equation's dependence on droplet diameter; Eqn. 10, used to determine the temperature at which CHF occurs, is less dependent on impinging mass flux and droplet diameter than Eqn. 9, used to determine CHF, by a factor of 1/5.55 seen as the exponent in Eqn. 10.

Table 2.2 Calculated CHF for water sprayed at 0.035lb/ft^3-s.

	Calculated CHF	
	W/m^2	BTU/h-ft^2
Liu et al. (1999)	532093	168727
Jia & Qui (2003)	504935	160115
Mudawar & Valentine (1989)	1357339	430412

Eqns. 7 through 12 were used in determining the surface temperatures at which CHF is predicted to occur, as well as to predict the curve shape prior to CHF. Both Eqns. 5 and 6 use an experimentally determined ratio parameter based upon the amount of spray that is evaporated compared to the amount of spray applied to the surface to predict heat flux values before surface temperatures associated with CHF. Because experimental ratios could not be determined for our experimental tests, these parameters were estimated to be functions of surface temperature. Figure 2.4 shows the estimated values for the expulsion rate (ε) used in Eqn. 5 and the evaporation ratio (r_e) used in Eqn. 6. The ratios were approximated as S curves with the same general characteristics and opposite boundary conditions to fit the desired purpose in their respective equations. The S curve function was used because the slope of the ratio parameter drastically impacts the slope of the predicted boiling curve. General boiling curves, such as those in Figure 2.1, show the boiling curve at surface temperatures less CHF starting with a minimal slope increasing to a much higher slope and then decreasing to a minimal slope again. Support for S curve behavior can be found in the physical observation of surface conditions: At first the slope is minimal due during observable flooded surface conditions where a portion of the sprayed liquid does not evaporate but runs off the hot surface. Then, as the surface temperature rises, the droplets impact the surface and stay on the surface until evaporated. As

the surface continues to increase in temperature, the droplet rate of evaporation increases until droplets evaporate almost instantaneously as they impact the surface.

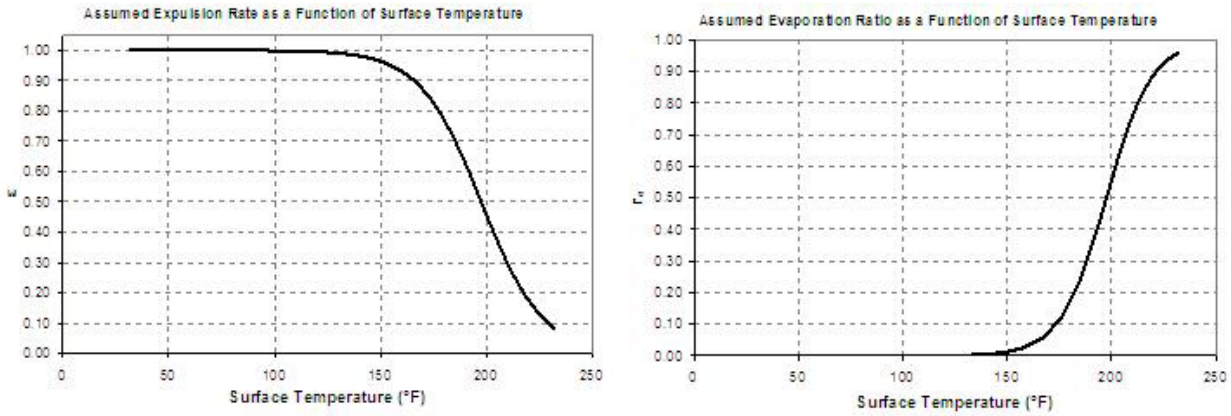

Figure 2.4 Estimated expulsion rate (ε) and evaporation ratio (r_e) used in Eqns. 4 and 6 to generate curves seen in Figure 2.3.

For transition evaporation, the general predictions using Eqn. 12 are again assumed to over-predict expected values because of their dependence on an estimated droplet velocity used in the above analysis and the dependence on impinging mass flux. But general curve shape is confirmed by predictions from Eqn. 16 for surface temperatures significantly above the predicted CHF surface temperature.

2.7 Summary

Spray cooling has been described as it relates to the more extensively studied pool boiling. The evaporation of a liquid droplet is similar to the boiling of pooled liquid in that it can be divided into regimes based upon the surface temperature and method of heat transfer.

Many researchers have experimentally examined how different parameters affect the heat transferred during spray cooling including: Surface parameters, droplet dynamics, spray characteristics, and spray geometry. Correlations developed through previous studies were used to predict a CHF for water sprayed on a heated surface at 0.035lb/ft2-s of approximately 120000 BTU/h-ft2 (or 378 kW) to occur at a surface temperature of approximately 232°F (111°C).

Experimental methods used to determine surface temperatures included the use of a metal ingot insulted to produce a one-dimensional temperature gradient between a heat source and the test surface and infrared thermography, which provides a non-contact method of determining local temperature values.

CHAPTER 3 - Experimental Facility Description

3.1 The Use of Infrared Thermography

Many of the previous studies examining spray cooling used a metal ingot that allowed only one-dimensional conduction to determine surface temperatures necessary to calculate heat flux removed by spray cooling. This experimental practice assumes a uniform temperature at the surface. However, this assumption is not strictly valid since phase change of individual fluid droplets is assumed to be the primary mode of heat transfer and the entire surface does not experience contact with the sprayed fluid at a single point in time. Thus, it follows that the surface temperature will vary where and when the droplets strike. The use of infrared (IR) thermography allows the surface to be viewed in such a way that local surface temperatures may be observed. Theoretically, the spatial differences in local surface temperature caused when a droplet contacts and is subsequently evaporated from the surface may be observed.

3.2 Selection of Testing Surface Material

In order to measure local surface temperatures during spray cooling, the IR camera must be able to clearly view the sprayed surface. A clear view cannot be obtained by viewing the surface from the side being sprayed since the fluid droplets emit their own IR energy and would block the view of the surface. To view the temperatures at the surface without seeing the fluid droplets themselves a thin metal sheet should be used as the heated surface and viewed from the side opposite of the spray. NiChrome (80% Nickel, 20% Chromium) was chosen for the filament for four reasons: high electrical resistivity, high thermal conductivity, availability, and cost.

The selected metal must have a high electrical resistivity so that a thin foil could act as an electrical resister and generate heat internally when minimal power is applied. NiChrome is

commonly used in convection heat flux applications where current is applied to a NiChrome wire exposed to flow in order to determine the associated heat transfer. With an electrical resistivity reported as 0.000108 Ohm-cm (www.MatWeb.com), NiChrome is one of the more resistive metals available that also has a high enough thermal conductivity to minimize temperature gradients within the metal. Table 3.1 lists the electrical resistivity and thermal conductivity of different metals that were considered for testing.

Table 3.1 Metal Electrical Resistivity and Thermal Conductivity (www.MatWeb.com)

Metal	Electrical Resistivity		Thermal Conductivity	
	Ohm-in x 10^5	Ohm-cm x 10^4	BTU/h-ft-°F	W/m-K
Copper	0.067	0.017	222	385
Titanium	4.64	1.18	11.2	19.3
NiChrome	4.25	1.08	7.7	13.4
High Carbon Steel	2.36	0.60	11 - 30	19 - 52
Zinc	0.233	0.0592	64.7	112

High thermal conductivity is necessary so that the temperature difference through the thickness of the sheet would be minimal. Ideally, the temperature profile seen on the side of the sheet not exposed to spray should accurately represent the surface temperature profile on the sprayed surface. Figures 3.1 and 3.2 are plots that show the analytical nodal temperature results generated from an ANSYS® simulation of 0.005-inch (0.125mm) thick NiChrome sheet exposed to both gradual and step-wise heat flux profiles at the front surface (represents the surface exposed to spray during testing).

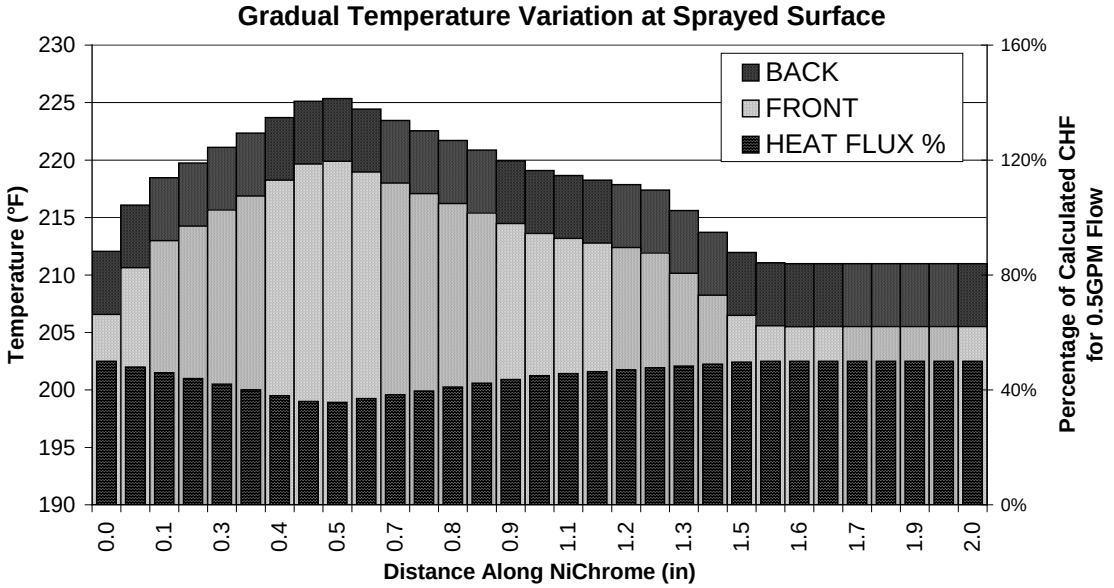

Figure 3.1 ANSYS nodal temperature results for 0.005-inch thick NiChrome exposed to a gradual heat flux profile at the front surface.

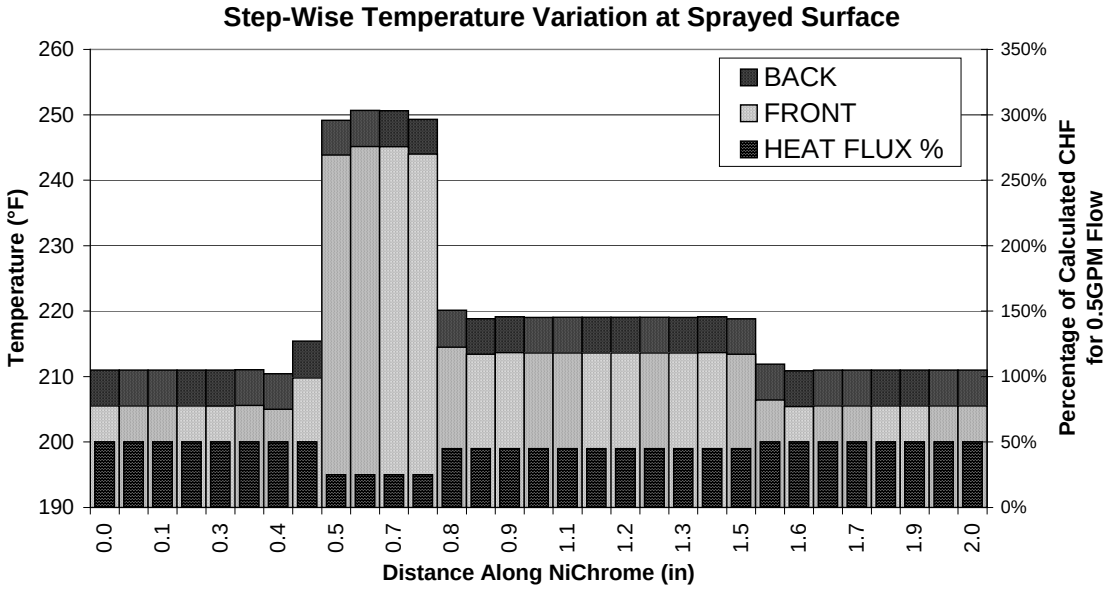

Figure 3.2 ANSYS nodal temperature results for 0.005-inch thick NiChrome exposed to a step-wise heat flux profile on the front surface.

In Figures 3.1 and 3.2, heat flux is shown as a percentage of the calculated critical heat flux ($798x10^3$ BTU/h-ft^2 or 2.52 MW/m^2) for 0.5 gallons per minute (GPM) water spray found using Mudawar and Valentine's (1989) critical heat flux correlation (see Chapter 2: Literature

Review). All other methods of heat transfer were considered negligible in these calculations because the magnitude of heat transfer due to spray cooling greatly exceeds that for corresponding radiation and convective heat loss. Results show a 5.4°F (3°C) temperature difference between the exposed front surface and the back IR viewed surface, which is well within reason of the anticipated uncertainty expected to be on the order of ±10°F (±5.6°C). Variation of surface temperature is clearly depicted in the temperature profile of the back, IR viewed, surface for both gradual and step-wise heat flux profiles.

For the experiments conducted here, it was necessary to obtain thin sheets NiChrome. Of the available options, the thinnest and most cost effective (100mm x 100mm x 0.125mm) sheet was selected for testing. Titanium was also examined as a possible testing material, but was not used due to its increased cost and limited availability.

With the metal material selected, the next step was determining the area of the surface that would be sprayed. This was important because a larger surface area would require that more power be supplied to the NiChrome to produce the same heat flux. Power would be supplied to the surface by a direct current (DC) power supply as opposed to an AC power supply so that there was no observable variation in the applied power over time that may affect the experimental results. Estimates for the necessary heat flux were calculated from Mudawar & Valentine's (1989) correlations for 0.2 GPM spray (approximately 459 $x10^3$ BTU/h-ft^2 or 1.45 MW/m^2). It was necessary that the NiChrome be supplied with a very high direct current (DC) because only a small voltage drop could be realized across the NiChrome. Safety is a major concern when working with a high current source and any fluid. Thus, it was decided that the NiChrome sheet would be cut into a strip whose surface area would minimize the required current while also remaining large enough to view local surface temperatures based on the estimated 130 micrometer spray droplet diameter. The surface was optimized to a size of 5/16" by 2".

3.3 Thermal Data Collection Assembly

Once the material and dimensions of the spray surface were determined, it was necessary to construct an assembly to support the material during testing and any equipment necessary for

data collection. The thermal data collection assembly consists of three main parts: the spray chamber, the IR camera support structure, and the heated surface assembly.

The spray chamber is a 2-foot cube made of 2x4 square-inch lumber and 3/16-inch thick plastic panels. Figure 3.3 is a drawing of the spray chamber and IR camera set-up. The chamber aids in the containment of the spray after vaporization and captures liquid run-off. The chamber has four circular openings: two are used for equipment access, a third is a drain for run-off liquid, and the fourth is a support for the heated surface assembly.

It is necessary that the IR camera views the heated surface from the opposite side of the spray, so the camera is affixed and held steady by a support structure located below the spray chamber. The camera is attached to the support structure via the terminal intended for tripod mounting.

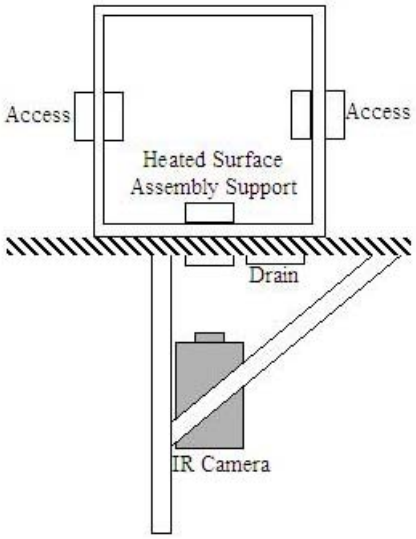

Figure 3.3 Spray chamber and IR camera support configuration

The heated surface assembly provides support for the NiChrome filament. A picture of this assembly can be seen in Figure 3.4. On each side of the assembly are two copper pieces that act as busses for the applied DC power and clamps used to hold the NiChrome filament in place. Between the two copper busses, two Teflon inserts topped with high temperature ceramic pieces form a physical separation. Both the Teflon and the ceramic are electrical isolators, making the NiChrome filament the only electrical path for the applied power. The NiChrome filament is

bolted between the two copper pieces through slots so that the filament can be pulled taut during spraying. It should be noted that the picture shown is not completely assembled for testing. The assembly shown in Figure 3.4 does not include the Extreme Tape ® or masking tape needed to prevent fluid leakage through the assembly.

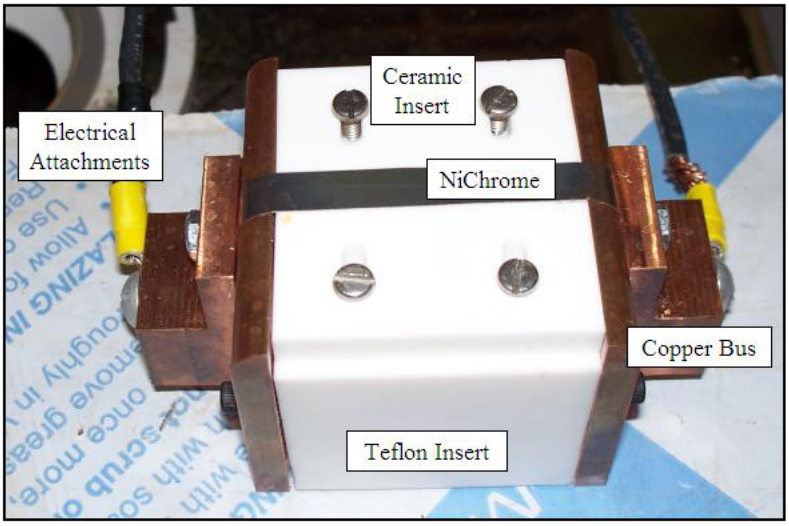

Figure 3.4 Picture of Heated Surface Assembly

The heated surface assembly is affixed with nylon screws to a plastic, cylindrical stage 3” in diameter. The stage slides on and off the heated surface assembly support (indicated in Figure 3.3) without allowing fluid leakage to the camera below. The center of the heated surface assembly is essentially hollow, allowing the IR camera a clear view of the NiChrome filament, as depicted in Figure 3.5. Further detail about the heated surface assembly is provided in Chapter 4 Experimental Procedure.

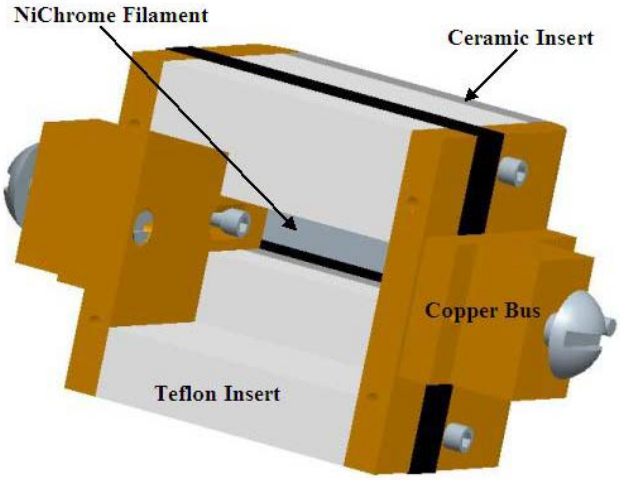

Figure 3.5 Heated Surface Assembly view of hollow center.

The IR camera views the unsprayed side of the filament as pictured in Figure 3.6 below. The NiChrome filament is the metallic piece in the center of the image. Directly below the NiChrome filament in the image is a piece of steel attached to the Teflon insert that is used in post-processing to determine the reflected temperature necessary to correctly determine the NiChrome surface temperature (see Chapter 5 Data Post-Processing for further description).

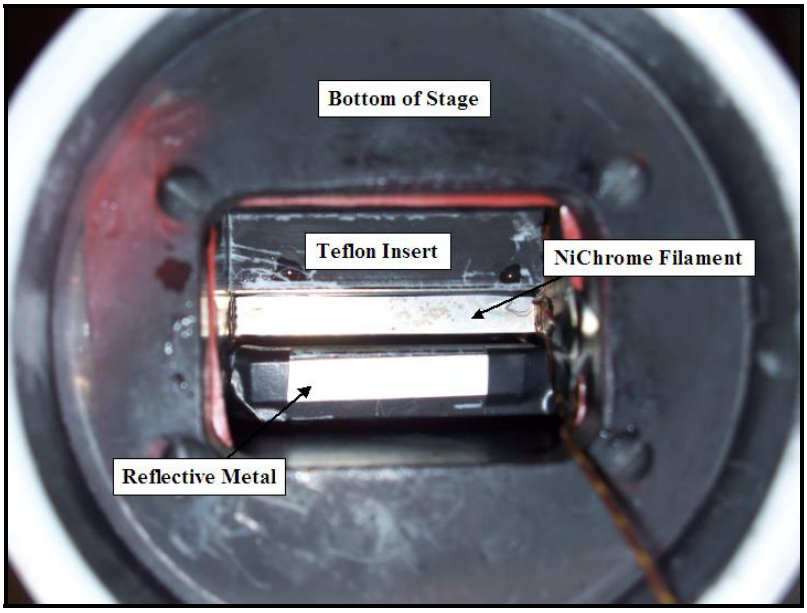

Figure 3.6 Picture of the inside of the heated surface assembly viewed from below where the IR camera is mounted.

3.4 Flow Assembly

An experimental facility was constructed to obtain the experimental data necessary to determine the heat transfer coefficient for spray cooling. The facility consists of two main assemblies: (1) The flow assembly that supplies sprayed fluid to the surface and (2) the heated assembly that contains the heated surface exposed to the spray as well as the necessary data collection equipment.

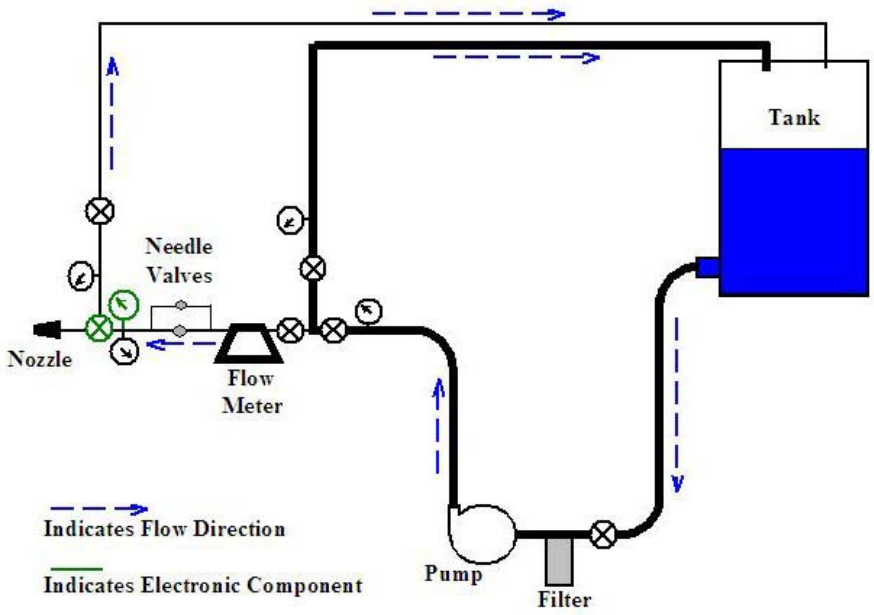

Figure 3.7 A representative schematic of the experimental flow loop.

The flow assembly forms a loop (a schematic is shown in Figure 3.7) with a 55-gallon tank reservoir, a 1-micron filter, a centrifugal pump, a coriolis flow meter, a three-way solenoid valve, and a full cone spray nozzle. Components are connected mainly with schedule 40 PVC piping and fittings as well as some steel piping. The primary line consists of 1-1/2" diameter PVC piping. The secondary line consists of 3/8" and 1/4" Swagelok steel piping from the supply line inlet to the solenoid valve. The return line from the solenoid valve to the tank is composed of PVC 3/4" piping composes. Assembly components are arranged as follows:

The tank outlet is placed 6" from the bottom of the tank at an elevation of approximately 7 feet above ground level. Elevation of the tank is necessary to create ample pressure at the inlet of the

pump. From the tank, the fluid passes through a Pentek DGD-2501 Dual Gradient Density Filter that filters the fluid first with a 25-micron pre-filter then with a 1-micron post-filter contained in a Pentek 10" Big Blue HFPP 1.5" Housing. After filtered, the fluid enters a Goulds Pump. Pump specifications can be located in Appendix C.

Once pumped, the fluid is divided between two paths. The first path is a re-circulating path that feeds the bulk of the fluid back into the tank. A restricting needle valve allows a small portion of the flow to be directed through the secondary line that supplies the spray nozzle.

Before reaching the nozzle the fluid first passes through a Micro Motion ELITE Flow Meter CMF025 that combined with the RFT9739 Field-Mounted Transmitter measures the fluid's temperature, density, and flow rate. The coriolis flow meter is pre-calibrated and set to measure density over the range of 60 to 70 pounds per cubic foot, temperature over the range of 50 to 100 degrees Fahrenheit, and flow rate over a range from 0 to 2 gallons per minute. Following the flow meter is a small system composed of two needle valves placed in parallel to allow for user controlled flow restriction to control pressure at the spray nozzle.

Next the pressure of the fluid is measured with a Viatran pressure transducer calibrated for a range of 0 to 100 pounds per square inch. The Viatran calibration can be found in Appendix C. At the same location a needle pressure indicator is used to ascertain the validity of the electronically read pressure measurement.

Following the pressure measurement, the flow passes through a Parker 3-Way solenoid valve used to direct the fluid through one of two paths. When the solenoid is inactivate the flow passes through a return line where a ball valve is used to generate a pressure loss similar to that experienced through the nozzle. When active, the flow passes through a 2-foot flexible line before it was expelled through a BETE WL ¼ nozzle.

The BETE WL ¼ nozzle selection was based on multiple criteria: Spray pattern, spray distribution, droplet size, and operating flow rates. This BETE nozzle produces a 90-degree, full cone spray that encompasses the area of interest as depicted in Figure 3.8. In order to assume

that the mass flux at the intended spray surface is uniform, the manufacturer's information for spray distribution (Appendix C) were used to locate a nozzle that generates a more uniform spray over a significant area. It was also necessary to spray at a low flow rate without misting the fluid. The BETE WL ¼ nozzle produces droplets with a Sauter Mean Diameter (D32) of 130 micrometers at 0.2 GPM. An operational range from 0.13 GPM to 0.74 GPM at pressures from 10 psi to 400 psi allows the nozzle to meet low mass flux rate at the intended surface with a low-pressure system and minimal spray distance.

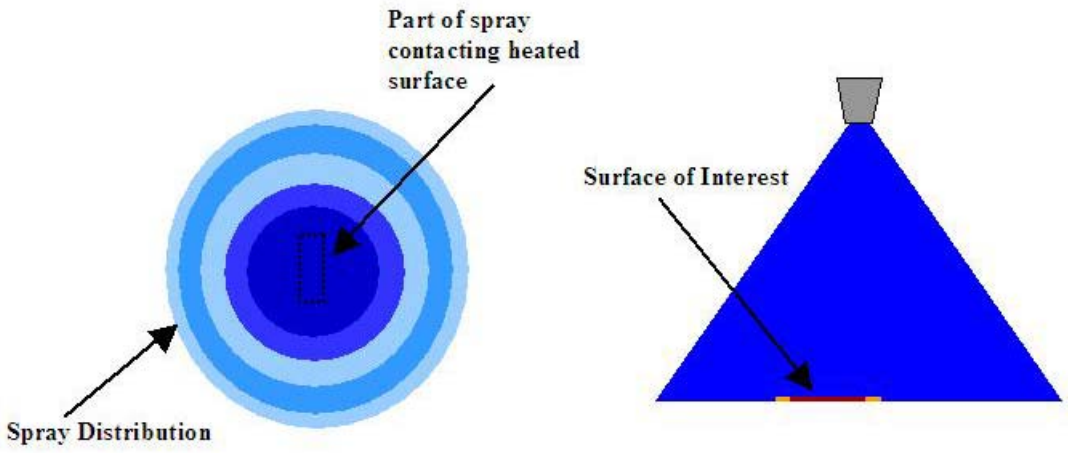

Figure 3.8 Depiction of how surface of interest is placed within the spray area.

The nozzle support structure, seen in Figure 3.9, allows 3-dimensional manipulation of the nozzle outlet in relation to the heated surface and holds the nozzle in a fixed position through testing.

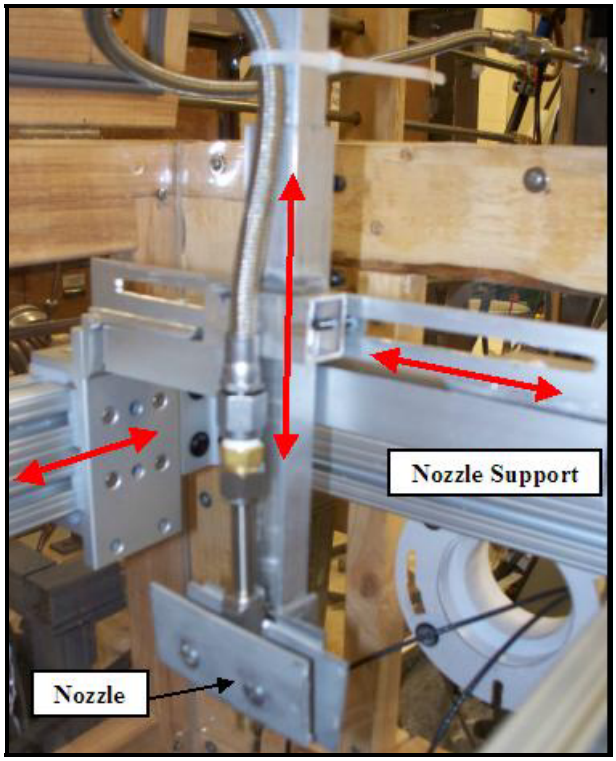

Figure 3.9 The nozzle support allows three degrees of freedom.

3.5 System Measurements

A National Instruments SCB-68 connector block is used to obtain measurements. A National Instruments NI PCI-6259 DAQ Card supports the connector block and receives seven separate signals: Flow rate, fluid temperature, fluid density, fluid pressure, approximate NiChrome surface temperature, voltage drop across the NiChrome filament, and current supplied to the NiChrome. Flow rate, fluid temperature, and fluid density signals are supplied by the Micro Motion flow meter. The fluid pressure signal is received from the Viatran pressure transducer. Approximate NiChrome surface temperature is measured with a 36-gage type K beaded thermocouple mounted so that the bead touches the surface with only physical contact. Voltage drop across the NiChrome filament is measured directly with a differential voltage channel. Supplied current is obtained using a Fluke i410 AC/DC Current Clamp that produces a signal of 1 millivolt per ampere. Figure 3.10 is a wiring diagram that shows how the signals are obtained.

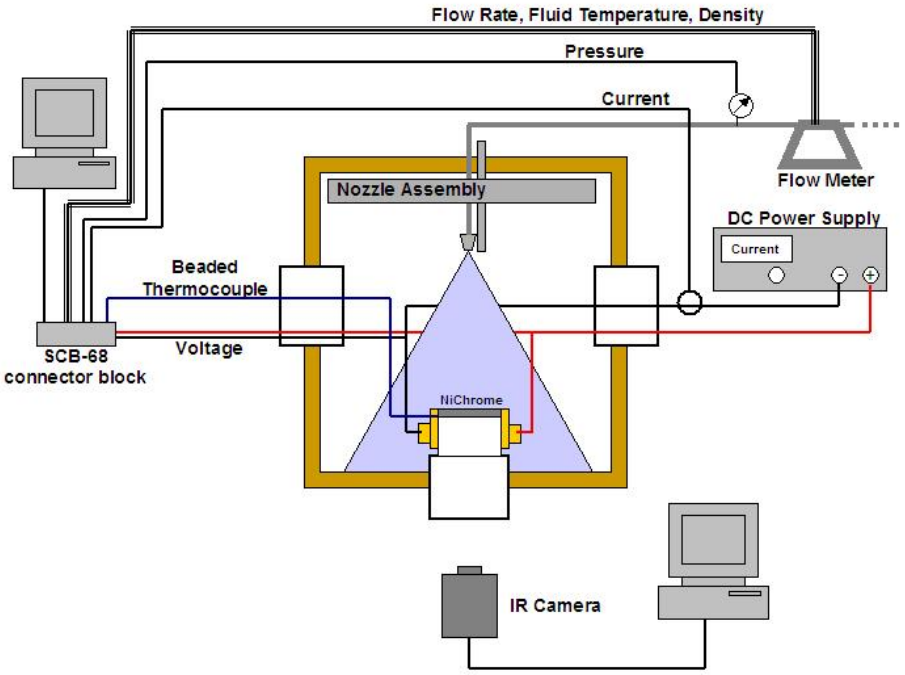

Figure 3.10 Measurement signals wiring diagram.

National Instruments LabVIEW software is used to process the signals. Figure 3.11 is the block diagram developed to record the measurements. A set of measurements is recorded every 5 seconds. Each set records 10,000 voltage samples at a frequency of 50,000Hz. Each signal is converted to display measured values using a calibration equation as shown in Table 3.2.

Table 3.2 Recorded Signal Summary.

Signal	Range	Calibration Equation	Units	Uncertainty Associated with Voltage Reading
Pressure	-10V – 10V	P = 16.878v + -2.4037	psi	0.0026 psi
Density	-5V – 5V	D = 2.5v + 57.5	lb/ft^3	0.0002 lb/ft^3
Fluid Temperature	-5V – 5V	T = 17.36V + 37.5	°F	0.001 °F
Flow Rate	-5V – 5V	F = 0.0002f	GPM	
Voltage	-5V – 5V		V	0.000076 V
Current	-1V – 1V	I = 100*V	A	0.0076 A

3.6 Summary

The experimental facility used in the data collection process consists of a NiChrome filament supported in a copper, Teflon, and high temperature ceramic assembly positioned in a spray chamber in such a way that an IR camera can view the unsprayed surface of the NiChrome. An assembly of PVC and steel pipes and fittings generates spray though a BETE WL ¼ nozzle that is positioned by an assembly housed within the spray chamber. Data is collected with Flir Systems IR imaging equipment and LabVIEW data acquisition.

CHAPTER 4 - Experimental Procedure

The experimental procedure consists of five main steps that will now be covered individually in detail:

1. Placing the NiChrome filament
2. Pre-heating the NiChrome filament
3. Pre-test flow collection
4. Spray data collection
5. Post-test flow collection

4.1 Placing the NiChrome Filament

A new NiChrome strip was used for each test. Strips are sheared from 100mm x 100mm sheet into 5/16-inch strips. Two holes are punched into the center of each end of the strip approximately ¼ -inch from the each end. The strip is then placed into the heated surface assembly to form the strip to the intended shape. Care is taken to make sure the strip is not kinked or marred during the entire set up process and throughout testing.

Figure 4.1 shows an exploded view of the assembly. On each side of the assembly are two copper pieces (3,4) that act as busses for the applied DC power as well as clamps to hold the NiChrome filament (1) in place. In Figure 4.1, the NiChrome strip is shown formed for testing. Between the two copper busses, two Teflon inserts (7) topped with 0.25-inch thick 1” x 2” ultra-high temperature, machinable, glass-mica ceramic tiles (2) form a physical separation. Both the Teflon and the ceramic are electrical isolators, making the NiChrome filament the only electrical path for the applied power. The NiChrome filament is bolted between the two copper pieces through slots so that the filament can be pulled taut during spraying. A 0.063-inch thick rubber gasket (5) forms a seal between the Teflon and copper surfaces and the supporting stage (6).

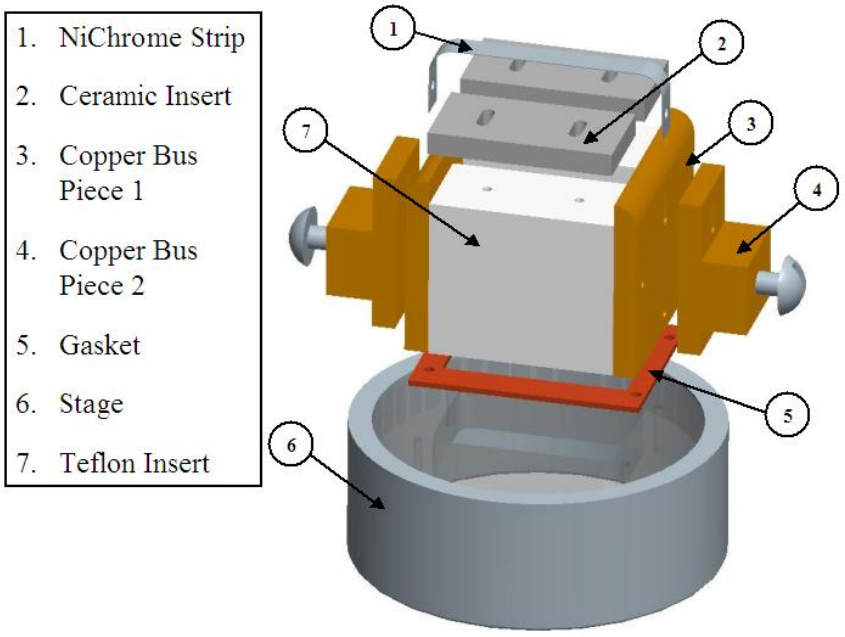

Figure 4.1: Heated Surface Complete Assembly.

Once the NiChrome filament is formed, it is removed from the assembly. Next, two approximately 3/8-inch rubber O-rings and a 36-gage type K glass insulated thermocouple are added to one side of the assembly as shown in Figure 4.2 below. The bead of the thermocouple is set so that it will contact the bottom side of the NiChrome filament approximately 1/8-inch from the copper bus. The thermocouple is used to generate a real-time temperature reading that is associated with the NiChrome surface temperature. The temperature measured by the thermocouple is not assumed accurate because of high contact resistance but is used to characterize the heating and cooling response time of the NiChrome filament. So that when the temperature measured by the thermocouple appears steady, the NiChrome surface is said to be at steady state. The two O-rings act as compressible spacers within the assembly. As the length of NiChrome filament extends as it is heated, the O-rings assist to retain the tension created when the assembly is at room temperature. Once the O-rings and thermocouple are in place, the copper piece is placed back into the assembly.

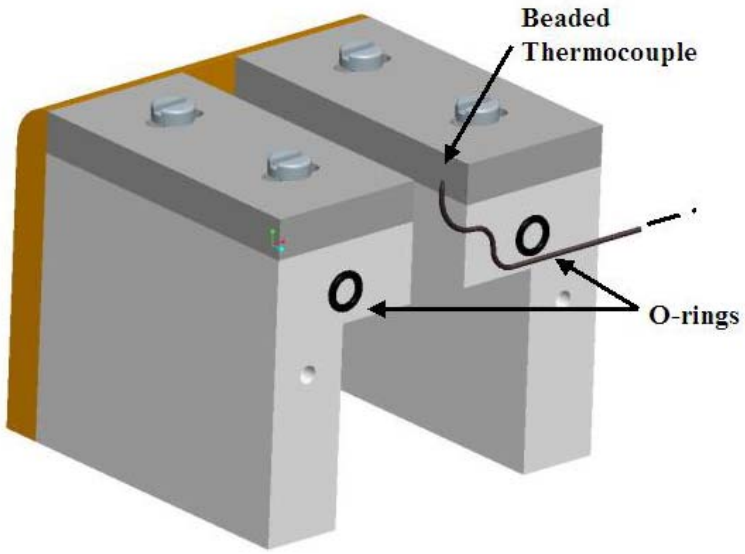

Figure 4.2 A solid model showing placement of O-rings and beaded thermocouple.

Next, Extreme Tape® is added to the heated assembly to help prevent fluid leakage into the cavity formed by the copper pieces and Teflon inserts, which keeps the viewed side of the NiChrome strip dry. First, the tape is cut in half lengthwise into two equal strips approximately 1/2" wide. These two strips are stretched between the two copper busses and across the ceramic inserts so that there is a very slight overhang (approximately 1/16-inch) as seen in Step 1 of Figure 4.3 so that the NiChrome strip will contact the tape. The strips of tape are held in place by another piece of Extreme Tape® stretched around the entire assembly so that holes drilled in the copper pieces remain uncovered as seen in Step 2 of Figure 4.3. (It should be noted that the tape does not contain an adhesive and only sticks to itself when it is stretched.)

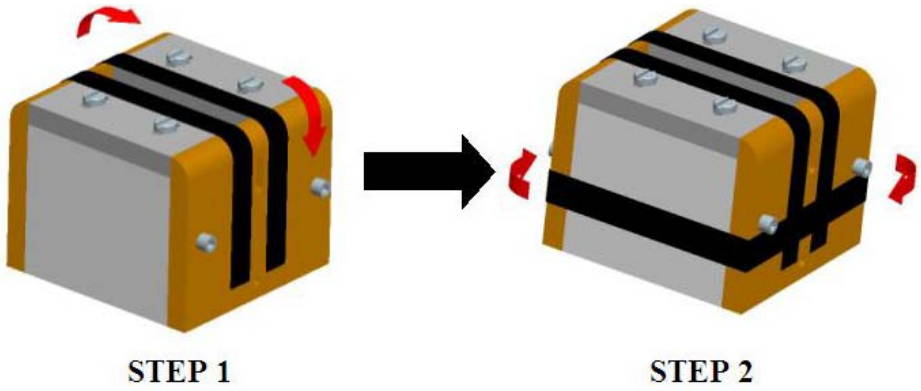

Figure 4.3: Placement of Extreme Tape®

After the tape is carefully placed, the formed NiChrome filament is placed on top of the tape. The two additional parts that form the copper busses are then attached via a screw at the bottom of copper bus piece 2. Figure 4.4 depicts where a C-clamp is then used to fix the copper pieces tight against the ceramic inserts, compressing the o-rings as much as possible.

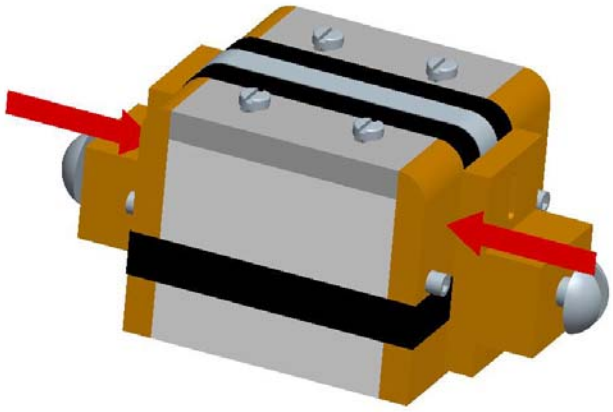

Figure 4.4: Clamp attachment point during NiChrome filament placement.

Placing the clamp hinges the copper pieces at the central screw, which attaches the copper to the Teflon inserts as shown in Figure 4.5a below. The formed NiChrome strip is then pulled tight across the ceramic insert between the copper pieces by the two upper screws, which are placed in slots and drawn tightly down. After the NiChrome is tightly fixed, the clamp is removed. The clamp is then used to right the copper pieces vertically as shown in Figure 4.5b so that the NiChrome is pulled taut and the screws that will hold the stage in place will go in correctly.

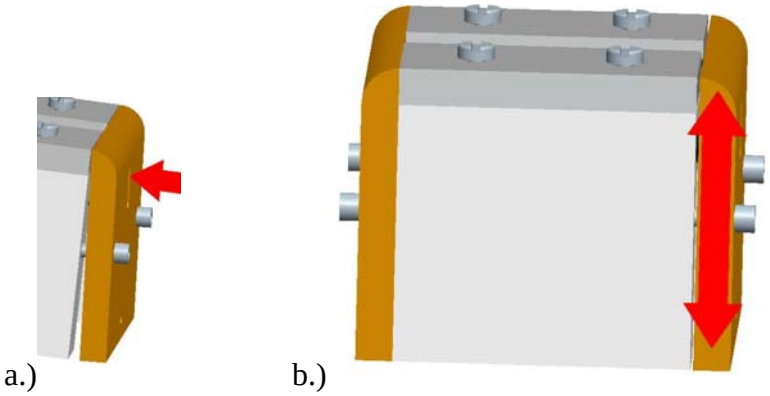

Figure 4.5 A solid model showing (a) the copper bus piece hinged at the center screw when the C-clamp is placed (b) the copper bus piece righted vertically.

The heated assembly is placed on a plastic cylindrical stage shown in Figure 4.6 that slide-fits onto the heated surface assembly support described in Chapter 3: Experimental Facility Description.

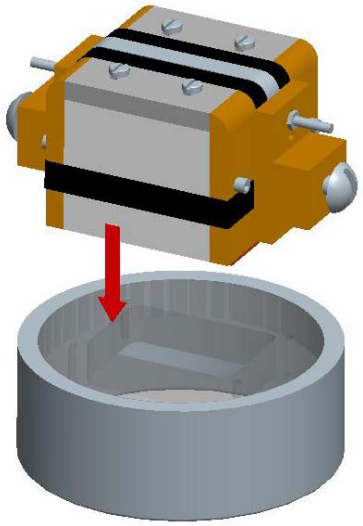

Figure 4.6: Heated Surface Assembly attachment to Stage.

4.2 Pre-Heating the NiChrome Filament

After the NiChrome filament is in place, the NiChrome is exposed to at least five heating cycles to aid in the removal of any manufacturer added surface treatments and so the integrity of the

assembly can be assessed before spray testing. To begin to administer these cycles the entire heated assembly is attached to the power supply and the data acquisition system is set to record temperature and power measurements. The IR camera is positioned to view the NiChrome and the IR camera settings are adjusted to reflect those values shown in Table 4.1.

Table 4.1: Infrared camera settings for testing.

Camera Setting	Assigned Value
Emissivity	0.24
Reflection Temperature	78°F
Ambient Temperature	72.5°F

While recording information with the data acquisition, the strip is heated at least five times by applying power to the heated assembly with the HP 6269B DC Power Supply. Regulating the current to the NiChrome circuit varies the power applied to the system. On the DC power supply, the voltage regulation is set to the maximum allowable so that voltage is not regulated. Then slow and small adjustments of the current limiter knob are used regulate the total applied power. The power is slowly increased for approximately 1.5 to 2 minutes until the infrared camera reads a temperature near to, but not exceeding 550°F. Power is then slowly decreased to zero for approximately 30 seconds, and the process is repeated. The heating cycle data collection is discontinued after all five applications and stored for reference only.

During this process, the NiChrome filament must be monitored visually. As the applied power is increased the temperature of the filament rises and the strip experiences thermal expansion. If the filament is not adequately tensioned in the assembly, the filament will raise from the assembly creating a visible gap that will allow leakage during testing. If expansion is observed, the filament must be re-tightened in the assembly and reheated until no visible gap is observed. If the filament re-tightening is required, the previous applications of power are still considered as part of the five necessary for completion of the pre-heating task.

Once preheated, the NiChrome filament is left in the heated surface assembly. Half-inch masking tape is used to cover the assembly in order to minimize fluid entry into the assembly component seams. The masking tape must cover all the component seams except the seam between the two copper pieces that form the copper bus and the seam between the assembly and the stage, which is filled with a rubber gasket. Figure 4.7 shows the assembly before and after masking tape is applied.

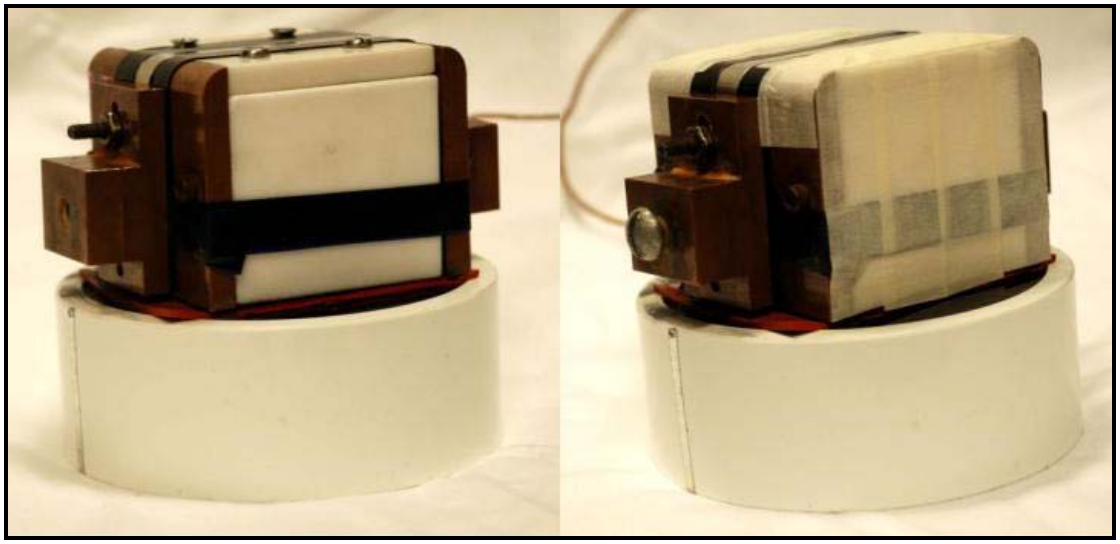

Figure 4.7: Photos of Heated Surface Assembly before (left) and after (right) masking tape is applied.

4.3 Flow Collection

Prior to each spray test, the spray nozzle position and fluid supply flow rate must be set to obtain the desired mass flux. Mass flux data taken before and after spray testing are used to characterize the mass flux during spray testing. Mass flux is determined by collecting fluid in the mass collector for a specified amount of time. Figure 4.8 is a representation of the mass collector used in testing. The mass collector is assembled from machined aluminum. It is comprised of a slotted rectangular section welded to an aluminum plate to form a watertight seal. The plate is then attached to a stage similar to that used for the heated surface assembly. The mass collector is detailed in Appendix C. The time of collection is determined by trial and error and set so that mass collector is approximately ¾ full at the end of the test to ensure the most

fluid is collected without the mass collector overflowing or droplets reflecting off the fluid's surface. During mass flux testing, the mass collector is placed in the spray chamber with the collector opening oriented in the same manner as the NiChrome strip during spray cooling testing.

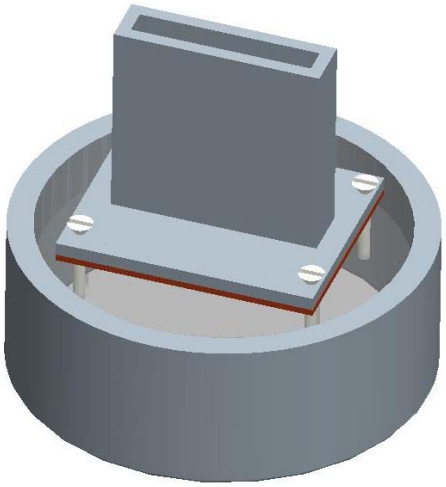

Figure 4.8: Mass collector.

Before fluid is collected, the reserve tank is filled so that fluid level is approximately 6 inches from the tank's top rim. The system pump is then run for approximately 20 minutes so that the fluid experiences an initial increase in temperature that will vary less drastically during testing. During all testing, the tank's fluid level is monitored and refilled as necessary so that it does not drop below 15 inches from the tank's top rim. The tank is refilled with fluid that is from a new source for water experiments, or from collected run-off for experiments with Fluid 1 or Fluid 2.

To begin testing, the mass collector is placed in the spray chamber and the pump and data acquisition equipment (flow meter and pressure transducer) are turned on. System parameters are monitored with the LabVIEW file flow.vi that is found in Appendix E. Simultaneously, a switch is used to activate the three-way solenoid valve, allowing fluid to spray through the nozzle. A stopwatch is also activated to limit length of the test. When the stopwatch time reaches the time of collection previously determined during flow collection experiments, the switch is used to deactivate the solenoid valve and stop fluid flow.

After the fluid is collected, the mass collector is removed from the spray chamber with care taken not to spill any of the collected fluid. The outside of the mass collector is dried thoroughly using a dry towel. The mass of the filled collector is measured using a sliding balance and recorded. The fluid is then disposed of and the entire mass collector is dried with compressed air and a dry towel. The mass of the emptied collector is found using the sliding balance and recorded. The mass flux is calculated by finding the mass difference between the filled and emptied collector and dividing it by the time span of the collection and the two dimensional area of the collector (1.75 inches by 0.25 inches).

Adjustments are then made to the spray flow rate and nozzle position, and the mass collection process is repeated until a specified mass flux is realized. The data acquisition is then set to record data and at least five trials are completed. The data recorder is restarted just prior to the next collection. The trials are conducted multiple times to observe repeatability. To conclude repeatable results, the measured mass difference between the filled and emptied mass collector must not vary more than 0.2 grams for all five trials. If the system reflects an inconsistent measurement by these standards, flow collection experiments are repeated until consistency is achieved.

After the spray data collection is complete (Processed discussed in the following section), the mass flux is measured in the same manner as discussed above. At least three tests are completed to reflect the repeatability of the mass flux measurement during the spray data collection process. In the event that inconsistent measurements are observed, additional mass flux data sets are collected since the spray data has already been collected with system settings. System settings are not adjusted at any point during post-spray flow collection.

4.4 Spray Data Collection

Once the mass flux has been set, the mass collector is removed from the spray chamber and the heated assembly is placed in a similar position so that the top surface of the NiChrome filament is in the same location as the top of the mass collector was previously. The heated assembly is

connected to the power supply and the data acquisition equipment is turned on. The LabVIEW file ChannelReadings3.vi (Appendix E) is used to collect data during the entire length of the test. The IR camera is placed below the spray chamber and directed to view the bottom of the NiChrome filament through the cavity formed by the copper pieces and Teflon inserts. IR camera settings are set to the values previously listed in Table 4.1. At this point the body of the IR camera (excluding the lens) is shrouded with a plastic sheet to protect the electrical components from any possible fluid leakage. If the IR camera is observed to be wet at any time during data collection, the test is stopped and the entire process, including replacement of a new NiChrome strip, is restarted.

While no power is applied to the NiChrome filament, two software-created rectangular areas are positioned so that they are inscribed within each of the metal strips (the NiChrome and steel strips) in the camera's view. These rectangular areas are set so that the camera operator can read the average temperature of the pixel within each rectangular area in real time. Additionally, two software-created points are added: one that equals the average surface temperature of the NiChrome (the average surface temperature of Area 1 in Figure 4.9) and another that is equal to the average NiChrome surface temperature but is positioned within the area inscribed within the steel strip (Point 2 in Figure 4.9). An infrared image is then recorded in case validation of point placement is necessary at any time during the post-processing procedure. These points, set before power is applied to the system, remain in their set positions for the entire length of the spray cooling test and will be used in post-processing to set system parameters to generate accurate surface temperature measurements.

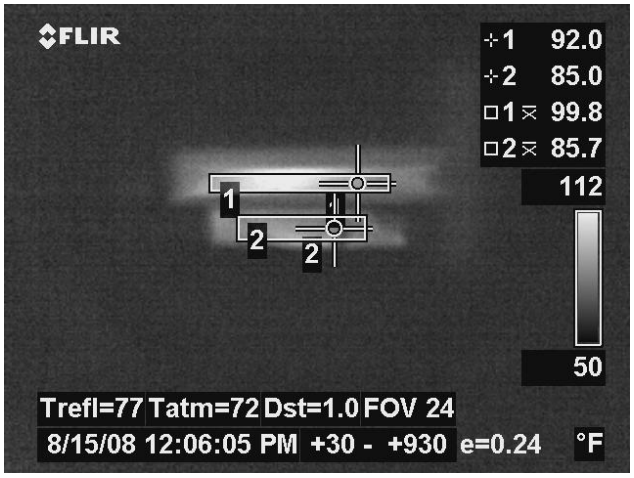

Figure 4.9: Example of area and point placement for testing with Flir IR camera. (Image taken from heat leakage Test 1.)

At this point, the LabVIEW file is set to record data. The fluid supply system is started and spray is applied to the heated assembly. Power is applied in steps by adjusting the current limiter on the power supply in the same manner as during pre-heating of the NiChrome filament. Figure 4.10 is an example of how power is varied over time during the data collection. As seen in the figure, the applied power is changed approximately every 2 minutes.

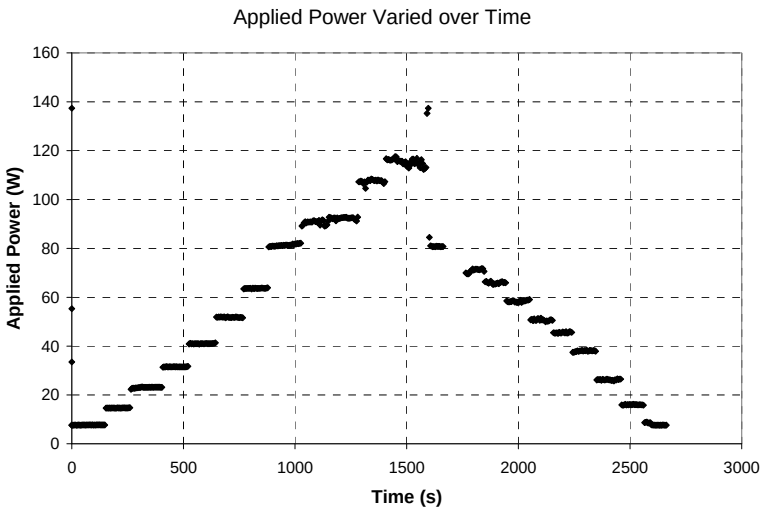

Figure 4.10: Example plot of how applied power is varied over time during testing. Example extracted from Test 8.

The temperature recorded by the beaded thermocouple is monitored. Once the measured temperature starts to stabilize, three infrared images are recorded and the power level is increased. Figure 4.11 is an example of the beaded thermocouple temperature measurement over time. It should be noted that the beaded thermocouple does not accurately represent the NiChrome surface temperature but it does mimic the dynamic of the surface's temperature. The camera's lens cap or an alternative protective cover was used to protect the camera from any fluid leakage between image capturing and to minimize heat exposure to the internal sensor.

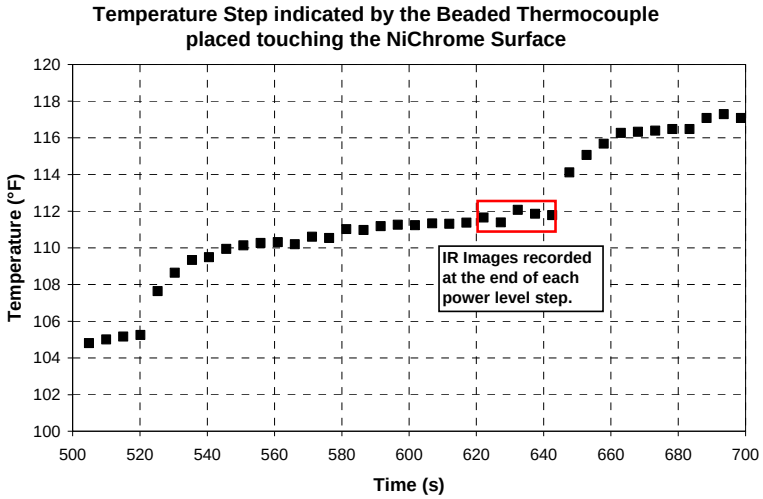

Figure 4.11: Measured temperature near NiChrome surface over one power level step.

This process is continued until the NiChrome surface appears red hot as shown in Figure 4.12, as this is assumed to be at or beyond critical heat flux (CHF). The power applied is immediately decreased slightly. The intent is that the surface remains dry but does not fail due to raising temperatures. If CHF is observed on only a portion of the NiChrome filament's surface, the power level is deceased in the same manner as if the entire strip was visually red hot.

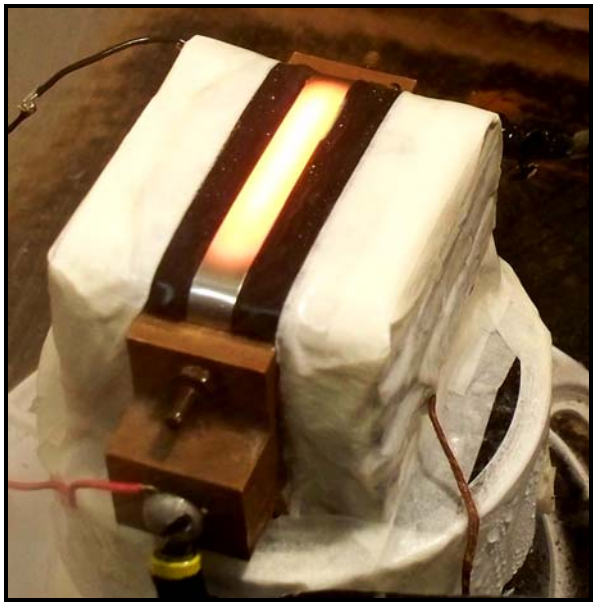

Figure 4.12: Picture of NiChrome filament glowing red hot while being sprayed during spray testing.

Infrared images are then recorded as the power is decreased in steps until no power is applied. The data collection and spray from the nozzle are stopped. For each test and fluid tested the number of power level steps will vary, but an attempt is made to maintain at least 20 steps per test with emphasis on recording steps after observed CHF and before the filament is re-wetted because those steps relate to the widest rage of varying heat flux for a spray cooled surface.

The five main steps in the data collection process, (1) placing the NiChrome filament, (2) pre-heating the NiChrome filament, (3) pre-test flow collection, (4) spray data collection, and (5) post-test data collection, have been described in detail above.

CHAPTER 5 - Data Post-Processing

Once all the data has been collected for a spray test (including mass flux data before and after spray data, spray data, and IR images), the data is processed to generate results. First the images are processed to show accurate surface temperatures using QuickVIEW, freeware available through Flir Systems. Subsequently, data recorded during mass flux and spray cooling is processed using codes generated in MatLAB to effectively calculate characteristic values of system settings measured during testing. Additional coding further processes the IR images and reports NiChrome surface temperatures measured.

5.1 QuickVIEW Processing

Each IR image contains the areas and points positioned prior the image collection process as described in Chapter 4: Experimental Procedure. These two points are used to determine the measured IR camera's reflected temperature and the NiChrome surface temperature. Point 1 (Sp1 in Figure 5.1) represents the average surface temperature of the NiChrome strip (Represented by Area 1 – Ar1 in Figure 5.1). Point 2 (Sp2 in Figure 5.1) represents the camera's reflected temperature. In order for the IR image to display accurate surface temperatures, the camera's reflective temperature and the surface emissivity must be defined independently for each image.

The first step is setting the user-defined Reflection Temperature. The correct reflective temperature is determined by increasing or decreasing the Reflected Temperature object parameter in QuickVIEW until the temperature value of Point 2 (Sp2 in Figure 5.1) equals the value entered as the object parameter to one decimal place. If the value of the point on the reflected surface falls equally between two values inputted for Reflected Temperature, the lower value is used.

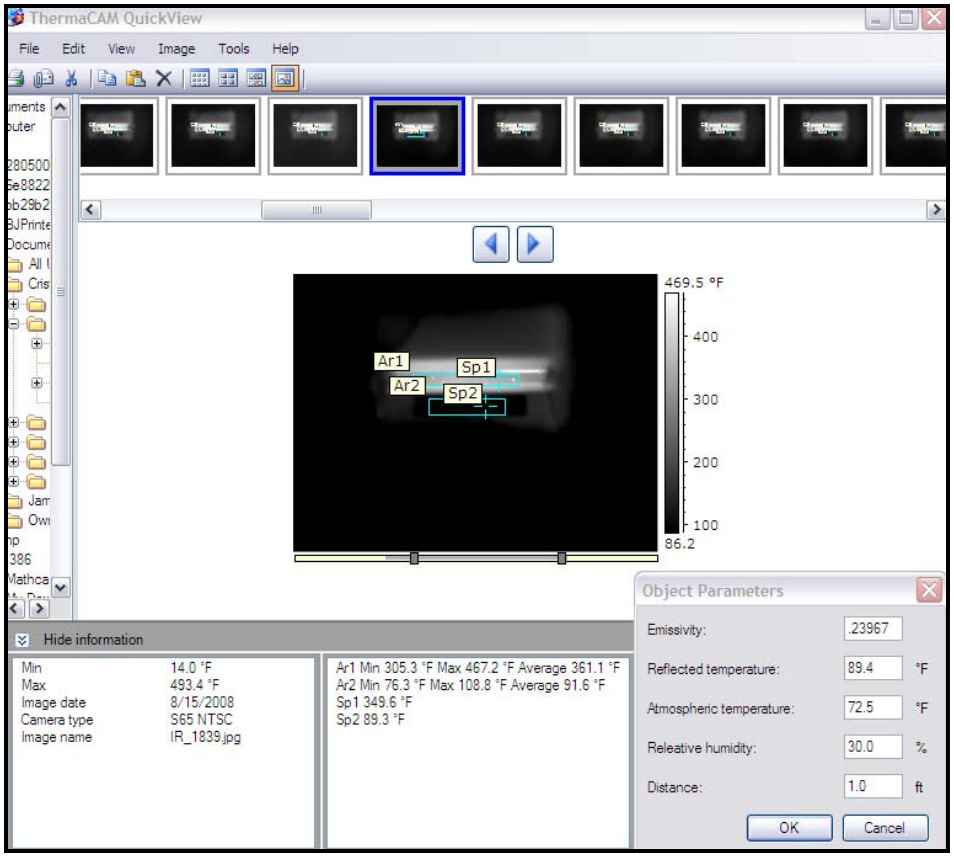

Figure 5.1 QuickVIEW screen shot

Next, the Emissivity is set in a similar manner. The emissivity correlation equation (Defined in Appendix A),

$$\varepsilon = A - (A - B)e^{(-T/\tau)} \qquad \text{Eqn. 5.1}$$

where A = 0.23715, B = 1.74931, and τ = 54.68912,

is used to set the user-defined Emissivity by substituting the temperature displayed for Point 1, to the nearest degree F (Sp1 in Figure 5.1), into the equation as T. The calculated emissivity value is then entered, to 5 decimal places, and QuickVIEW adjusts the image to fit the set parameters and gives a new temperature for Point 1. This value is again entered into the emissivity calibration equation and set as the Emissivity until the calculated emissivity is equal to the one previously entered. The final user-defined Reflected Temperature and Emissivity are manually recorded for each image.

To minimize the error associated with the IR image displayed temperature range being represented by pixel values between 0 and 255, adjustments are made to the grayscale at the right of the image. The highest and lowest values represented are shown at the top and bottom of the grayscale respectively. These values change when the Reflected Temperature and Emissivity parameters are adjusted because the software uses the user-defined object parameters to associate the energy detected to a surface temperature. In order for processing to remain accurate, the highest value shown on the grayscale is adjusted to be approximately equal the maximum temperature value in Area 1 without exceeding the upper limit of the camera's range (approximately 1000°F). The minimum grayscale temperature is set so that it reduces the grayscale temperature range, but remains lower than the Reflected Temperature and above the lower limit of the camera's range (approximately 15°F). High and low values are then manually recorded for each image.

All images are manually processed in the same manner unless the temperature variation across the NiChrome surface is too significant to be represented by a single temperature value, which is the case if CHF occurs on only a section of the NiChrome as it did in Test 1. For this case, the image is simply processed twice using the same Reflected Temperature values, but different Emissivity values. Image processing is also altered if a fluid droplet impedes the view of either Point 1 or Point 2. For this case, attempts are made to adjust the point placement in the image taken before any power was applied to a location that also represents the surface temperature but is not impeded by fluid droplets in subsequent IR images. If this is not reasonable, the data point is removed from the data set.

5.2 MatLAB Processing

After the IR images are processed with the QuickVIEW software, three separate MatLAB generated codes (code texts located in Appendix E) are used to continue the post processing of the data. These codes process the mass flux, LabVIEW test data, and image test data.

Calculation of Mass Flux

The mass flux reported for each spray test is determined using a generated MatLAB code. In the code, the mass flux of each trial is determined by dividing the mass collected in the mass collector by the period of collection and the inlet area of the collector as shown in Eqn. 5.2.

$$\dot{m}'' = \frac{\Delta m_{mass\_collector}}{t_{collection} A_{inlet}} \qquad \text{Eqn. 5.2}$$

In Eqn. 5.2, $\Delta m_{collector}$ is the mass of the filled collector minus the mass of the collector empty of fluid and $t_{collection}$ is the time allotted for mass collection. The inlet area of the mass collector, A_{inlet}, is nominally 0.25" x 1.75.

The mass flux reported for each spray test is calculated as the average calculated mass flux from trials conducted before spray data collection plus the average calculated mass flux after spray data collection divided by two. The overall uncertainty associated with reported mass flux is estimated to be ±15%.

System Data Code Calculations

A separate MatLAB code is used to calculate the average, standard deviation, maximum, and minimum values for system data (pressure, spray fluid temperature, flow rate, applied current, voltage drop, and thermocouple temperature reading) recorded during the heated surface testing. These values are monitored for drastic changes to confirm the stability of the system during data collection. Additionally, system data is used to support the reliability of the mass collection tests run before and after the heated surface testing to determine the mass flux.

Image Processing Code Calculations

The post processing of each image is completed separately from the mass flux and system data calculations. The code first determines significant jumps (> 0.3A) in the applied current followed by at least 6 stable data points to define the power levels from the LabVIEW system data. Each power level is characterized by averaged system data (pressure, spray fluid temperature, flow rate, applied current, etc) for the last 25 points in the defined power level. If

the power level does not contain 25 points, every point in the level is used to define the averages that represent system conditions at that power level.

To determine the surface temperatures within each image, a user-defined line is used. The coordinates of this line are determined prior to running the post-processing code and are also entered into the test summary input file. Each image is opened individually and the red pixel value (a numeral between 0 and 255 used as part of the pixel's color definition) is read in. Because the image is gray scale, the red, blue, and yellow pixel values are all equal in magnitude. Figure 5.2, below, is an image showing the user-defined line highlighted in red. A well-defined line will run in the center and across the length of the NiChrome strip between the copper buses without highlighting end conditions.

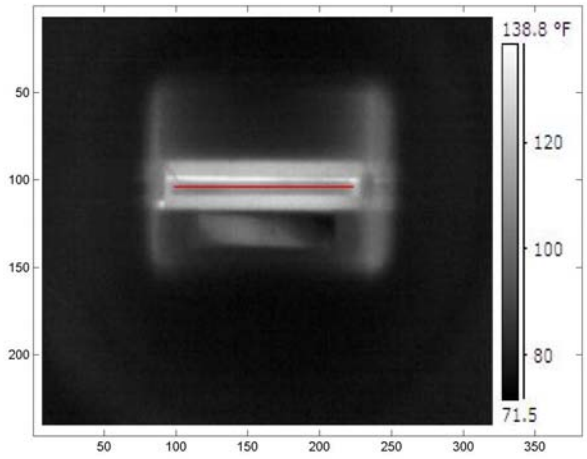

Figure 5.2: Image of user-defined line used in image post processing extracted from Test 8.

Nodal temperatures are determined for a specified number points equidistantly spaced along the selected line. The locations of these points are determined by dividing the line into equal segments and defining points at the segment intersections as is depicted for three points in Figure 5.3.

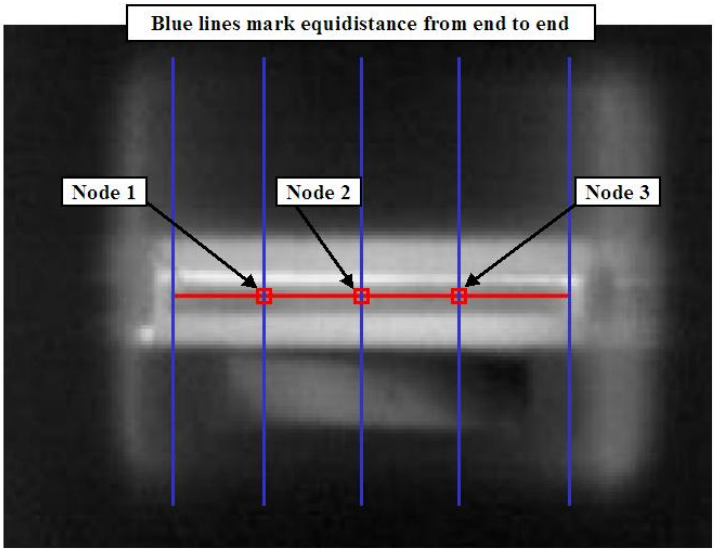

Figure 5.3: Example of the Location of Three Individually Reported Nodal Temperatures

Each of the point coordinates is used as the coordinate for the center pixel of a node. The center pixel value, along with all 8 surrounding pixel values (as shown in Figure 5.4) is averaged to generate a nodal value. A linear scale is defined between the highest and lowest temperatures reported in the grayscale at the right of the image and their corresponding pixel values. This linear scale is then used to convert the nodal value to a represented temperature value. The approximate uncertainty associated with using a nodal temperature value is estimated to be ±10°F at 300°F.

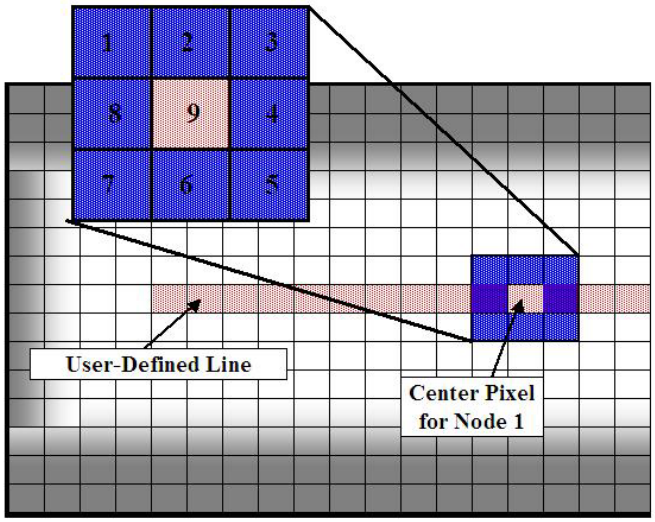

Figure 5.4 Schematic of Pixel Selection for Node Formation

Calculation of Spray Cooling Heat Flux

Once the system parameters and the nodal temperatures at each power level have been calculated, the code determines the heat flux removed by the fluid spray on a nodal basis. For these quasi-steady state tests (support for the use of a quasi-steady state model is located in Appendix A), the calculated heat flux removed by the spray is equal to the heat flux generated by current passing through the resistive NiChrome filament minus the heat loss to the surroundings through convection and radiation heat transfer. Heat loss through conduction heat transfer is considered negligible. An analysis based on experimental results that validates the neglecting of conduction heat transfer is located in Appendix A. This relationship is shown in Eqn. 5.3.

$$q''_{spray} = q''_{generated} - q''_{radiation,bottom} - q''_{radiation,top} - q''_{convection} \qquad \text{Eqn. 5.3}$$

Generated heat flux, $q''_{generated}$, is calculated as the applied power divided by the area of associated generation. The applied power is determined by squaring the current measured at the associated power level and multiplying by the NiChrome resistance. The area associated with power generation is equal to the NiChrome filament's width multiplied by the length between the copper electrical busses.

$$q''_{generated} = \frac{I^2 R}{wl} \qquad \text{Eqn. 5.4}$$

Since NiChrome filament resistance is determined per unit length (see discussion on experimental validation of reported NiChrome resistance in Appendix A), Eqn. 5.4 can be simplified to

$$q''_{generated} = \frac{I^2 R'}{w} \qquad \text{Eqn. 5.5}$$

With the estimated uncertainty of ±7.5% for the applied current, ±5.5% for the resistance per unit length, and ±4.5% for the NiChrome filament width, the estimated uncertainty for generated heat flux is ±17%.

The heat lost to radiation heat transfer is calculated as

$$q''_{radiation} = \sigma\varepsilon\left(T^4_{surface} - T^4_{reference}\right) \qquad \text{Eqn. 5.6}$$

where σ is the Stefan-Boltzmann Constant (0.1714e-8 BTU/h-ft^2-R^4 or 5.670e-8 W/m^{2}K^4), ε is the applied image emissivity value set during QuickVIEW post processing, $T_{surface}$ is the nodal temperature in absolute temperature units, and $T_{reference}$ is the spray fluid temperature for calculated radiation heat loss from the top-sprayed surface ($q"_{radiation,top}$ in Eqn. 5.3) and the image reflected temperature set during QuickVIEW post processing for the bottom-viewed surface ($q"_{radiation,bottom}$ in Eqn. 5.3) in absolute temperature units. An overall uncertainty of ±30% is associated with this radiation heat loss calculation (Detail on how uncertainty was estimated is located in Appendix A).

Arguments can be made that radiation heat transfer from the sprayed surface to the impinging droplets is a substantial mechanism of heat transfer for phase change especially when an insulating vapor layer has formed at the surface. Calculations in this study do not determine whether or not a vapor layer is present at the surface; therefore, radiation heat loss from the

sprayed surface is subtracted for all collected data. Figure 5.5 shows that the magnitude of heat loss due to radiation at all measured surface temperatures is minimal compared to the calculated heat loss removed by the spray.

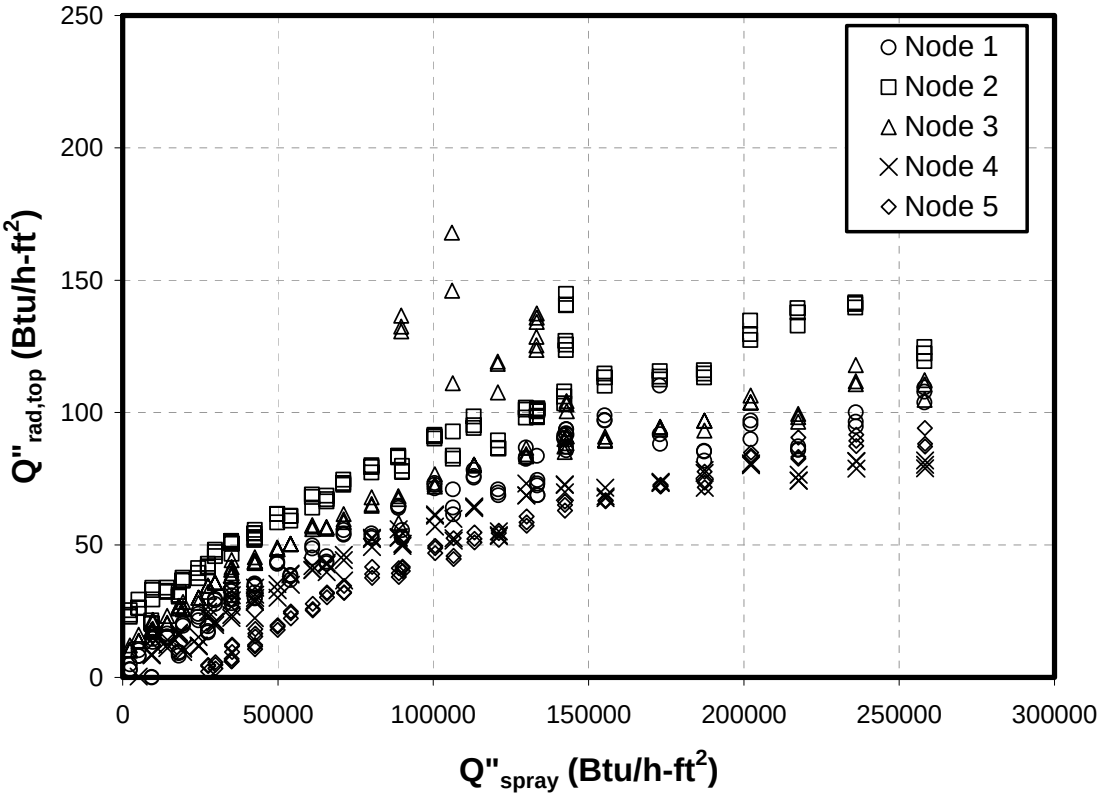

Figure 5.5 Calculated heat loss to radiation from the sprayed surface compared to calculated spray cooling heat flux.

The heat lost to convection heat transfer is approximated as

$$q''_{convection} = \left(\frac{\overline{Nu} k_f}{L} \right) \left(T_{surface} - T_{reference} \right) \qquad \text{Eqn. 5.7}$$

where $\overline{Nu}$ is the average Nusselt number correlated to naturally convective heat loss from a downward facing horizontal heated surface. It should be noted that this correlation determines an average, not local, Nusselt number and assumes the ends of the surface are free and air can flow around the surface and continue to rise. While this is not the case for this particular

application, it provides a reasonable quantitative value with an associated increase in uncertainty. In Eqn. 5.7 above, k_f represents the thermal conductivity of air; L, the characteristic length, is defined as the surface's width; $T_{surface}$ is the nodal surface temperature, and $T_{reference}$ is the image reflected temperature set during QuickVIEW post processing.

Incropera and DeWitt (2002) report the average Nusselt Number for the correlation can be calculated as

$$\overline{Nu} = 0.27 Ra_L^{1/4} \qquad \text{for } \left(10^5 \le Ra_L \le 10^{10}\right) \qquad \text{Eqn. 5.8}$$

where

$$Ra_L = \frac{g\beta\left(T_{surface} - T_{reference}\right)L^3}{\nu\alpha} \qquad \text{Eqn. 5.9}$$

In the above equation, g is the force of gravity, β is the volumetric thermal expansion coefficient, ν is the kinematic fluid viscosity, and α is the thermal diffusivity.

Treating air as an ideal gas,

$$\beta = \frac{1}{\left(\frac{T_{surface} + T_{reference}}{2}\right)} \qquad \text{Eqn. 5.10}$$

The overall uncertainty related to the convection heat loss calculation is approximated as ±53.5%. The overall uncertainty for spray cooling heat flux is estimated as ±18% (See Appendix A for details of this calculation).

5.3 Summary

After the data has been collected, it was post-processed with the Flir QuickVIEW software and the experimentally determined NiChrome emissivity so that pixel values can be correlated to accurate temperature values. The data was then processed further using generated MatLAB

codes that calculate the test mass flux, local surface temperatures, and corresponding local heat flux removed by spray. Data from each test is summarized and the results are plotted.

CHAPTER 6 - Experimental Results

Experimental tests were completed for variations of mass flux, spray fluid, and spray angle. A summary of test parameters for each valid test is shown in Table 6.1. Tests are grouped in relevant sections based upon spray fluid and spray angle. The highlighted color for each section corresponds to the color scheme used in all data plots. Data sets plotted individually are located in Appendix B. The format applied to these and all other plots is discussed below. Additionally, data has been grouped and plotted in order to discuss the effects of varying mass flux, spray fluid, and spray angle.

Table 6.1 Matrix of experimental parameters tested

Test #	Fluid	Spray Angle (degrees)	Mass Flux (lb/ft^2-s)
1	Water	90	0.0459
3	Water	90	0.0272
4	Water	90	0.0364
5	Water	90	0.0349
6	Fluid 1	90	0.0355
7	Fluid 1	90	0.0266
8	Fluid 1	90	0.0506
9	Fluid 2	90	0.0465
10	Fluid 2	90	0.0356
11	Fluid 2	90	0.0240
13	Water	45	0.0362
14	Water	45	0.0446
15	Water	45	0.0225
16	Water	10	0.0215
18	Water	10	0.0378

6.1 Formatting and Notation for Data Plots

Each test data set was used to generate a plot of spray heat flux (BTU/h-ft^2) vs. ΔT (surface temperature minus impinging fluid temperature in °F). An example of a plot is shown below in Figure 6.1. Circular, hollow, black data points represent individual nodal measurements. These

values are first averaged over time and then averaged to represent the entire heated surface and plotted as green diamonds in the figure below. (Tables of individual nodal measurements averaged over time are located in Appendix B.) The color green establishes the group from Table 6.1 that the test data set belongs to: in this case Fluid 2 sprayed at 90°. The diamond shape establishes that the mass flux in the moderate range near 0.035lb/ft^2-s. Square shaped data points represent mass flux of approximately 0.045lb/ft^2-s, and triangle, 0.025lb/ft^2-s. The outline color of the data point signifies whether the surface is increasing (red outline) or decreasing (blue outline) in temperature. Data sets are labeled by the spray fluid, spray angle, and mass flux in lb/ft^2-s.

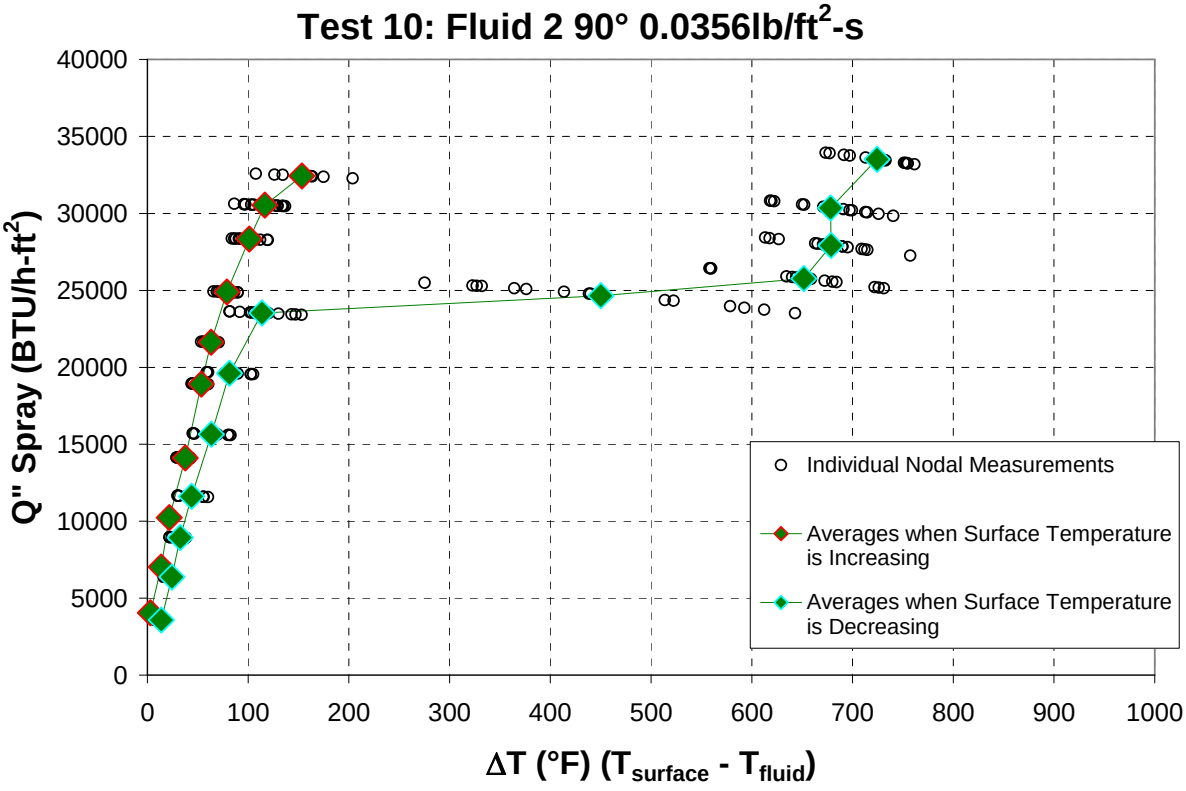

Figure 6.1 Example plot representing one test data set.

Five phases of cooling can be generalized for every test in the data set. The phases described below are labeled A through E in Figures 6.2 and 6.3 on the following pages. Every test, no matter what particular parameter was tested, experience five phases. Each phase is described by both physical and graphical observations.

A. *Initial heating of the surface* - In the first five to seven power levels the liquid tends to form a large pool or multiple large droplets remain on the surface that dissipate by flooding off either end of the strip. As the surface temperature rises, the thickness of the pools or droplets formed at the surface decreases and the liquid appears to run off the surface at a higher frequency. (In tests with spray angles other than 90°, run-off occurs mainly at the end of the strip opposite of the spray.) During this phase, the heat flux varies linearly with change in temperature. The image labeled A in Figure 6.3 is an image selected from the three images taken at data point A in the plot. The NiChrome filament appears fairly uniform in surface temperature, which suggests that a pool of liquid covers the surface at this power level.

B. *Surface conditions near CHF* - Rising surface temperatures further causes intermittent areas to appear dry and then quickly re-wet. These dry spots increase in both size and duration as the surface temperature continues to rise. Graphically, there is an increase in the temperature range of the individually measured nodes indicting non-uniform surface temperatures where the surface is drying. Image B in Figure 6.3 is an image selected from this stage at point B labeled in the plot. The surface temperature has become significantly less uniform than that in Image A. This is an effect of the surface experiencing localized dry spots.

C. *Surface conditions after CHF* – The power increase following point B causes the surface to appear completely dry and surface temperatures increase to a point where the surface is visually bright red in color. The power is immediately lowered slightly to avoid catastrophic conditions. After the power is reduced, the surface continues to appear visually red. Data points are recorded after the power level is adjusted, and CHF is said to have occurred between two power levels: the last power level recorded before and directly after the rapid increase in surface temperature. In other words, between the power levels corresponding to the last set of collect IR images and the power level that directly follows, even if IR images were not collect and the power was quickly reduced. The range formed between the two settings defines CHF. Image C corresponds to data point C in the plot. The surface temperature is the highest at this power level. In some tests, CHF occurs on only a section of

the strip as shown in Figure 6.4. In this event, data points are defined separately for the CHF and non-CHF sides of the surface.

D. *Film boiling followed by re-wetting of the surface* – As the surface temperature is decreased following the occurrence of CHF, the surface remains visually red, but the intensity fades. In this phase, referred to as film boiling, the surface appears dry and droplets are not observed impacting the surface. The surface is re-wetted by an area of liquid pooling at the surface and then expanding to cover the entire surface. Re-wetting does not necessarily occur immediately following the decrease in applied power, but may happen at any point in the power level. Additionally the presence of a liquid pool at the surface does not always lead to complete re-wetting; Dry areas can remain stable until the power level is decreased further. A significant temperature drop represents re-wetting graphically. Image D, corresponding to point D in the plot, captures the surface just prior to rewetting. A cooler area at the bottom of the strip indicates a liquid pool has formed at the surface.

E. *After rewetting* – Once the surface is completely covered by a liquid pool, the surface remains completely wetted for the remainder of the test. The surface appears visually scarred from the extreme temperatures following CHF. The presence of view-obscuring liquid droplets is evident in the IR image due to the extreme temperature conditions causing seals to leak. As the surface temperature decreases, the NiChrome temperature appears more uniform then the previous stage, but less uniform than conditions when surface temperatures were increasing. Data points return close to those from raising surface temperatures, but experience a slightly lower slope. Image E, corresponding to point E, captures the surface during this stage.

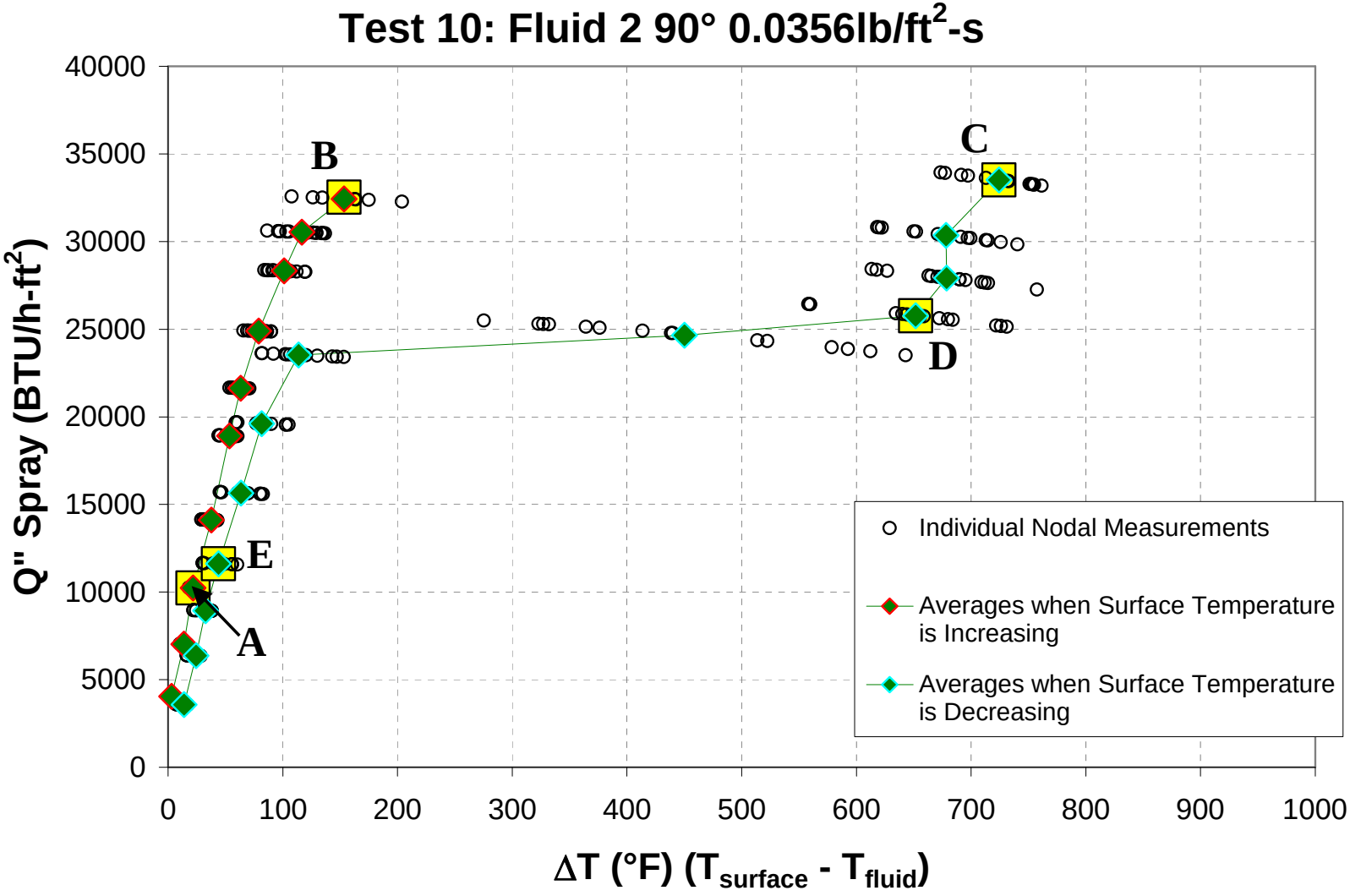

Figure 6.2 Particular data points corresponding to IR images in Figure 6.3

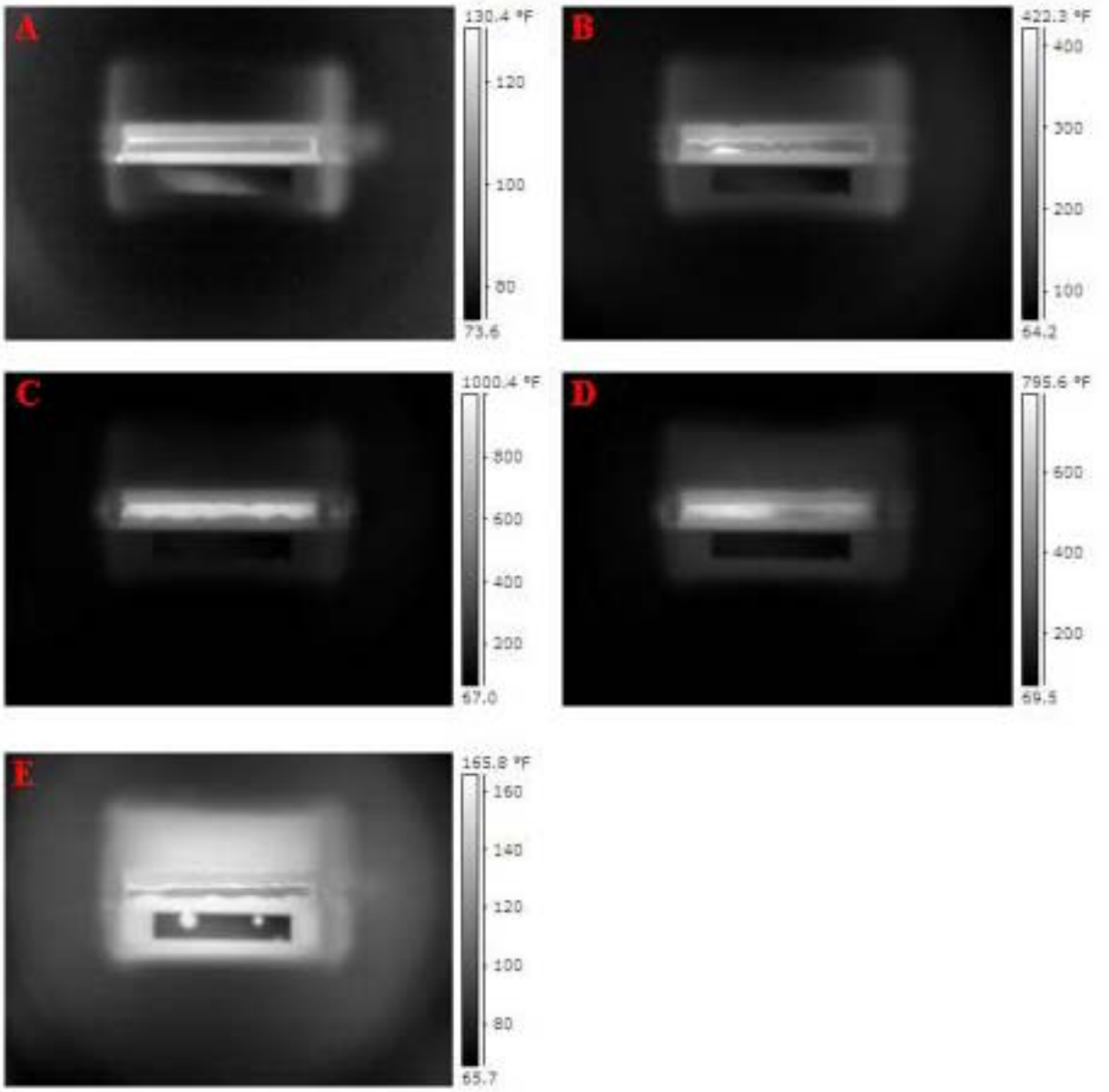

Figure 6.3 IR images corresponding to particular data points labeled in Figure 6.2.

Figure 6.4 Image from Test 5 where CHF occurs only at the right side of the NiChrome surface.

All data sets were processed in the same fashion and are presented in the same format. Data from tests exposed to varying test parameters can then be compared and discussed.

6.2 Discussion on the Effects of Changing Mass Flux

Water Sprayed at 90° with Varying Mass Flux

The data from tests previously discussed were grouped so that all tests with water spray at 90° for varying mass flux are plotted and compared: During initial heating of the surface (region highlighted by box 1 in Figure 6.5), the change in heat flux with temperature remains constant at approximately 330 BTU/h-ft^2 per °F for all tests plotted as observed from Figure 6.5. This suggests that heat flux for water in this region is independent of mass flux. During testing it was observed that, when power was initially applied, the surface flooded and excess liquid ran off either end of the NiChrome filament. Therefore, it follows that increasing the mass flux does not significantly affect the amount of heat transfer but more likely the amount of run off.

As the data nears CHF (region highlighted by box 2 in Figure 6.5), the slope of heat flux and surface temperature is observed to increase but remains constant at approximately 1300 BTU/hr-ft^2 per °F for varying mass flux over the entire region. This trend has been observed in water spray cooling experiments conducted by Mudawar and Valentine (1989) and is described as nucleate boiling, a heat transfer regime independent of mass flux.

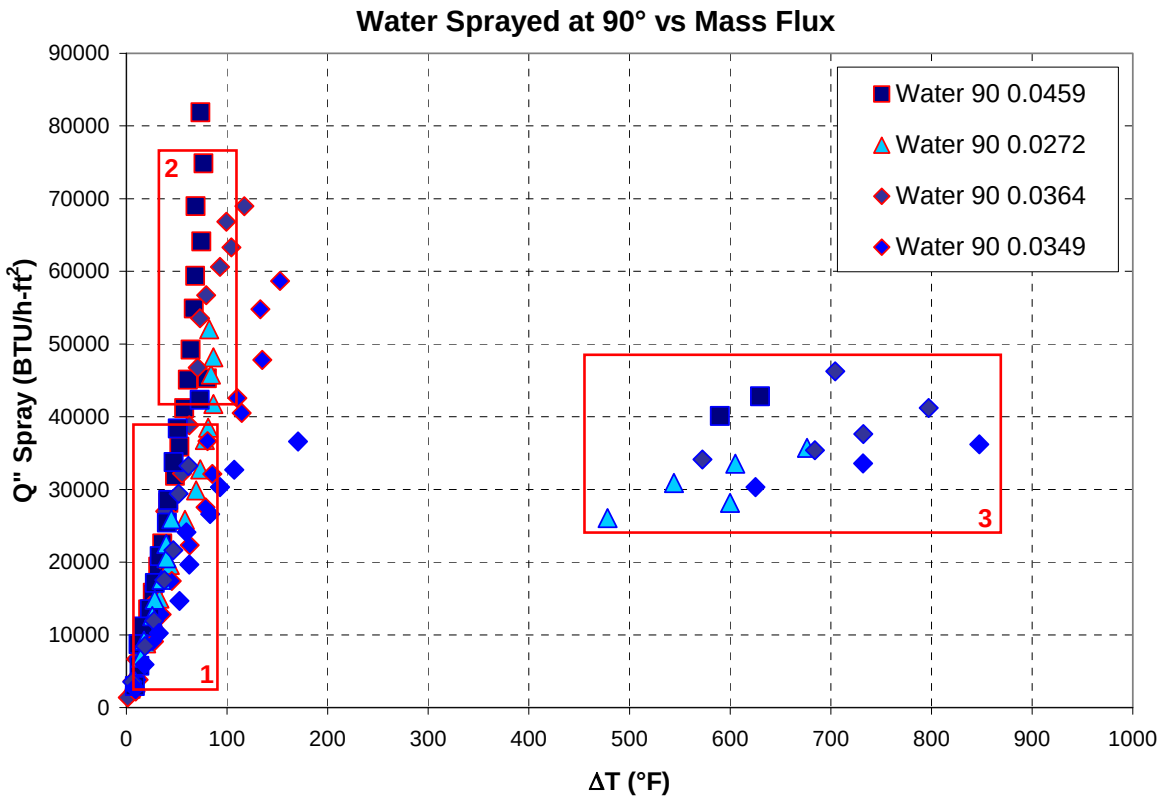

Figure 6.5 Water sprayed normal (90°) to the surface with varying mass flux.

The CHF (plotted in Figure 6.6a based on the heat flux before the occurrence of CHF with a y-error bar indicating the maximum possible heat flux for the immediately following power setting) is observed to increase linearly as mass flux is increased at an approximate rate of 1.6×10^6 BTU/h-ft^2 per lb/ft^2-s. This implies that the CHF of water is dependent on mass flux. The temperature before and after CHF occurs varies too greatly for any trend to be observed about how temperatures at CHF may vary with mass flux.

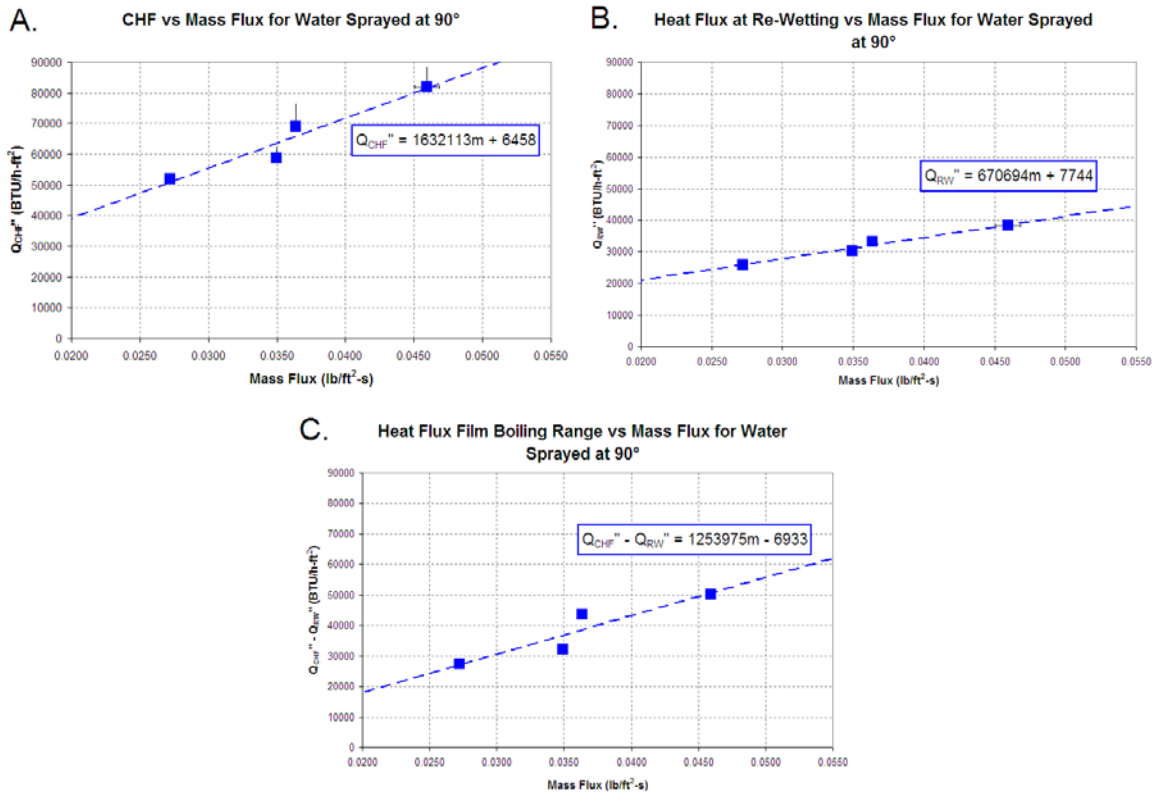

Figure 6.6 CHF (A), heat flux at re-wetting (B), and heat flux in the film boiling range (C) vs mass flux for water sprayed at 90°

In the film boiling region, the region bounded by the occurrence of CHF and re-wetting of the surface (highlighted by box 3 in Figure 6.5), the data suggests heat flux may be decreasing linearly with respect to decreasing surface temperatures. Data also suggests that the slope may be decreasing as mass flux decreases, but these notions cannot be definitively supported due to an insufficient number of data in some tests and uncertainties in heat flux and temperature measurements. It is evident that the range of heat flux for data in the film boiling region increases linearly as mass flux is increased at an approximate rate of 6.7×10^5 BTU/h-ft^2 per lb/ft^2-s as shown in Figure 6.6c.

It then follows that the estimated heat flux at surface re-wetting (plotted in Figure 6.6b based on the heat flux after the surface re-wets with a y-error bar indicating the heat flux from the preceding power setting) also increases linearly as mass flux is increased. The rate is approximated to be 1.25×10^6 BTU/h-ft^2 per lb/ft^2-s.

Fluid 1 Sprayed at 90° with Varying Mass Flux

Similar tests were conducted with Fluid 1 as the spray fluid were also grouped and examined. Trends observed for the effects of varying mass flux of Fluid 1 are similar to those previously described for water.

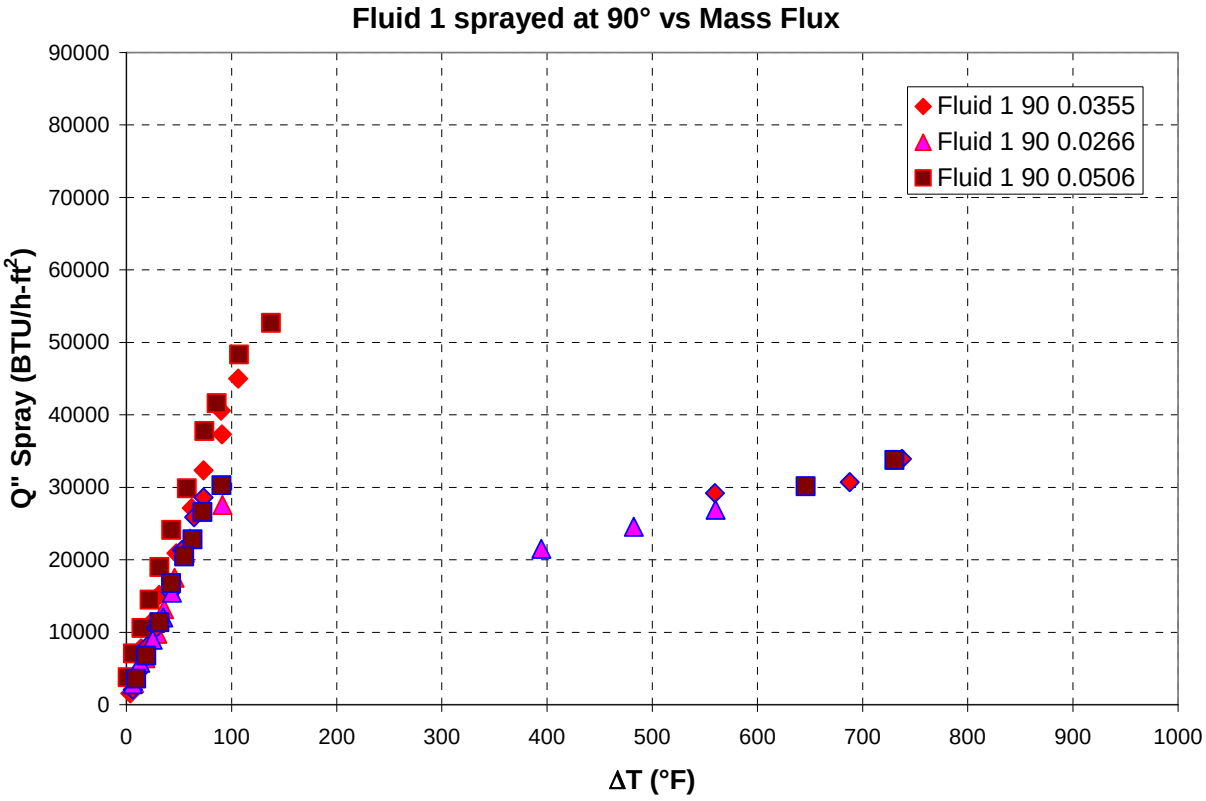

Figure 6.7 Fluid 1 sprayed normal (90°) to the surface with varying mass flux

As was the case for water, the initial linear slope of heat flux and mass flux is reasonably constant at approximately 330 BTU/h-ft^2 per °F (observed from Figure 6.7) suggesting the heat flux in this phase has no significant dependence on mass flux.

Also, the estimated CHF (plotted in Figure 6.8a) is observed to increase linearly as mass flux is increased at an approximate rate of 0.99x10^6 BTU/h-ft^2 per lb/ft^2-s for Fluid 1. The range of heat flux for data in the film boiling region (plotted in Figure 6.8b) decreases linearly with decreasing mass flux at an approximate rate of 0.82x10^6 BTU/h-ft^2 per °F. Additionally, the

estimated heat flux at surface re-wetting (plotted in Figure 6.8) is observed to increase linearly as mass flux is increased at an approximate rate of 3.58×10^5 BTU/h-ft^2 per lb/ft^2-s.

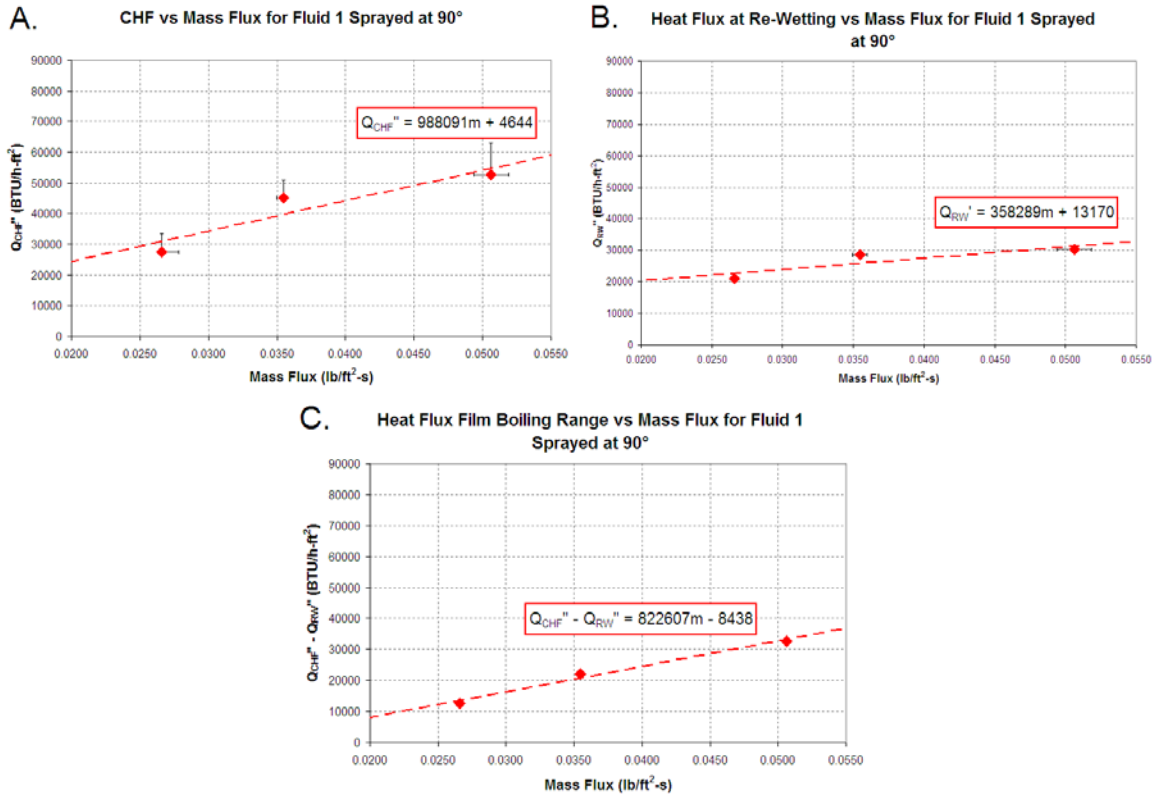

Figure 6.8 CHF (A), heat flux at re-wetting (B), heat flux in the film boiling range (C) vs mass flux for Fluid 1 sprayed at 90°

The data differs from that recorded with water in that a constant slope is not evident as heat flux approaches CHF. This may suggest that due to differences in fluid properties, nucleate boiling does not occur. This notion is inconclusive due to the fact that CHF was achieved at a lower power setting, decreasing the possible region and, therefore, fewer data points were available. Instead, it is noted that the slope of heat flux and temperature gradually decreases as CHF is approached. Many experimentalists have observed this trend of decreasing slope prior to the occurrence of CHF in both pool boiling and spray cooling tests.

Additionally, data in the film boiling region for Fluid 1 does support a linear trend between decreasing heat flux and temperature, but notions that the slope may be decreasing as mass flux

decreases can not be definitively concluded from the existing data. Data actually may suggest that the slope during film boiling is constant, and, therefore, heat flux in this region may not be highly dependent on mass flux for Fluid 1.

Fluid 2 Sprayed at 90° with Varying Mass Flux

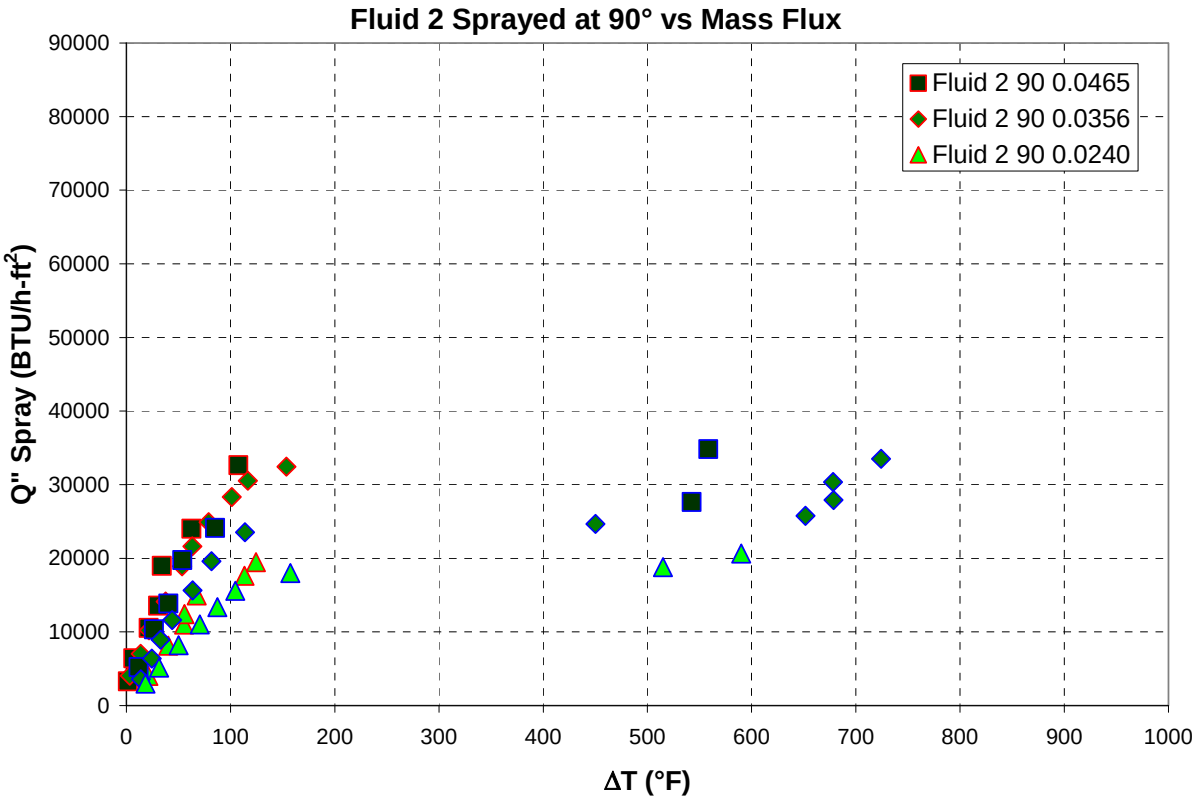

Figure 6.9 Fluid 2 sprayed normal (90°) to the surface with varying mass flux

Varying mass flux with Fluid 2 as the spray fluid once again leads to trends similar to those described for water and Fluid 1: The initial linear slope of change in heat flux with change in mass flux is considered generally constant at approximately 330 BTU/h-ft^2 per °F (observed from Figure 6.9). It is less conclusive to define this particular trend due to the fact that the CHF value is lower than that of previously tested fluids so fewer data points were recorded in this phase.

Also, the estimated CHF (plotted in Figure 6.10a) is observed to increase linearly as mass flux is increased at a rate of approximately 0.59x10^6 BTU/h-ft^2 per lb/ft^2-s for Fluid 2. The range of

heat flux for data in the film boiling region (plotted in Figure 6.10c) again increases as the mass flux is increased. The rate is approximately 0.25×10^6 BTU/h-ft^2 per °F for Fluid 2. The estimated heat flux at surface re-wetting (plotted in Figure 6.10b) is observed to increase linearly as mass flux is increased at a rate of approximately 3.84×10^5 BTU/h-ft^2 per lb/ft^2-s

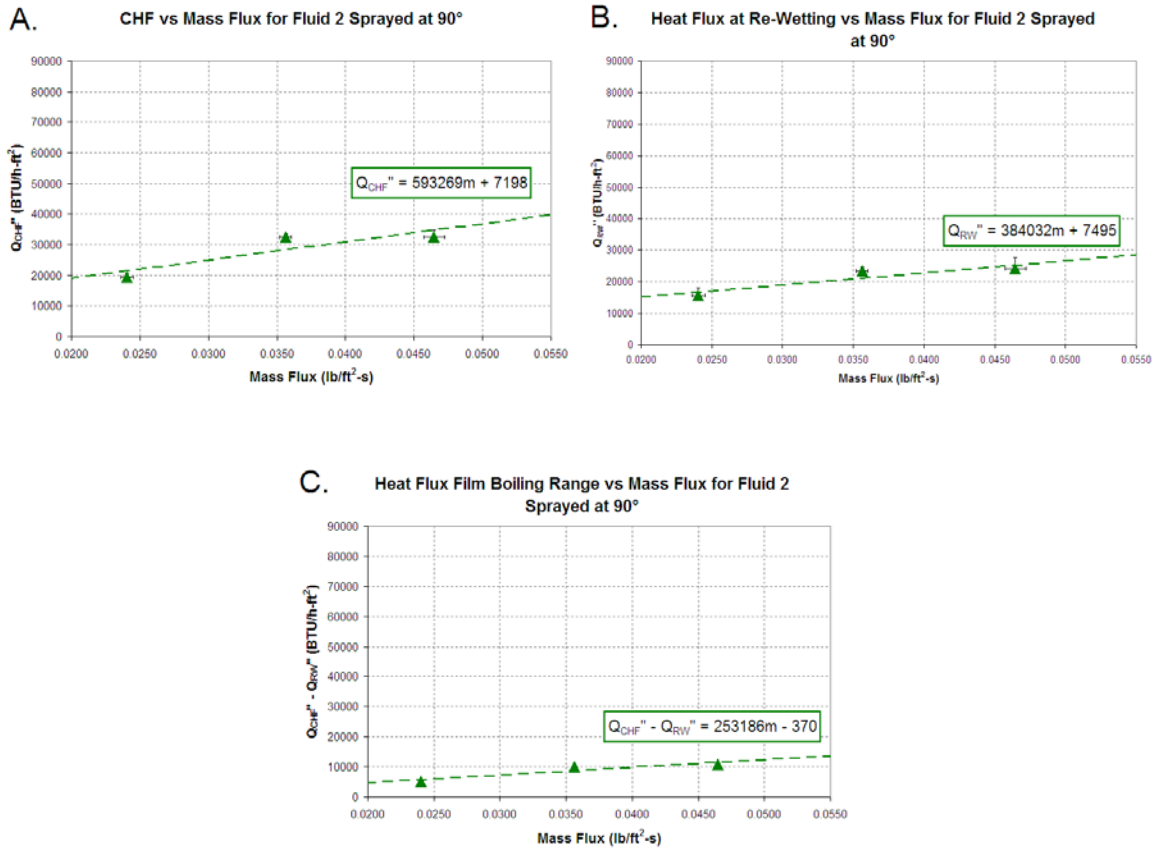

Figure 6.10 CHF (A), heat flux at re-wetting (B), heat flux in the film boiling range (C) vs mass flux for Fluid 2 sprayed at 90°

Fluid 2 data is similar to Fluid 1 in that the slope of heat flux and temperature decreases as CHF is approached. Fluid 1 data is similar to water data in that it too suggests heat flux during film boiling may be decreasing linearly with decreasing surface temperatures and the slope may be decreasing as mass flux decreases, but is inconclusive due to an insufficient number of data in some tests and uncertainties in heat flux and temperature measurements.

6.3 Discussion on the Effects of Different Spray Fluids

Data from tests conducted with different spray fluids at similar mass flux were also plotted and examined for trends that may suggest some dependence on fluid properties. Fluid properties for water, Fluid 1, and Fluid 2 are listed in Table 6.2. The three fluids are very similar in density while the specific heat, latent heat, surface tension, and thermal conductivity decrease from water to Fluid 1 and further to Fluid 2. Dynamic viscosity, the property varying the most among the three liquids, increases from water to Fluid 1 and is even higher for Fluid 2. This suggests that highly evident data trends are likely dependent upon dynamic viscosity. Less substantial trends may be dependent on any of the other fluid properties. The exception is density; no real conclusions can be drawn about the effects of varying density from the tested fluids of similar densities.

Table 6.2 Fluid properties at atmospheric pressure and room temperature for water, Fluid 1, and Fluid 2

Property	**Units**	**Water**		**Fluid 1**		**Fluid 2**	
Density	**lb/ft^3** (kg/m^3)	**62.31**	(998)	**62.95**	(1008)	**63.58**	(1018)
Specific Heat	**BTU/lb-°F** (J/g-K)	**0.9986**	(4.18)	**0.8959**	(3.75)	**0.7952**	(3.33)
Latent Heat	**BTU/lb** (kJ/kg)	**1048**	(2438)	**873**	(2031)	**702**	(1632)
Dynamic Viscosity	**lb/ft-h** (Pa-s)	**2.2**	(0.00089)	**31.5**	(0.01302)	**60.3**	(0.02491)
Surface Tension	**lb/ft** (N/m)	**4.93E-03**	(0.072)	**4.30E-03**	(0.063)	**3.68E-03**	(0.054)
Thermal Conductivity	**BTU/h-ft-°F** (W/m-K)	**0.35**	(0.61)	**0.29**	(0.51)	**0.23**	(0.40)

Properties calculated based on the fluid mass fraction and properties listed on www.webbook.NIST.gov and www.dow.com

Various Fluids Sprayed at 90° with Mass Flux near 0.045lb/ft^2-s

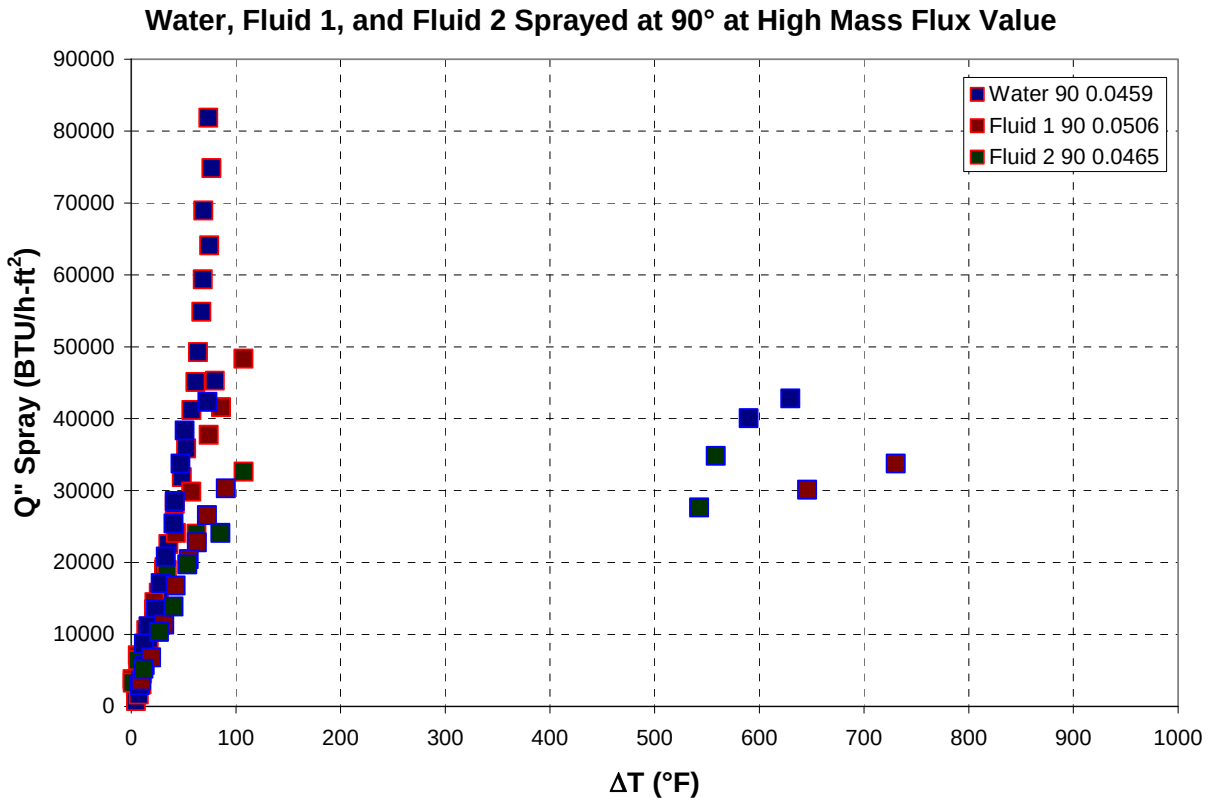

Figure 6.11 Water, Fluid 1, and Fluid 2 sprayed normal (90°) to the surface at a mass flux near 0.045lb/ft^2-s

Data for test completed with mass flux near 0.045lb/ft^2-s realize the same trend in heat flux at initial heating of a constant slope regardless of the spray fluid. This suggests that heat flux in this phase is not highly dependent on the spray fluid's properties. As the data approaches CHF, the slope formed by the data appears to decreases at a higher rate as the fluid viscosity is increased and the other properties listed in Table 6.2 decrease. The presence of data points in this region close to CHF suggest that Fluid 1 and Fluid 2 are more stable at heat fluxes near CHF than water. This follows from the idea that the trend of decreasing slope is not evident in the water data because cooling in this state is unstable; therefore, intrinsic fluctuations quickly send the surface to CHF while in tests with Fluid 1 and Fluid 2 the surface was stable enough to counteract these fluctuations. Fluid 2 may be considered more stable with respect to Fluid 1 based upon the same reasoning. Similar trends were observed in data taken at moderate (near

0.035lb/ft^2-s) and low (near 0.025lb/ft^2-s) mass flux. Plots for moderate and low mass flux are located in Appendix B.

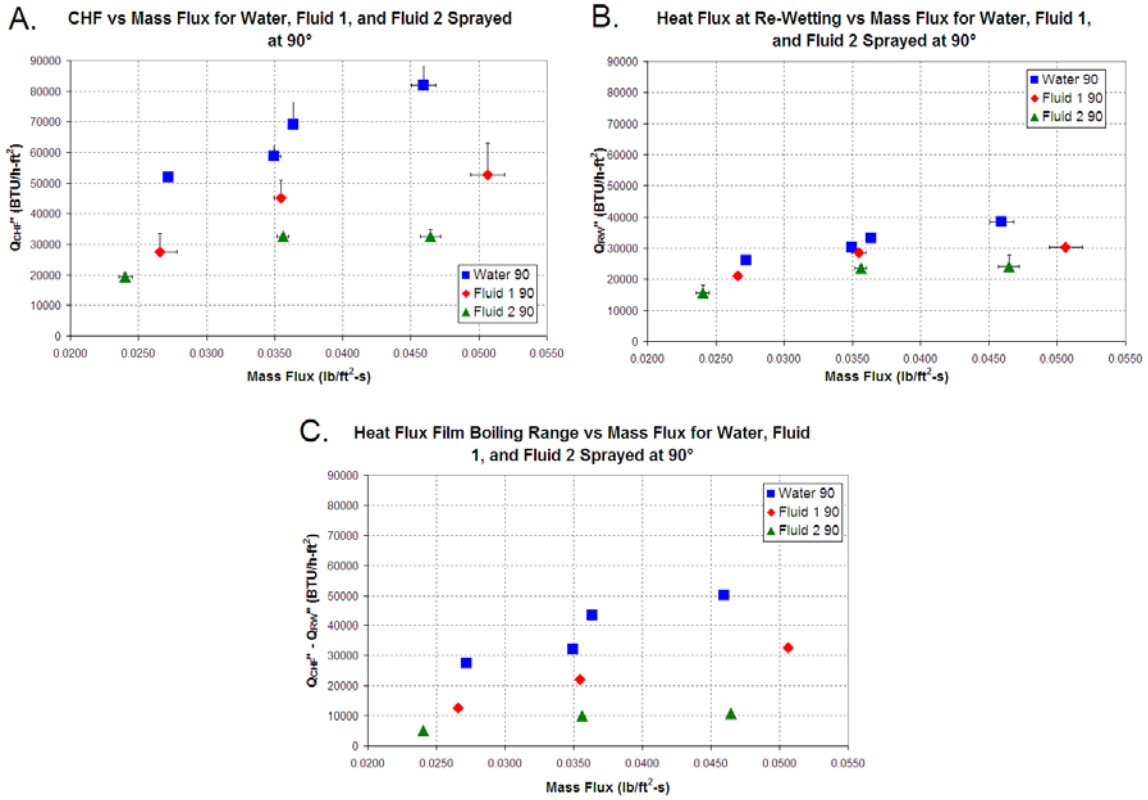

Figure 6.12 CHF (A), heat flux at re-wetting (B), and heat flux in the film boiling range (C) plotted for water, Fluid 1, and Fluid 2 for varying mass flux

Additionally, the estimated CHF appears to decrease as the fluid viscosity is increased and the other properties decrease for all variation of mass flux (see Figure 6.12a and 6.12b) and the heat flux at re-wetting decreases linearly with decreasing mass flux and may be weakly dependent upon fluid properties. Therefore, it follows that the heat flux range for the film boiling region is also decreasing with decreasing surface properties (see Figure 6.12c). This suggests that the film boiling region is dependent on spray fluid properties.

In order to further evaluate the effect of the spray fluid's viscosity and surface tension on CHF values, the spray efficiency of the heat flux removed by the fluid spray at CHF

$$\varepsilon = \frac{Q''_{CHF}}{\dot{m}'' h_{fg}} \qquad \text{Eqn. 6.1}$$

is plotted with respect to the non-dimensional ratio of viscous forces and surface tension, the Capillary Number.

$$Ca = \frac{\mu\left(\frac{\dot{m}''}{\rho}\right)}{\sigma} \qquad \text{Eqn. 6.2}$$

Characteristic spray velocity is defined as mass flux divided by the fluid density as suggested by Yao & Cox (2002). Data suggest a linear relation between the parameters as shown in Figure 6.13.

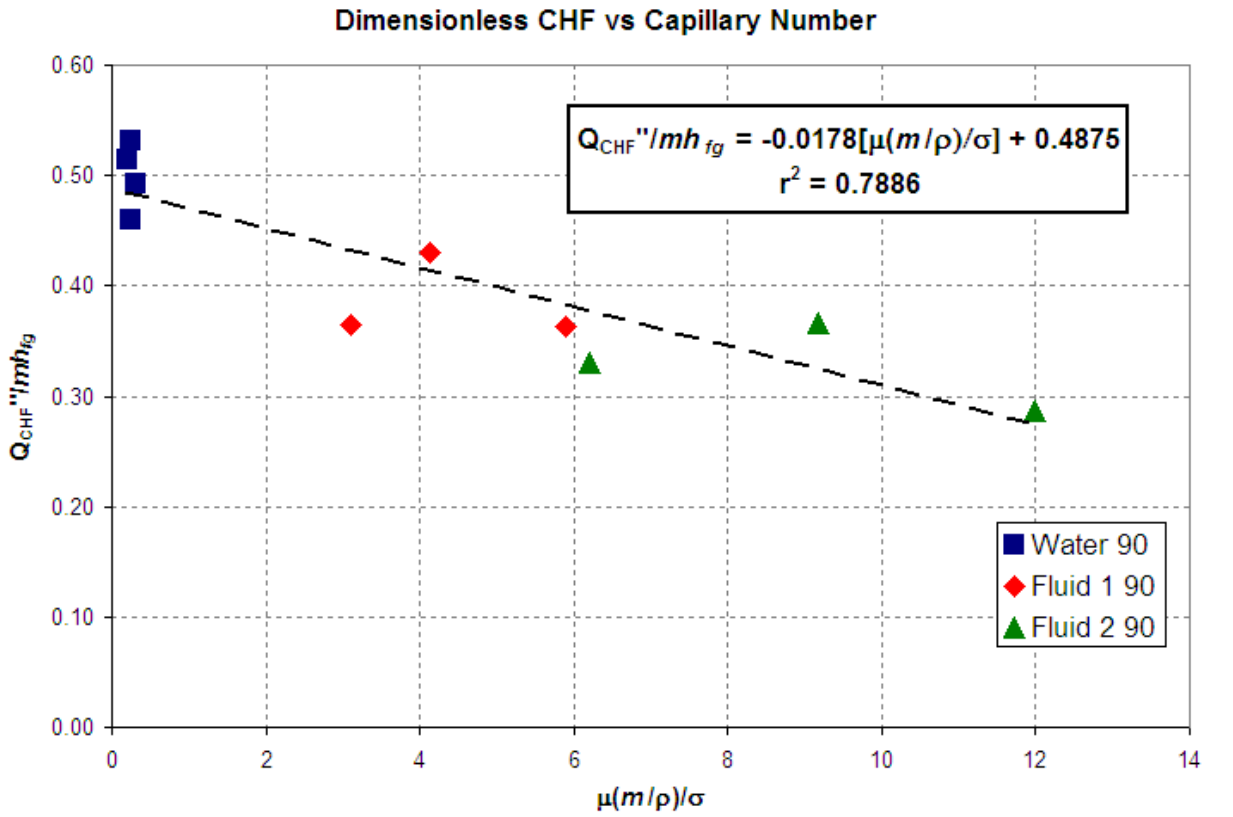

Figure 6.13 Plot of spray efficiency and the non-dimensional capillary number

Spray efficiency can also be compared to the Nusselt Number

$$Nu \equiv \frac{hd}{k_f} \qquad \text{Eqn. 6.3}$$

where h is the heat transfer coefficient before CHF and d is an estimated mean droplet diameter

times the Prandlt Number

$$\mathrm{Pr} = \frac{\mu c_p}{k_f} \qquad \text{Eqn. 6.4}$$

to observe the additional effects of fluid thermal conductivity and specific heat as seen in Figure 6.14. Again, an approximate linear correlation can be established.

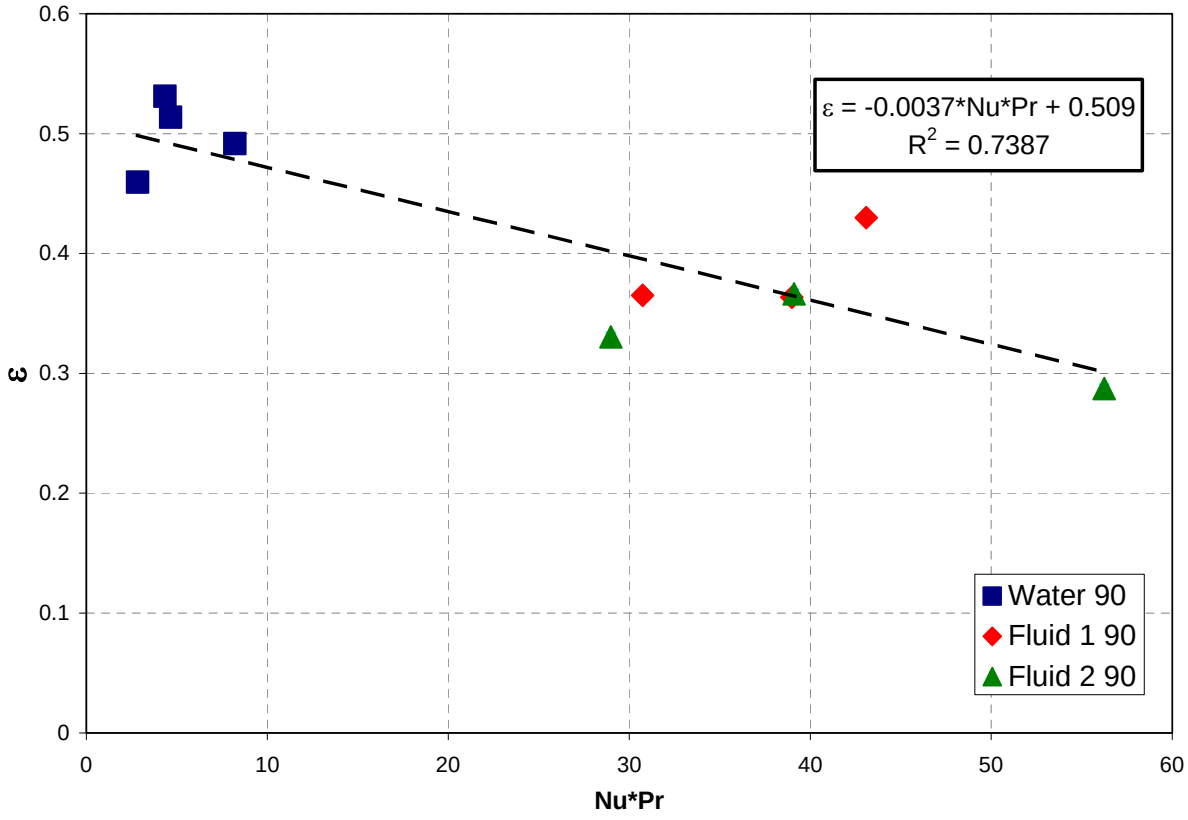

Figure 6.14 Plot of the spray efficiency vs the Nusselt Number times the Prandlt Number

The combined effects of fluid surface tension, thermal conductivity, and specific heat are observed by comparing the spray efficiency to the Nusselt Number times the Prandlt Number divided by the Capillary Number (Figure 6.15).

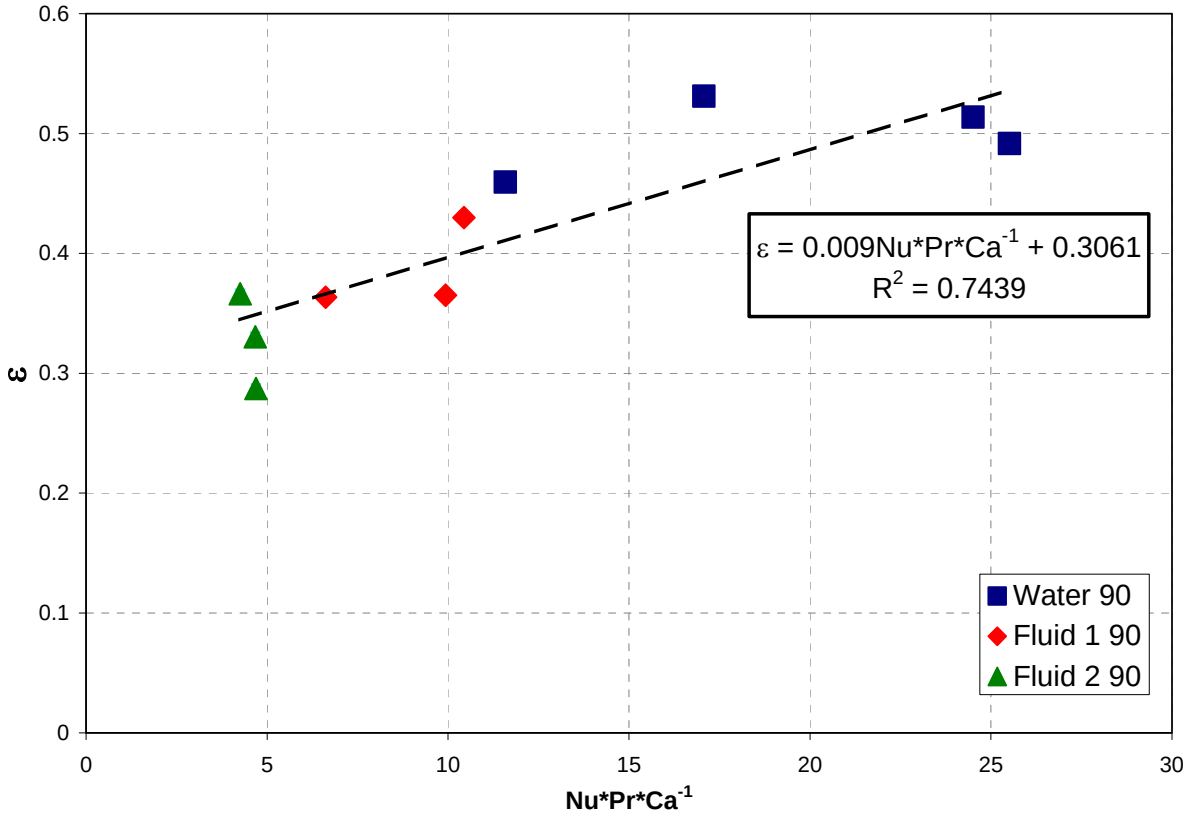

Figure 6.15 Plot of the spray efficiency vs the Nusselt Number times the Prandlt Number divided by the Capillary Number

The combination of $Nu*Pr*Ca^{-1}$ removes the effects due to fluid viscosity and still produces an linear relation with spray efficiency. Therefore, it is evident that spray efficiency is primarily affected by the spray fluid's surface tension and thermal conductivity in collaboration with the specific heat.

6.4 Discussion on the Effects of Spray Angle

Data collected for water sprayed at spray angles of approximately 45° and 10° were also examined. Figure 6.16 shows data collected at different spray angles at a mass flux near 0.025lb/h-ft^2.

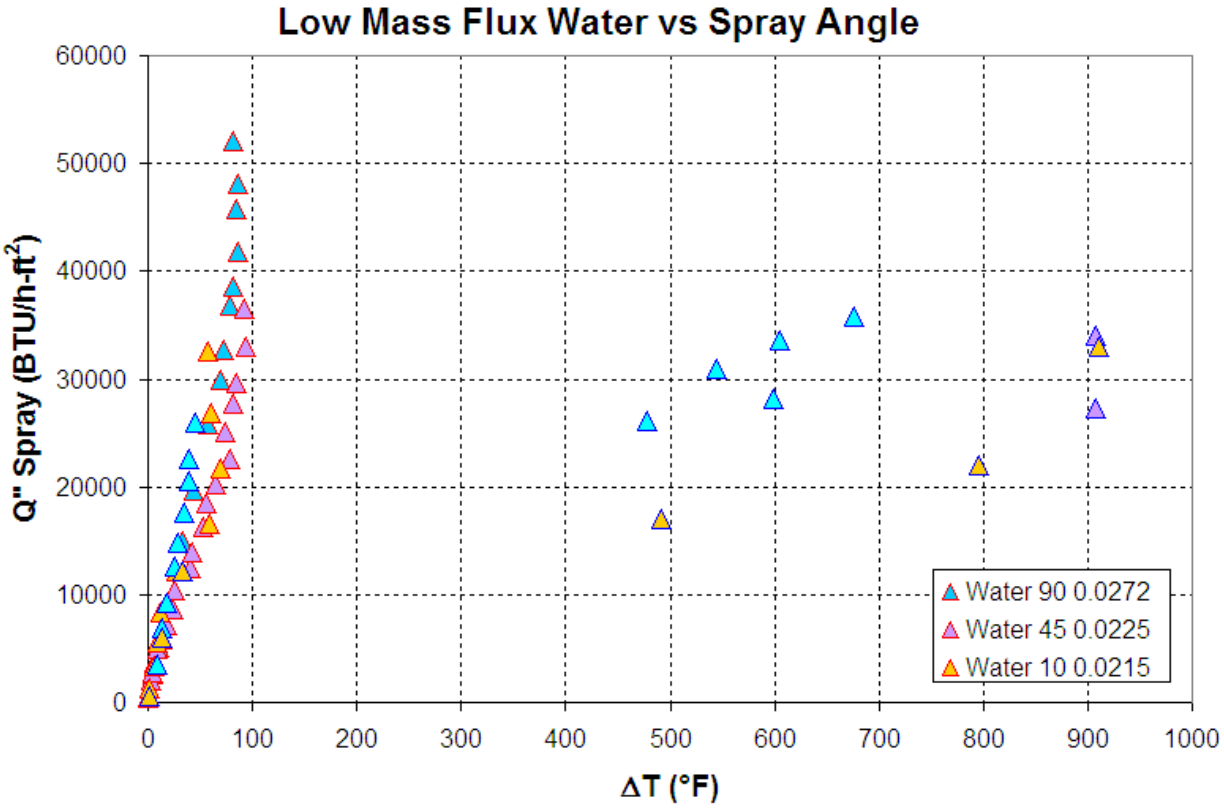

Figure 6.16 Water sprayed normal (90°), 45°, and 10° to the surface at a mass flux near 0.025lb/ft^2-s

Data collected for these tests also realize a constant increase in heat flux with temperature just after initial heating; suggesting that heat flux in this region is not highly dependent on mass flux and fluid properties, but also shows no real dependence on spray angle. Additionally, a significant increase in the slope of heat flux and temperature is observed before the estimated CHF as was noted in other water tests and was presumed to indicate nucleate boiling. This implies that the increase in slope is independent of spray angle. Data collected for mass flux near 0.035lb/h-ft^2 shows similar trends (see plot in Appendix B).

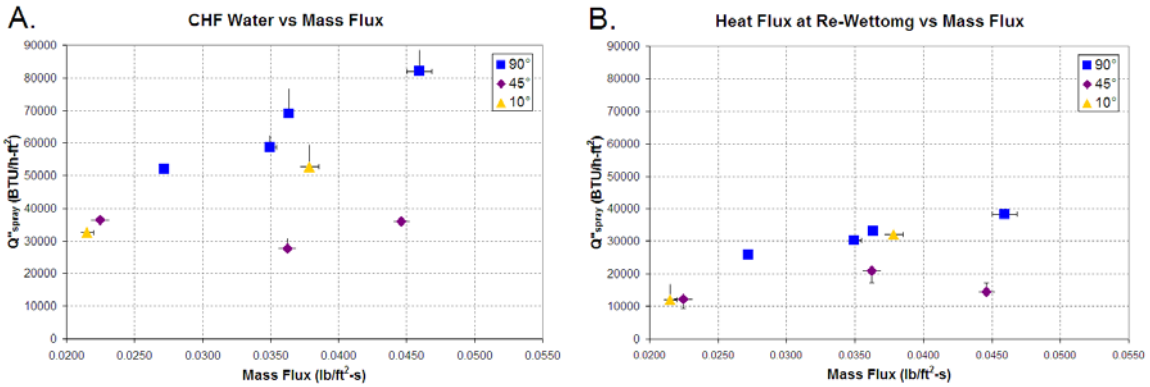

Figure 6.17 CHF (A) and heat flux at re-wetting (B) plotted for Water, Fluid 1, and Fluid 2 at varying mass fluxes

Plots of the estimated CHF and estimated heat flux at re-wetting are shown in Figures 6.17a and 6.17b, respectively. Data suggest that CHF values may be optimal at a normal (90°) spray angle, but a 10° spray angle may also effective. This may be due to the increase momentum created by the tangential velocity hindering the formation of a vapor layer at the surface. The CHF and heat flux at re-wetting for data collected at a 45° spray angle is notably less than that for data collected at 90° and 10° spray angles. Although inconclusive due to the uncertainty in calculated heat flux at the lower mass flux, data may support the notion that a spray angle of 45° is less effective than 90° or 10° spray angles.

6.5 Data Comparison to Existing Correlations

Data collected for water sprayed at a 90° spray angle at approximately 0.035lb/ft^2-s was compared to the predicted to the correlations discussed in Chapter 2. Heat flux data recorded before the occurrence of CHF does not appear to follow to the plotted correlations as seen in Figure 6.18. The estimated surface temperature at which CHF is expected to occur determined by the Mudawar & Valentine (1989) correlation does seem to follow the experimental data. Data within the film boiling region follows the general curve shape defined by the Yao & Cox (2002) correlation, but Yao & Cox (2002) under-predict the magnitude.

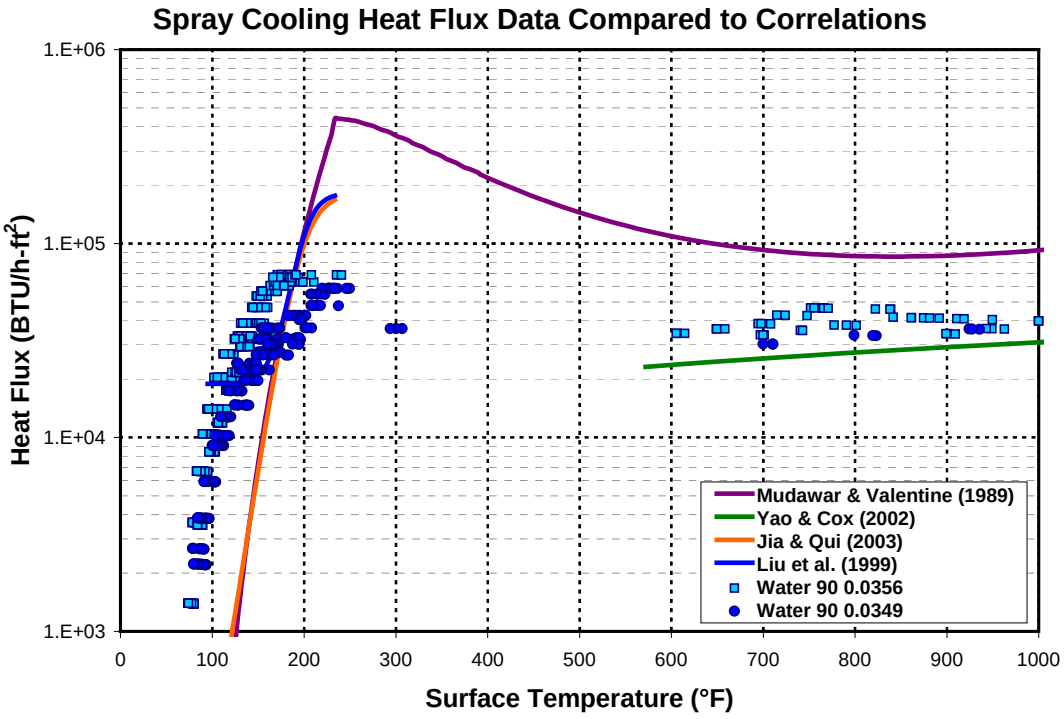

Figure 6.18 Experimental data compared to correlations

6.6 Summary of Results

The following conclusion were drawn based upon trends evident in the collected data:

- Initial heat flux varies linearly with temperature and is not highly dependent upon mass flux, fluid properties, or spray angle.
- Critical heat flux increases linearly with increasing mass flux and varying spray fluid properties.
- Non-dimensionalized spray efficiency can be approximated by the linear relation to the Capillary Number (a ration of viscous forces and surface tension) as

$$\varepsilon = -0.0178 * [Ca] + 0.4875 \qquad \text{Eqn. 6.5}$$

- Non-dimensionalized spray efficiency can be approximated by the linear relation to the Nusselt Number times the Prandlt Number as

$$\varepsilon = -0.0037 * [Nu * \mathrm{Pr}] + 0.509 \qquad \text{Eqn. 6.6}$$

- Non-dimensionalized spray efficiency can be approximated by the linear relation to the Nusselt Number times the Prandlt Number divided by the Capillary Number as

$$\varepsilon = 0.009 * \left[\frac{Nu * \mathrm{Pr}}{Ca} \right] + 0.3061 \qquad \text{Eqn. 6.7}$$

- Heat flux at re-wetting increases linearly with increasing mass flux and may be weakly dependent on fluid properties.
- The range of the film boiling region increases with increasing mass flux.
- Data suggests that critical heat flux reaches a minimal level at a 45° spray angle, but definitive conclusions are not supported for the effect of spray angle.

CHAPTER 7 - Conclusions

A facility was designed and constructed to experimentally determine the effects of varied low mass flux, spray fluid, and spray angle on the amount of heat flux removed the fluid spray. IR thermography served as a viable non-contact method of determining the spray cooled surface temperature. To capture local surface conditions, a NiChrome strip filament was used to generate heat internally with an applied current: The strip used was very thin (0.005in or 0.125mm thick) so that temperature characteristics from the sprayed surface could be perceived from an infrared depiction of the alternate unsprayed surface.

The experimental facility used in the data collection process consists of a NiChrome filament supported in a copper, Teflon, and high temperature ceramic assembly positioned in a spray chamber in such a way that an IR camera can view the unsprayed surface of the NiChrome. An assembly of PVC and steel pipes and fittings generated spray though a BETE WL ¼ nozzle that was positioned by an assembly housed within the spray chamber. Data was collected with Flir Systems IR imaging equipment and LabVIEW data acquisition.

Data collection for each test included five main steps: (1) placing the NiChrome filament, (2) pre-heating the NiChrome filament, (3) pre-test flow collection, (4) spray data collection, and (5) post-test data collection. Recorded IR images were first processed using the Flir Systems QuickVIEW software to apply the appropriate reflected temperature and emissivity determined by an experimental correlation. IR images were then passes through a number of sequences in a MatLAB code to correlate pixel values to spray surface temperatures and calculate the heat loss to spray cooling at each quasi-steady state adjusted by increasing or decreasing the applied current.

Tests were conducted for mass flux ranging from 0.025lb/ft^2-s to 0.045lb/ft^2-s of water, Fluid 1, or Fluid 2 at angles of 90°, 45°, or 10°. Results for individual tests were presented as the calculated local heat flux removed by spray cooling and the corresponding local temperature

difference defined as the surface temperature minus the spray fluid temperature. Results from all valid tests were examined to determine the effects of mass flux, spray fluid, and spray angle.

The data suggested that:

- Initial heat flux varies linearly with temperature and is not highly dependent upon mass flux, fluid properties, or spray angle.
- Critical heat flux increases linearly with increasing mass flux and varying spray fluid properties.
- Non-dimensionalized spray efficiency can be approximated by the linear relation to the Capillary Number (a ration of viscous forces and surface tension) as

$$\varepsilon = -0.0178 * [Ca] + 0.4875 \qquad \text{Eqn. 6.5}$$

- Non-dimensionalized spray efficiency can be approximated by the linear relation to the Nusselt Number times the Prandlt Number as

$$\varepsilon = -0.0037 * [Nu * \mathrm{Pr}] + 0.509 \qquad \text{Eqn. 6.6}$$

- Non-dimensionalized spray efficiency can be approximated by the linear relation to the Nusselt Number times the Prandlt Number divided by the Capillary Number as

$$\varepsilon = 0.009 * \left[\frac{Nu * \mathrm{Pr}}{Ca} \right] + 0.3061 \qquad \text{Eqn. 6.7}$$

- Heat flux at re-wetting increases linearly with increasing mass flux and may be weakly dependent on fluid properties.
- The range of the film boiling region increases with increasing mass flux.
- Data suggests that critical heat flux reaches a minimal level at a 45° spray angle, but definitive conclusions are not supported for the effect of spray angle.

Table 7.1 lists the observed slopes of heat flux and temperature difference for water sprayed at 90° with changing mass flux to similar observations made for Fluid 1 and Fluid 2 sprayed at 90°.

Table 7.1 Observation of the effects of varying mass flux for water, Fluid 1, and Fluid 2

	$Q"_{spray}$ / ΔT initially	CHF / Mass Flux	DT Range of Film Boiling / Mass Flux	Re-Wetting Heat Flux / Mass Flux
Units	BTU/h-ft^2 per °F	BTU/h-ft^2 per lb/ft^2-s	BTU/h-ft^2 per lb/ft^2	BTU/h-ft^2 per lb/ft^2-s
Water	330 for all	$2.0x10^6$	$1x10^6$	$6.7x10^5$
Fluid 1	330 for all	$1.0x10^6$	$0.8x10^6$	$3.6x10^5$
Fluid 2	330 for all	$0.6x10^6$	$0.25x10^6$	$3.8x10^5$

Future studies may make efforts to characterize the mass flux and droplet velocity variation across the sprayed surface in order to better define the mechanism of spray that affects heat transfer from a fluid spayed especially when sprayed at an angle. Additional tests conducted with the fluid sprayed at angles between 90°, 45°, and 10° may lead to a better understanding of how spray angle may affect spray efficiency. Further design of a larger heated surface with better protection against leaking would better capture surface temperature variations at locations encompassed by the entire cooling spray. This information would be valuable for use in optimizing spray cooling configurations to generate more uniform heat removal.

References

Automation Creations Inc., 2008, "MatWeb.Com," **2007-2008**.

Choi, K. J., and Yao, S. C., 1987, "Mechanisms of Film Boiling Heat Transfer of Normally Impacting Spray," International Journal of Heat and Mass Transfer, **30**(2) pp. 311.

Del Giudice, S., and Comini, G., 1979, "Dropwise Evaporation," Journal of Heat Transfer, **101**(3) pp. 441.

Faghri, A., and Zhang, Y., 2006, "Transport phenomena in multiphase systems," Elsevier, Burlington, MA.

Flir Systems, 2004, "ThermaCAM S65 Operation Manual."

FLIR Systems, Inc., 2005, "www.Flirthermography.com," **2007 - 2008**.

Freund, S., Pautsch, A. G., Shedd, T. A., 2007, "Local Heat Transfer Coefficients in Spray Cooling Systems Measured with Temperature Oscillation IR Thermography," International Journal of Heat and Mass Transfer, **50**(9) pp. 1953.

Ghodbane, M., Holman, J.P. 1991, "Experimental Study of Spray Cooling with Freon-113," International Journal of Heat and Mass Transfer, **34**(4) pp. 1163.

Goodfellow, 2008, "www.Goodfellow.com," **2007-2008** pp. Alloy - Electrical Properties.

Grissom, W. M., Wierum, F.A., 1981, "Liquid Spray Cooling of a Heated Surface," International Journal of Heat and Mass Transfer, **24**(2) pp. 261.

Horacek, B., Kiger K.T., Kim J., 2005, "Single Nozzle Spray Cooling Heat Transfer Mechanisms," International Journal of Heat and Mass Transfer, **48**(8) pp. 1425.

Incropera, F.P., and DeWitt, D.P., 2002, "Fundamentals of Heat and Mass Transfer," John Wiley & Sons, United States, pp. 981-907,916.

Isachenko, V. P., Kushnyrev, V.I., Gorin, S.V., 1979, "Experimental Study of Heat Transfer in Cooling of a Vertical Surface by a Liquid Spray," Heat Transfer: Soviet Research, **11**(4) pp. 142.

Jia, W., and Qiu, H., 2003, "Experimental Investigation of Droplet Dynamics and Heat Transfer in Spray Cooling," Experimental Thermal and Fluid Science, **27**(7) pp. 829.

Lin, L., Ponnappan, R., 2003, "Heat Transfer Characteristics of Spray Cooling in a Closed Loop," International Journal of Heat and Mass Transfer, **46**(20) pp. 3737.

Liu, Z., Wang, J, 2000, "Study of Film Boiling Heat Transfer for Water Jet Impinging on High Temperature Flat Plate," International Journal of Heat and Mass Transfer, **44**(13) pp. 2475.

Moriyama, A., Araki, A., Yamagami, M., Mase, K., 1987, "LOCAL HEAT-TRANSFER COEFFICIENT IN SPRAY COOLING OF HOT SURFACE." Transactions of the Iron and Steel Institute of Japan, **28**(2) pp. 104.

Mudawar, I., and Valentine, W. S., 1989, "Determination of the Local Quench Curve for Spray-Cooled Metallic SurfacesJ," Journal of Heat Transfer, **7**(2) pp. 107-107-121.

Pais, M. R., Chow, J.C., Mahefkey, E.T., 1992, "Surface Roughness and its Effects on the Heat Transfer Mechanism in Spray Cooling," Journal of Heat Transfer, **114**(1) pp. 211.

Qiao, Y. M., and Chandra, S., 1997, "Experiments on Adding a Surfactant to Water Drops Boiling on a Hot Surface," Proceedings: Mathematical, Physical and Engineering Sciences, **453**(1959) pp. 673-689.

Sargent, S. R., Hedlund, C.R., Ligrani, P.M., 1998, "An Infrared Thermography Imaging System for Convective Heat Transfer Measurements in Complex Flows," Measurement Science Technology, **9**(12) pp. 1974.

Schaff, F., 2000, "Beyond the Visible: The ABCs of IR," Photonics Spectra, **34**(4) pp. 146.

Schmidt, J., Boye, H., 2001, "Influence of Velocity and Size of the Droplets on the Heat Transfer in Spray Cooling," Chemical Engineering Technology, **24**(3) pp. 255.

Silk, E. A., Kim, J., Kiger, K., 2006, "Spray Cooling of Enhanced Surfaces: Impact of Structured Surface Geometry and Spray Axis Inclination," International Journal of Heat and Mass Transfer, **49**(25) pp. 4910.

Webb, B. W., Queiroz, M., Oliphant, K,N., Bonin, M.P., 1992, "Onset of Dry-Wall Heat Transfer in Low-Mass-Flux Spray Cooling," Experimental Heat Transfer, **5**(1) pp. 33.

Yao, S. C., Cox, T.L., 2002, "A General Heat Transfer Correlation for Impacting Water Sprays on High-Temperature Surfaces," Experimental Heat Transfer, **15**(4) pp. 207.

APPENDIX A - Experimental Determination of NiChrome Properties, Assumption Validation Analysis, and Uncertainty Estimations

A.1 Experimental Determination of NiChrome Surface Emissivity as a Function of Surface Temperature

To capture accurate temperature measurements using IR thermography, it was necessary to determine the emissivity of the surface whose temperature is to be recorded. In this case, the NiChrome filament emissivity needed to be determined. Emissivity is found to be dependent on surface temperature, so it is necessary to complete an emissivity study that captures the surface emissivity starting from room temperature up to maximum temperature of interest, 550°F.

Misconceptions with Flir Infrared Camera

Initial testing with the Flir ThermaCAM S65 IR Camera used the visual display as output. An example of the visual display output is seen in Figure A.1. Videos of the display were recorded in grayscale so that individual pixels in each frame could be represented by a single value. The video files were delimitated into frames. The value of the pixel was correlated to a temperature value based on a linear fit between the high and low temperature values labeled on the linear grayscale at the right of the screen. Temperatures recorded in this manner were found to be unrepeatable. Flir representatives provided further explanation: Flir post-processing software must be utilized in order for the grayscale at the right to be linear with temperature and a reflected temperature must be established in order to take into account the IR sensor reflecting its own temperature in the observed metal.

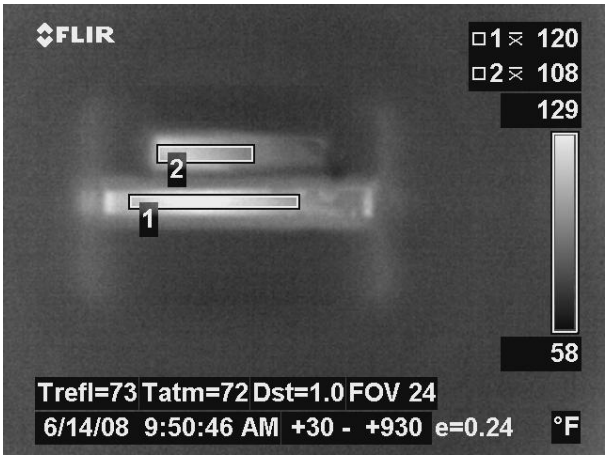

Figure A.1 Example of IR camera screen output

Flir's freeware, QuickVIEW, was obtained and used in future testing so that the temperatures were correctly represented by the pixel color value. In order to use the freeware, it was necessary that images be collected and saved using the camera so the images were in the proper format to be manipulated with the software. Video could not be used because the standard jpeg format does not allow parameter changes with QuickVIEW. Additionally, a metallic strip with very low emissivity was attached to a Teflon insert in the heated assembly as seen in Figure A.2. The metallic strip was placed so that the temperature reflected by the strip would represent the reflected temperature of the IR sensor in the NiChrome Filament. All other surfaces were painted with high heat flat black spray paint.

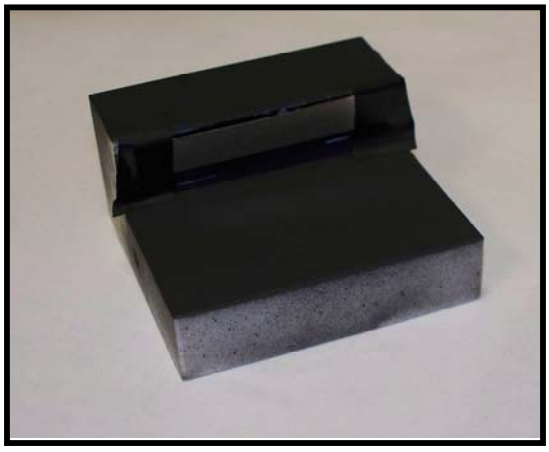

Figure A.2 Metallic strip placed on Teflon to establish a reflected temperature.

Emissivity Data Collection

Once camera operation and interpretation were understood, data collection could be completed and used to determine surface emissivity as a function of surface temperature. Heating the NiChrome to a known temperature and then adjusting the emissivity setting in the camera until the temperature measured with the camera equaled the known temperature would determine surface emissivity.

A copper block heated with cartridge heaters with a fin used to create a uniform temperature at the fin surface seen in Figure A.3 was used to heat the NiChrome. The face of the fin was placed so that it sat flush with the top of the NiChrome strip placed in the heated surface assembly. Insulation was applied to all other surfaces of the copper and an insulatory weight was used to supply contact pressure between the copper and the NiChrome.

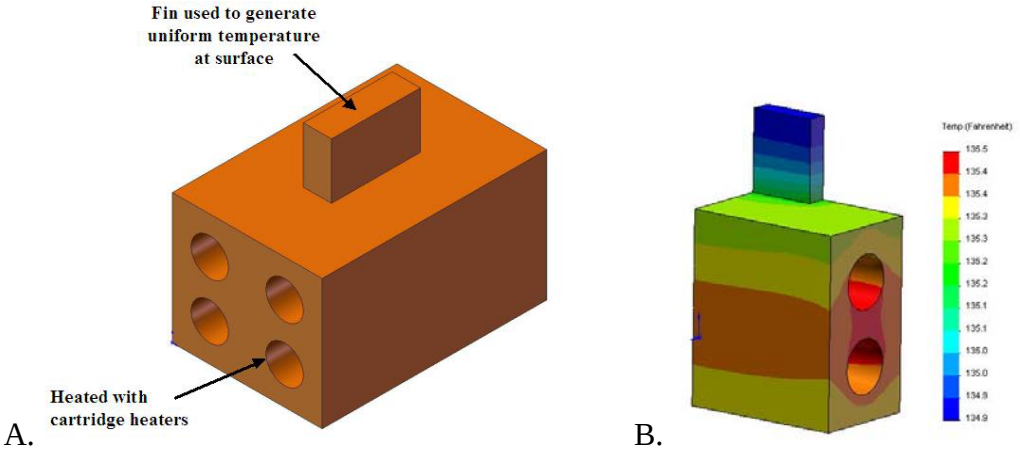

Figure A.3 (A)A solid model model of finned copper clock used to generate a uniform surface temperature (B) ANSYS model showing 1D conduction through fin of copper block.

Two 36-gage type K glass insulated thermocouples were welded intrinsically to the viewed surface of the NiChrome so that a temperature could be observed between the two leads as seen in Figure A.4. Using the QuickVIEW freeware, an area was defined to observe the average reflected temperature seen in the non-heated metallic surface. The reflected temperature parameter was adjusted so that the average temperature reflected by the non-heated metallic strip was equal to the set parameter. Two points were selected within the corresponding thermocouple leads. Emissivity was adjusted individually for each point represented by each

thermocouple so that the recorded temperature was equal to the average temperature recorded by the thermocouple at that time within ±0.5°F.

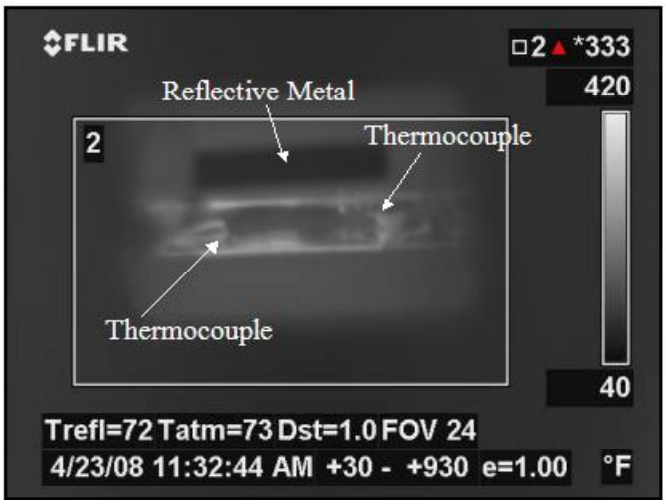

Figure A.4 IR image of intrinsically mounted thermocouples used to determine NiChrome surface emissivity.

Looking at Figure A.4 closely, it is evident that the thermocouple lead placement is clearer for the thermocouple to the left of the image compared to that on the right side. Additionally, the fin surface is dimensionally shorter than the entire NiChrome surface so the most uniform temperature is found in the area of direct contact. Emissivity values associated with temperatures recorded from left thermocouple were used to develop the emissivity correlation as a function of surface temperature. A total of five tests were completed in the described fashion. Figure A.5 is a graph of all the recorded data. The data suggest that the surface emissivity at lower surface temperatures is higher (approximately 0.50) compared to higher surface temperatures (approximately 0.25). The change in emissivity as surface temperature is increased is significant over the surface temperatures from 130°F to 200°F then begins to lessen and becomes asymptotic to 0.25 around 300°F. This value follows the reported emissivity of 0.25 for rolled NiChrome (Flir Manual, 2004).

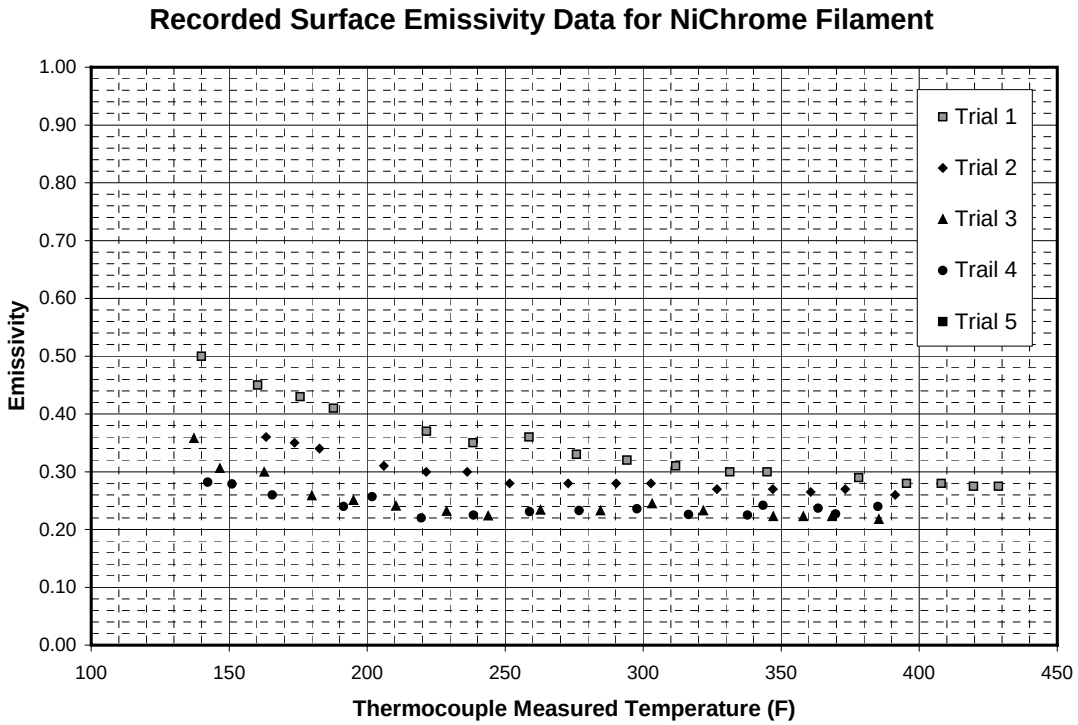

Figure A.5 Data plot of emissivity vs surface temperature.

NiChrome Emissivity Correlation Results

Collected data with the exception of Trial 1 (which was negated due to the testing being conducted on a previously non-heated NiChrome strip) and data points recorded near room temperature were used to determine a correlation that relates surface emissivity to surface temperature. A correlation to fit the data's trend was developed in the form of

$$\varepsilon = A - (A-B)*e^{(-T/\tau)} \qquad \text{Eqn A.1}$$

and least square fit was used to determine constants A, B, and τ while ε is the determined emissivity and T is the recorded surface temperature recorded by the thermocouple. A plot of the correlated equation fit and associated uncertainty is shown in Figure A.6.

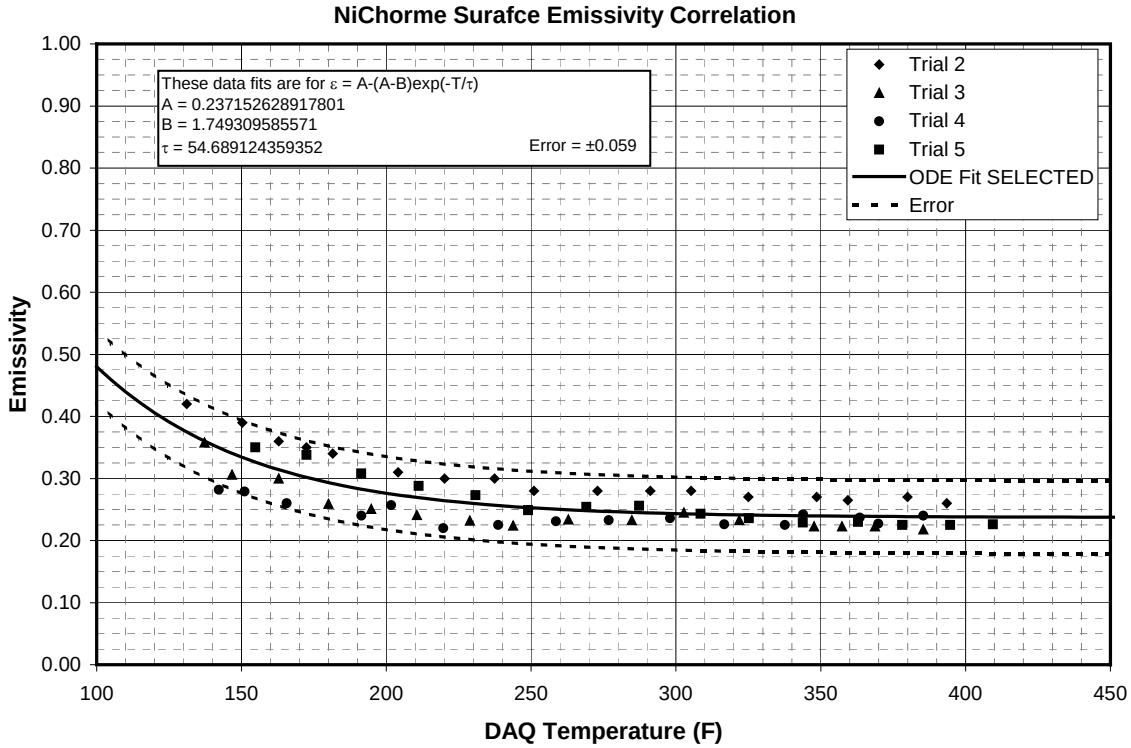

Figure A.6 NiChrome surface emissivity correlation and associated error.

The uncertainty estimated and plotted in Figure A.6 is highly influenced by data collected at surface temperatures below 200°F. Therefore uncertainty estimates for this analysis use an uncertainty value of 0.059 for surface temperatures from 130°F to 200°F, 0.0375 from 200°F to 250°F, and 0.025 for surface temperatures measured above 250°F even though the calibration curve was fit using all the collected data.

A.2 The Use of a Quasi-Steady State Model for Local Heat Transfer

A quasi-steady state model is employed for this analysis because the time constant associated with the heat removed by spray cooling is much higher than that experienced from other forms of heat transfer. An analysis was completed to determine the effective time constant associated with conduction heat transfer, convective heat transfer and an effective heat transfer coefficient was developed for the spray cooling heat transfer.

A time constant for conduction heat transfer can be determined by

$$\tau = \frac{mc_p L}{kA} \qquad \text{Eqn A.2}$$

and an associated time constant assuming a first-order response for a hot surface exposed to convection heat transfer is

$$\tau = \frac{mc_p}{hA} \qquad \text{Eqn A.3}$$

Employing this model using a representative high and low value for the heat transfer coefficients determined for natural convection from a surface facing downward and using an effective heat transfer coefficient for spray cooling defined as

$$h_{spray} \equiv \frac{Q''_{Spray}}{(T_{surface} - T_{fluid})} \qquad \text{Eqn A.4}$$

Calculations based upon Eqns. A.2 through A.4 are summarized below.

NiChrome Properties

Density: 8400 kg/m3

Specific Heat: 450 J/kg-K

Thermal Conductivity: 13.4 W/m-K

Thickness: 0.000125m

Area: 0.0403225m^2

Free Convection Heat Transfer Coefficient

High Value: 129.7 W/m^2-k

Low Value: 9.0 W/m^2-k

Effective Spray Cooling Heat Transfer Coefficient

High Value 2805.5 W/m^2-k

Low Value 158.8 W/m^2-k

Conductivity Time Constant (***5x Time Constant)***

1.79 s (8.96 s)

Free Convection Time Constant		*(5x Time Constant)*
3.64	s	(18.21 s)
52.22	s	(261.12s)
Spray Cooling Time Constant		***(5x Time Constant)***
0.17	s	(0.84 s)
2.97	s	(14.87 s)

If it estimated that 5 times constants are needed to achieve steady state, all values reach 5 time constants in less than 20 seconds with the exception of free convection at high heat transfer coefficient values that occur at high surface temperatures where the magnitude of heat transfer to free convection is much less than that of spray cooling so any transient effects are negligible.

A.3 Analysis to Support Neglecting Conduction Heat Transfer in the Local Heat Transfer Model

Conduction heat losses are assumed negligible for experimental testing. This assumption is based upon results generated from a preliminary test where the NiChrome filament was heated and no spray cooling was applied. Instead, the spray surface was insulated with an approximately 0.25” thick piece of fiberglass high temperature insulation. IR images were captured at several power levels after the system was allowed to time to reach steady state. Processed images were then used to ascertain a coordinating conduction heat flux for each individual pixel within the NiChrome filament. Figure A.7 is a surface plot that depicts the total magnitude of heat flux per pixel. The majority of pixels were found to experience less than 0.04W conduction heat loss with a maximum total heat loss of 0.24W at the upper boundary of the surface where pixel temperature values are not applied to overall results.

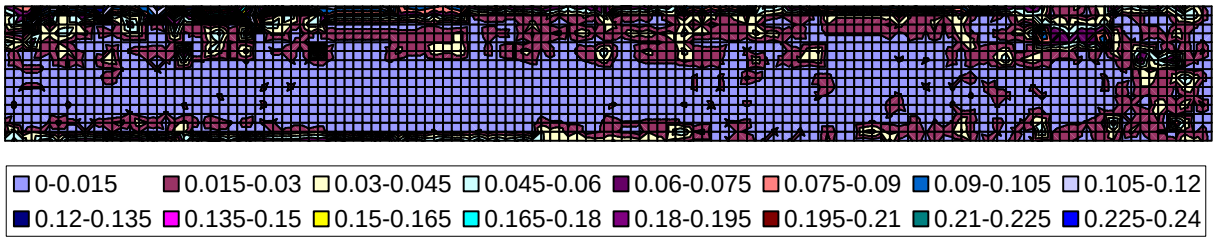

Figure A.1: Total conduction heat loss per pixel (in Watts) for NiChrome at approximately 345°F.

The calculated convection and radiation heat loss from the view surface based upon the above-mentioned correlations for the above image were 0.268W and 0.164W, respectively for an associated 0.25" x 2" area. In comparison to the magnitude of these heat loss values in addition to the magnitude of generated heat (11W), the heat loss associated with conduction is considered negligible. Therefore the equation for local heat transfer during spray cooling in the experimental set up can be written as

$$q''_{spray} = q''_{generated} - q''_{radiation,bottom} - q''_{radiation,top} - q''_{convection} \qquad \text{Eqn A.5}$$

A.4 Calculations Used to Estimate Uncertainty

The estimated uncertainty for the data reported has been determined in the following manner.

Estimated uncertainty in heat flux removed by spray cooling:

$$Q''_{spray} = Q''_{Gen} - Q''_{Rad} - Q''_{Conv} \qquad \text{Eqn A.6}$$

$$Q''_{Spray} = \left(\frac{I^2 R'}{w}\right) - \left(\sigma\varepsilon\left(T^4_{Surface} - T^4_{Fluid}\right) + \sigma\varepsilon\left(T^4_{Surface} - T^4_{\text{Re flected}}\right)\right) - \left(\left[\frac{\left(0.27\frac{g\left(\frac{2}{T_{Surface}+T_{\text{Re flected}}}\right)\left(T_{Surfaec}-T_{\text{Re flected}}\right)w^3}{\nu\alpha}\right)k_f}{w}\right]\left(T_{Surface} - T_{\text{Re flected}}\right)\right) \qquad \text{Eqn A.7}$$

Power Generation

Applied Current:

Standard Equipment Error: Values range from 0.675A at 5A to 3.125A at 75A

$$\pm 0.035 * \text{measurement} + 0.5 \qquad \text{Eqn A.8}$$

DAQ Error: 10 volt range on a rounding 16 bit card

$$u_{DAQ} = \frac{10}{2^{17}}\left(1000\,\tfrac{\text{A}}{\text{V}}\right) = \pm 0.076\text{A} \qquad \text{Eqn A.9}$$

Averaging: The current is measured by the DAQ so that 10,000 measurements are recorded at a frequency of 50,000Hz and the average and standard deviations are reported. Figure A.1a shows how the applied current is varied over the length of a single test. Figure A.1b shows how the measured current varies is a single power level of that test. The standard

deviation (A.1b) associated with a single power level is relatively equal to the average standard deviation of current for the entire test (A.1c). Further, the average standard deviation associated with a single test is consistent with the average standard deviation for all tests shown in Figure A.2. Therefore, the estimated uncertainty associated with applied current is approximated by the average of the test average standard deviation multiplied by the 95% confidence interval for 10,000 data points with one degree of freedom.

$$u_{i,avg} = 0.47 * t_{95,9999} = \pm 0.89\text{A} \qquad \text{Eqn. A.10}$$

The total estimated uncertainty associated with applied current is determined as the root sum square of the standard equipment error (at 20A), DAQ error, and averaging error:

$$u_{current} = \sqrt{1.2^2 + 0.076^2 + 0.89^2} = \pm 1.50\text{A} \qquad \text{Eqn A.11}$$

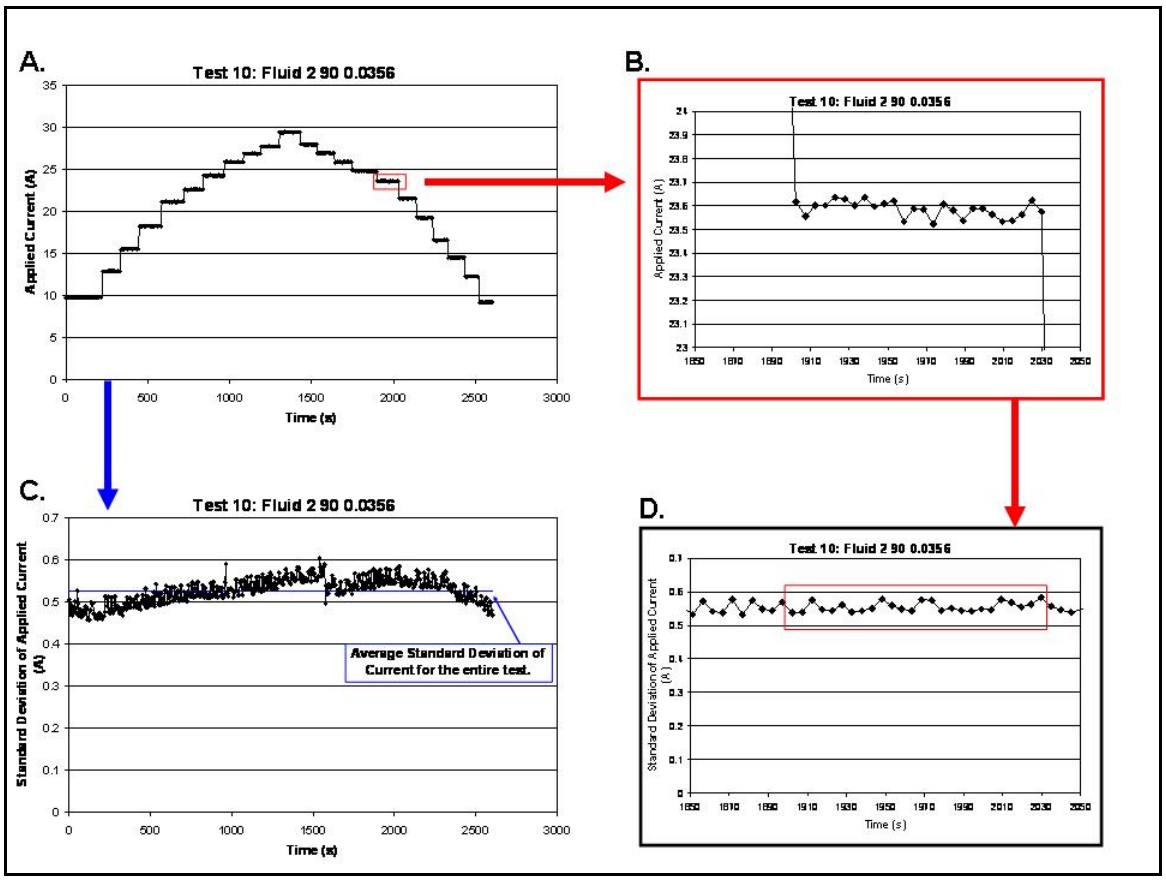

Figure A.2 Depiction of standard deviation of applied current for one test

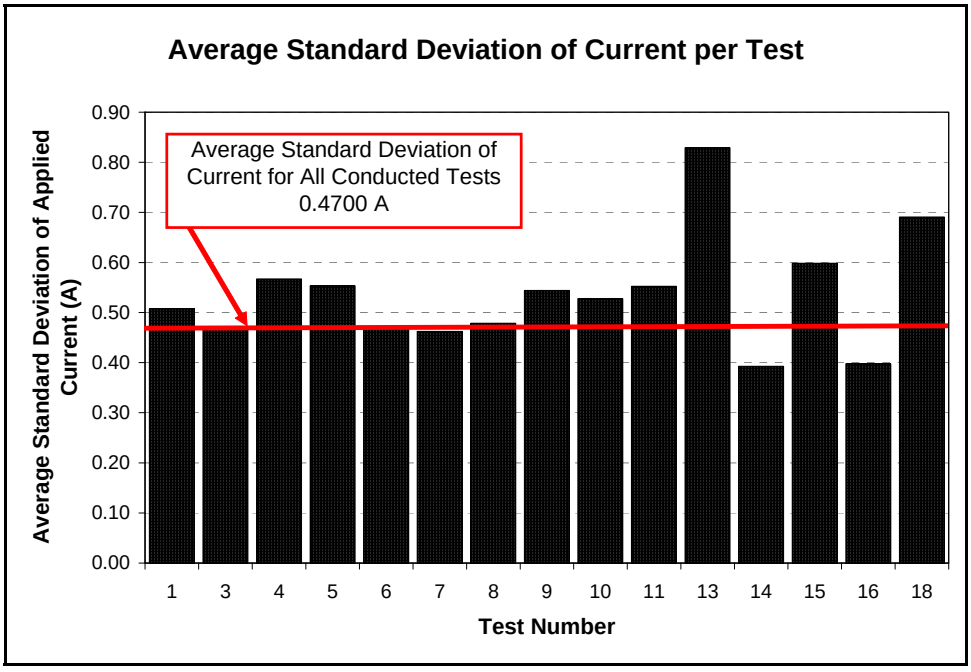

Figure A.3 Average standard deviation of applied current for all tests

Filaments Width:

Measurements were collected after the filaments were sheared to characterize the average filament width. The width was recorded for each filament in three locations: at the center and approximately 1 inch from the center in either direction. The measurements were then averaged to find an average filament width of 0.3151 inches and an associated standard deviation of 0.006776 inches.

Table A.1Width measurement recorded for NiChrome filaments used in testing

Strip	Left	Middle	Right	Average	
6/14	0.3250	0.3235	0.3225	0.3237	
6/16	0.3150	0.3130	0.3110	0.3130	
6/17	0.3350	0.3305	0.3275	0.3310	
6/19	0.3085	0.3100	0.3140	0.3108	
6/21(1)	0.3285	0.3195	0.3100	0.3193	
6/21(2)	0.3165	0.3130	0.3070	0.3122	
6/22	0.3160	0.3150	0.3130	0.3147	
6/23(1)	0.3020	0.3010	0.3010	0.3013	
6/23(2)	0.3150	0.3150	0.3145	0.3148	
10/6(1)	0.3185	0.3210	0.3195	0.3197	
10/6(2)	0.3080	0.3140	0.3180	0.3133	
10/24	0.3030	0.3075	0.3085	0.3063	
11/4	0.3165	0.3135	0.3100	0.3133	
Unlabeled 1	0.3090	0.3120	0.3100	0.3103	
Unlabeled 2	0.3160	0.3230	0.3310	0.3233	
Unlabeled 3	0.3185	0.3175	0.3180	0.3180	
Unlabeled 4	0.3145	0.3125	0.3080	0.3117	
Unlabeled 5	0.3125	0.3140	0.3160	0.3142	
			Avg	**0.3151**	**in**
			St Dev	**0.006776**	**in**
			Uncertainty	**0.014297**	**in**

The estimated uncertainty associated with width is approximated by

$$u_w = 0.3151 * t_{95,17} = \pm 0.0143 \,\text{inches} \qquad \text{Eqn. A.12}$$

Resistance per Unit Length:

Manufacturer provided information (www.goodfellow.com) lists the volumetric resistance of the NiChrome sheet as 0.000108 Ω-cm. Resistance per unit length was determined by multiplying the volumetric resistance by the filaments average width and thickness:

$$R' = \frac{\rho}{wt} = 0.027 \frac{\Omega}{in} \qquad \text{Eqn A.13}$$

Resistances were also measured at various lengths across the previously used NiChorme filaments and one un-used strips. The change in resistance over length was determined as the linear slope of the total measured resistance with length as seen in Figure A.4. There are uncertainties associated with this test, but the measured values show a range in resistance per unit length from 0.026 to 0.029 Ω pre inch. Therefore, the uncertainty associated with using the manufacturer specifications for volumetric resistance will be estimated as half the difference between the measured data or ±0.0015 Ω/in.

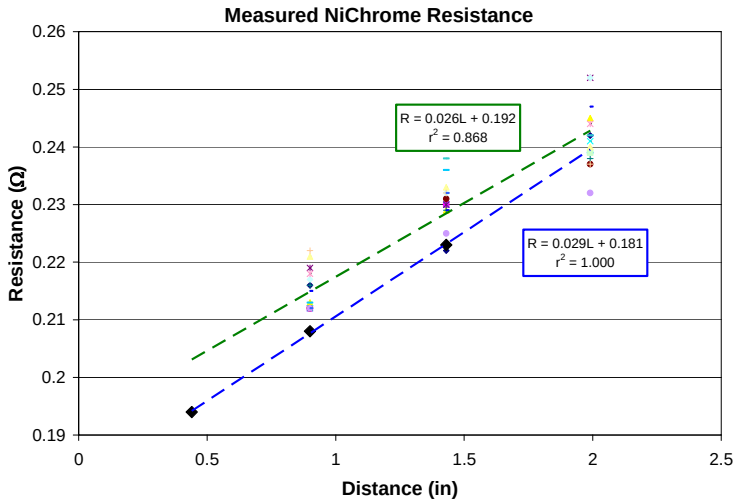

Figure A.4 Measured resistance of NiChrome filaments at varied lengths

The volumetric change in resistance due to changes in temperature is listed as 0.00005 μΩ-cm per Kelvin, which is considered to be negligible.

It follows that the total uncertainty associated with generated power is estimated as

$$\mu_{Q,gen} = \sqrt{(2 * \mu_i)^2 + (\mu_w)^2 + (\mu_{R'})^2} = 17.00\% \qquad \text{Eqn A.14}$$

where μ is the uncertainty expressed as a percentage of the nominal values 10A, 0.3151in, and 0.027Ω/in respectively. Values range from 45.6% at 5A to 11.8% at 75A.

Radiation Heat Transfer

Heat lost to radiation is calculated as

$$q''_{Rad} = \varepsilon\sigma\left(T^4_{Surface} - T^4_{\text{Referance}}\right) \qquad \text{Eqn A.15}$$

Surface Temperature

Surface temperature is the nodal temperature averaging the value of 9 pixels. The surface temperature is subject to a standard error from the IR camera, temperature difference through the thickness of the NiChrome filament, and errors associated with emissivity and range settings used in QuickVIEW post processing.

The Flir ThermaCAM S65 IR camera reports a standard error of a minimum of ±3.6°F or ±2% of the measurement, which is ±5.36°F at 300°F.

The temperature gradient through the NiChrome discussed in Chapter 3 is ±5.4°F.

The effect of associated error in emissivity and reflected temperature was determined experimentally by selecting a point on a processed IR image within the QuickVIEW software and changing the settings. The difference between new temperature and the processed temperature was then averages for both the high and low emissivity and reflected temperature values. Table A.2 lists the values.

Table A.2 Surface temperature error associated with emissivity calibration and reflected temperature

Nodal Temperature (°F)	Emissivity				Reflected Temperature				Total %
	High	Low	Avg	%	High	Low	Avg	%	
110	111.2	108.7	1.3	1.1	104.7	114.9	5.1	4.6	4.8
322	341.2	305.9	17.7	5.5	313.8	329.8	8.0	2.5	6.0
796.8	854.3	748.9	52.7	6.6	792.1	801.4	4.6	0.6	6.6

The high and low emissivity values were determined by considering the standard error of the IR camera, error associated with the thermocouples used when determining emissivity, and the calibration fit of ±0.025. The high and low reflected temperatures were determined as ±5°F from the original value base on the general observed 10°F temperature difference seen across the reflective strip. A general uncertainty of ±6% is assumed for this analysis.

The effect of averaging the 9 pixels is at most 5% because the post-processing code ignores any data points that do not meet this criterion. The average percentage of the using 9 pixels to form a nodal temperature over the nodal temperature is plotted in Figure A.5, below.

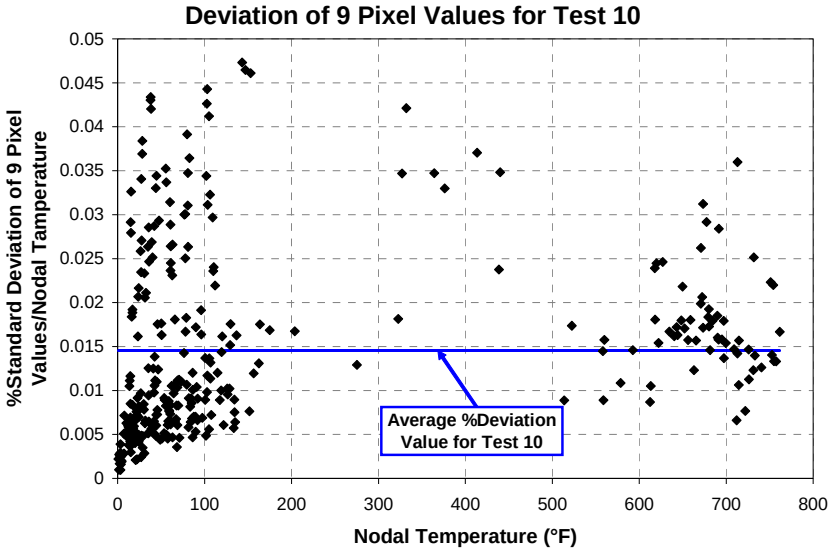

Figure A.5 Standard deviation of averaging 9 pixel values over recorded temperature for one test

The average percentage of the standard deviation associated with averaging 9 pixel values over the surface temperature measurement was recorded for all tests and is listed in Table A.3. The average ±1.42% is used to complete the analysis. The associated uncertainty is determined as

$$\mu_{9,node} = 1.42 * t_{95,8} = \pm 3.3\% \qquad \text{Eqn A.16}$$

Table A.3 Percentage of standard deviation associated with averaging 9 pixels over the recorded surface temperature per test

Test #	%Std/Temp
1	1.34
3	1.36
4	2.02
5	1.73
6	1.00
7	1.87
8	1.33
9	1.21
10	1.45
11	1.94
13	1.25
14	1.49
15	0.80
16	1.40
17	1.20
18	1.24
Average	1.42

Additionally, there is an uncertainty related to the scaling of pixel values to temperatures since pixels can only have integer values from 0 to 255. The pixelation of an image is determined as the temperature range divided by the pixel value associated with the max minus the pixel value associated with the minimum. The percentage of pixelation over the average recorded temperature value ranges from .1% to .6% as shown in Figure A.6.

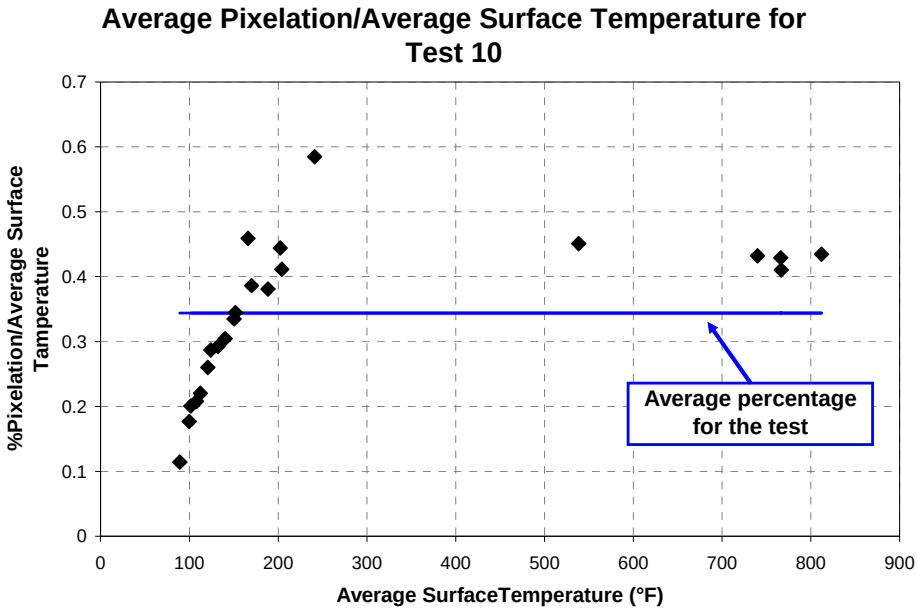

Figure A.6 Percentage of pixelation over average surface temperature for Test 10

The average value has been recorded for each test (Figure A.7) and the overall average is the estimated uncertainty. The associated uncertainty is ±0.034%.

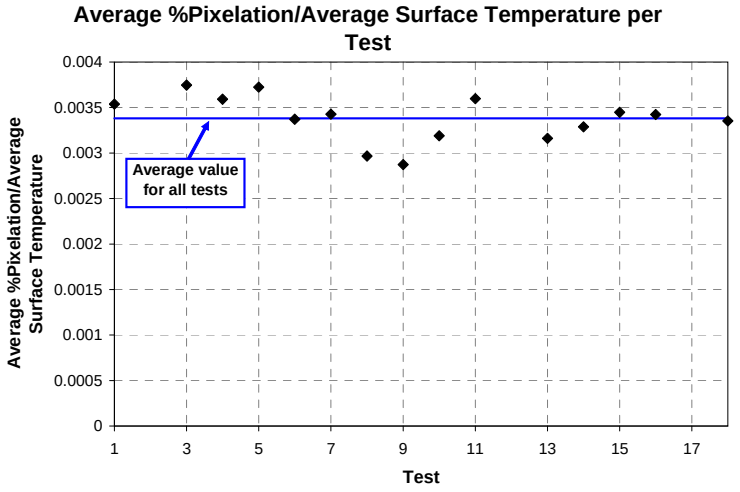

Figure A.7Average percent pixelation over average surface temperature per test

So the uncertainty associated with the surface temperature is the root sum square of the IR camera standard error, the temperature measurement errors associated with emissivity and

reflected temperature, the error associated with using a 9-pixel average, and the pixelation error. The total uncertainty in measured surface temperature is

$$\mu_{Tsurface} = \sqrt{\left(\frac{u_{IRcamera}}{300}\right)^2 + \left(\mu_{e,Trefl}\right)^2 + \left(\mu_{9\,pixel}\right)^2 + \left(\mu_{pixelation}\right)^2} = 14.8\% \qquad \text{Eqn. A.17}$$

Fluid Temperature

The estimated uncertainty associated with the spray fluid temperature is determined based upon the standard error from the flow meter that measures the temperature and the error associated with the DAQ equipment. The flow meter reports an error of ±(1+0.5%*measurement, °C) which is ±2°F at 80°F. The DAQ uses a 10 volt range and a rounding 16 bit converter so using the calibration of 17.36°F/V generates and associated uncertainty of ±0.001°F and, therefore assumed negligible. The total uncertainty is estimated as the flow meter uncertainty.

Reflected Temperature

The uncertainty associated with reflected temperature is ±5°F as discussed when determining the surface temperature uncertainty.

Surface Emissivity

The uncertainty associated with emissivity is estimated to be ±0.025 as discussed in section A.1 of Appendix A.The overall uncertainty for radiation heat transfer was determined by applying the uncertainties to nominal values for a surface at 300° radiating to 80°F (fluid temperature) and 90°F (reflected temperature) and then determining the average percent change of the final values, respectively. These percentages were then used to determine the overall associated uncertainty of radiation heat loss adding an additional term of 20% to account for assumptions made in using the fluid and reflected temperatures as the reference temperatures. This generates an uncertainty in radiation heat loss as approximately ±30%.

Convection Heat Transfer

The estimated uncertainty associated with the calculation of convection heat transfer is based upon a surface uncertainty of ±14.8%, a reflected temperature uncertainty of ±5°F, and the estimated correlation uncertainty of ±30%. The uncertainty associated with the correlation was increased to ±50% to account for the difference in the application: the surface is not open for air to flow around the ends and the value is used as a local heat transfer coefficient instead of the intended average heat transfer coefficient. Because the magnitude of convection heat transfer is significantly less than the calculated spray cooling heat transfer, the total uncertainty has minimal effects. The convection heat transfer uncertainty is found by applying each uncertainty to nominal values of 300°F surface temperature and 90°F reflected temperature (having an associated heat transfer coefficient of 4.1W/m^2-K) then averaging the percent difference from the nominal value and taking the associated root sum square. This method estimates the total uncertainty in convection heat transfer to be ±53.5%, which is quite large, but the magnitude of heat lost to convection heat transfer is much smaller than the heat generated and the spray cooling heat flux.

Determining the Spray Cooling Heat Flux

It follows that the total estimated uncertainty to be associated with spray cooling heat flux values was determined by applying the individual uncertainties for heat generation, radiation heat loss, and convection heat loss to values extracted from experimental data at relatively low and high values in the range as shown in Table A.4. The maximum of the two is reported as ±17.9% for uncertainty of the spray cooling heat flux.

Table A.4 Calculations to determine uncertainty associated with spray cooling heat flux

	Q_conv (W/m^2)	Q_rad (W/m^2)	Q_applied (W/m^2)	Q_spray (W/m^2)
High Nominal Value	4047	5938	209210	199224

+	1.09%	1.07%	17.86%	17.93%
-	1.09%	1.07%	17.86%	
Low Nominal Value	5.5	7.3	5905	5893
+	0.05%	0.04%	17.04%	17.04%
-	0.05%	0.04%	17.04%	

Calculation of the Mass Flux

The test mass flux is calculated as the mass of the mass collector filled with collected fluid minus the mass of the empty mass collector divided by the inlet area and the collection time.

$$\dot{m}'' = \frac{m_{full} - m_{empty}}{At} \qquad \text{Eqn. A.18}$$

The balance used to determine the mass of the collector is assumed accurate to ±1.5g and the collection time is assumed accurate to approximately ±3s. To determine the uncertainty associated with the inlet area, the notion that some water droplets that impact the surrounding area may reflect into the collection. The inlet area was determined to be 0.452 square inches while the area of the surrounding structure was determined to be 0.544 square inches. If it is assumed that 25% of the outer structure reflects droplets into the collector, an uncertainty of 13.6% can be associated with the inlet area.

For most tests (with the exception of tests 13 – 16 because data was collect by alternate staff) mass was collected in trials before and after the spray data was collected and the average before was averaged with the average after and reported as the test mass flux. The standard deviation associated for trials before and after were then averaged and reported for each test and multiplied by the 95% confidence interval for 8 values with one degree of freedom. The average for all of the tests was then determined to be ±4.4%. The total mass flux uncertainty was defined as the root sum square of the calculated mass flux and the averaging of the trials, so that the total mass flux uncertainty is estimated to be ±14.8%.

APPENDIX B - All Measured Data

B.1 Summary of Collected Data

Table B.1 Summary table of parameter tested

Test #	Fluid	Spray Angle	Mass Flux (lb/ft^2-s)	Nozzle Distance from Center of NiChrome (inches)	Month	Day	Year
1	Water	90	0.0459	6.25	6	14	2008
3	Water	90	0.0272	10.50	6	16	2008
4	Water	90	0.0364	8.50	6	17	2008
5	Water	90	0.0349	8.50	6	18	2008
6	Fluid 1	90	0.0355	9.00	6	21	2008
7	Fluid 1	90	0.0266	11.00	6	21	2008
8	Fluid 1	90	0.0506	6.50	6	22	2008
9	Fluid 2	90	0.0465	9.00	6	23	2008
10	Fluid 2	90	0.0356	11.25	6	23	2008
11	Fluid 2	90	0.0240	16.75	6	23	2008
13	Water	45	0.0362	8.50	10	6	2008
14	Water	45	0.0446	8.50	10	6	2008
15	Water	45	0.0225	11.50	10	24	2008
16	Water	10	0.0215	6.25	10	24	2008
18	Water	10	0.0378	4.50	11	4	2008

- Where Spray angle is defined as the angle between the spray axis and the heated surface where spray normal to the surface as shown in Figure B.1 is 90.

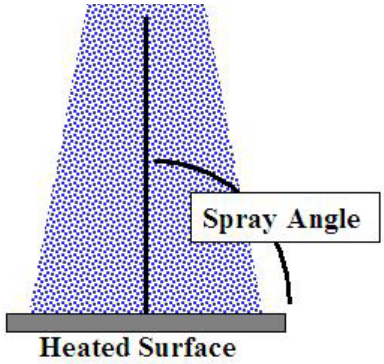

Figure B.1 Definition of spray angle

- Where Distance from Center of NiChrome is defined as the height for tests at 90° and the hypotenuse for tests at 45° or 10°.

- All heat flux is that calculated as removed by the spray in BTU/h-ft^2.
- All temperature measurements are ΔT ($T_{surface} - T_{fluid}$) in °F.

B.2 Test Data Summaries

Test 1

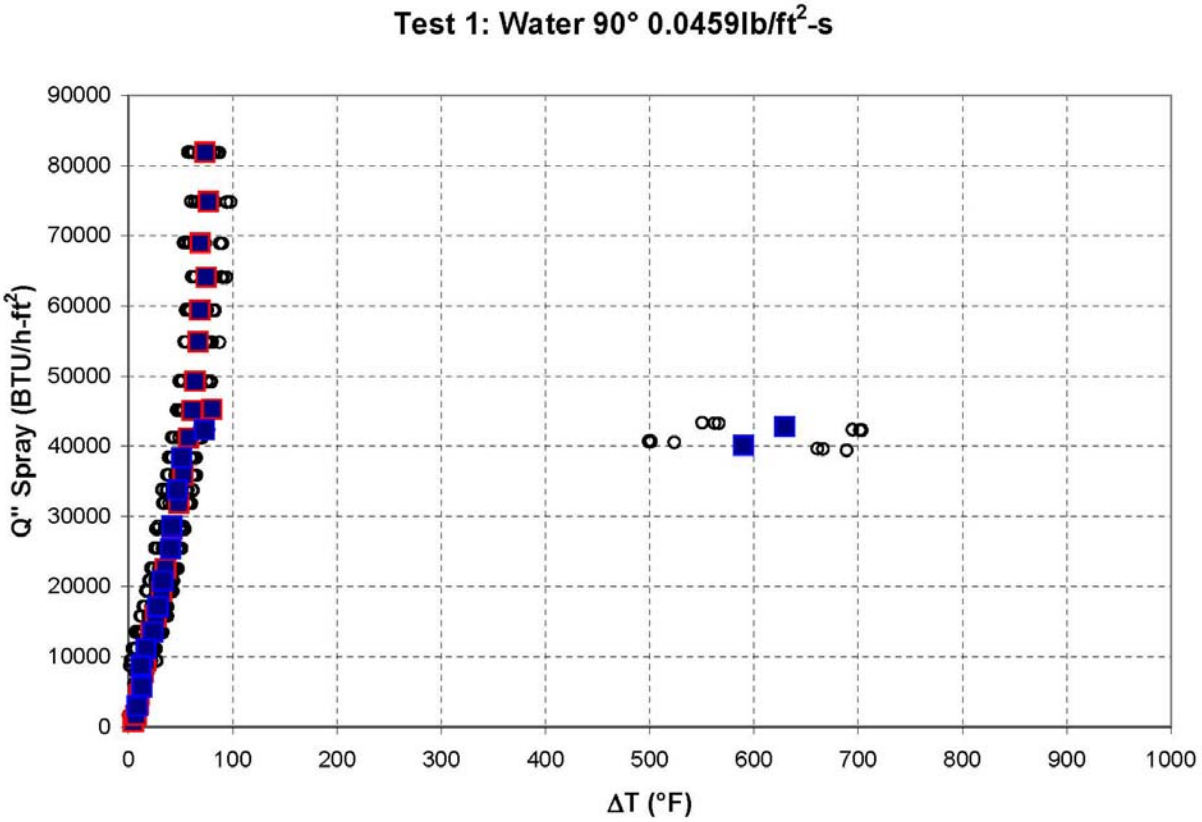

Figure B.2 Test 1 spray heat flux (BTU/h-ft^2) vs $T_{surface}$ - T_{liquid} (°F)

Table B.2 Test 1 summary data

Test	1		
Fluid	Water	**Avg Pressure (psi)**	22.3
Spray Angle	90	**Avg Fluid Temp (°F)**	82.4
Mass Flux (lb/ft^2-s)	0.0459	**Avg Flow Rate (GPM)**	0.202
Min Q"$_{spray}$ (BTU/h-ft^2)	743	**min ΔT (°F)**	4.7
Max Q"$_{spray}$ (BTU/h-ft^2)	81869	**max ΔT (°F)**	629.6
Q"$_{spray}$ before	81869	**ΔT before CHF (°F)**	73.6
Max possible Q"$_{spray}$	88609		

Table B.3 Test 1 nodal values

Step #	T_1 (°F)	Q''_1 (BTU/h-ft^2)	T_2 (°F)	Q''_2 (BTU/h-ft^2)	T3 (°F)	Q''_3 (BTU/h-ft^2)	T_4 (°F)	Q''_4 (BTU/h-ft^2)	T_5 (°F)	Q''_5 (BTU/h-ft^2)	T_{fluid} (°F)	T_{avg} (°F)	Q''_{avg} (BTU/h-ft^2)
1	3.8	745	0.0	0	5.6	741	-2.9	750	-7.4	750	80.2	4.7	743
2	7.2	1633	0.0	0	7.6	1632	-0.4	1644	-7.7	1644	80.6	7.4	1633
3	11.1	3057	0.0	0	10.7	3057	7.5	3065	-5.2	3075	80.9	9.8	3060
4	12.4	4547	0.0	0	11.8	4548	6.9	4559	-3.9	4566	81.3	10.4	4551
5	15.5	6143	0.0	0	14.9	6144	6.0	6164	-2.8	6168	81.6	12.1	6151
6	17.7	7730	0.0	0	16.5	7733	7.5	7753	-1.1	7758	82.0	13.9	7739
7	21.7	9426	26.7	9413	20.7	9429	12.1	9449	2.8	9463	82.4	16.8	9436
8	25.2	11079	0.0	0	23.2	11084	14.7	11104	4.0	11121	82.6	16.8	11097
9	27.1	13462	31.8	13450	26.2	13464	16.5	13487	7.3	13506	82.7	21.8	13474
10	32.8	15777	36.6	15767	29.9	15785	20.6	15807	12.2	15826	83.0	26.4	15793
11	37.5	19349	41.6	19338	35.8	19353	26.6	19376	17.5	19397	82.4	31.8	19363
12	42.7	22543	46.5	22533	38.7	22554	28.2	22580	22.2	22594	82.1	35.7	22561
13	49.8	28137	53.2	28127	42.5	28156	36.0	28172	27.1	28194	82.2	41.7	28157
14	57.1	31836	59.5	31830	49.7	31856	41.2	31878	34.0	31896	82.3	48.3	31859
15	61.8	35850	63.9	35844	54.8	35869	45.0	35894	37.7	35912	81.4	52.6	35874
16	68.6	41168	67.9	41170	58.8	41195	49.9	41218	42.6	41236	81.5	57.6	41197
17	73.3	45080	72.3	45083	61.5	45113	51.9	45138	47.4	45149	81.7	61.3	45113
18	79.0	49202	77.0	49207	63.7	49243	50.8	49277	49.2	49281	81.9	63.9	49242
19	79.5	54836	79.3	54837	67.7	54869	54.8	54902	54.0	54905	82.0	67.0	54870
20	74.8	59363	82.1	59343	70.6	59374	57.8	59408	57.0	59410	82.2	68.4	59380
21	81.0	64092	91.2	64064	76.2	64105	61.0	64145	63.2	64140	82.4	74.5	64109
22	73.0	68946	89.1	68901	67.8	68961	53.8	68997	60.2	68981	83.0	68.8	68957
23	82.1	74835	95.4	74798	80.1	74841	60.1	74894	65.7	74880	83.2	76.7	74849
24	86.4	81834	83.1	81843	75.8	81864	58.4	81910	64.3	81895	83.4	73.6	81869
25	80.1	45292	0.0	0	0.0	0	0.0	0	0.0	0	83.7	80.1	45292
125	0.0	0	0.0	0	0.0	0	559.5	43316	699.8	42299	83.7	629.6	42807
26	70.1	42340	75.8	42325	0.0	0	0.0	0	0.0	0	83.8	72.9	42333
126	0.0	0	0.0	0	0.0	0	507.9	40641	671.9	39534	83.8	589.9	40088
27	62.6	38335	61.5	38338	0.0	0	40.2	38391	40.2	38391	84.0	51.1	38364
28	57.7	33721	58.0	33720	0.0	0	38.7	33769	34.2	33780	84.0	47.2	33748
29	50.7	28529	52.0	28526	0.0	0	34.9	28568	29.1	28582	82.7	41.7	28551
30	47.9	25406	50.1	25400	42.8	25419	34.1	25441	26.7	25458	82.6	40.3	25425
31	39.7	20805	41.9	20799	35.7	20815	27.1	20836	20.6	20850	82.8	33.0	20821
32	34.9	17123	36.7	17118	31.1	17132	23.7	17150	15.3	17167	83.0	28.3	17138
33	30.0	13494	31.8	13490	26.5	13503	19.4	13519	10.5	13534	83.1	23.6	13508
34	0.0	0	0.0	0	24.8	11129	18.7	11143	7.0	11161	83.4	16.8	11144
35	0.0	0	0.0	0	19.7	8713	14.6	8724	2.3	8732	83.6	12.2	8723
36	14.7	5737	0.0	0	15.1	5736	9.4	5747	-2.3	5748	83.7	13.1	5740
37	8.5	2947	11.1	2942	9.5	2945	4.6	2949	-7.0	2948	83.8	8.4	2946

Test 3

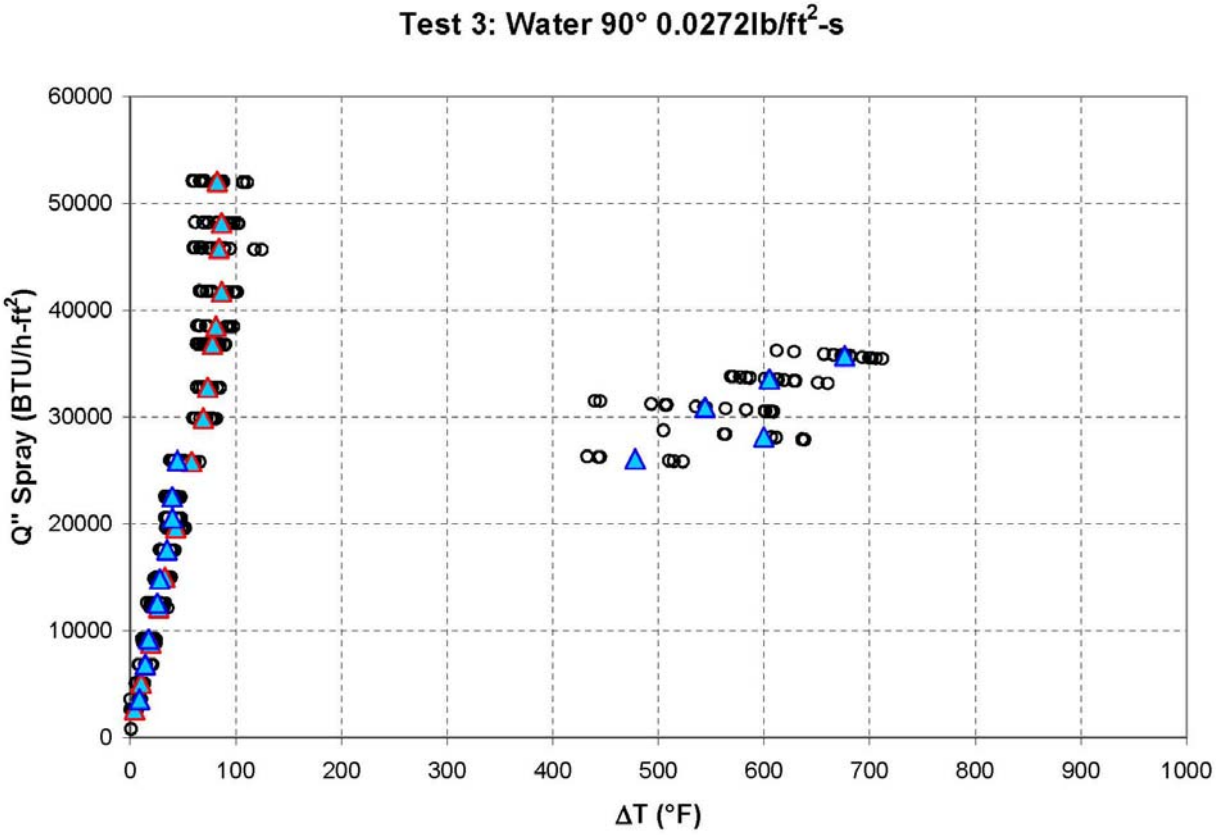

Figure B.3 Test 3 spray heat flux (BTU/h-ft^2) vs $T_{surface}$ - T_{liquid} (°F)

Table B.4 Test 3 summary data

Test	3		
Fluid	Water	**Avg Pressure (psi)**	21.9
Spray Angle	90	**Avg Fluid Temp (°F)**	82.0
Mass Flux (lb/ft^2-s)	0.0272	**Avg Flow Rate (GPM)**	0.197
Min Q"$_{spray}$ (BTU/h-ft^2)	2597	**min ΔT (°F)**	4.1
Max Q"$_{spray}$ (BTU/h-ft^2)	52052	**max ΔT (°F)**	676.4
Q"$_{spray}$ before	52052	**ΔT before CHF (°F)**	82.3
Max possible Q"$_{spray}$	53381		

Table B.5 Test 3 nodal values

Step #	T_1 (°F)	Q''_1 (BTU/h-ft^2)	T_2 (°F)	Q''_2 (BTU/h-ft^2)	T3 (°F)	Q''_3 (BTU/h-ft^2)	T_4 (°F)	Q''_4 (BTU/h-ft^2)	T_5 (°F)	Q''_5 (BTU/h-ft^2)	T_{fluid} (°F)	T_{avg} (°F)	Q''_{avg} (BTU/h-ft^2)
2	2.3	2602	4.1	2597	6.1	2592	3.8	2598	-0.6	2608	79.6	4.1	2597
3	10.4	5088	11.7	5085	13.0	5081	10.6	5087	5.7	5099	80.0	10.3	5088
4	19.5	8836	21.2	8831	23.5	8825	20.1	8834	13.3	8851	80.3	19.5	8836
5	27.5	12158	27.8	12157	31.7	12147	26.4	12161	21.0	12175	80.5	26.9	12160
6	34.1	14998	34.6	14997	37.2	14990	31.2	15006	27.4	15016	80.7	32.9	15001
7	45.1	19617	43.5	19621	49.0	19606	40.3	19629	38.0	19635	80.9	43.2	19622
8	62.5	25805	59.2	25814	60.5	25810	54.1	25828	54.3	25827	81.2	58.1	25817
9	80.3	29851	70.4	29879	72.0	29874	61.9	29902	61.2	29904	81.4	69.2	29882
10	74.1	32768	81.7	32746	77.7	32757	69.1	32781	63.9	32795	81.6	73.3	32770
11	83.9	36804	89.5	36788	81.8	36810	70.8	36840	64.1	36858	81.7	78.0	36820
12	0.0	0	92.3	38480	95.5	38471	72.4	38536	64.8	38556	81.9	81.3	38511
13	91.7	41733	99.0	41712	99.2	41711	75.3	41778	67.5	41799	82.1	86.5	41746
14	119.9	45688	90.7	45775	77.8	45811	69.6	45834	62.3	45853	82.3	84.1	45792
15	102.0	48124	95.1	48145	84.3	48176	75.3	48201	75.3	48200	82.6	86.4	48169
16	108.2	51978	86.7	52041	85.4	52044	69.5	52088	61.7	52109	82.8	82.3	52052
17	688.2	35642	704.5	35510	667.8	35804	683.5	35681	637.8	36026	83.0	676.4	35733
18	595.1	33620	626.9	33390	611.8	33504	599.1	33595	592.1	33641	83.1	605.0	33550
19	506.7	31133	529.8	30986	582.3	30677	599.3	30563	502.5	31169	83.3	544.1	30906
20	0.0	0	0.0	0	628.4	27955	627.5	27961	543.4	28519	83.4	599.8	28145
21	0.0	0	0.0	0	515.9	25865	440.1	26278	0.0	0	83.6	478.0	26071
22	0.0	0	49.0	25911	50.6	25907	38.2	25939	41.2	25931	83.7	44.7	25922
23	0.0	0	43.6	22513	45.4	22508	34.2	22536	35.6	22533	83.9	39.7	22523
24	0.0	0	44.5	20538	47.0	20531	33.7	20565	34.1	20564	84.1	39.8	20550
25	0.0	0	38.5	17544	41.7	17535	30.2	17564	28.8	17567	84.3	34.8	17553
26	0.0	0	30.3	14831	33.1	14824	25.2	14844	23.4	14849	84.4	28.0	14837
27	0.0	0	28.9	12570	32.5	12561	23.0	12584	18.5	12595	84.6	25.7	12577
28	0.0	0	18.7	9211	23.3	9200	16.3	9217	11.5	9228	84.1	17.5	9214
29	0.0	0	14.9	6832	20.0	6820	14.2	6833	8.3	6845	82.0	14.4	6832
30	0.0	0	9.3	3576	0.0	0	8.0	3579	-0.5	3584	81.9	8.6	3577

Test 4

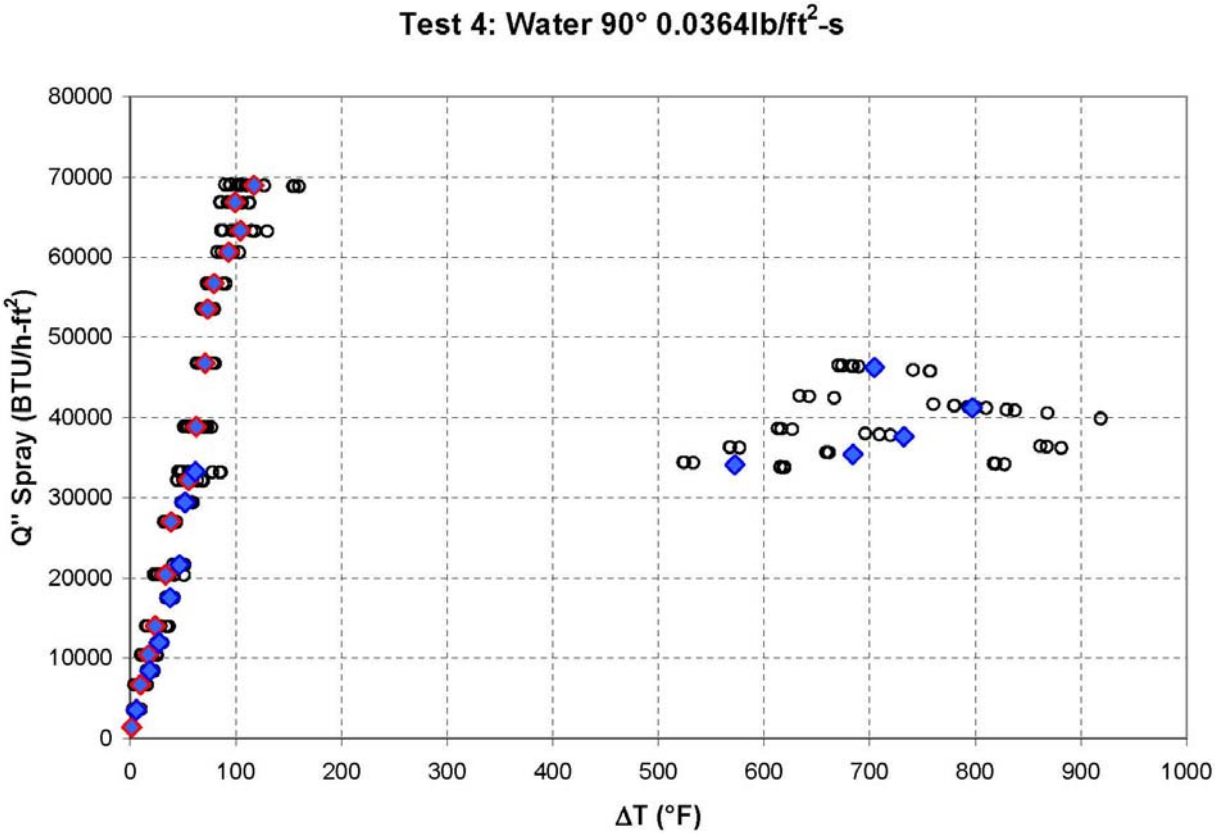

Figure B.4 Test 4 spray heat flux (BTU/h-ft^2) vs $T_{surface}$ - T_{liquid} (°F)

Table B.6 Test 4 summary data

Test	4		
Fluid	Water	**Avg Pressure (psi)**	22.1
Spray Angle	90	**Avg Fluid Temp (°F)**	80.4
Mass Flux (lb/ft^2-s)	0.0364	**Avg Flow Rate (GPM)**	0.199
Min Q"$_{spray}$ (BTU/h-ft^2)	1391	**min ΔT (°F)**	1.4
Max Q"$_{spray}$ (BTU/h-ft^2)	68956	**max ΔT (°F)**	797.1
Q"$_{spray}$ before	68956	**ΔT before CHF (°F)**	117.1
Max possible Q"$_{spray}$	76756		

Table B.7 Test 4 nodal values

		Q''_1		Q''_2		Q''_3		Q''_4		Q''_5			Q''_{avg}
Step #	T_1 (°F)	(BTU/h-ft^2)	T_2 (°F)	(BTU/h-ft^2)	T3 (°F)	(BTU/h-ft^2)	T_4 (°F)	(BTU/h-ft^2)	T_5 (°F)	(BTU/h-ft^2)	T_{fluid} (°F)	T_{avg} (°F)	(BTU/h-ft^2)
1	0.4	1393	1.7	1390	1.9	1389	-1.1	1396	-4.5	1398	78.3	1.4	1391
2	7.8	3625	5.7	3630	7.9	3625	3.0	3636	-0.5	3643	78.7	6.1	3629
3	0.0	0	11.4	6679	14.8	6670	8.5	6686	3.9	6697	79.0	9.7	6683
4	0.0	0	18.4	10406	23.8	10392	15.5	10413	10.5	10426	79.2	17.1	10409
5	0.0	0	24.3	14003	33.1	13979	21.5	14010	15.7	14025	79.4	23.6	14004
6	0.0	0	36.0	20402	43.4	20381	30.8	20416	24.3	20432	79.5	33.6	20408
7	0.0	0	43.5	26983	0.0	0	39.5	26994	32.6	27012	79.7	38.5	26996
8	0.0	0	59.0	32178	66.8	32155	50.8	32200	44.5	32217	79.9	55.3	32187
9	0.0	0	67.0	38825	73.4	38807	57.2	38852	52.3	38865	80.1	62.5	38837
10	0.0	0	78.6	46756	0.0	0	68.4	46784	65.6	46791	80.2	70.8	46777
11	0.0	0	78.2	53537	0.0	0	72.4	53553	69.2	53562	80.4	73.3	53551
12	0.0	0	80.2	56719	0.0	0	78.7	56723	78.9	56722	80.5	79.3	56721
13	0.0	0	96.0	60620	0.0	0	88.2	60642	95.0	60623	80.6	93.1	60628
14	103.8	63307	102.3	63311	111.5	63284	87.0	63354	116.7	63269	80.8	104.3	63305
15	110.0	66799	93.4	66846	98.8	66831	90.3	66855	104.4	66815	81.0	99.4	66829
16	156.3	68838	93.0	69026	0.0	0	103.5	68997	115.4	68963	81.1	117.1	68956
17	0.0	0	679.0	46458	0.0	0	682.7	46428	751.7	45843	81.3	704.5	46243
18	806.7	41218	647.5	42596	777.7	41500	835.2	40923	918.6	39892	81.4	797.1	41226
19	0.0	0	0.0	0	618.6	38595	708.2	37907	870.1	36340	81.5	732.3	37614
20	0.0	0	0.0	0	570.7	36292	660.2	35662	821.3	34233	81.6	684.1	35396
21	0.0	0	0.0	0	527.0	34403	617.7	33816	0.0	0	81.7	572.3	34109
22	0.0	0	47.0	33283	56.2	33260	60.7	33247	82.8	33185	81.8	61.7	33244
23	0.0	0	48.5	29435	51.5	29427	49.6	29432	58.0	29410	81.8	51.9	29426
24	0.0	0	0.0	0	47.8	21644	43.6	21655	48.4	21642	80.7	46.6	21647
25	0.0	0	40.9	17532	39.1	17537	34.3	17549	36.3	17544	80.8	37.6	17541
26	0.0	0	28.6	11922	30.2	11918	25.2	11930	25.5	11930	80.9	27.4	11925
27	0.0	0	18.8	8437	22.0	8430	17.6	8440	15.8	8444	81.1	18.5	8438
28	0.0	0	6.7	3541	0.0	0	8.1	3539	2.7	3543	81.2	5.9	3541

Test 5

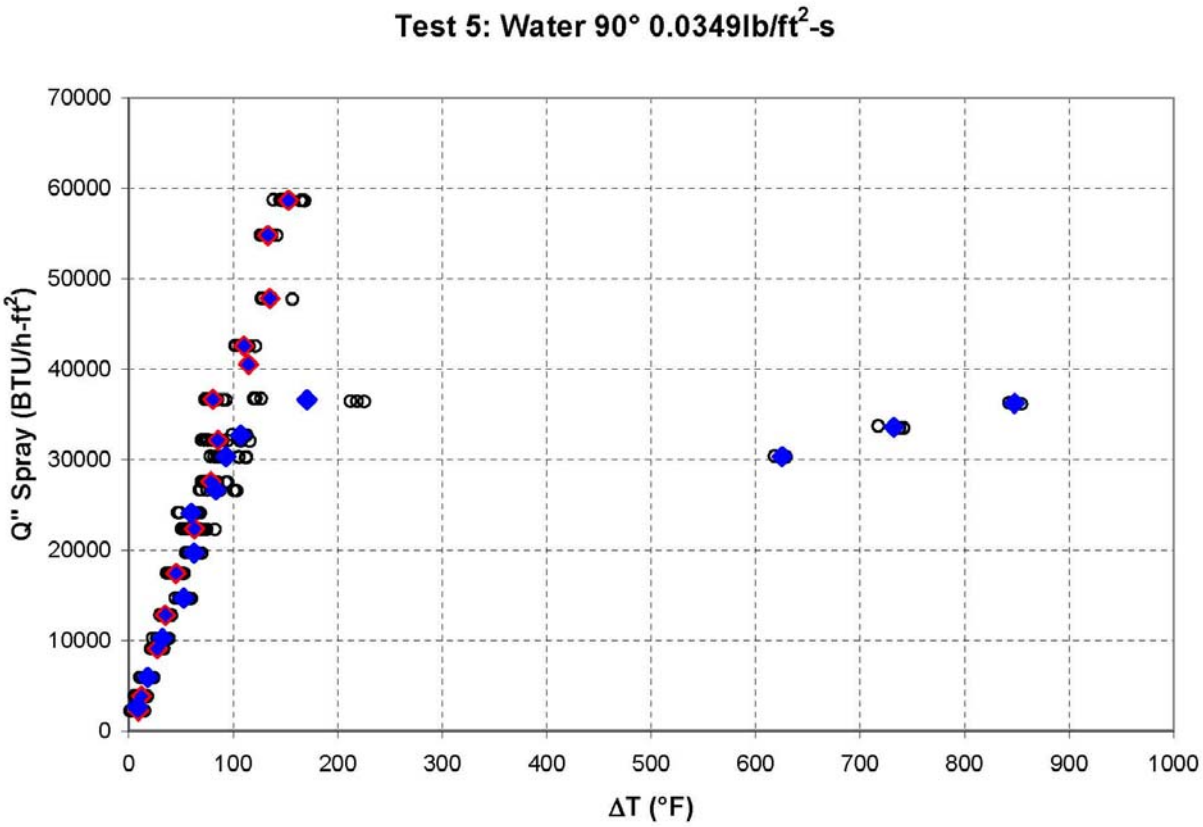

Figure B.5 Test 5 spray heat flux (BTU/h-ft^2) vs $T_{surface}$ - T_{liquid} (°F)

Table B.8 Test 5 summary data

Test	5		
Fluid	Water	**Avg Pressure (psi)**	21.8
Spray Angle	90	**Avg Fluid Temp (°F)**	80.2
Mass Flux (lb/ft^2-s)	0.0349	**Avg Flow Rate (GPM)**	0.198
Min Q"$_{spray}$ (BTU/h-ft^2)	2216	**min ΔT (°F)**	8.2
Max Q"$_{spray}$ (BTU/h-ft^2)	58682	**max ΔT (°F)**	847.6
Q"$_{spray}$ before	58682	**ΔT before CHF (°F)**	152.8
Max possible Q"$_{spray}$	62476		

Table B.9 Test 5 nodal values

Step #	T_1 (°F)	Q"$_1$ (BTU/h-ft^2)	T_2 (°F)	Q"$_2$ (BTU/h-ft^2)	T3 (°F)	Q"$_3$ (BTU/h-ft^2)	T_4 (°F)	Q"$_4$ (BTU/h-ft^2)	T_5 (°F)	Q"$_5$ (BTU/h-ft^2)	T_{fluid} (°F)	T_{avg} (°F)	Q"$_{avg}$ (BTU/h-ft^2)
1	10.1	2216	14.6	2205	13.0	2209	6.5	2224	1.8	2227	78.4	9.2	2216
2	13.7	3831	17.5	3822	15.1	3828	8.7	3842	5.5	3847	78.8	12.1	3834
3	33.0	9075	31.5	9079	28.6	9086	22.6	9101	21.4	9104	79.0	27.4	9089
4	38.8	12791	38.2	12792	36.4	12797	31.6	12809	30.5	12812	79.3	35.1	12800
5	51.8	17394	48.7	17403	47.1	17407	40.8	17424	37.2	17433	79.5	45.1	17412
6	71.7	22310	64.6	22330	61.5	22338	57.4	22349	59.1	22345	79.7	62.9	22335
7	90.7	27510	79.1	27543	77.5	27547	74.5	27556	71.6	27563	80.0	78.7	27544
8	109.9	32073	91.2	32128	75.4	32173	71.1	32185	79.2	32163	80.2	85.4	32144
9	89.4	36625	80.2	36650	77.1	36659	77.8	36657	78.1	36657	80.4	80.5	36650
10	116.8	42547	107.9	42573	105.7	42580	0.0	0	0.0	0	80.6	110.1	42567
11	0.0	0	129.3	47832	140.6	47798	0.0	0	0.0	0	80.8	135.0	47815
12	0.0	0	129.0	54808	137.2	54783	0.0	0	0.0	0	81.1	133.1	54795
13	0.0	0	146.9	58699	145.9	58703	166.2	58641	152.2	58684	81.3	152.8	58682
14	0.0	0	114.5	40523	0.0	0	0.0	0	0.0	0	81.5	114.5	40523
114	0.0	0	0.0	0	0.0	0	0.0	0	847.6	36217	81.5	847.6	36217
15	0.0	0	122.5	36750	0.0	0	218.7	36452	0.0	0	81.6	170.6	36601
115	0.0	0	0.0	0	0.0	0	0.0	0	732.2	33577	81.6	732.2	33577
16	0.0	0	107.2	32705	0.0	0	0.0	0	0.0	0	81.8	107.2	32705
116	0.0	0	0.0	0	0.0	0	0.0	0	625.1	30335	81.8	625.1	30335
17	0.0	0	87.6	30329	0.0	0	110.0	30266	81.6	30346	82.0	93.0	30314
18	0.0	0	82.2	26629	0.0	0	97.0	26587	70.6	26659	80.0	83.3	26625
19	0.0	0	63.8	24086	0.0	0	67.1	24077	48.0	24127	79.7	59.6	24097
20	0.0	0	65.1	19661	0.0	0	66.4	19658	55.8	19686	79.8	62.4	19668
21	0.0	0	53.5	14676	0.0	0	58.5	14662	46.0	14696	79.9	52.6	14678
22	0.0	0	34.5	10227	0.0	0	36.8	10221	25.5	10250	80.0	32.3	10233
23	0.0	0	23.1	5903	0.0	0	19.3	5912	11.6	5931	80.2	18.0	5915
24	0.0	0	10.1	2658	0.0	0	6.3	2666	-1.4	2677	80.3	8.2	2662

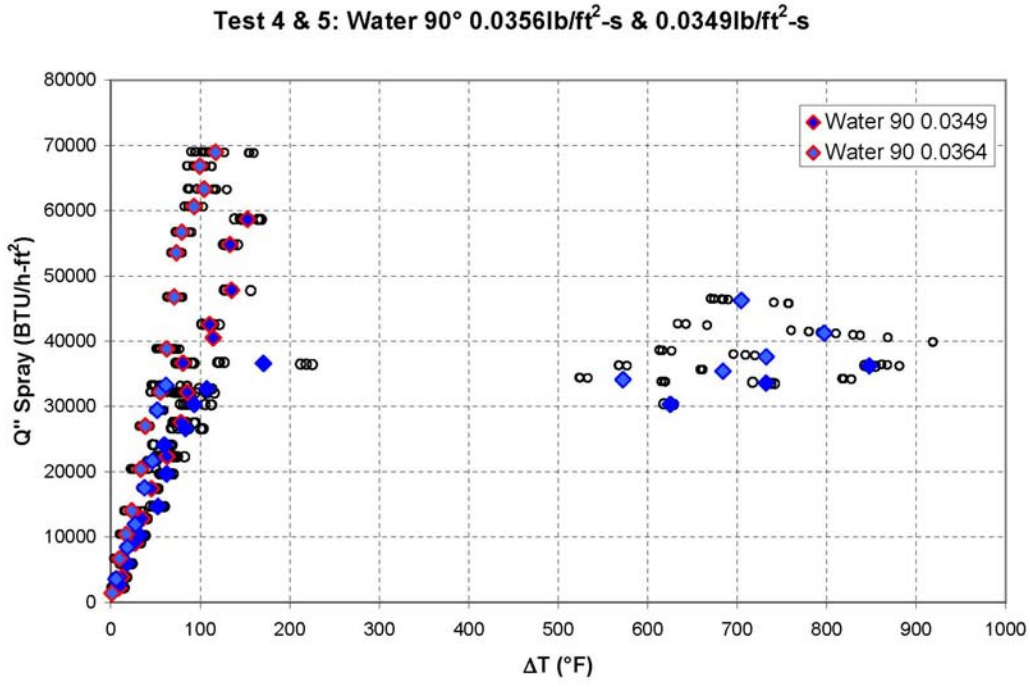

Figure B.6 Test 4 & Test 5 spray heat flux (BTU/h-ft2) vs Tsurface - Tliquid (°F)

Test 6

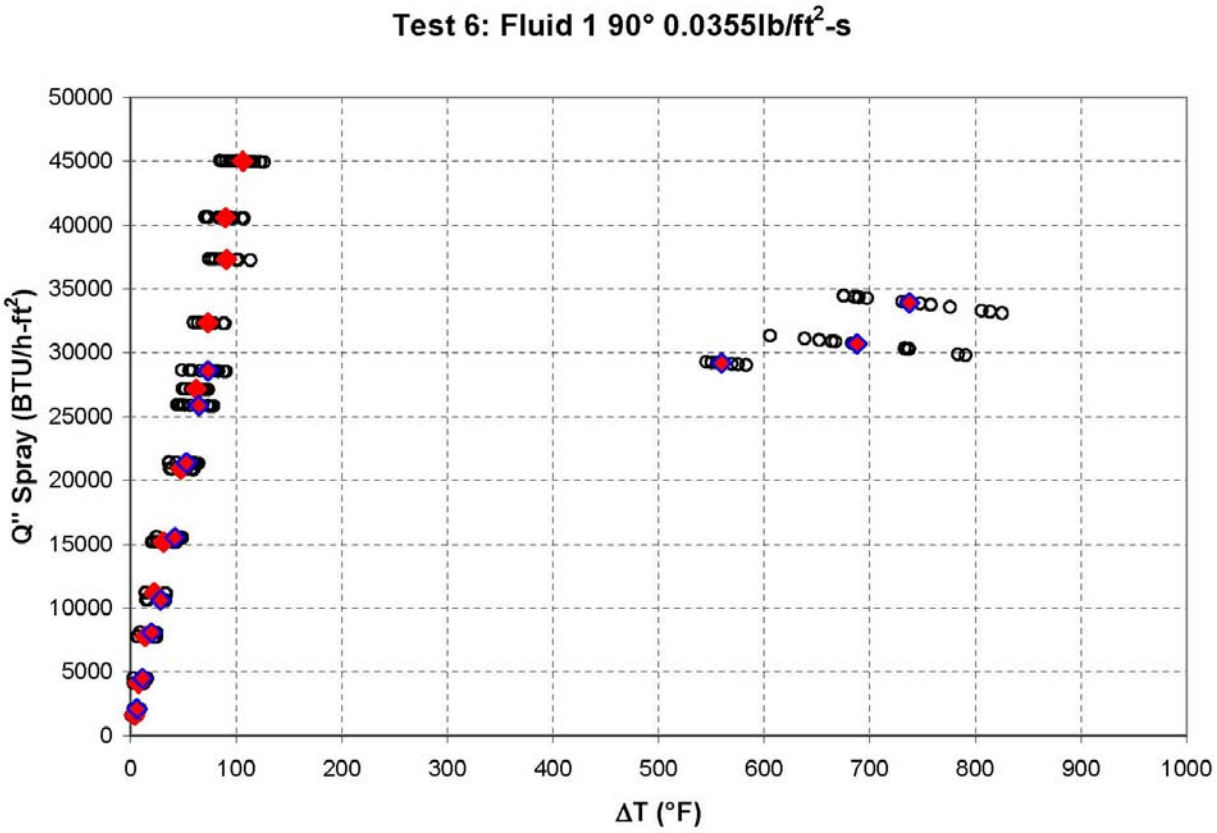

Figure B.7 Test 6 spray heat flux (BTU/h-ft^2) vs $T_{surface}$ - T_{liquid} (°F)

Table B.10 Test 6 summary data

Test	6		
Fluid	Fluid 1	**Avg Pressure (psi)**	21.2
Spray Angle	90	**Avg Fluid Temp (°F)**	85.8
Mass Flux (lb/ft^2-s)	0.0355	**Avg Flow Rate (GPM)**	0.198
Min Q"$_{spray}$ (BTU/h-ft^2)	1586	**min ΔT (°F)**	3.7
Max Q"$_{spray}$ (BTU/h-ft^2)	45013	**max ΔT (°F)**	737.4
Q"$_{spray}$ before	45013	**ΔT before CHF (°F)**	106.3
Max possible Q"$_{spray}$	50813		

Table B.11 Test 6 nodal values

Step #	T_1 (°F)	Q"$_1$ (BTU/h-ft^2)	T_2 (°F)	Q"$_2$ (BTU/h-ft^2)	T3 (°F)	Q"$_3$ (BTU/h-ft^2)	T_4 (°F)	Q"$_4$ (BTU/h-ft^2)	T_5 (°F)	Q"$_5$ (BTU/h-ft^2)	T_{fluid} (°F)	T_{avg} (°F)	Q"$_{avg}$ (BTU/h-ft^2)
1	-0.4	1595	6.4	1580	0.0	0	1.0	1592	-4.7	1598	83.6	3.7	1586
2	4.3	4101	11.9	4083	0.0	0	5.6	4098	-0.4	4111	84.3	7.3	4094
3	12.6	7767	0.0	0	23.6	7739	12.9	7766	6.7	7781	84.6	14.0	7763
4	21.4	11189	0.0	0	33.0	11159	21.4	11189	14.5	11206	84.8	22.6	11186
5	30.3	15170	0.0	0	41.6	15140	30.5	15169	22.5	15189	85.0	31.2	15167
6	48.6	20895	0.0	0	56.8	20873	47.0	20899	38.1	20923	85.2	47.6	20898
7	60.7	27147	70.5	27120	70.8	27119	58.0	27154	50.5	27174	85.5	62.1	27143
8	71.5	32353	81.7	32324	81.3	32325	71.0	32354	61.1	32381	85.7	73.3	32347
9	92.4	37320	105.5	37283	94.8	37313	85.5	37339	76.2	37365	85.8	90.8	37324
10	90.6	40591	106.2	40546	96.3	40575	84.3	40608	72.3	40640	85.8	89.9	40592
11	114.0	44992	120.6	44973	111.1	45000	94.2	45048	91.4	45055	86.0	106.3	45013
12	814.9	33214	763.7	33712	737.7	33948	692.0	34337	678.6	34446	86.1	737.4	33931
13	769.9	30005	717.8	30474	673.7	30839	641.7	31081	635.8	31126	86.3	687.8	30705
14	0.0	0	570.0	29130	563.0	29176	548.6	29268	557.1	29214	86.4	559.7	29197
15	86.2	28552	84.9	28556	83.4	28560	60.9	28620	51.0	28644	86.6	73.3	28586
16	75.7	25843	76.1	25842	74.0	25848	52.0	25905	44.7	25923	86.4	64.5	25872
17	62.1	21353	60.8	21356	61.9	21353	43.4	21401	36.4	21417	86.4	52.9	21376
18	46.5	15515	48.0	15511	46.3	15515	45.1	15519	24.7	15568	86.6	42.1	15525
19	30.0	10615	32.5	10609	31.9	10611	32.0	10610	15.7	10648	86.7	28.4	10619
20	19.9	8068	23.5	8059	24.0	8058	22.3	8062	9.2	8091	86.9	19.8	8068
21	10.4	4495	14.8	4486	15.4	4484	13.2	4489	2.5	4504	87.0	11.3	4491
22	3.1	2097	7.4	2094	8.8	2091	5.2	2097	-3.3	2098	87.2	6.1	2095

Test 7

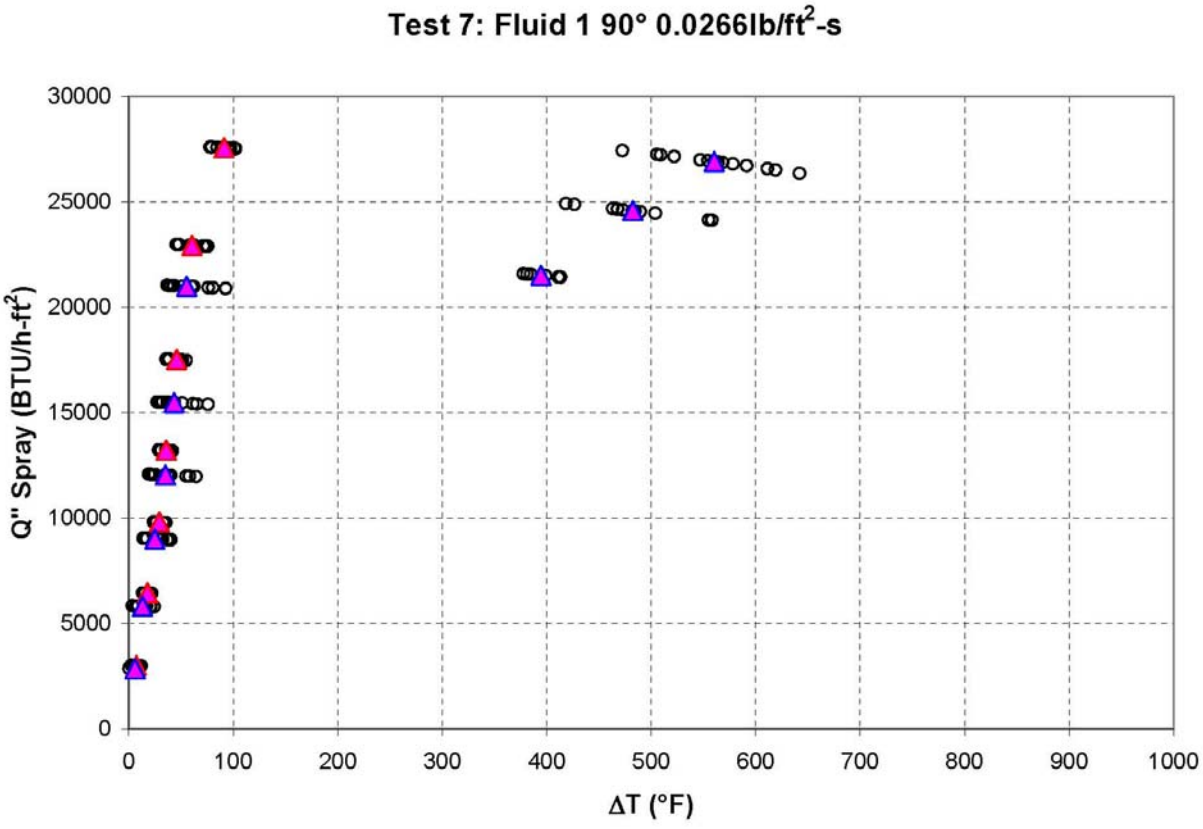

Figure B.8 Test 7 spray heat flux (BTU/h-ft^2) vs $T_{surface}$ - T_{liquid} (°F)

Table B.12 Test 7 summary data

Test	7		
Fluid	Fluid 1	**Avg Pressure (psi)**	18.7
Spray Angle	90	**Avg Fluid Temp (°F)**	88.0
Mass Flux (lb/ft^2-s)	0.0266	**Avg Flow Rate (GPM)**	0.189
Min Q"$_{spray}$ (BTU/h-ft^2)	2843	**min ΔT (°F)**	6.1
Max Q"$_{spray}$ (BTU/h-ft^2)	27562	**max ΔT (°F)**	560.3
Q"$_{spray}$ before	27562	**ΔT before CHF (°F)**	91.2
Max possible Q"$_{spray}$	33488		

Table B.13 Test 7 nodal values

		Q"$_1$		Q"$_2$		Q"$_3$		Q"$_4$		Q"$_5$			Q"$_{avg}$
Step #	**T_1 (°F)**	**(BTU/h-ft^2)**	**T_2 (°F)**	**(BTU/h-ft^2)**	**T3 (°F)**	**(BTU/h-ft^2)**	**T_4 (°F)**	**(BTU/h-ft^2)**	**T_5 (°F)**	**(BTU/h-ft^2)**	**T_{fluid} (°F)**	**T_{avg} (°F)**	**(BTU/h-ft^2)**
1	7.4	2992	9.2	2988	11.3	2982	5.2	2997	3.2	3002	86.5	7.2	2992
2	20.5	6423	21.4	6420	0.0	0	15.2	6436	14.2	6439	86.9	17.8	6430
3	33.8	9786	34.3	9785	0.0	0	24.7	9810	24.7	9810	87.1	29.4	9798
4	39.9	13191	0.0	0	0.0	0	38.2	13195	29.5	13219	87.5	35.9	13202
5	52.2	17492	0.0	0	0.0	0	48.3	17503	37.3	17533	87.6	45.9	17509
6	73.7	22895	0.0	0	0.0	0	60.8	22932	47.0	22971	87.8	60.5	22933
7	99.4	27538	0.0	0	0.0	0	93.8	27555	80.5	27593	88.0	91.2	27562
8	574.5	26819	624.0	26478	566.4	26872	525.9	27124	510.7	27209	88.2	560.3	26900
9	504.3	24446	0.0	0	509.6	24418	478.2	24599	437.5	24813	88.3	482.4	24569
10	381.1	21573	0.0	0	407.7	21448	0.0	0	0.0	0	88.5	394.4	21511
11	83.0	20915	58.0	20984	0.0	0	41.7	21025	38.8	21032	88.6	55.4	20989
12	67.5	15407	44.4	15468	0.0	0	30.3	15502	31.2	15500	88.8	43.3	15470
13	59.1	11973	37.3	12031	0.0	0	22.6	12065	21.3	12068	89.0	35.1	12034
14	38.8	8966	30.7	8986	0.0	0	16.2	9020	14.4	9023	89.1	25.0	8999
15	21.9	5790	15.5	5805	0.0	0	8.8	5819	6.2	5824	89.3	13.1	5809
16	6.5	2842	5.7	2843	0.0	0	0.0	2853	-1.6	2854	89.4	6.1	2843

Test 8

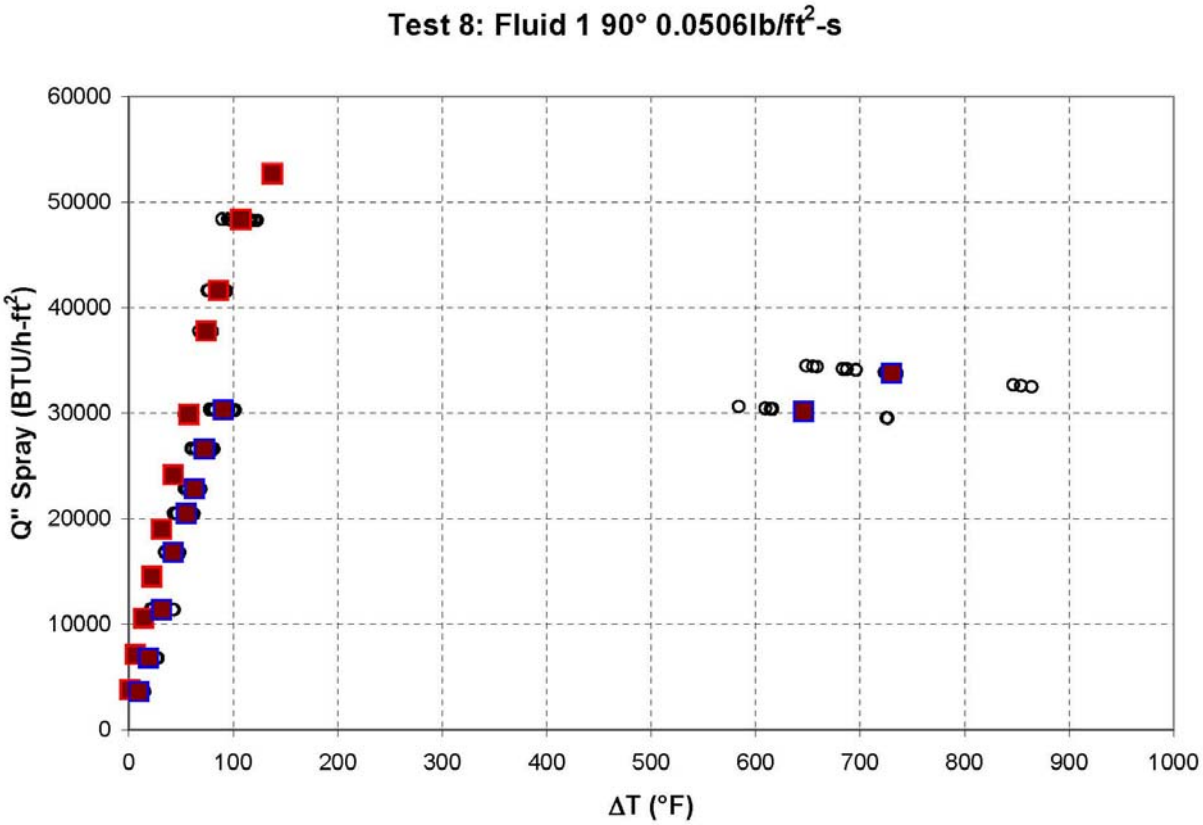

Figure B.9 Test 8 spray heat flux (BTU/h-ft^2) vs $T_{surface}$ - T_{liquid} (°F)

Table B.14 Test 8 summary data

Test	8		
Fluid	Fluid 1	**Avg Pressure (psi)**	21.9
Spray Angle	90	**Avg Fluid Temp (°F)**	86.1
Mass Flux (lb/ft^2-s)	0.0506	**Avg Flow Rate (GPM)**	0.203
Min Q"$_{spray}$ (BTU/h-ft^2)	3596	**min ΔT (°F)**	1.3
Max Q"$_{spray}$ (BTU/h-ft^2)	52693	**max ΔT (°F)**	730.3
Q"$_{spray}$ before	52693	**ΔT before CHF (°F)**	137.5
Max possible Q"$_{spray}$	62956		

Table B.15 Test 8 nodal values

Step #	T_1 (°F)	$Q"_1$ (BTU/h-ft^2)	T_2 (°F)	$Q"_2$ (BTU/h-ft^2)	T3 (°F)	$Q"_3$ (BTU/h-ft^2)	T_4 (°F)	$Q"_4$ (BTU/h-ft^2)	T_5 (°F)	$Q"_5$ (BTU/h-ft^2)	T_{fluid} (°F)	T_{avg} (°F)	$Q"_{avg}$ (BTU/h-ft^2)
1	-0.9	3784	1.2	3779	2.0	3777	0.9	3780	-0.1	3782	84.8	1.3	3778
2	4.7	7096	6.9	7090	8.3	7087	6.7	7091	4.9	7095	85.2	6.3	7092
3	12.6	10587	15.4	10579	16.1	10578	15.4	10579	12.6	10587	85.5	14.4	10582
4	20.4	14497	22.8	14491	24.2	14487	22.6	14491	20.6	14496	85.6	22.1	14492
5	30.3	19005	33.1	18998	33.2	18997	31.1	19003	29.3	19008	85.8	31.4	19002
6	41.8	24121	44.1	24114	45.1	24112	42.8	24118	40.0	24126	85.9	42.8	24118
7	58.0	29866	58.5	29865	59.6	29862	56.7	29870	54.3	29876	86.0	57.4	29868
8	74.9	37755	77.6	37747	76.5	37750	72.3	37762	69.8	37769	86.0	74.2	37757
9	88.0	41603	92.9	41588	85.8	41609	82.5	41618	80.0	41625	86.3	85.8	41609
10	106.1	48336	112.3	48318	119.2	48297	98.7	48358	99.8	48354	86.5	107.2	48333
11	0.0	0	0.0	0	0.0	0	0.0	0	137.5	52693	86.7	137.5	52693
12	688.8	34148	725.7	33838	727.9	33819	854.8	32576	654.0	34422	86.7	730.3	33761
13	0.0	0	0.0	0	689.2	29810	0.0	0	602.4	30480	86.3	645.8	30145
14	0.0	0	96.9	30287	0.0	0	94.7	30294	79.8	30335	86.2	90.5	30305
15	0.0	0	79.0	26588	0.0	0	76.3	26595	61.8	26635	86.2	72.4	26606
16	0.0	0	67.4	22799	62.8	22812	66.4	22802	54.8	22833	86.3	62.9	22811
17	0.0	0	58.2	20459	59.6	20455	58.0	20460	44.6	20496	86.4	55.1	20468
18	0.0	0	46.8	16779	0.0	0	45.9	16782	35.0	16811	86.5	42.5	16791
19	0.0	0	0.0	0	42.8	11344	29.9	11379	21.8	11399	86.7	31.5	11374
20	0.0	0	0.0	0	27.1	6771	17.9	6795	12.1	6809	86.8	19.0	6792
21	0.0	0	0.0	0	14.6	3584	9.1	3597	4.6	3607	86.9	9.4	3596

Test 9

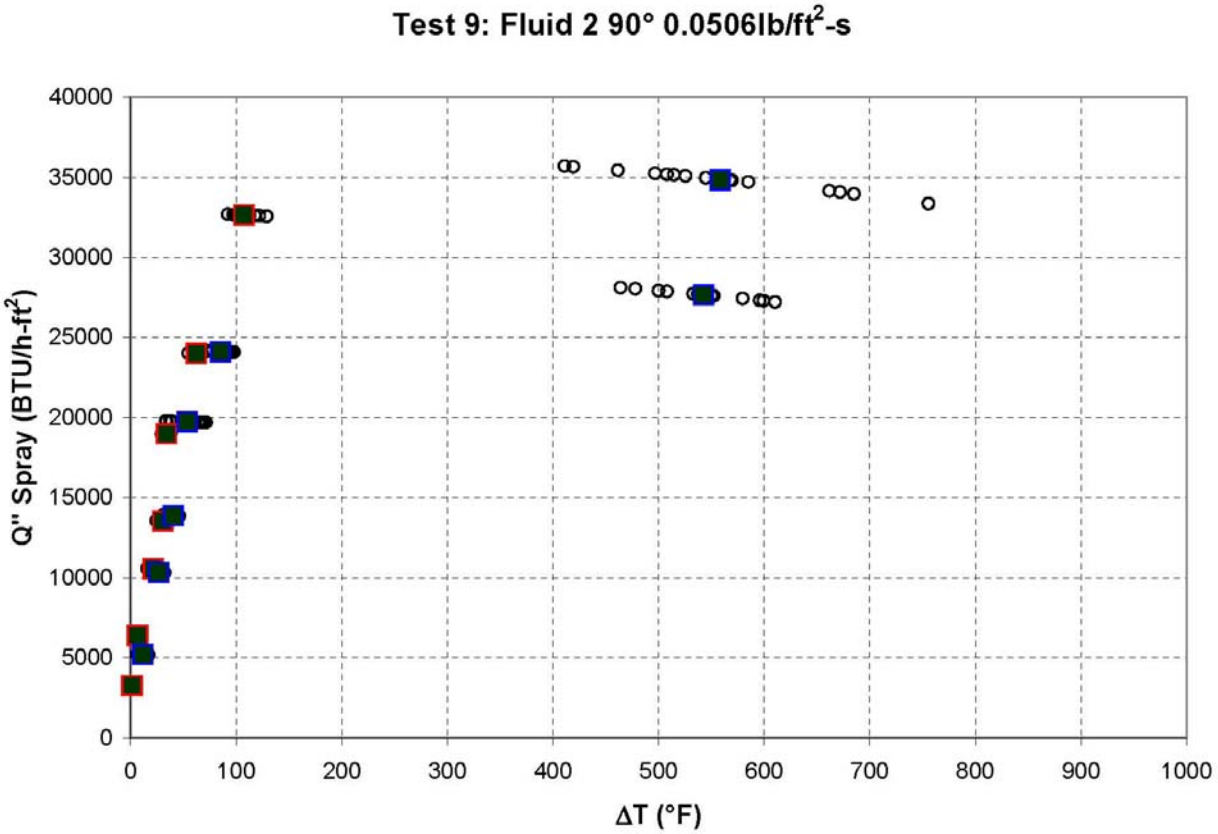

Figure B.10 Test 9 spray heat flux (BTU/h-ft^2) vs $T_{surface}$ - T_{liquid} (°F)

Table B.16 Test 9 summary data

Test	9		
Fluid	Fluid 2	**Avg Pressure (psi)**	18.6
Spray Angle	90	**Avg Fluid Temp (°F)**	87.3
Mass Flux (lb/ft^2-s)	0.0465	**Avg Flow Rate (GPM)**	0.185
Min Q"$_{spray}$ (BTU/h-ft^2)	3284	**min ΔT (°F)**	1.5
Max Q"$_{spray}$ (BTU/h-ft^2)	34822	**max ΔT (°F)**	558.4
Q"$_{spray}$ before	32641	**ΔT before CHF (°F)**	107.4
Max possible Q"$_{spray}$	34822		

Table B.17 Test 9 nodal values

		Q"$_1$		Q"$_2$		Q"$_3$		Q"$_4$		Q"$_5$			Q"$_{avg}$
Step #	**T_1 (°F)**	**(BTU/h-ft^2)**	**T_2 (°F)**	**(BTU/h-ft^2)**	**T3 (°F)**	**(BTU/h-ft^2)**	**T_4 (°F)**	**(BTU/h-ft^2)**	**T_5 (°F)**	**(BTU/h-ft^2)**	**T_{fluid} (°F)**	**T_{avg} (°F)**	**(BTU/h-ft^2)**
1	-2.7	3292	0.9	3285	0.0	0	2.0	3282	-4.4	3293	85.9	1.5	3284
2	5.3	6409	7.6	6404	0.0	0	10.1	6398	3.7	6412	86.1	6.7	6406
3	19.3	10566	21.1	10562	27.7	10545	23.3	10556	16.2	10574	86.3	21.5	10561
4	30.2	13544	29.1	13547	36.5	13528	31.4	13541	24.8	13558	86.5	30.4	13544
5	31.3	18989	30.8	18990	35.8	18977	37.2	18973	35.5	18978	86.8	34.1	18981
6	62.2	24007	61.3	24009	66.0	23996	64.1	24002	58.2	24018	87.0	62.4	24006
7	100.0	32663	100.8	32660	107.2	32642	106.2	32645	122.7	32596	87.2	107.4	32641
8	430.5	35603	516.4	35135	536.4	35014	608.1	34534	700.7	33827	87.4	558.4	34822
9	480.6	28027	529.6	27744	562.4	27537	564.4	27521	575.9	27451	87.6	542.6	27656
11	72.7	24155	74.4	24151	93.0	24100	91.0	24105	95.0	24094	87.9	85.2	24121
12	33.6	19796	38.3	19785	60.4	19728	66.4	19712	69.3	19704	88.1	53.6	19745
13	32.7	13883	36.0	13875	45.3	13852	44.1	13855	44.2	13855	88.3	40.5	13864
14	20.9	10359	23.6	10352	31.0	10333	28.6	10339	28.5	10340	88.5	26.5	10345
15	6.7	5214	11.7	5204	16.9	5192	13.5	5200	10.3	5207	88.7	11.8	5204

Test 10

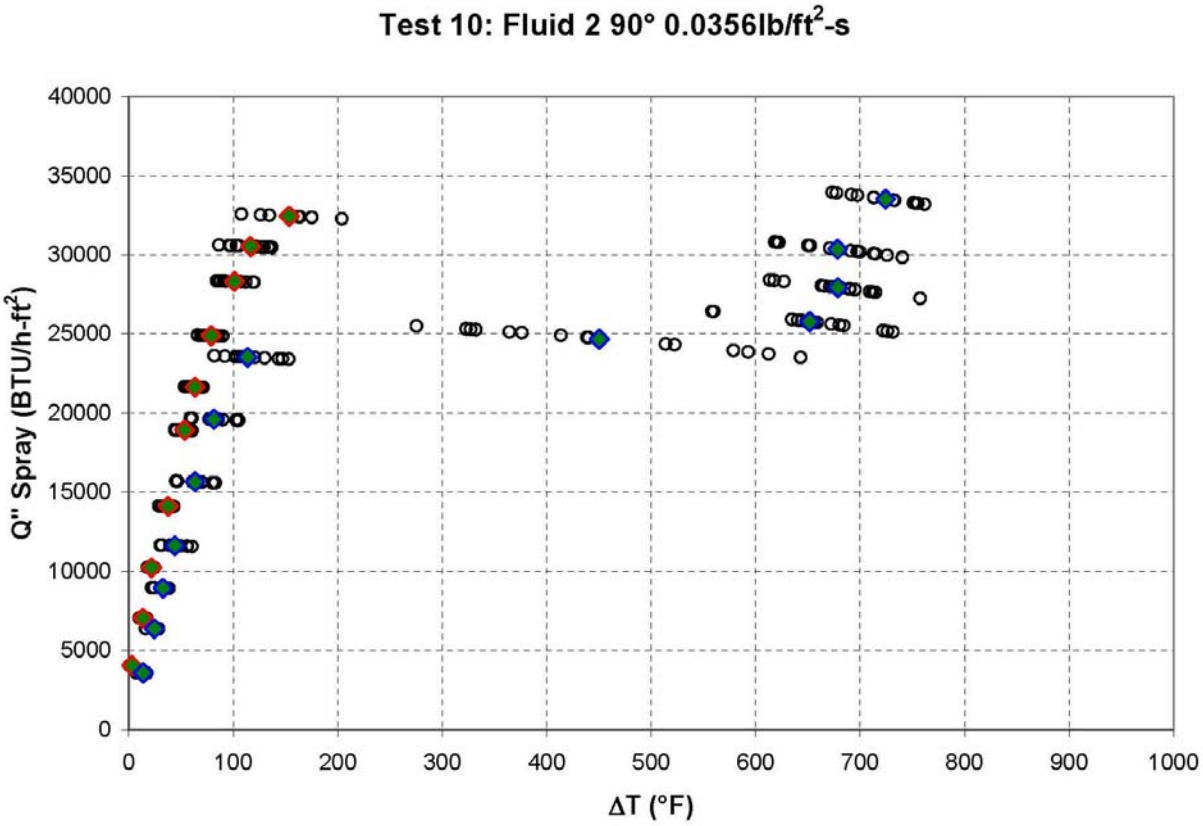

Figure B.11 Test 10 spray heat flux (BTU/h-ft^2) vs $T_{surface}$ - T_{liquid} (°F)

Table B.18 Test 10 summary data

Test	10		
Fluid	Fluid 2	**Avg Pressure (psi)**	19.3
Spray Angle	90	**Avg Fluid Temp (°F)**	87.5
Mass Flux (lb/ft^2-s)	0.0356	**Avg Flow Rate (GPM)**	0.190
Min Q"$_{spray}$ (BTU/h-ft^2)	3577	**min ΔT (°F)**	3.1
Max Q"$_{spray}$ (BTU/h-ft^2)	33519	**max ΔT (°F)**	724.3
Q"$_{spray}$ before	32438	**ΔT before CHF (°F)**	153.5
Max possible Q"$_{spray}$	33519		

Table B.19 Test 10 nodal values

Step #	T_1 (°F)	$Q"_1$ (BTU/h-ft^2)	T_2 (°F)	$Q"_2$ (BTU/h-ft^2)	T3 (°F)	$Q"_3$ (BTU/h-ft^2)	T_4 (°F)	$Q"_4$ (BTU/h-ft^2)	T_5 (°F)	$Q"_5$ (BTU/h-ft^2)	T_{fluid} (°F)	T_{avg} (°F)	$Q"_{avg}$ (BTU/h-ft^2)
1	3.5	4045	4.4	4043	3.5	4045	2.8	4047	1.4	4051	86.2	3.1	4046
2	15.3	7028	15.7	7027	13.6	7032	12.5	7035	11.1	7039	86.3	13.6	7032
3	24.2	10224	22.7	10228	21.7	10231	20.4	10234	19.2	10238	86.4	21.7	10231
4	42.1	14099	42.7	14097	39.2	14107	34.4	14120	29.6	14132	86.6	37.6	14111
5	59.2	18899	57.9	18902	53.9	18913	51.5	18920	44.7	18939	86.8	53.5	18914
6	69.5	21615	67.2	21621	64.2	21630	60.5	21640	55.4	21654	87.0	63.4	21632
7	88.6	24865	0.0	0	80.6	24888	77.9	24896	68.5	24922	87.2	78.9	24893
8	109.1	28300	112.6	28289	97.4	28334	97.5	28334	89.0	28359	87.3	101.1	28323
9	126.8	30501	132.3	30485	128.8	30496	98.9	30583	96.0	30591	87.5	116.6	30531
10	0.0	0	0.0	0	180.8	32353	156.8	32429	122.8	32531	87.6	153.5	32438
11	755.5	33247	746.8	33326	700.8	33721	693.9	33781	0.0	0	87.8	724.3	33519
12	704.7	30146	722.6	29995	650.6	30575	683.3	30323	630.1	30731	87.9	678.3	30354
13	695.2	27796	728.0	27515	669.9	28000	680.9	27911	619.3	28380	88.1	678.6	27920
14	647.7	25814	726.4	25175	678.8	25572	646.3	25824	558.9	26432	88.2	651.6	25764
15	561.7	24068	564.6	24009	429.9	24797	340.3	25229	354.4	25179	88.5	450.2	24656
16	147.8	23428	121.8	23508	109.0	23545	105.0	23557	85.1	23612	88.7	113.7	23530
17	103.6	19551	86.7	19600	79.8	19620	77.9	19625	59.6	19674	88.6	81.5	19614
18	81.2	15600	66.8	15641	62.3	15653	61.0	15657	45.9	15697	88.4	63.4	15650
19	57.2	11581	46.4	11610	45.4	11613	40.5	11626	30.6	11651	88.3	44.0	11616
20	38.1	8917	35.5	8924	35.6	8923	31.6	8933	22.8	8955	88.0	32.7	8930
21	28.0	6356	27.1	6358	27.0	6359	23.8	6367	16.4	6384	87.9	24.4	6365
22	15.3	3573	15.6	3573	16.8	3570	14.1	3576	7.4	3591	87.7	13.8	3577

Test 11

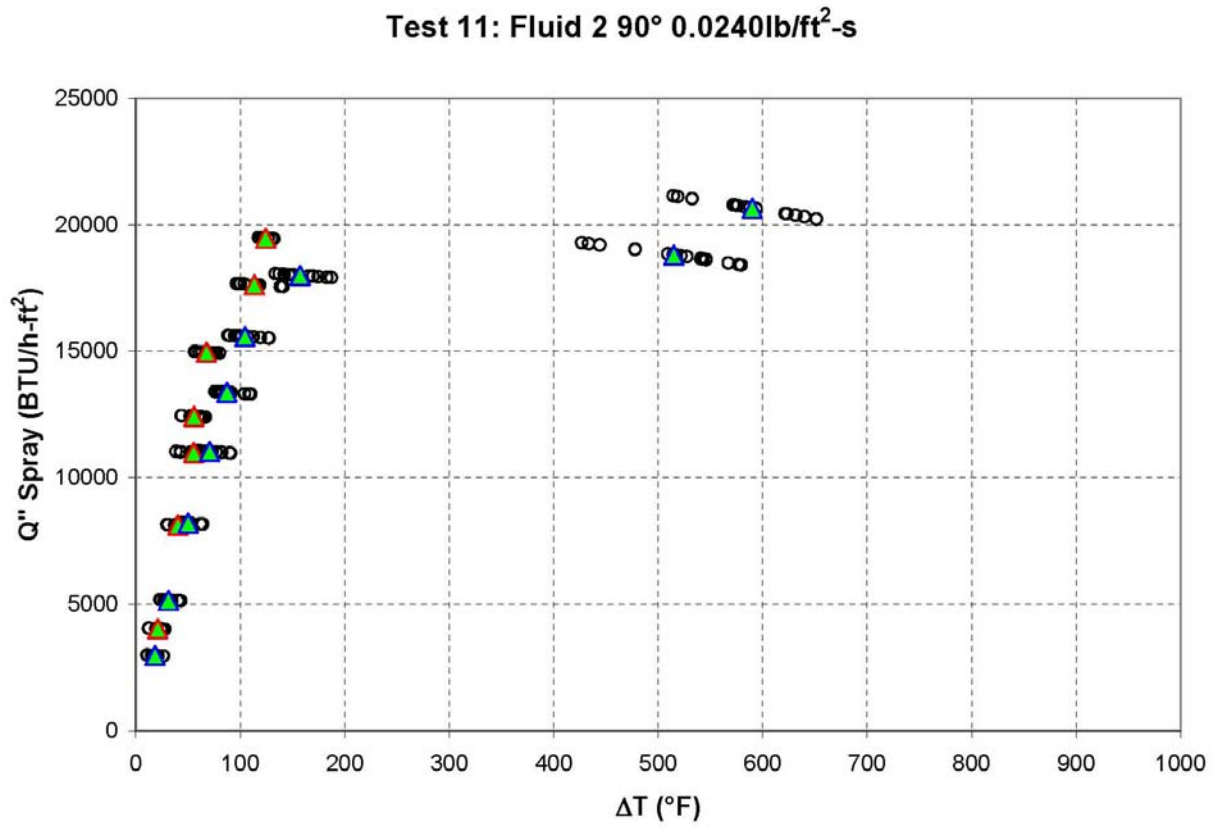

Figure B.12 Test 11 spray heat flux (BTU/h-ft^2) vs $T_{surface}$ - T_{liquid} (°F)

Table B.20 Test 11 summary data

Test	11		
Fluid	Fluid 2	**Avg Pressure (psi)**	16.7
Spray Angle	90	**Avg Fluid Temp (°F)**	86.2
Mass Flux (lb/ft^2-s)	0.0240	**Avg Flow Rate (GPM)**	0.177
Min Q"$_{spray}$ (BTU/h-ft^2)	2972	**min ΔT (°F)**	18.4
Max Q"$_{spray}$ (BTU/h-ft^2)	20658	**max ΔT (°F)**	590.0
Q"$_{spray}$ before	19476	**ΔT before CHF (°F)**	124.4
Max possible Q"$_{spray}$	20658		

Table B.21 Test 11 nodal values

		Q"$_1$		Q"$_2$		Q"$_3$		Q"$_4$		Q"$_5$			Q"$_{avg}$
Step #	**T_1 (°F)**	**(BTU/h-ft^2)**	**T_2 (°F)**	**(BTU/h-ft^2)**	**T3 (°F)**	**(BTU/h-ft^2)**	**T_4 (°F)**	**(BTU/h-ft^2)**	**T_5 (°F)**	**(BTU/h-ft^2)**	**T_{fluid} (°F)**	**T_{avg} (°F)**	**(BTU/h-ft^2)**
1	24.5	4020	27.2	4013	0.0	0	20.0	4031	12.5	4048	84.7	21.0	4028
2	45.2	8113	47.0	8108	0.0	0	38.1	8132	30.5	8151	85.4	40.2	8126
3	62.5	10977	64.5	10971	0.0	0	53.2	11001	41.4	11031	85.6	55.4	10995
4	60.3	12420	64.9	12407	0.0	0	53.7	12437	43.9	12463	85.8	55.7	12432
5	72.1	14949	76.4	14937	0.0	0	64.6	14970	57.2	14989	86.0	67.6	14961
6	116.4	17627	139.8	17558	0.0	0	100.7	17672	96.9	17682	86.1	113.4	17635
7	131.3	19456	0.0	0	0.0	0	119.4	19491	122.3	19482	86.3	124.4	19476
8	576.9	20757	628.6	20399	637.6	20332	585.2	20702	521.8	21102	86.5	590.0	20658
9	530.2	18727	565.6	18505	544.0	18642	500.5	18902	434.8	19256	86.6	515.0	18806
10	154.0	18014	181.5	17927	154.3	18013	139.5	18058	0.0	0	86.7	157.3	18003
11	95.8	15614	124.6	15530	110.3	15573	92.6	15623	99.5	15604	86.9	104.5	15589
12	81.4	13394	107.5	13319	90.0	13370	78.4	13402	78.9	13401	87.0	87.3	13377
13	66.8	11046	87.6	10988	72.7	11029	63.2	11055	62.6	11057	87.1	70.6	11035
14	47.9	8212	62.9	8171	52.9	8199	44.3	8221	42.4	8226	87.2	50.1	8206
15	30.2	5162	41.9	5131	33.5	5154	27.6	5168	23.7	5178	87.4	31.4	5159
16	18.0	2973	26.1	2954	21.1	2966	15.6	2979	11.2	2989	87.5	18.4	2972

Test 13

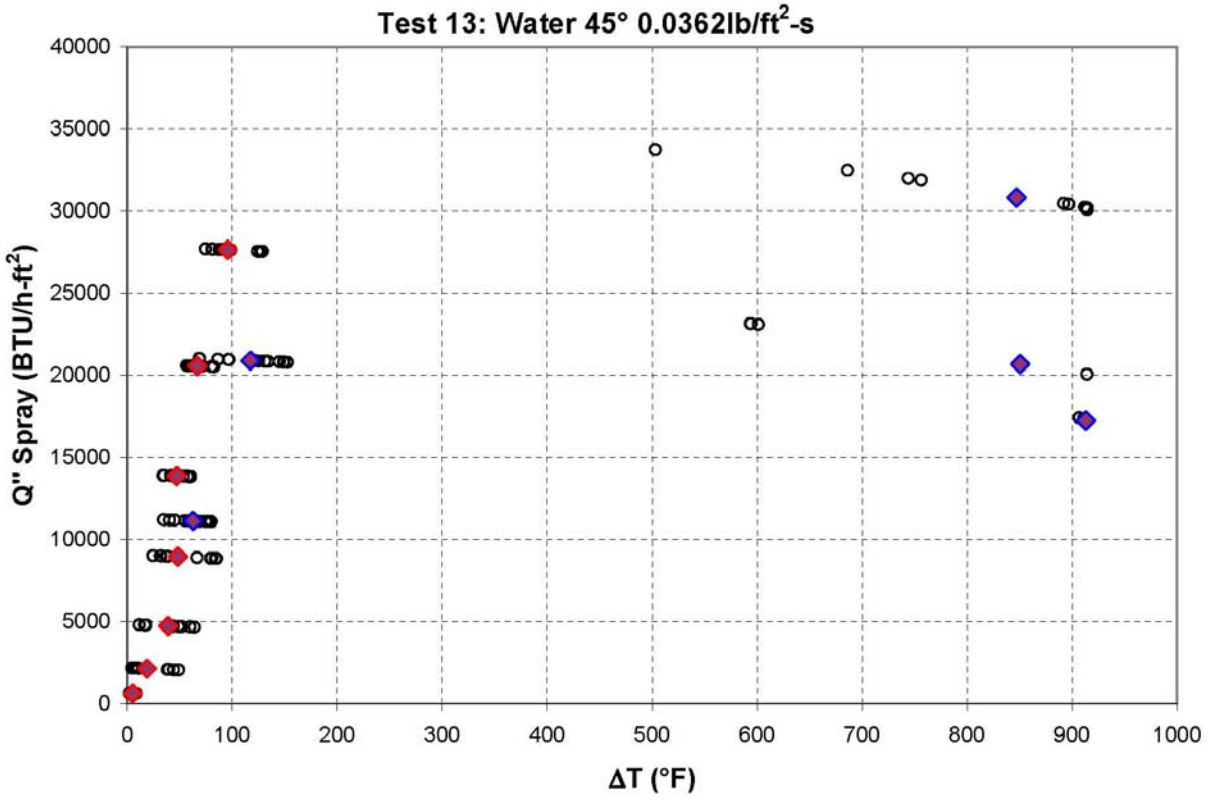

Figure B.13 Test 13 spray heat flux (BTU/h-ft^2) vs $T_{surface}$ - T_{liquid} (°F)

Table B.22 Test 13 summary data

Test	13		
Fluid	Water	**Avg Pressure (psi)**	12.6
Spray Angle	45	**Avg Fluid Temp (°F)**	85.2
Mass Flux (lb/ft^2-s)	0.0362	**Avg Flow Rate**	0.157
Min Q"$_{spray}$ (BTU/h-	629	**min ΔT (°F)**	5.2
Max Q"$_{spray}$ (BTU/h-	30826	**max ΔT (°F)**	913.2
Q"$_{spray}$ before	27642	**ΔT before CHF (°F)**	95.5
Max possible Q"$_{spray}$	30826		

Table B.23 Test 13 nodal values

Step #	T_1 (°F)	Q''_1 (BTU/h-ft^2)	T_2 (°F)	Q''_2 (BTU/h-ft^2)	T3 (°F)	Q''_3 (BTU/h-ft^2)	T_4 (°F)	Q''_4 (BTU/h-ft^2)	T_5 (°F)	Q''_5 (BTU/h-ft^2)	T_{fluid} (°F)	T_{avg} (°F)	Q''_{avg} (BTU/h-ft^2)
1	2.2	633	7.5	626	8.2	625	2.9	632	-2.0	633	83.6	5.2	629
2	16.5	2137	23.3	2121	0.0	0	19.8	2130	15.8	2139	84.0	18.8	2132
3	34.0	4742	43.4	4716	0.0	0	40.1	4725	38.0	4731	84.4	38.9	4729
4	38.5	8975	47.8	8949	53.6	8933	47.8	8949	52.9	8935	84.8	48.1	8948
5	36.8	13894	44.2	13875	50.6	13858	45.0	13873	58.6	13837	85.1	47.0	13867
6	57.7	20590	61.9	20579	68.5	20561	64.5	20572	81.6	20524	85.3	66.8	20565
7	78.6	27690	94.7	27646	92.0	27653	86.0	27670	126.5	27552	85.5	95.5	27642
8	648.4	32704	856.8	30774	908.5	30236	914.3	30162	906.8	30255	85.7	847.0	30826
9	596.2	23131	914.1	20065	914.1	20065	914.1	20065	914.1	20065	85.9	850.5	20678
10	0.0	0	910.6	17331	914.0	17205	914.0	17205	914.0	17205	86.0	913.2	17236
11	74.6	21014	103.3	20938	135.2	20846	124.7	20877	148.7	20805	86.2	117.3	20896
12	39.9	11188	57.1	11145	73.3	11102	77.6	11090	64.9	11125	86.5	62.6	11130

Test 14

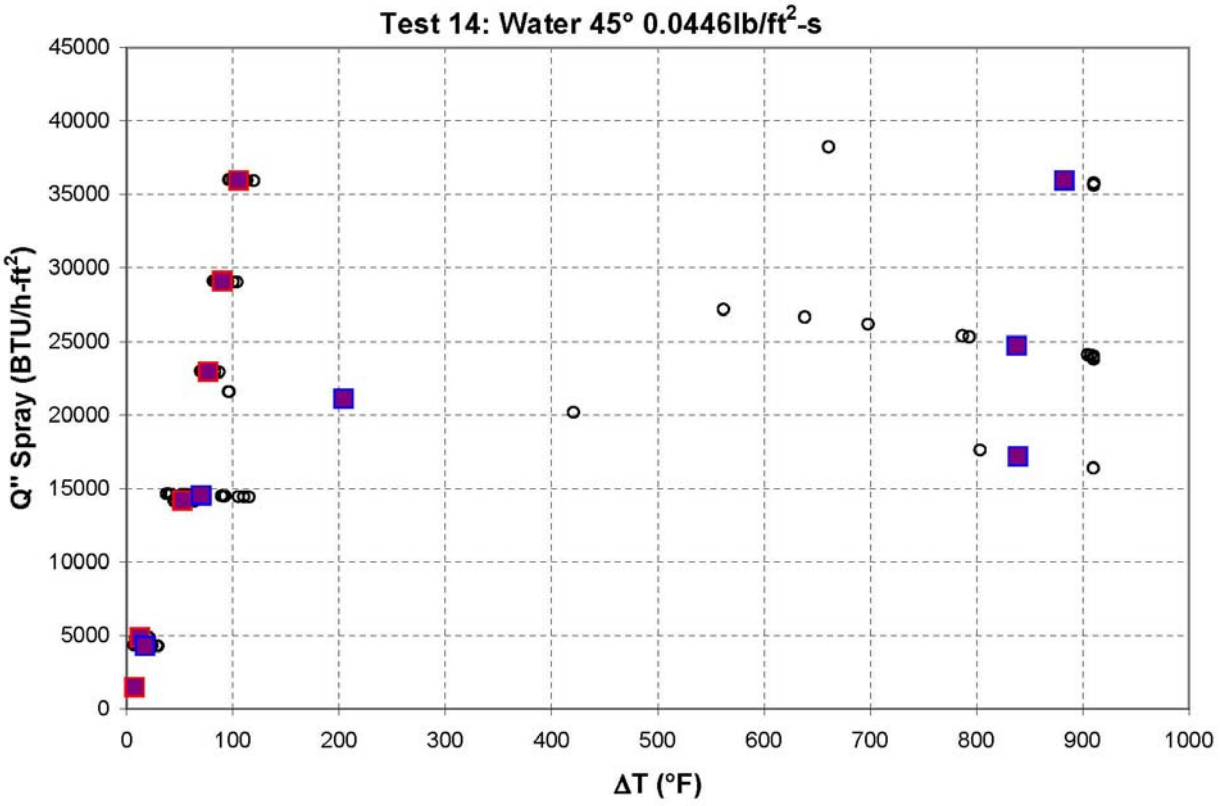

Figure B.14 Test 14 spray heat flux (BTU/h-ft^2) vs $T_{surface}$ - T_{liquid} (°F)

Table B.24 Test 14 summary data

Test	14		
Fluid	Water	**Avg Pressure (psi)**	10.3
Spray Angle	45	**Avg Fluid Temp (°F)**	89.3
Mass Flux (lb/ft^2-s)	0.0446	**Avg Flow Rate**	0.135
Min Q"$_{spray}$ (BTU/h-	1482	**min ΔT (°F)**	7.4
Max Q"$_{spray}$ (BTU/h-	35976	**max ΔT (°F)**	882.6
Q"$_{spray}$ before	35976	**ΔT before CHF (°F)**	105.3
Max possible Q"$_{spray}$	35976		

Table B.25 Test 14 nodal values

		Q"$_1$		Q"$_2$		Q"$_3$		Q"$_4$		Q"$_5$			Q"$_{avg}$
Step #	**T_1 (°F)**	**(BTU/h-ft^2)**	**T_2 (°F)**	**(BTU/h-ft^2)**	**T3 (°F)**	**(BTU/h-ft^2)**	**T_4 (°F)**	**(BTU/h-ft^2)**	**T_5 (°F)**	**(BTU/h-ft^2)**	**T_{fluid} (°F)**	**T_{avg} (°F)**	**(BTU/h-ft^2)**
1	7.4	1482	-1.1	1504	-2.2	1507	-4.2	1511	-5.9	1515	88.1	7.4	1482
2	20.9	4823	12.1	4847	11.3	4849	9.0	4855	9.0	4855	88.3	12.4	4846
3	60.4	14154	50.0	14183	50.9	14181	50.4	14182	49.5	14184	88.6	52.2	14177
4	85.4	22928	74.4	22959	72.4	22965	76.3	22954	75.2	22957	88.8	76.7	22953
5	94.6	29080	88.5	29098	86.4	29104	89.0	29096	91.8	29088	89.2	90.1	29093
6	111.1	35959	109.6	35964	100.0	35991	100.8	35989	105.0	35977	89.6	105.3	35976
7	0.0	0	0.0	0	827.1	36512	910.3	35691	910.3	35691	89.7	882.6	35965
8	713.8	25958	816.8	24938	839.4	24721	910.2	23944	910.2	23930	89.8	838.1	24698
9	0.0	0	0.0	0	204.3	21107	0.0	0	0.0	0	90.1	204.3	21107
109	0.0	0	0.0	0	0.0	0	0.0	0	838.9	17206	90.1	838.9	17206
10	39.7	14622	53.4	14587	56.1	14580	91.1	14481	110.0	14424	90.2	70.1	14539
11	8.0	4332	14.0	4318	13.1	4321	22.6	4297	28.7	4281	90.5	17.3	4310

Test 15

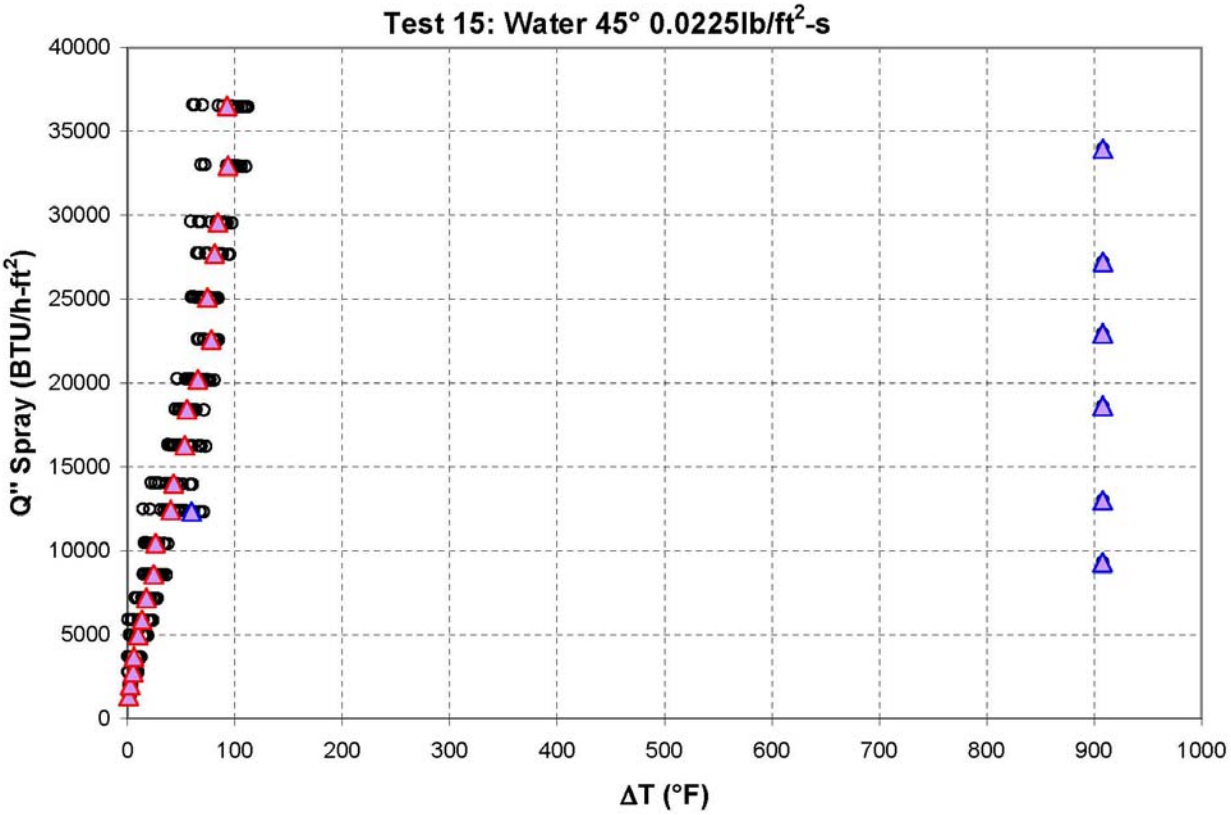

Figure B.15 Test 15 spray heat flux (BTU/h-ft^2) vs $T_{surface}$ - T_{liquid} (°F)

Table B.26 Test 15 summary data

Test	15		
Fluid	Water	**Avg Pressure (psi)**	13.7
Spray Angle	45	**Avg Fluid Temp (°F)**	89.7
Mass Flux (lb/ft^2-s)	0.0225	**Avg Flow Rate**	0.153
Min Q"$_{spray}$ (BTU/h-	1344	**min ΔT (°F)**	1.0
Max Q"$_{spray}$ (BTU/h-	36509	**max ΔT (°F)**	908.2
Q"$_{spray}$ before	36509	**ΔT before CHF (°F)**	92.7
Max possible Q"$_{spray}$	36509		

Table B.27 Test 15 nodal values

		Q"$_1$		Q"$_2$		Q"$_3$		Q"$_4$		Q"$_5$			Q"$_{avg}$
Step #	T_1 (°F)	(BTU/h-ft^2)	T_2 (°F)	(BTU/h-ft^2)	T3 (°F)	(BTU/h-ft^2)	T_4 (°F)	(BTU/h-ft^2)	T_5 (°F)	(BTU/h-ft^2)	T_{fluid} (°F)	T_{avg} (°F)	(BTU/h-ft^2)
5	-7.7	1360	1.0	1344	-1.1	1349	-8.2	1360	-13.3	1360	88.8	1.0	1344
6	-4.9	2025	3.7	2005	1.4	2011	-5.8	2026	-11.0	2029	88.9	2.5	2008
7	0.4	2787	8.8	2766	6.3	2773	-2.1	2792	-7.6	2799	89.1	5.2	2775
8	1.6	3702	11.2	3679	9.4	3683	1.7	3702	-4.3	3715	89.2	6.0	3691
9	8.3	4975	17.9	4951	15.0	4958	6.8	4979	0.9	4993	89.4	9.8	4971
10	11.7	5886	21.6	5861	19.8	5866	11.4	5887	3.0	5906	89.4	13.5	5881
11	16.7	7194	24.3	7174	23.6	7176	15.0	7198	7.8	7215	89.4	17.5	7191
12	22.0	8599	30.8	8576	30.8	8576	22.0	8599	16.4	8613	89.5	24.4	8592
13	27.9	10450	31.3	10441	30.7	10443	22.5	10464	17.7	10476	89.7	26.0	10455
14	41.9	12432	52.0	12404	48.5	12414	32.1	12457	26.3	12471	89.8	40.2	12436
15	46.4	14000	53.5	13981	49.9	13991	34.8	14031	30.3	14042	90.0	43.0	14009
16	55.8	16272	60.9	16257	63.9	16249	45.5	16299	39.8	16314	90.1	53.2	16278
17	54.1	18442	56.3	18436	65.2	18412	52.9	18445	48.0	18458	90.4	55.3	18439
18	71.2	20209	73.2	20203	70.9	20210	54.2	20256	57.6	20246	90.6	65.4	20225
19	78.9	22585	84.4	22569	82.5	22575	67.5	22617	76.8	22591	90.8	78.0	22587
20	78.8	25074	82.0	25065	80.5	25069	62.1	25119	67.6	25104	91.0	74.2	25086
21	83.0	27703	82.9	27703	91.3	27679	65.3	27750	82.6	27703	91.2	81.0	27708
22	85.5	29572	90.8	29558	88.8	29563	64.5	29629	91.3	29556	91.4	84.2	29576
23	95.8	32946	103.4	32924	101.8	32929	69.6	33017	96.6	32943	91.5	93.4	32952
24	96.2	36500	92.3	36511	110.3	36459	64.3	36587	100.4	36488	91.7	92.7	36509
25	908.2	33966	908.2	33966	908.2	33966	908.2	33966	908.2	33951	91.8	908.2	33963
26	908.1	27224	908.1	27224	908.1	27224	908.1	27224	908.1	27209	91.9	908.1	27221
27	908.1	22964	908.1	22964	908.1	22964	908.1	22964	908.1	22949	91.9	908.1	22961
28	908.0	18640	908.0	18640	908.0	18640	908.0	18640	908.0	18625	92.0	908.0	18637
29	908.0	13012	908.0	13012	908.0	13012	908.0	13012	908.0	12997	92.0	908.0	13009
30	907.9	9308	907.9	9308	907.9	9308	907.9	9308	907.9	9293	92.1	907.9	9305
31	67.3	12330	70.6	12321	61.5	12346	38.5	12405	0.0	0	92.1	59.5	12351

Test 16

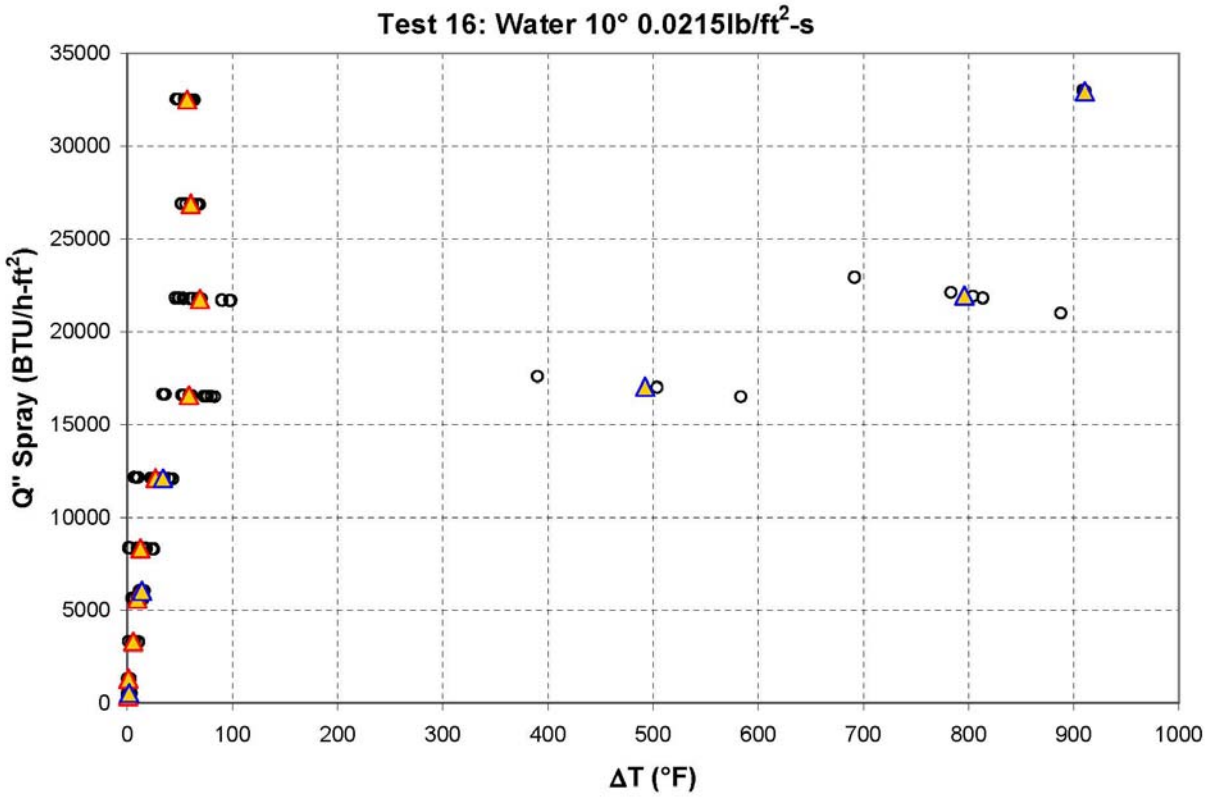

Figure B.16 Test 16 spray heat flux (BTU/h-ft^2) vs $T_{surface}$ - T_{liquid} (°F)

Table B.28 Test 16 summary data

Test	16		
Fluid	Water	**Avg Pressure (psi)**	14.2
Spray Angle	10	**Avg Fluid Temp (°F)**	88.4
Mass Flux (lb/ft^2-s)	0.0215	**Avg Flow Rate**	0.157
Min Q"$_{spray}$ (BTU/h-	387	**min ΔT (°F)**	0.7
Max Q"$_{spray}$ (BTU/h-	32956	**max ΔT (°F)**	910.6
Q"$_{spray}$ before	32522	**ΔT before CHF (°F)**	56.9
Max possible Q"$_{spray}$	32956		

Table B.29 Test 16 nodal values

Step #	T_1 (°F)	Q"$_1$ (BTU/h-ft^2)	T_2 (°F)	Q"$_2$ (BTU/h-ft^2)	T3 (°F)	Q"$_3$ (BTU/h-ft^2)	T_4 (°F)	Q"$_4$ (BTU/h-ft^2)	T_5 (°F)	Q"$_5$ (BTU/h-ft^2)	T_{fluid} (°F)	T_{avg} (°F)	Q"$_{avg}$ (BTU/h-ft^2)
1	-8.3	406	0.0	0	0.0	0	0.7	387	-1.3	392	86.3	0.7	387
2	-7.6	1328	0.0	0	0.0	0	1.7	1309	0.3	1312	87.1	1.0	1310
3	-3.5	3338	8.3	3310	0.0	0	4.9	3319	3.7	3321	87.5	5.6	3317
4	2.8	5645	0.0	0	0.0	0	12.5	5621	12.8	5621	87.7	9.4	5629
5	0.8	8361	15.0	8327	0.0	0	19.4	8316	14.6	8328	87.9	12.4	8333
6	8.4	12164	24.1	12127	28.9	12115	42.3	12080	30.2	12112	88.2	26.8	12119
7	34.6	16643	52.5	16597	56.9	16585	74.4	16537	74.7	16536	88.3	58.6	16580
8	49.1	21826	64.8	21786	76.9	21752	95.2	21702	59.6	21799	88.6	69.1	21773
9	53.0	26912	62.8	26887	0.0	0	65.5	26879	0.0	0	88.7	60.4	26893
10	0.0	0	58.8	32517	61.0	32511	0.0	0	50.8	32538	88.9	56.9	32522
11	908.8	33008	911.0	32942	911.0	32942	911.0	32942	911.0	32942	89.0	910.6	32956
12	691.4	22942	783.2	22123	813.5	21822	887.6	21013	804.1	21917	89.0	796.0	21964
13	0.0	0	0.0	0	503.6	17011	583.4	16514	390.0	17602	89.0	492.4	17042
14	39.4	12100	35.1	12111	34.8	12112	31.2	12121	29.0	12127	89.1	33.9	12114
15	14.1	6054	16.0	6049	14.6	6052	11.4	6060	13.3	6056	89.2	13.9	6054
16	-0.5	544	1.6	542	1.5	542	-0.7	545	2.1	541	89.2	1.7	542

Test 17

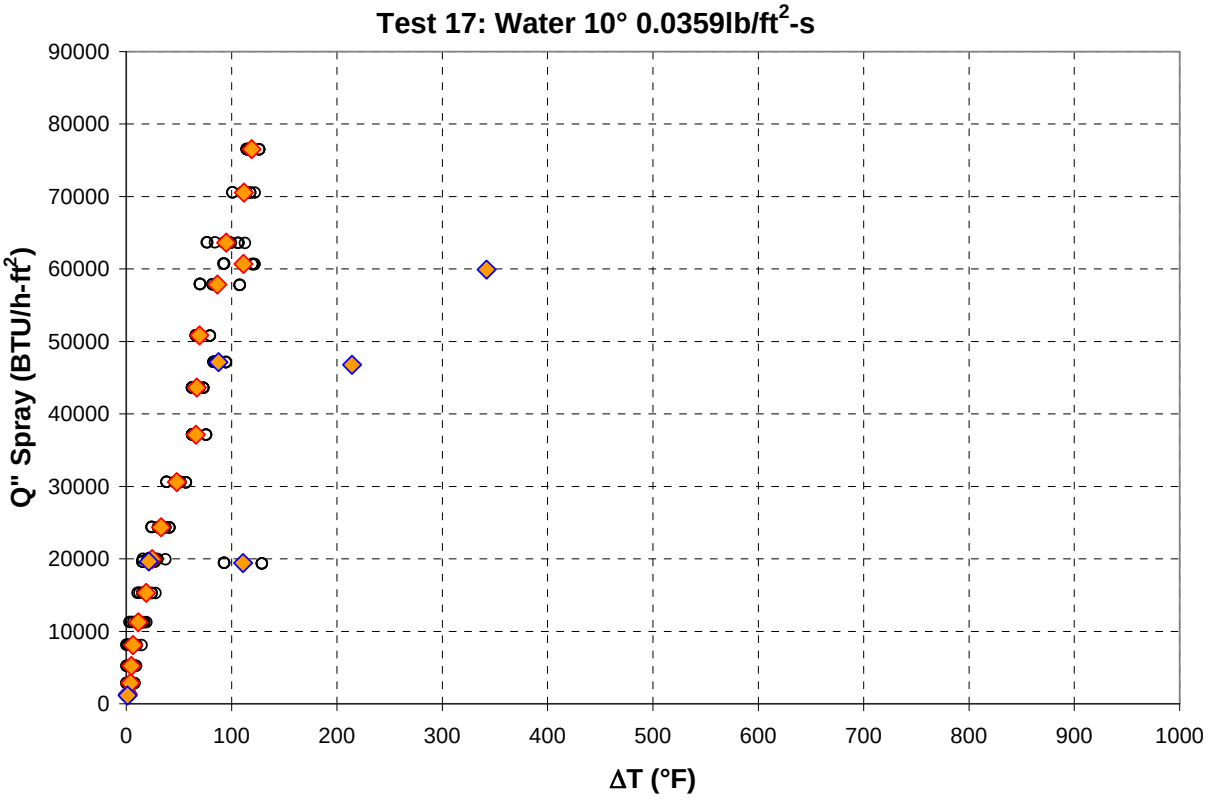

Figure B.17 Test 17 spray heat flux (BTU/h-ft^2) vs $T_{surface}$ - T_{liquid} (°F)

Table B.30 Test 17 summary data

Test	17		
Fluid	Water	**Avg Pressure (psi)**	16.5
Spray Angle	10	**Avg Fluid Temp (°F)**	85.6
Mass Flux (lb/ft^2-s)	0.0359	**Avg Flow Rate**	0.171
Min Q"$_{spray}$ (BTU/h-	1159	**min ΔT (°F)**	1.3
Max Q"$_{spray}$ (BTU/h-	76523	**max ΔT (°F)**	342.1
Q"$_{spray}$ before	76523	**ΔT before CHF (°F)**	118.9
Max possible Q"$_{spray}$	76523		

Table B.31 Test 17 nodal values

		Q"$_1$		Q"$_2$		Q"$_3$		Q"$_4$		Q"$_5$			Q"$_{avg}$
Step #	**T_1 (°F)**	**(BTU/h-ft^2)**	**T_2 (°F)**	**(BTU/h-ft^2)**	**T3 (°F)**	**(BTU/h-ft^2)**	**T_4 (°F)**	**(BTU/h-ft^2)**	**T_5 (°F)**	**(BTU/h-ft^2)**	**T_{fluid} (°F)**	**T_{avg} (°F)**	**(BTU/h-ft^2)**
1	0.1	1352	3.4	1345	0.0	0	-3.9	1361	0.0	0	83.5	1.7	1348
2	4.2	2866	7.3	2858	3.9	2867	-3.1	2882	0.5	2874	83.6	4.0	2866
3	3.6	5242	8.8	5229	6.1	5236	-1.7	5253	0.7	5248	83.8	4.8	5239
4	5.3	8124	10.6	8112	7.1	8120	-0.6	8138	2.7	8130	83.9	6.4	8122
5	10.1	11268	17.4	11250	13.5	11260	5.0	11280	11.5	11265	84.0	11.5	11265
6	19.2	15303	25.5	15286	17.9	15306	13.0	15318	0.0	0	84.1	18.9	15303
7	23.0	19982	31.0	19962	25.0	19977	19.3	19992	0.0	0	84.3	24.6	19978
8	30.4	24365	41.1	24337	37.1	24347	24.0	24381	0.0	0	84.4	33.1	24357
9	51.4	30581	56.6	30567	46.3	30595	38.2	30616	0.0	0	84.5	48.1	30590
10	62.9	37155	75.7	37120	63.5	37153	62.7	37155	0.0	0	84.6	66.2	37146
11	73.3	43610	69.6	43620	62.6	43639	62.6	43639	0.0	0	84.7	67.0	43627
12	68.5	50830	66.1	50836	67.3	50833	66.5	50835	79.5	50801	84.8	69.6	50827
13	70.1	57913	107.9	57811	82.0	57882	0.0	0	0.0	0	84.8	86.6	57869
14	84.7	63658	101.1	63614	98.6	63619	0.0	0	0.0	0	85.0	94.8	63630
15	104.2	70576	119.2	70534	111.7	70555	0.0	0	0.0	0	85.2	111.7	70555
16	114.5	76536	126.2	76502	116.0	76532	0.0	0	0.0	0	85.2	118.9	76523
17	119.8	60671	121.7	60666	92.7	60747	0.0	0	0.0	0	85.3	111.4	60695
117	0.0	0	0.0	0	0.0	0	0.0	0	342.1	59912	85.3	342.1	59912
18	84.8	47165	94.7	47137	83.1	47169	0.0	0	0.0	0	85.4	87.5	47157
118	0.0	0	0.0	0	0.0	0	214.4	46791	0.0	0	85.4	214.4	46791
19	15.5	19648	26.9	19621	21.7	19634	0.0	0	0.0	0	85.5	21.3	19634
119	0.0	0	0.0	0	0.0	0	92.9	19466	128.8	19363	85.5	110.9	19415
20	-0.5	1160	0.3	1160	0.9	1160	-0.3	1160	2.6	1159	85.6	1.3	1159

Test 18

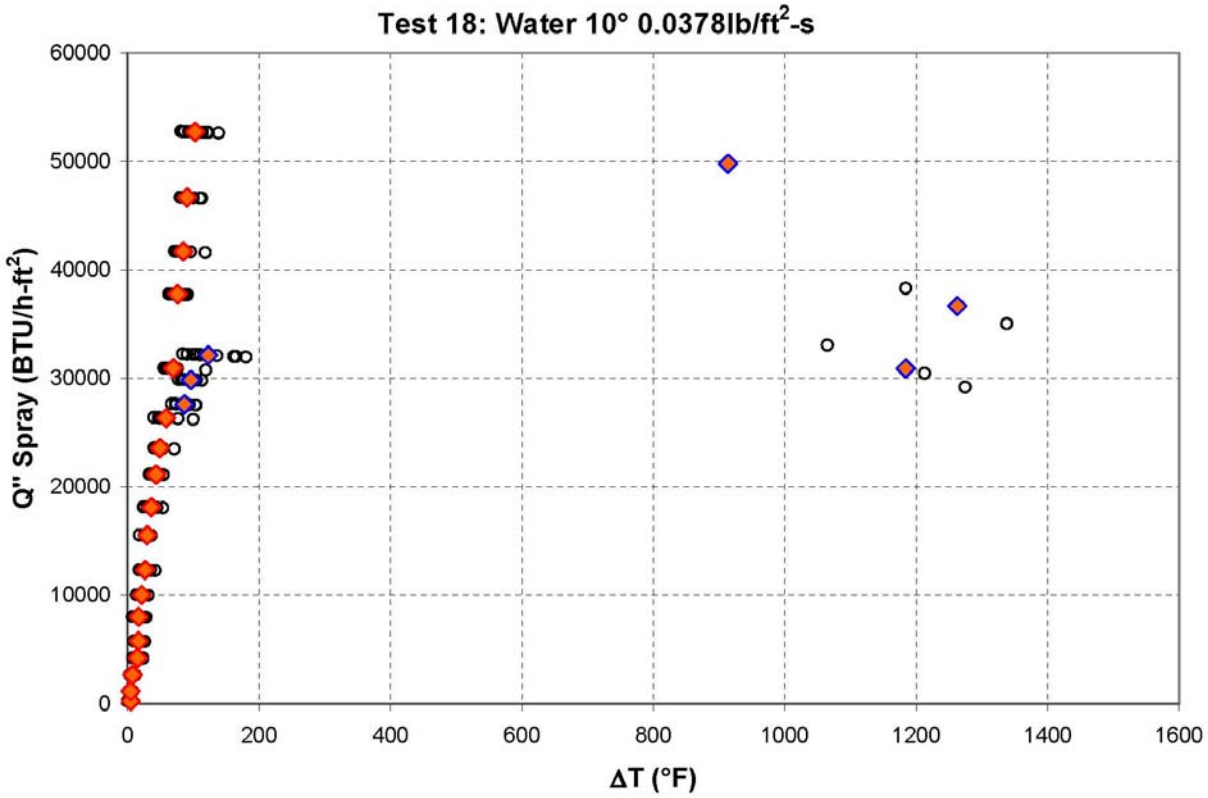

Figure B.18 Test 18 spray heat flux (BTU/h-ft^2) vs $T_{surface}$ - T_{liquid} (°F)

Table B.32 Test 18 summary data

Test	18		
Fluid	Water	**Avg Pressure (psi)**	17.6
Spray Angle	10	**Avg Fluid Temp (°F)**	85.5
Mass Flux (lb/ft^2-s)	0.0378	**Avg Flow Rate (GPM)**	0.174
Min Q"$_{spray}$ (BTU/h-	244	**min ΔT (°F)**	4.5
Max Q"$_{spray}$ (BTU/h-	52723	**max ΔT (°F)**	1262.3
Q"$_{spray}$ before	52723	**ΔT before CHF (°F)**	103.0
Max possible Q"$_{spray}$	59719		

Table B.33 Test 18 nodal values

Step #	T_1 (°F)	Q''_1 (BTU/h-ft^2)	T_2 (°F)	Q''_2 (BTU/h-ft^2)	T3 (°F)	Q''_3 (BTU/h-ft^2)	T_4 (°F)	Q''_4 (BTU/h-ft^2)	T_5 (°F)	Q''_5 (BTU/h-ft^2)	T_{fluid} (°F)	T_{avg} (°F)	Q''_{avg} (BTU/h-ft^2)
1	2.5	249	6.0	242	0.0	0	5.9	242	-0.2	255	84.1	4.8	244
2	3.5	1176	7.4	1167	0.0	0	5.2	1172	2.1	1179	84.2	4.5	1174
3	4.9	2672	8.9	2662	0.0	0	10.5	2659	4.6	2672	84.3	7.2	2666
4	9.5	4239	15.3	4225	20.6	4211	20.7	4211	10.6	4236	84.4	15.3	4224
5	10.7	5796	16.5	5782	24.0	5762	18.7	5776	13.0	5790	84.6	16.6	5781
6	9.5	8030	15.8	8015	24.0	7994	20.1	8005	14.2	8019	84.7	16.7	8013
7	15.3	10051	21.1	10037	26.8	10022	24.3	10029	20.2	10039	84.9	21.5	10035
8	18.4	12352	23.6	12339	33.3	12314	31.2	12320	26.2	12333	85.0	26.6	12331
9	23.1	15560	28.8	15546	34.9	15530	33.6	15533	28.2	15547	85.1	29.7	15543
10	26.9	18144	33.7	18127	39.3	18112	39.9	18111	40.7	18108	85.3	36.1	18120
11	37.7	21164	41.6	21154	48.6	21135	47.9	21137	41.5	21154	85.4	43.5	21149
12	40.5	23592	47.4	23574	53.1	23559	51.0	23564	53.6	23557	85.6	49.1	23569
13	45.5	26381	52.0	26364	62.0	26337	59.2	26345	75.2	26298	85.7	58.8	26345
14	58.4	30956	67.2	30932	69.9	30925	67.0	30933	85.1	30879	85.8	69.5	30925
15	67.7	37797	74.3	37779	79.6	37764	79.0	37766	79.8	37764	85.9	76.1	37774
16	75.0	41735	84.0	41710	92.4	41687	96.8	41674	76.1	41732	86.1	84.9	41707
17	82.1	46709	92.2	46681	0.0	0	107.6	46637	80.4	46713	86.2	90.6	46685
18	89.0	52763	109.6	52705	127.2	52654	0.0	0	86.1	52771	86.3	103.0	52723
20	913.4	49811	913.4	49797	913.4	49782	913.4	49807	913.4	49782	86.6	913.4	49796
21	1183.9	38308	1337.7	35044	0.0	0	0.0	0	1265.2	36678	86.6	1262.3	36677
22	1064.6	33072	1274.3	29196	0.0	0	0.0	0	1212.6	30471	86.7	1183.9	30913
23	91.5	32237	124.2	32147	0.0	0	168.9	32014	106.6	32197	86.8	122.8	32149
24	81.6	29913	109.6	29838	0.0	0	0.0	0	97.9	29870	87.0	96.4	29874
25	71.3	27648	100.5	27571	0.0	0	0.0	0	87.8	27605	87.1	86.6	27608

Effects of Varied Spray Fluid Properties

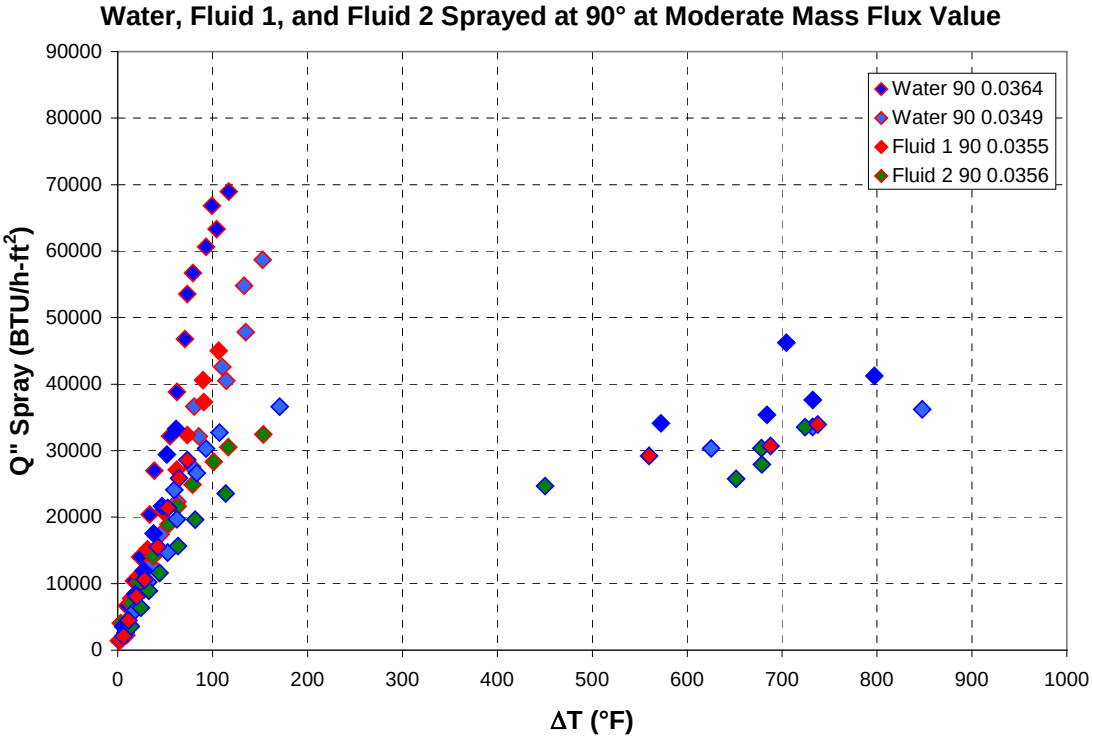

Figure B.19 Plot of water, Fluid 1, and Fluid 2 sprayed at 90° at a moderate mass flux

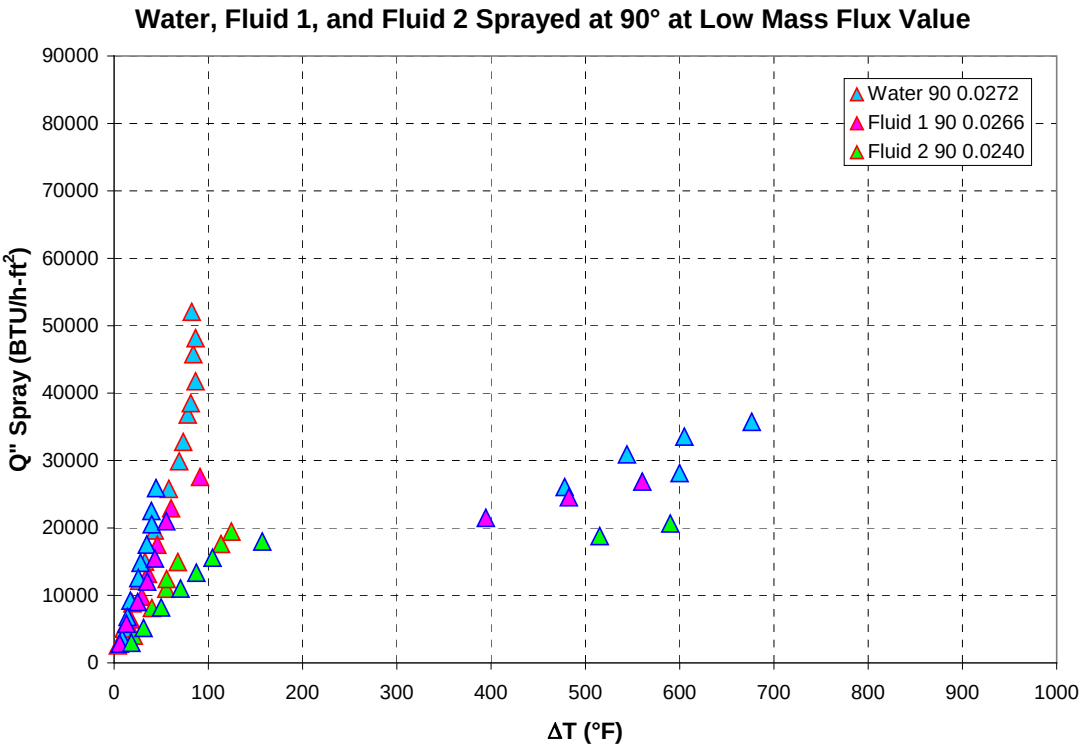

Figure B.20 Plot of water, Fluid 1, and Fluid 2 sprayed at 90° at a low mass flux

Effects of Spray Angle

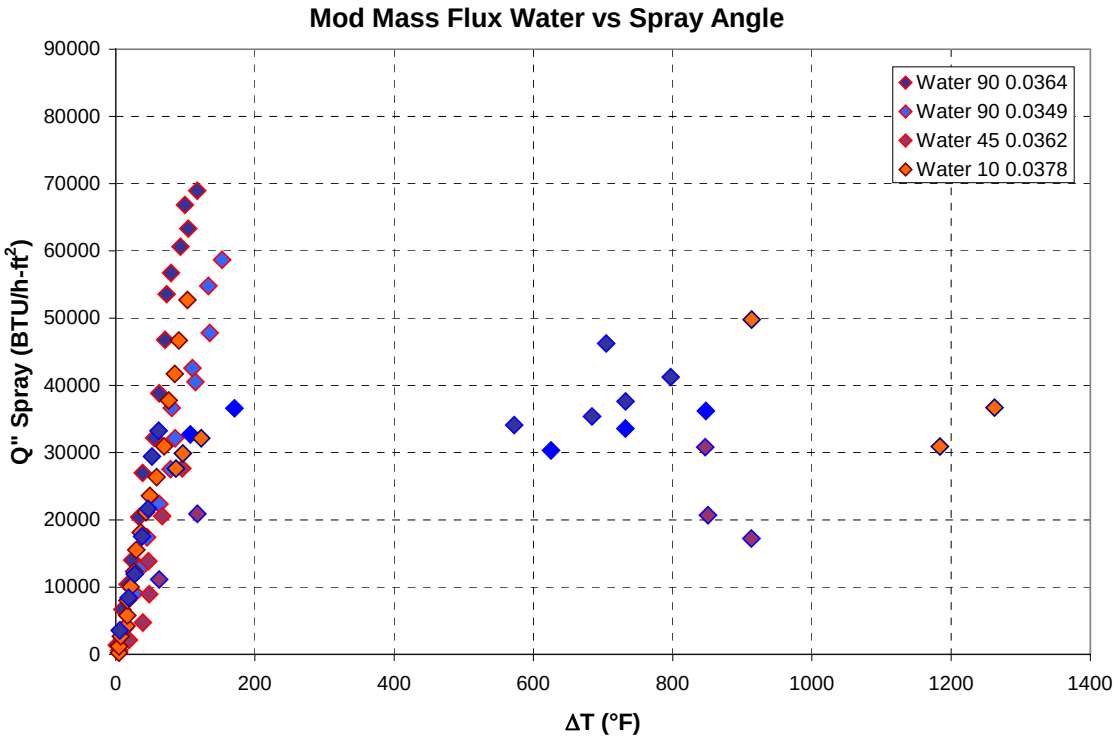

Figure B.21 Water sprayed normal (90°), 45°, and 10° to the surface at a mass flux near 0.035lb/ft^2-s

APPENDIX C - Specifications for Components / Materials

C.1 Pump Curve

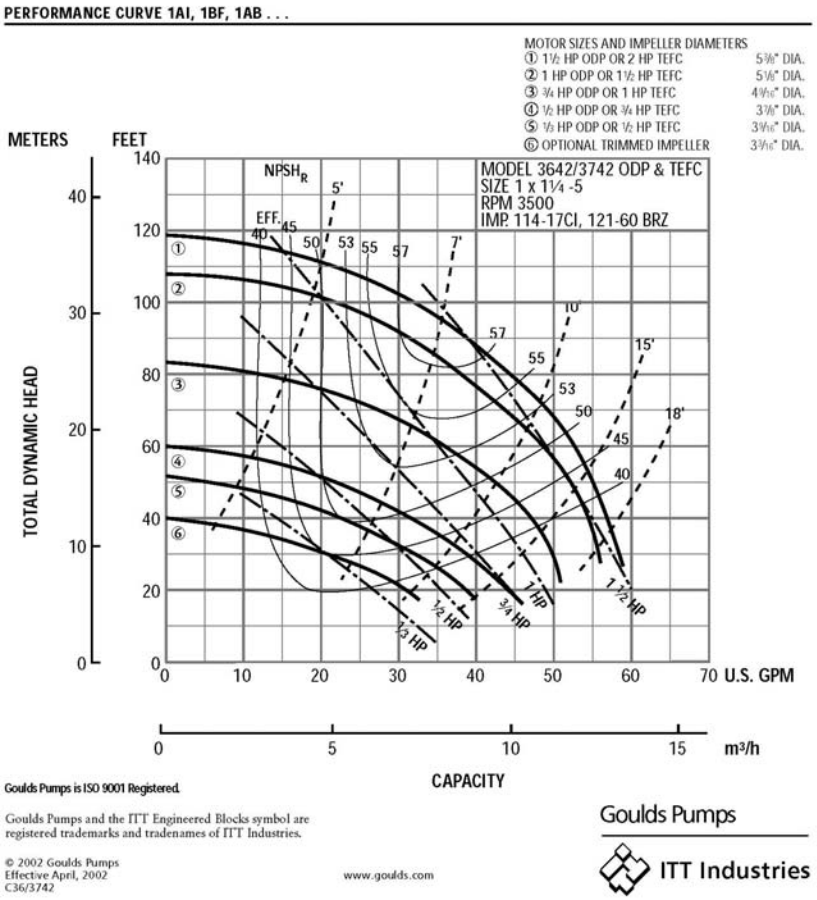

Figure C.1 Pump curve

Goulds Pump 1 ½ HP TEFC

Approx 105ft of head at 1GPM

Maximum Temperature: 212°F (100°C)

Maximum working pressure: 125 PSI

Motor: 60 Hz, 3500 RPM

C.2 IR Camera

TECHNICAL SPECIFICATIONS

IMAGING PERFORMANCE	
Thermal:	
Field of view/min focus distance	24°x18° /0.3 m (with 35 mm lens)
Spatial resolution (IFOV)	1.3 mrad
Thermal sensitivity	0.08°C at 30°C
Image frequency	50/60 Hz non-interlaced
Focus	Automatic or manual
Electronic zoom function	2,4,8 interpolating
Detector type	Focal Plane Array (FPA), uncooled microbolometer 320 x 240 pixels
Spectral range	7.5 to 13µm
Digital image enhancement	Normal and enhanced
Visual:	
Built-in digital video	640 x 480 pixels, full color
IMAGE PRESENTATION	
Video output	RS170 EIA/NTSC or CCIR/PAL composite video and IEEE-1394 FireWire output (full radiometric data)
Viewfinder	Built-in, high-resolution color LCD (TFT)
External display	4" LCD with integrated remote control
MEASUREMENT	
Temperature range	-40°C to +1,500°C (-40°F to +2,732°F) Up to +2,000°C (3632°F), optional
Accuracy	±2°C, ±2% of reading
Measurement mode	Spot/manual (up to 10 movable), automatic placement and reading of max. and min. temperature within area. Area (circle or box, up to 10 movable), isotherm (2), line profile, Delta T
Atmospheric transmission correction	Automatic, based on inputs for distance, atmospheric temperature and relative humidity
Optics transmission correction	Automatic, based on signals from internal sensors
Emissivity correction	Variable from 0.1 to 1.0 or select from listings in pre-defined materials list
Reflected ambient temperature correction	Automatic, based on input of reflected temperature
External optics/window correction	Automatic, based on input of optics/window transmission and temperature

Figure C.2 ThermaCAM S65 technical specifications from product brochure

C.3 MicroMotion Flow Meter

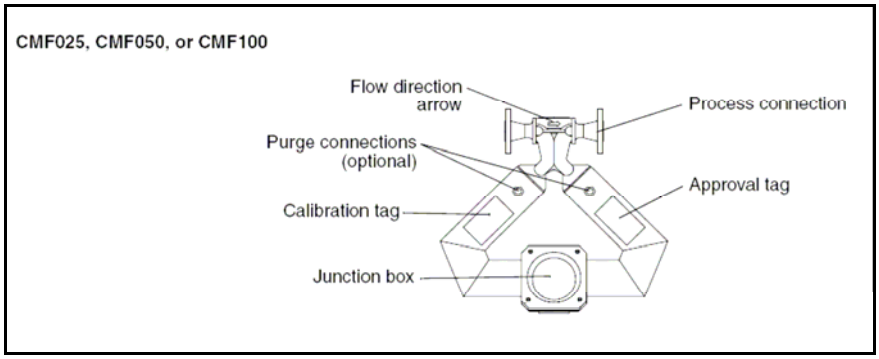

Figure C.3 MiCroMotion Elite CMF025 flow meter used in flow assembly

Micro Motion Flow Meter CFM 025 used to measure

Volumetric Flow Rate (0-2 gpm)

Temperature (50°-100°F)

Density (60 – 70 $^{lb}/_{ft\wedge 3}$)

Appendix
A

RFT9739 Specifications

Performance specifications

Sensor model		Mass flow accuracy*
ELITE	liquid	±0.10% ± [(zero stability / flow rate) x 100]% of rate
	gas	±0.50% ± [(zero stability / flow rate) x 100]% of rate
F-Series	liquid	±0.20% ± [(zero stability / flow rate) x 100]% of rate
	gas	±0.70% ± [(zero stability / flow rate) x 100]% of rate
D (except DH38), DT and DL	liquid	±0.15% ± [(zero stability / flow rate) x 100]% of rate
	gas	±0.65% ± [(zero stability / flow rate) x 100]% of rate
DH38	liquid	±0.15% ± [(zero stability / flow rate) x 100]% of rate
	gas	±0.50% ± [(zero stability / flow rate) x 100]% of rate

Sensor model		Mass flow repeatability*
ELITE	liquid	±0.05% ± [½(zero stability / flow rate) x 100]% of rate
	gas	±0.25% ± [(zero stability / flow rate) x 100]% of rate
F-Series	liquid	±0.10% ± [½(zero stability / flow rate) x 100]% of rate
	gas	±0.35% ± [(zero stability / flow rate) x 100]% of rate
D (except DH38), DT and DL	liquid	±0.05% ± [½(zero stability / flow rate) x 100]% of rate
	gas	±0.30% ± [(zero stability / flow rate) x 100]% of rate
DH38	liquid	±0.05% ± [½(zero stability / flow rate) x 100]% of rate
	gas	±0.25% ± [(zero stability / flow rate) x 100]% of rate

		Density accuracy		Density repeatability	
Sensor model		*g/cc*	*kg/m³*	*g/cc*	*kg/m³*
ELITE (except CMF010P)	liquid only	±0.0005	±0.5	±0.0002	±0.2
ELITE CMF010P	liquid only	±0.002	±2.0	±0.001	±1.0
F-Series	liquid only	±0.002	±2.0	±0.001	±1.0
D6, D12, D25, D40, DH100, DH150	liquid only	±0.002	±2.0	±0.001	±1.0
DH6, DH12, DH38	liquid only	±0.004	±4.0	±0.002	±2.0
D65, DL65, DT65, D100, DT100, D150, DT150, DH300	liquid only	±0.001	±1.0	±0.0005	±0.5
D300, D600, DL100, DL200	liquid only	±0.0005	±0.5	±0.002	±2.0

Sensor model	Temperature accuracy	Temperature repeatability
All sensors	±1°C ± 0.5% of reading in °C	±0.02°C

** Flow accuracy includes the combined effects of repeatability, linearity, and hysteresis. All specifications for liquids are based on reference conditions of water at 68 to 77°F (20 to 25°C) and 15 to 30 psig (1 to 2 bar), unless otherwise noted. For values of zero stability, refer to product specifications for each sensor.*

Figure C.4 Model RFT9739 specifications from Micro Motion Instruction Manual, 2000.

C.4 Actual Flow Loop Configuration

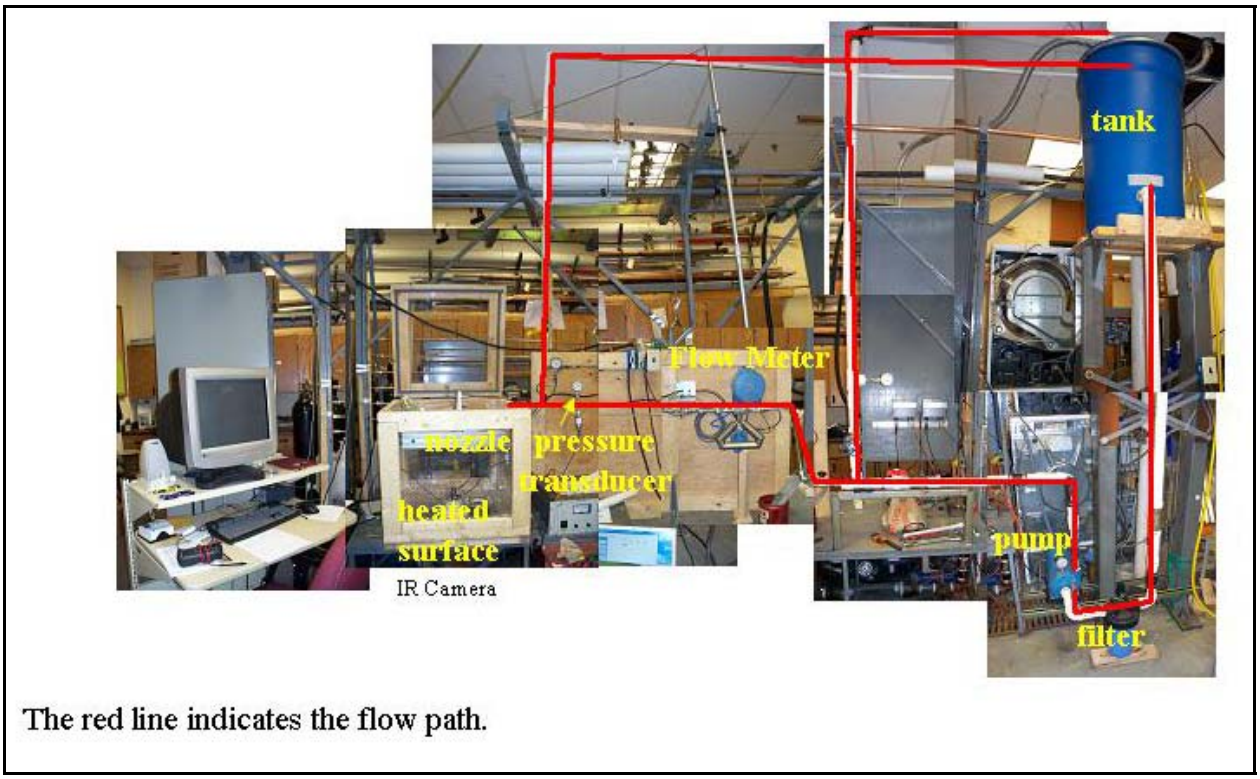

Figure C.5 Mosaic of constructed flow loop configuration

C.5 Nozzle Specifications

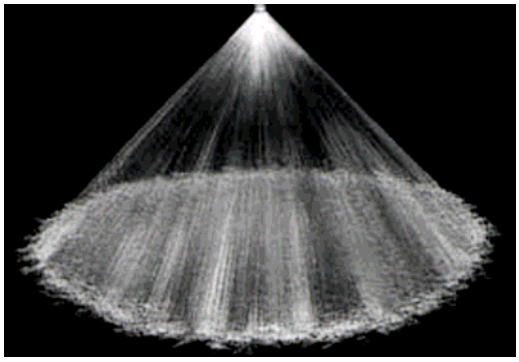

Figure C.6 Picture of spray from the BETE nozzle

Table C.34 Nozzle performance

Male or Female Pipe Size	Nozzle Number	K Factor	GALLONS PER MINUTE @ PSI										Approx. Orifice Dia. (in.)
			10 PSI	20 PSI	30 PSI	40 PSI	60 PSI	80 PSI	100 PSI	150 PSI	200 PSI	400 PSI	
1/8	WL 1/4	0.044	0.13	0.18	0.22	0.25	0.30	0.35	0.38	0.47	0.53	0.74	0.043
	WL 1/2	0.088	0.26	0.36	0.44	0.50	0.60	0.69	0.77	0.93	1.07	1.48	0.055
	WL 3/4	0.132	0.39	0.54	0.66	0.75	0.91	1.04	1.15	1.40	1.60	2.21	0.072

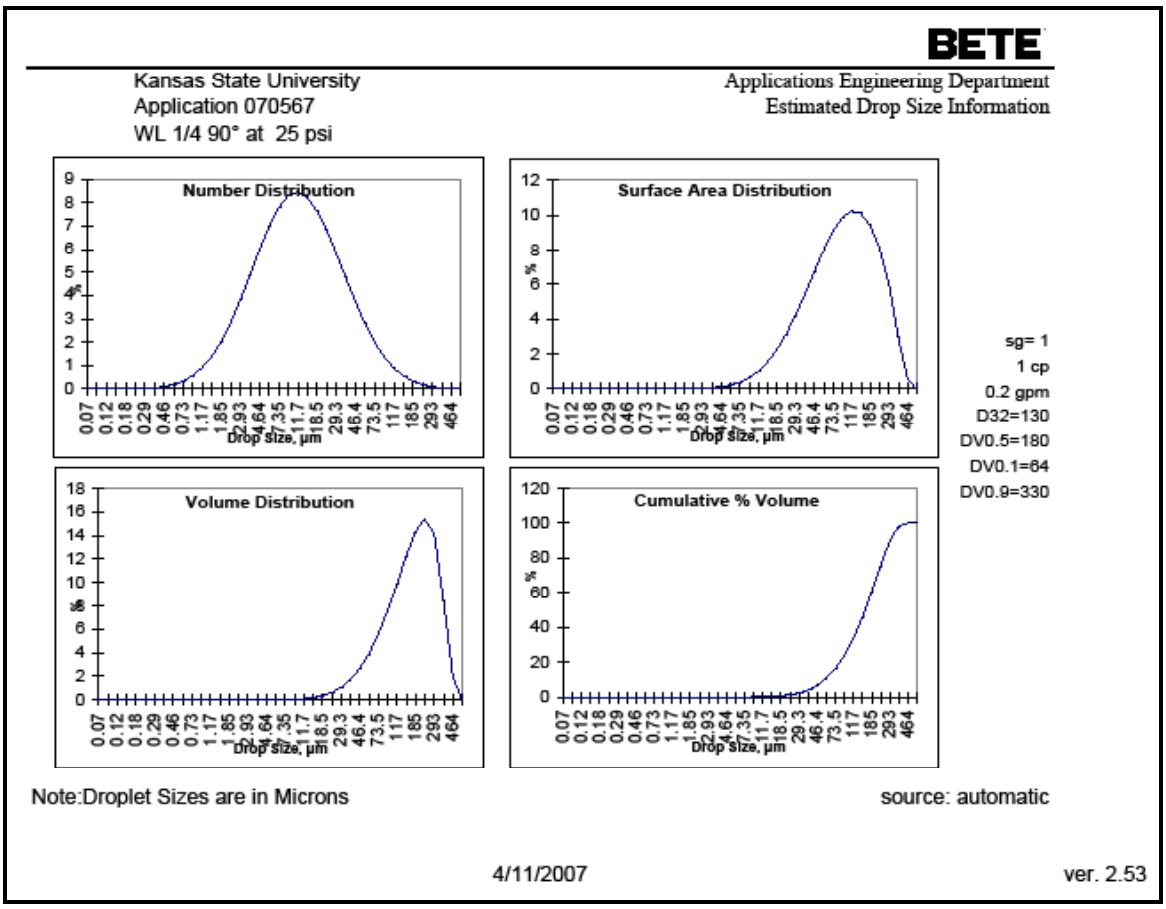

Figure C.7 Estimated droplet size distribution for the BETE WL 1/4 at 0.2GPM

C.6 Viatran Pressure Transducer Calibration

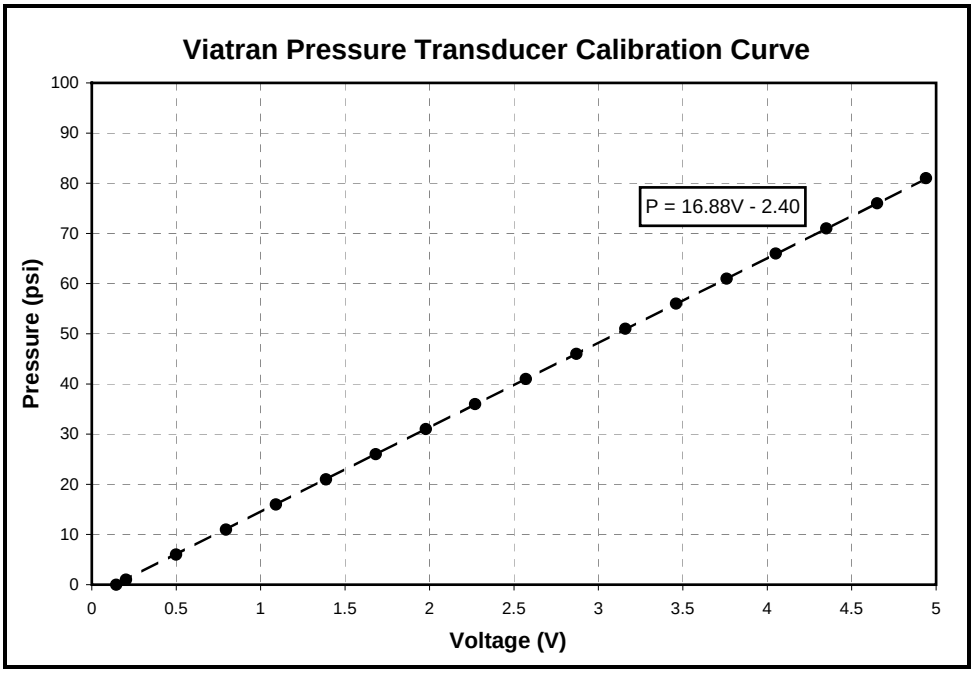

Figure C.8 Calibration plot for Viatran pressure transducer

APPENDIX D - Component Drawings

D.1 Heat Surface Assembly

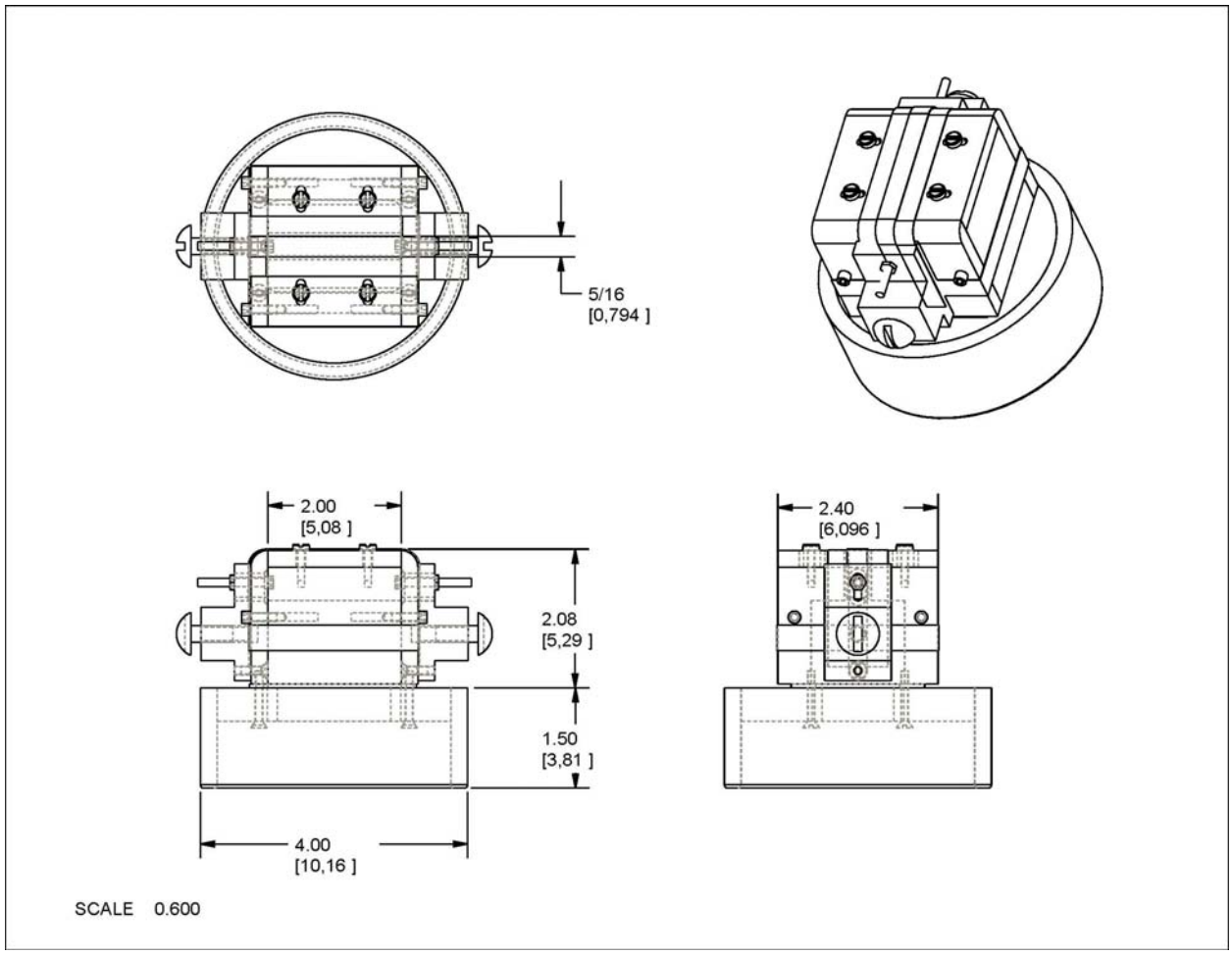

Figure D.1 Heated Surface Assembly Drawing

D.2 Mass Collector

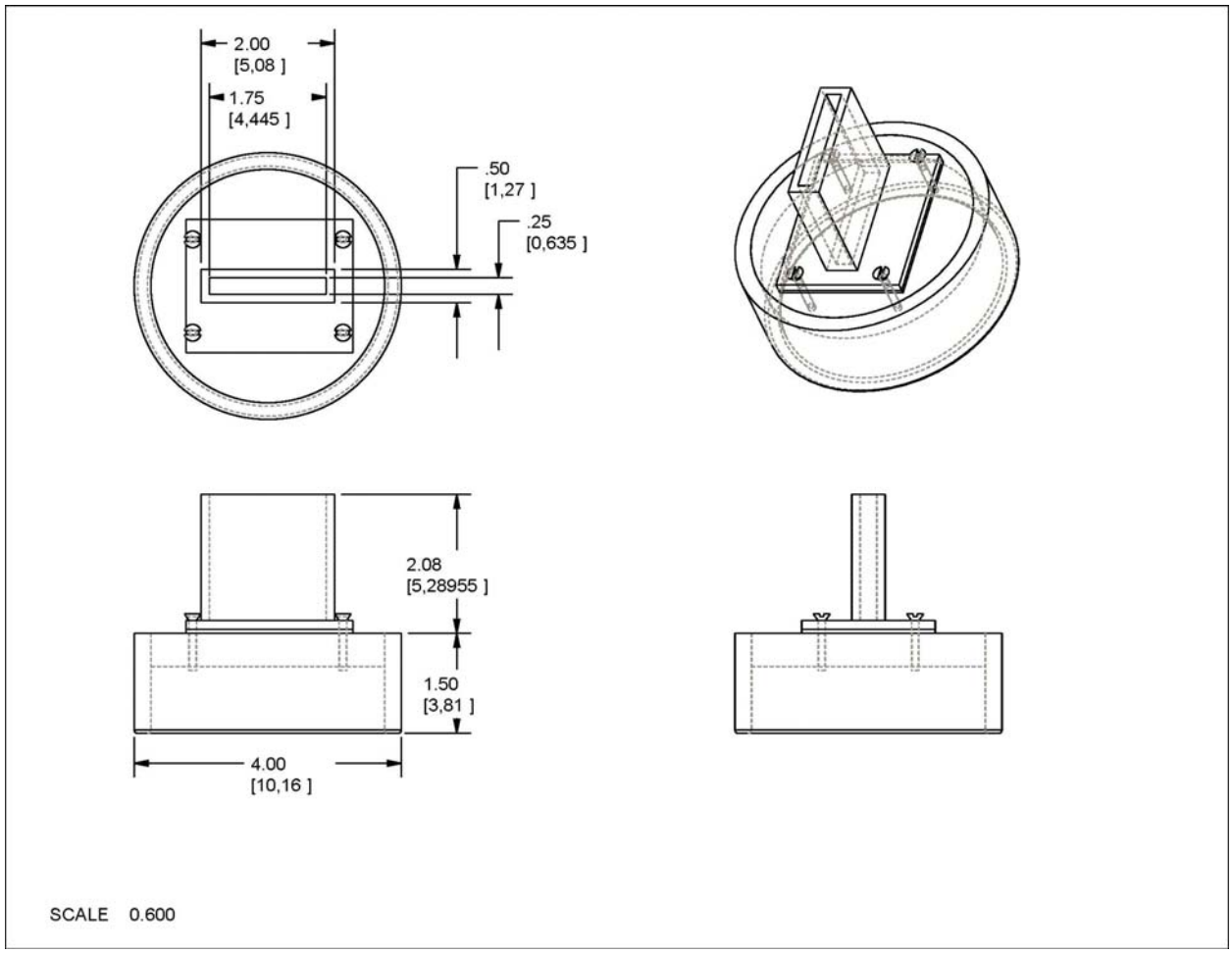

Figure D.2 Mass Collector Drawing

APPENDIX E - Processing Codes

E.1 MatLAB Code

Mass Flux

```
%Data Location
extension = 'C:\Documents and Settings\Cristina Pedotto\Desktop\Spray Cooling\Test Data and Results';
%Read in the input data file
input_data_filename = sprintf('%s\\Input Summary.xls',extension);
input_data = xlsread(input_data_filename, 'Input');

for test = 1:1:size(input_data,1)
output_file_name = sprintf('%s\\Test %i\\Test%i nodal results.xls',extension,test,test);
%Open Excel
Excel = actxserver ('Excel.Application');
File=output_file_name;
if ~exist(File,'file')
ExcelWorkbook = Excel.workbooks.Add;
ExcelWorkbook.SaveAs(File,1);
ExcelWorkbook.Close(false);
end
invoke(Excel.Workbooks,'Open',File);

  if input_data(test,10) == 1
    %Read in Mass Flux Data
    processing_data_filename = sprintf('%s\\Test %i\\Test%i Processing.xls',extension,test,test);
    pretest_mass_data = xlsread(processing_data_filename, 'F1');
    posttest_mass_data = xlsread(processing_data_filename, 'F2');
    pretest_flow_data_filename = sprintf('%s\\Test %i\\Flow%ia.lvm',extension,test,test);
    if posttest_mass_data(1,2) ~= 0
      posttest_flow_data_filename = sprintf('%s\\Test %i\\Flow%ib.lvm',extension,test,test);
      posttest_flow_data = dlmread(posttest_flow_data_filename);
    else
      posttest_flow_data = zeros(3,4);
    end
    pretest_flow_data = dlmread(pretest_flow_data_filename);

    %Ignore non-relevant mass flux trails
    n = 1; n_max = size(pretest_mass_data,1);
    while n <= n_max
      if pretest_mass_data(n,5) == 0
        pretest_mass_data(n,:) = [];
        n_max = n_max-1;
      else
        n=n+1;
      end
    end
    if posttest_mass_data(1,2) ~= 0
      n = 1; n_max = size(posttest_mass_data,1);
      while n <= n_max
        if posttest_mass_data(n,5) == 0
          posttest_mass_data(n,:) = [];
          n_max = n_max-1;
        else
          n=n+1;
        end
      end
      mass_flux(size(pretest_mass_data,1)+size(posttest_mass_data,1),1) = zeros;
    end
```

```
    %Summarize mass flux data
    mass_flux(size(pretest_mass_data,1),1) = zeros;
    for i = 1:1:size(pretest_mass_data,1)
       if pretest_mass_data(i,5) == 1
          mass_flux(i,1) = i;
          mass_flux(i,2) = pretest_mass_data(i,2) - pretest_mass_data(i,3); %g
          mass_flux(i,3) = mass_flux(i,2)/(1.75*.25*.0254^2)/1000/(pretest_mass_data(i,4)*60); %kg/m^2-s
          mass_flux(i,4) = mass_flux(i,3)*2.20462262/3.2808399^2; %lb/ft^2-s
       end
    end

    %Claculate Averages and Standard Deviations
    pretest_avg = mean(mass_flux(1:size(pretest_mass_data,1),4));
    pretest_stdev = std(mass_flux(1:size(pretest_mass_data,1),4));
    flag1 = 1;
    a = 1;
    for k = 2:1:size(pretest_flow_data,1)
       if pretest_flow_data(k,1) == 0 || pretest_flow_data(k,1) - pretest_flow_data(k-1,1) >10 || k == size(pretest_flow_data,1)
          flag2 = k;
          if k == size(pretest_flow_data,1)
             flag2 = k+1;
          end
          for j = flag1:1:flag2-1
             pressure(j-flag1+1) = pretest_flow_data(j,2);
             water_temp(j-flag1+1) = pretest_flow_data(j,6);
             flow_rate(j-flag1+1) = pretest_flow_data(j,8);
          end
          mass_flux(a,5) = mean(pressure);
          mass_flux(a,6) = std(pressure);
          mass_flux(a,7) = mean(water_temp);
          mass_flux(a,8) = std(water_temp);
          mass_flux(a,9) = mean(flow_rate);
          mass_flux(a,10)= std(flow_rate);
          flag1 = flag2;
          a = a + 1;
          clear pressure water_temp flow_rate;
       end
    end

    %Post Test Mass Tests
    if posttest_mass_data(1,2) ~= 0
       for i = 1:1:size(posttest_mass_data,1)
          if posttest_mass_data(i,5) == 1
             mass_flux(size(pretest_mass_data,1)+i,1) = i;
             mass_flux(size(pretest_mass_data,1)+i,2) = posttest_mass_data(i,2) - posttest_mass_data(i,3); %g
             mass_flux(size(pretest_mass_data,1)+i,3) =
mass_flux(size(pretest_mass_data,1)+i,2)/(1.75*.25*.0254^2)/1000/(posttest_mass_data(i,4)*60); %kg/m^2-s
             mass_flux(size(pretest_mass_data,1)+i,4) = mass_flux(size(pretest_mass_data,1)+i,3)*2.20462262/3.2808399^2; %lb/ft^2-s
          end
       end
       %Claculate Averages and Standard Deviations
       posttest_avg = mean(mass_flux(size(pretest_mass_data,1)+1:size(pretest_mass_data,1)+size(posttest_mass_data,1),4));
       posttest_stdev = std(mass_flux(size(pretest_mass_data,1)+1:size(pretest_mass_data,1)+size(posttest_mass_data,1),4));
       flag1 = 1;
       for k = 2:1:size(posttest_flow_data,1)
          if posttest_flow_data(k,1) == 0 || posttest_flow_data(k,1) - posttest_flow_data(k-1,1) >10 || k == size(posttest_flow_data,1)
             flag2 = k;
             if k == size(posttest_flow_data,1)
                flag2 = k+1;
             end
             for j = flag1:1:flag2-1
                pressure(j-flag1+1) = posttest_flow_data(j,2);
                water_temp(j-flag1+1) = posttest_flow_data(j,6);
                flow_rate(j-flag1+1) = posttest_flow_data(j,8);
             end
             mass_flux(a,5) = mean(pressure);
             mass_flux(a,6) = std(pressure);
             mass_flux(a,7) = mean(water_temp);
             mass_flux(a,8) = std(water_temp);
```

```
            mass_flux(a,9) = mean(flow_rate);
            mass_flux(a,10)= std(flow_rate);
            flag1 = flag2;
            a = a + 1;
            clear pressure water_temp flow_rate;
         end
      end
      clear a i k j flag1 flag2;
   else
      posttest_mass_data = zeros(3,5);
      posttest_avg = 0;
      posttest_stdev = 0;
   end

   %erase rows indicated to not be used for analysis
   s = size(mass_flux,1);
   n = 0;
   for i = 1:1:s
      i = i-n;
      if mass_flux(i,2) == 0
         mass_flux(i,:) = [];
         s = size(mass_flux,1);
         n = n+1;
      end
   end

   %Calculate Overall Averages
   for i = 2:1:10
      averages(1,i) = mean(mass_flux(:,i));
      stdevs(1,i) = std(mass_flux(:,i));
   end

   mass_flux(size(mass_flux,1)+1,:) = averages;
   mass_flux(size(mass_flux,1)+1,:) = stdevs;

   if posttest_avg ~= 0
      test_avg = (pretest_avg + posttest_avg)/2.0;
      test_stdev = (pretest_stdev + posttest_stdev)/2.0;
   else
      test_avg = pretest_avg;
      test_stdev = pretest_stdev;
   end

   summary_titles = {'PreTest','PostTest','Test','(lb/ft^2-s)'};
   xlswrite1(output_file_name, summary_titles, 'Mass Flux Data','A1');
   xlswrite1(output_file_name, pretest_avg, 'Mass Flux Data','A2');
   xlswrite1(output_file_name, pretest_stdev, 'Mass Flux Data','A3');
   xlswrite1(output_file_name, posttest_avg, 'Mass Flux Data','B2');
   xlswrite1(output_file_name, posttest_stdev, 'Mass Flux Data','B3');
   xlswrite1(output_file_name, test_avg, 'Mass Flux Data','C2');
   xlswrite1(output_file_name, test_stdev, 'Mass Flux Data','C3');
   titles = {'Trial','Dm (g)','Mass Flux (kg/m^2-s)', 'Mass Flux (lb/ft^2-s)',...
   'Avg. Pressure (psi)', 'Pressure StDev (psi)', 'Avg Water Temp (°F)',...
   'Water Temp StDev (°F)', 'Avg Flow Rate (GPM)','Flow Rate StDev (GPM)'};
   xlswrite1(output_file_name, titles, 'Mass Flux Data','A5');
   xlswrite1(output_file_name, mass_flux, 'Mass Flux Data', 'A6');
      %Close Excel
   invoke(Excel.ActiveWorkbook,'Save');
   Excel.Quit
   Excel.delete
   clear Excel
   clear mass_flux averages stdevs i pretest_mass_data posttest_mass_data...
   pretest_flow_data posttest_flow_data;
else
%Close Excel
   invoke(Excel.ActiveWorkbook,'Save');
   Excel.Quit
   Excel.delete
   clear Excel
```

```
   end
end
```

System Data Summary

```
%Data Location
extension = 'C:\Documents and Settings\Cristina Pedotto\Desktop\Spray Cooling\Test Data and Results';
%extension = input('Enter the location of the files:\n', 's');

%Read in the input data file
input_data_filename = sprintf('%s\\Input Summary.xls',extension);
input_data = xlsread(input_data_filename, 'Input');

for test = 1:1:size(input_data,1)
output_file_name = sprintf('%s\\Test %i\\Test%i nodal results.xls',extension,test,test);

%Open Excel
Excel = actxserver ('Excel.Application');
File=output_file_name;
if ~exist(File,'file')
ExcelWorkbook = Excel.workbooks.Add;
ExcelWorkbook.SaveAs(File,1);
ExcelWorkbook.Close(false);
end
invoke(Excel.Workbooks,'Open',File);

   if input_data(test,10) == 1
      %Read in Heat Data
      processing_data_filename = sprintf('%s\\Test %i\\Test%i Processing.xls',extension,test,test);
      heat_data_filename = sprintf('%s\\Test %i\\Heat%i.lvm',extension,test,test);
      heat_data = dlmread(heat_data_filename);

      %Calculate Overall Averages
      for i = 2:1:15
         averages(1,i) = mean(heat_data(:,i));
         stdevs(1,i) = std(heat_data(:,i));
         maxs(1,i) = max(heat_data(:,i));
         mins(1,i) = min(heat_data(:,i));
      end

      %heat_data(size(heat_data,1)+1,:) = averages;
      %heat_data(size(heat_data,1)+1,:) = stdevs;
      %heat_data(size(heat_data,1)+1,:) = maxs;
      %heat_data(size(heat_data,1)+1,:) = mins;

      titles = {'Time (s)','Pressure (psi)', ' ', 'Density (lb/ft^3)',' ',...
         'Water Temp (°F)',' ', 'Flow Rate (GPM)','Power (W)',' ',...
         'Voltage (V)',' ','Current (A)',' ','Beaded TC (°F)'};
      xlswrite1(output_file_name, titles, 'Heat Data','A1');
      xlswrite1(output_file_name, heat_data, 'Heat Data', 'A2');

      %Close Excel
      invoke(Excel.ActiveWorkbook,'Save');
      Excel.Quit
      Excel.delete
      clear Excel

      clear heat_data averages stdevs i;
   else
      %Close Excel
      invoke(Excel.ActiveWorkbook,'Save');
      Excel.Quit
      Excel.delete
      clear Excel
   end
end
```

Image Processing

```
%Data Location
extension = 'C:\Documents and Settings\Cristina Pedotto\Desktop\Spray Cooling\Test Data and Results';

%Read in the input data file
input_data_filename = sprintf('%s\\Input Summary.xls',extension);
input_data = xlsread(input_data_filename, 'Input');

for test = 13:1:14%size(input_data,1)
   output_file_name = sprintf('%s\\Test %i\\Test%i nodal results.xls',extension,test,test);

      if input_data(test,10) == 1

         %Open Excel
         Excel = actxserver ('Excel.Application');
         File=output_file_name;
         if ~exist(File,'file')
            ExcelWorkbook = Excel.workbooks.Add;
            ExcelWorkbook.SaveAs(File,1);
            ExcelWorkbook.Close(false);
         end
         invoke(Excel.Workbooks,'Open',File);

         %Read in Heat Data
         processing_data_filename = sprintf('%s\\Test %i\\Test%i Processing.xls',extension,test,test);
         heat_data_filename = sprintf('%s\\Test %i\\Heat%i.lvm',extension,test,test);
         heat_data = dlmread(heat_data_filename);

         %Process the DAQ file:
         %Find points to be considered power change
         changes(1) = 1;
         mark = 2;
         for j = 2:1:size(heat_data,1)
            a = abs(heat_data(j,13)-heat_data((j-1),13));
            if a > 0.5
               changes(mark) = j;
               mark = mark + 1;
            end
         end
         changes(mark) = j;

         %Finding averages
         n=0;
         for j = 2:1:size(changes,2)
            if (changes(j) - changes(j-1))<25
               length = changes(j) - changes(j-1);
            else
               length = 25;
            end

            for i = 1:1:length
            %for i = 1:1:(changes(j) - changes(j-1))
               for k = 1:1:15
                  step(i,k) = heat_data((changes(j)-length-1+i),k);
               end
            end

            %Forming matrix of averages
            if (size(step,1) > 6)
               step_avg = mean(step); %averages
               averages(j-1-n,1) = j-1-n; %Test number
               averages(j-1-n,2) = step(1,1); %start time
               averages(j-1-n,3) = step(size(step,1),1); %end time
               averages(j-1-n,4) = averages(j-1-n,3) - averages(j-1-n,2); %time step
               averages(j-1-n,5) = length; %number of data points used to define averages

               for k = 2:1:15
                  averages(j-1-n,k+4) = step_avg(1,k);
```

```
            end
        else
            n = n+1;
        end
        clear step;
    end

    %Define the NiChrome points
    x_start = input_data(test,12);
    x_end = input_data(test,13);
    y_center = input_data(test,14);
    points = 5; %Number of points selected from the NiChrome Surface
    section = int32(x_end - x_start)/(points*2);

    for p = 1:1:points
        x(p) = (2*p-1)*section + x_start;
        y(p) = y_center;
    end

    for i = 1:1:size(averages,1)
        if averages(i,13) == max(averages(:,13));
            Pmax_loc = i;
        end
    end

    %Read in Image Process Data
    QV_data_filename = sprintf('%s\\Test %i\\Test%i Processing.xls',extension, test, test);
    QV_data = xlsread(QV_data_filename, 'HT1');

    n = 0;
    QV_image_averages(size(QV_data,1),2) = zeros;
    for i = 1:1:size(QV_data,1)
        if mod((QV_data(i,2)-QV_data(1,2)),3) == 0
            n = n + 1;
            if i > 4
                if QV_data(i,2) - QV_data(i-3,2) == 1000
                    n = n - 1;
                end
            end
        end
        QV_image_averages(i,1) = QV_data(i,2); %Image Name
        QV_image_averages(i,2) = n;%Step Number
        QV_image_averages(i,3) = averages(n,17); %Avg Applied Current
        QV_image_averages(i,4) = averages(n,18); %Avg StDev Current
        QV_image_averages(i,5) = averages(n,10); %Avg Fluid Temperature
        QV_image_averages(i,6) = averages(n,11); %Avg StDev Temperature
    end

    %WARNING
    steps = (QV_data(size(QV_data,1),2) - QV_data(1,2) + 1 + 3*input_data(test,11))/3;
    if steps ~= size(averages,1)
        fprintf('ERROR: Inconsistant number of power increments!\nQuickVIEW file gives %i.\nLabVIEW file gives %i.\nTest
%i\n',steps,size(averages,1),test);
        %Close Excel
        invoke(Excel.ActiveWorkbook,'Save');
        Excel.Quit
        Excel.delete
        clear Excel
        return;
    end


    %Determine Pixelation
    pixelation = 9; %input('Enter pixelation [64,25,16,9,1]:');
    pixel = zeros(pixelation,1);

    mid_image = sprintf('%s\\Test %i\\Heat%i images\\1%.3i.jpg',extension,test,test,int16(steps/2));
    A = imread(mid_image);
    %Show selected region
```

```
for j = 1:1:size(A,2)
   for i = 1:1:size(A,1)
      if (j>=x_start-1 && j<=x_end+1 && i==y_center)
         A(i,j,1) = 255; A(i,j,2) = 0; A(i,j,3) = 0;
      end
   end
end
figure, image(A);
locations_filename = sprintf('%s\\Test %i\\Test %i selected line',extension,test,test);
saveas(gcf,locations_filename,'jpeg')

list_place = 0;%Set start of temperature listing

%Start Image Processing
for ww = 0:3:size(QV_data,1)-3 %Loops for each steady state test
   clear A B C D i j m n k avg avg_sq avg_temp h_avg_english h_avg_metric q_area sum;

   for k=1:1:3 %Loops for each frame in the test
      if ww == 0
         s = k;
      else
         s = ww+k;
      end
      filename = sprintf('%.4i',QV_data(s,2));
      image_filename = sprintf('%s\\Test %i\\Heat%i images\\%s.jpg',extension, test, test, filename);
      A = imread(image_filename);
      B = A;

      high_temp = QV_data(s,8);
      %if high_temp > 1014.0
      %    high_temp = 1014.0;
      %end
      low_temp = QV_data(s,9);
      %if low_temp < 14.0
      %    low_temp = 14.0;
      %end
      range = high_temp - low_temp;
      top_x = 333;
      top_y = 24;
      top = A(top_y,top_x,1);
      bottom_x = 333;
      bottom_y = 224;
      bottom = A(bottom_y,bottom_x,1);
      slope = (single(high_temp) - single(low_temp))/(single(top) - single(bottom));
      QV_data(s,12) = slope;
      intercept = single(high_temp) - slope*single(top);

      %Power => Heat Generation
      t = 0.000125; %m
      l = 2.0*.0254; %m
      w = (0.3151)*.0254;  %m
      Area = w*l; %m^2
      R_base = 0.000108; %Volumetric Resistance Ohm-cm
      RT = 0.00000000005*(5/9); % Thermal change Ohm-cm/F
      %R = 0.000108/(w*t)/100;%Ohms/m
      T_sat = 212; %°F

      for n = 1:1:(x_end - x_start + 1)
         %fprintf ('You are here ww = %i k = %i s = %i n = %i\n',ww, k, s, n);
         j = x_start + n - 1;
         i = y_center;
         pixel(1) = A(i-1, j-1);
         pixel(2) = A(i, j-1);
         pixel(3) = A(i+1, j-1);
         pixel(4) = A(i-1, j);
         pixel(5) = A(i, j);
         pixel(6) = A(i+1, j);
         pixel(7) = A(i-1, j+1);
         pixel(8) = A(i, j+1);
```

```
                pixel(9) = A(i+1, j+1);
                avg1(s) = mean(pixel)*slope + intercept;
                stdev1(s) = std(pixel)*slope;
                line_temperature(s,n) = avg1(s);
                temp_gradient(s,n + 3) = line_temperature(s,n);

                for p = 1:1:points
                   if j == x(p)
                      if QV_data(s,2) > 1999
                         base(s,1) = QV_image_averages(s,2)+100; %Step # for high side
                      else
                         base(s,1) = QV_image_averages(s,2); %Step # for even temp strip or low side
                      end
                      base(s,3*p-1) = mean(pixel)*slope + intercept;%Measured Surface Temperature °F
                      base(s,3*p) = std(pixel)*slope;%StDev of Measured Surface Temperature °F

                      T_ref = QV_data(ww+1,4);
                      T_fluid = QV_image_averages(s,5); %Avg Fluid Temp per step
                      base(s,3*points + 2) = QV_image_averages(s,3); %Average Current
                      base(s,3*points + 3) = QV_image_averages(s,4); %Average Std of Current over Step
                      base(s,3*points + 4) = T_fluid;
                      base(s,3*points + 5) = QV_image_averages(s,6);%Average StDev for Fluid Temp per Step
                      base(s,3*points + 6) = slope; %Pixelation °F
                      base(s,3*points + 7) = high_temp;
                      base(s,3*points + 8) = low_temp;

                      heat(s,1) = QV_image_averages(s,2); %Step Number
                      T(p) = mean(pixel)*slope + intercept;
                      heat(s,5*p - 3) = T(p);
                      R = (R_base+RT*(T(p)-72.5))/(w*t)/100;%Ohms/m
                      q_gen = QV_image_averages(s,3)^2*R/w;
                      heat(s,5*p - 1) = q_gen;
                      q_rad_bot(p) = 5.67e-8*QV_data(s,3)*(((T(p)+459.67)^4)-((T_ref+459.67)^4))*(5/9)^4;
                      q_rad_top(p) = 5.67e-8*QV_data(s,3)*(((T(p)+459.67)^4)-((T_fluid+459.67)^4))*(5/9)^4;
                      q_rad(p) = q_rad_bot(p) + q_rad_top(p);
                      heat(s,5*p) = q_rad(p);
                      q_conv(p) = 0.27*(0.0263/w)*abs(T(p)-T_ref)*(5/9)*((9.81*abs(T(p)-T_ref)*(5/9)*w^3)/(((T(p)+T_ref)*(5/9)/2)*15.89e-
6*22.5e-6))^(1/4);
                      heat(s,5*p+1) = q_conv(p);
                      q_spray(p) = q_gen-q_rad(p)-q_conv(p);
                      heat(s,5*p - 2) = q_spray(p); %(W/m2)
                      base(s,3*p+1) = q_spray(p)*.3171; %BTU/h-ft2
                      base1(s,:) = base(s,:);

                      if (base(s,3*p)/base(s,3*p-1)) < 0.065
                         if base(s,3*points + 7) > 1000
                            h_tol = 0;
                            l_tol = 0.30*range;
                         elseif base(s,3*points + 7) > 500
                            h_tol = 0.05*range;
                            l_tol = 0.30*range;
                         elseif base(s,3*points + 7) < 150
                            h_tol = 0.10*range;
                            l_tol = 0.10*range;
                         else
                            h_tol = 0.15*range;
                            l_tol = 0.20*range;
                         end
                         if T(p)<(high_temp - h_tol) && T(p)>(low_temp + l_tol)
                            for n = 1:1:3
                               for m = 1:1:3
                                  X = i-2+n;
                                  Y = j-2+m;
                                  B(X,Y,1) = 255; B(X,Y,2) = 0; B(X,Y,3) = 0;
                               end
                            end
                         end
                      end
```

```
                for i = 1:1:size(base,1)
                    if base(i,3*p-1) > 1000 && base(i,3*p-1) < 1050
                        base(i,3*p-1) = 1000.0;
                    end
                end
            end
        end
    end

    image(B);
    point_filename = sprintf('%s\\Test %i\\Test%i Point Locations\\%s-p',extension,test,test,filename);
    saveas(gcf,point_filename,'jpeg')

    temp_gradient(s,1) = QV_data(s,2);
    temp_gradient(s,2) = mean(line_temperature(s,:));
    temp_gradient(s,3) = std(line_temperature(s,:));
  end
end

summary = zeros(size(base,1),2*points); %allocate space for the summary file.

for p = 1:1:points
  for i = 1:1:size(base,1)
    if (base(i,3*p)/base(i,3*p-1)) < 0.065
      range = base(i,3*points+7) - base(i,3*points+8); %High Temp - low Temp
      if base(i,3*points + 7) > 1000
        h_tol = 0.0;
        l_tol = 0.30*range;
      elseif base(i,3*points + 7) > 500
        h_tol = 0.05*range;
        l_tol = 0.30*range;
      elseif base(i,3*points + 7) < 150
        h_tol = 0.10*range;
        l_tol = 0.10*range;
      else
        h_tol = 0.15*range;
        l_tol = 0.20*range;
      end
      summary(i,1) = base(i,1); %Step #
      if base(i,3*p-1)<=(base(i,3*points + 7) - h_tol) && base(i,3*p-1)>=(base(i,3*points + 8) + l_tol)
        list_place = list_place + 1;
        temp_list_base(list_place,1) = base(i,3*p-1)-base(i,3*points+4); %Temp Measurement (°F)
        temp_list_base(list_place,2) = base(i,3*p+1); %Spray Heat Flux (BTU/h-ft2)
        temp_list_base(list_place,3) = (base(i,3*p))/(base(i,3*p-1)); %Percent Node Stdev of measurement
        temp_list_base(list_place,4) = base(i,1); %Step #
        temp_list_base(list_place,5) = base(i,3*p);%9 Node StDev (°F)
        temp_list_base(list_place,6) = p; %point #
        summary(i,2*p) = base(i,3*p-1);%List measured nodal tempertures (°F)
        summary(i,2*p+1) = base(i,3*p+1); %List calculated Q"s (BTU/h-ft2)
      end
    end
  end
end

n = 1;
for i = 3:1:size(temp_list_base,1)
  if temp_list_base(i,4) == temp_list_base(i-1,4) && temp_list_base(i,4) == temp_list_base(i-2,4)
      temp_list(n,:) = temp_list_base(i-2,:);
      temp_list(n+1,:) = temp_list_base(i-1,:);
      temp_list(n+2,:) = temp_list_base(i,:);
      n = n+3;
  end
end

a = 0;
for i = 1:1:size(summary,1)
  if rem(i,3) == 0
    step_avg(i/3,1) = summary(i,1);%Step #
    ph = 1;
```

```
        for p = 1:1:points
            %if point does not exist in all three step images,
            %leave out of step average
            if summary(i-2,2*p) ~= 0 && summary(i-1,2*p) ~= 0 && summary(i,2*p) ~= 0
                Tn(p,1) = mean(summary(i-2:i,2*p));
                Tn(p,2) = max(summary(i-2:i,2*p));
                Tn(p,3) = min(summary(i-2:i,2*p));
                Q(p,1) = mean(summary(i-2:i,2*p+1));

                T9n(1,p) = base(i-2,3*p);
                T9n(2,p) = base(i-1,3*p);
                T9n(3,p) = base(i,3*p);
            else
                Tn(p,3)= 0;
                Q(p,1) = 0;
                T9n (1:3,p)= 0;
            end
            if Tn(p,1)>0
                step_avg(i/3,4*p-2) = Tn(p,1)-base(i,3*points+4); %Step Avg Nodal Temp (°F)
                step_avg(i/3,4*p-1) = Q(p,1);%Step Avg Q"s (BTU/h-ft2)
                step_avg(i/3,4*p) = Tn(p,2)-Tn(p,1);%Step max - avg Nodal Temp (°F)
                step_avg(i/3,4*p+1) = Tn(p,1)-Tn(p,3);%Step avg - min Nodal Temp (°F)
            else
                step_avg(i/3,4*p-2) = 0;
                step_avg(i/3,4*p-1) = 0;
                step_avg(i/3,4*p) = 0;
                step_avg(i/3,4*p+1) = 0;
            end
            clear Tn Q;
        end

        for p = 1:1:points
            if step_avg(i/3,4*p-2) > 0
                Tn1(ph,1) = step_avg(i/3,4*p-2)+base(i,3*points+4);%Nodal Temp
                Qn(ph,1) = step_avg(i/3,4*p-1);%Q" Spray
                ph = ph+1;
            end
        end

        if ph == 1
            Tn1 = zeros(points,1);
            Qn = zeros(points,1);
        end

        step_avg(i/3,4*points+2) = base(i,3*points+4); %Fluid Temp
        step_avg(i/3,4*points+3) = mean(Tn1(:,1))-base(i,3*points+4); %Avg Node Temp - Fluid Temp
        step_avg(i/3,4*points+4) = max(Tn1(:,1))-mean(Tn1(:,1));%Max Node Temp - Fluid Temp
        step_avg(i/3,4*points+5) = mean(Tn1(:,1))-min(Tn1(:,1));%Min Node Temp - Fluid Temp
        step_avg(i/3,4*points+6) = mean(Qn(:,1));% Avg Q" spray
        step_avg(i/3,4*points+7) = max(Qn(:,1))-mean(Qn(:,1));% Max - Avg Q" spray
        step_avg(i/3,4*points+8) = mean(Qn(:,1))-min(Qn(:,1));% Avg - min Q" spray

        un(i/3,1) = mean(Tn1(:,1));
        un(i/3,2) = mean(T9n(3,:));%Avg 9 node StDev

        clear Tn1 T9n Qn;

        un(i/3,3) = base(i,3*points+6); %Pixelation °F
        un(i/3,4) = base(i,3*points+2); %Average Current
        un(i/3,5) = base(i,3*points+3);%Average Std of Current over Step
        un(i/3,6) = base(i,3*points+3)/base(s,3*points+2); %Percent of Current
        un(i/3,7) = base(i,3*points+4);%Fluid Temperature
        un(i/3,8) = base(i,3*points+5);%Average StDev for Fluid Temp per Step
    end
end

n = 1; n_max = size(step_avg,1);
while n <= n_max
    if step_avg(n,4*points+6) == 0 || step_avg(n,4*points+3) < 0
```

```
            step_avg(n,:) = [];
            un(n,:) = [];
            n_max = n_max-1;
        else
            n = n+1;
        end
    end

    summary_titles = {'Step #','T1 (°F)','Q1 (BTU/h-ft2)','T2 (°F)',...
    'Q2 (BTU/h-ft2)', 'T3 (°F)', 'Q3 (BTU/h-ft2)','T4','Q4 (BTU/h-ft2)', 'T5',...
    'Q5 (BTU/h-ft2)'};
    xlswrite1(output_file_name, summary_titles, 'Image Data','A1');
    xlswrite1(output_file_name, summary, 'Image Data', 'A2');

    temp_list_titles = {'T (°F)','Q Spray (BTU/h-ft2)','%Std/temp'...
    'Step #', '9 Node Dev (°F)','Point #'};
    xlswrite1(output_file_name, temp_list_titles, 'Temp List','A1');
    xlswrite1(output_file_name, temp_list, 'Temp List', 'A2');

    step_avg_titles = {'Step #','T1 (°F)','Q"1 (BTU/h-ft2)','Tmax-T','T-Tmin',...
    'T2 (°F)','Q"2 (BTU/h-ft2)','Tmax-T','T-Tmin',...
    'T3 (°F)','Q"3 (BTU/h-ft2)','Tmax-T','T-Tmin',...
    'T4 (°F)','Q"4 (BTU/h-ft2)','Tmax-T','T-Tmin',...
    'T5 (°F)','Q"5 (BTU/h-ft2)','Tmax-T','T-Tmin',...
    'Tfluid (°F)','Tavg','D to T max','D to T min','Q"avg',...
    'D to Q" max', 'D to Q" min'};
    xlswrite1(output_file_name, step_avg_titles, 'Step Avg','A1');
    xlswrite1(output_file_name, step_avg, 'Step Avg', 'A2');

    un_titles = {'Avg Temp (°F)','T9avg (°F)','Pixelation (°F)',...
    'Avg Current (A)','StDev Current (A))', '%ISdDev/I', 'T fluid(°F)',...
    'T fluid StDev(°F)'};
    xlswrite1(output_file_name, un_titles, 'Uncertainty','A1');
    xlswrite1(output_file_name, un, 'Uncertainty', 'A2');

    heat_flux_titles = {'Step #', 'T1','Q" Spray (BTU/h-ft2)', 'Q" Gen',...
        'Q" Rad','Q" Conv','T2','Q" Spray (BTU/h-ft2)', 'Q" Gen',...
        'Q" Rad','Q" Conv','T3','Q" Spray (BTU/h-ft2)', 'Q" Gen',...
        'Q" Rad','Q" Conv','T4','Q" Spray (BTU/h-ft2)', 'Q" Gen',...
        'Q" Rad','Q" Conv','T4','Q" Spray (BTU/h-ft2)', 'Q" Gen',...
        'Q" Rad','Q" Conv'};
    xlswrite1(output_file_name, heat_flux_titles, 'Heat Flux','A1');
    xlswrite1(output_file_name, heat, 'Heat Flux', 'A2');


    %Close Excel
    invoke(Excel.ActiveWorkbook,'Save');
    Excel.Quit
    Excel.delete
    clear Excel

    clear heat_data averages stdevs i QV_image_averages QV_data...
        changes summary temp_gradient heat un step_avg base temp_list_base temp_list;
  end
end
```

E.2 LabVIEW Codes

National Instruments LabVIEW software is used to process the signals. Figure E.3 is the block diagram developed to record the measurements. A set of measurements is recorded every 5 seconds (1). Each set records 10,000 voltage samples at a frequency of 50,000Hz (2). After the samples are read, the measurements are separated. A software filter is used to minimize 60Hz noise from the pressure signal as indicated by the software filter function (3) shown in Figure E.3. The flow rate is defined by the frequency of the obtained signal. A low-pass software filter is used to eliminate high-frequency noise and all 10,000 filtered samples are then used to determine the signal's frequency (4). The calibration equation for each device is used to adjust each sample to the appropriate units. Applied power is determined arithmetically by multiplying each voltage sample by the corresponding current sample (5). Each data set is then averaged and both the arithmetic mean and standard deviation (6) with the exception of flow rate where only a single frequency can be established from the data set. When the writing function (7) is activated by the user, these values are recorded to a text file. Processes are very similar for reading collected during mass flux trials (flow.vi).

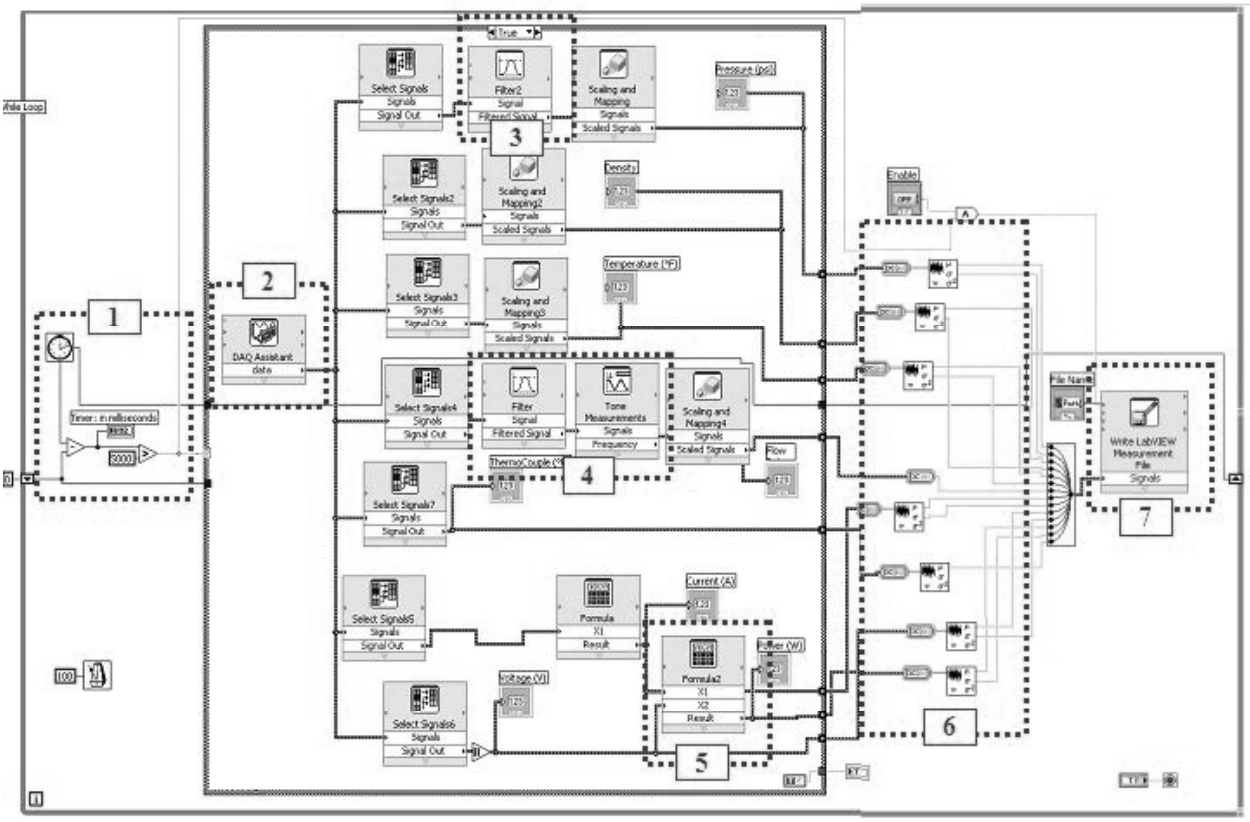

Figure E.1 ChannelReadings3.vi LabVIEW Block Diagram

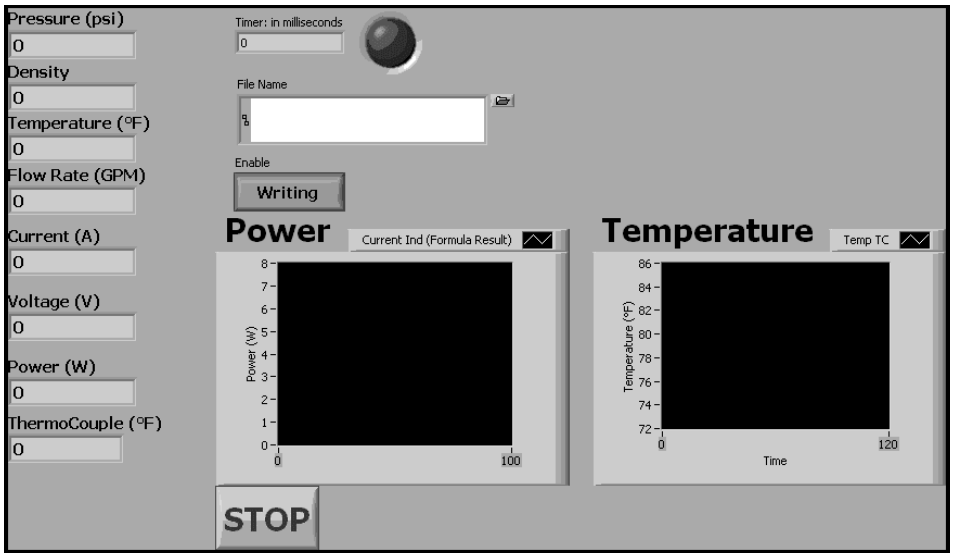

Figure E.2 ChannelReadings3.vi LabVIEW Front Pannel (User Interface)

Flow.vi

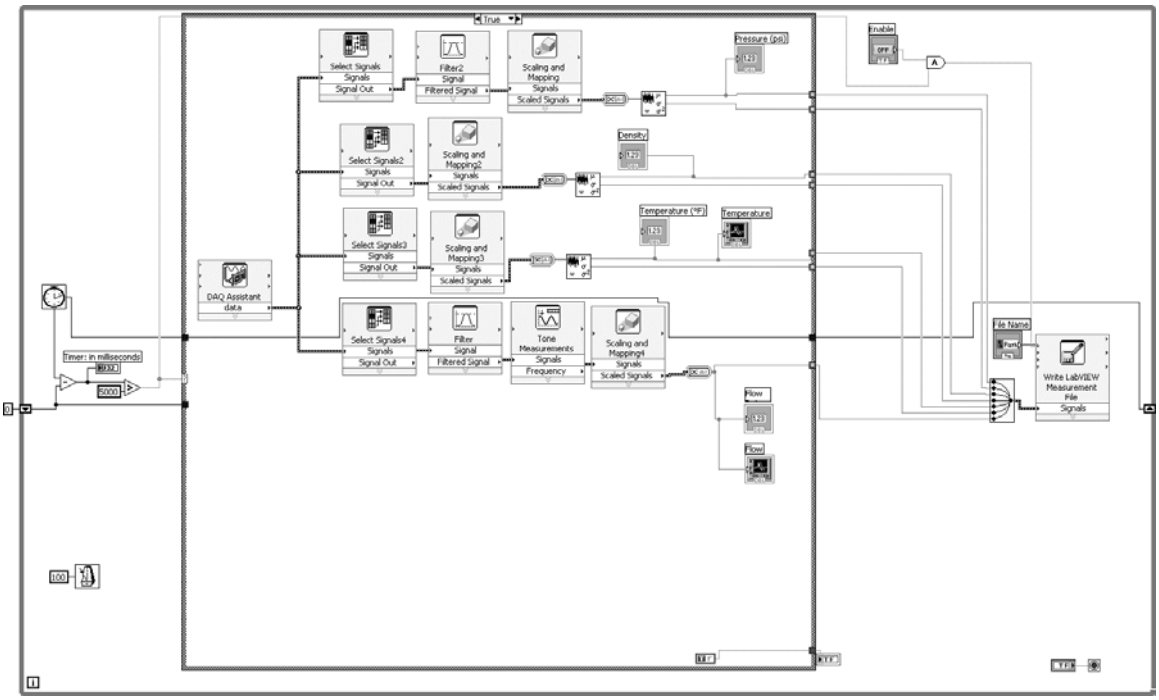

Figure E.3 Flow.vi LabVIEW Block Diagram

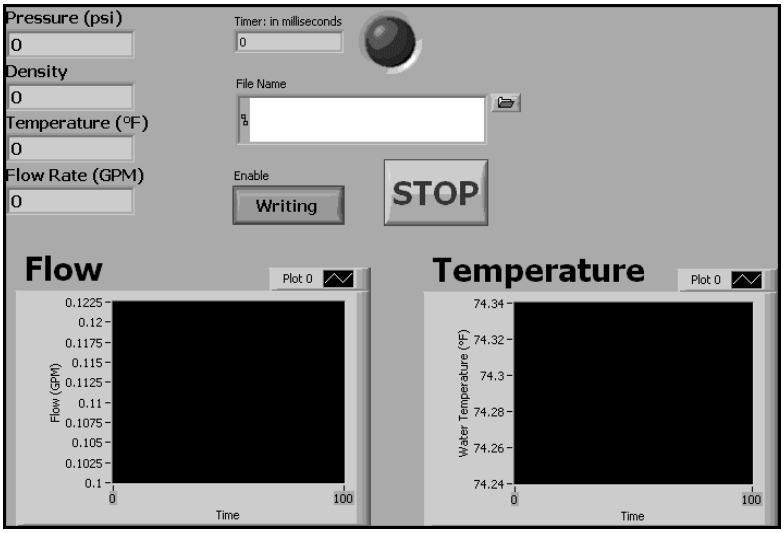

Figure E.4 Flow.vi LabVIEW Front Pannel (User Interface)